The Characterisation and Screening of Novel Aromatic Thin-Film Materials

John B. Henry

Degree of Doctor of Philosophy

The University of Edinburgh

2009

Frontispiece

"Science alone of all the subjects contains within itself the lesson of the danger of belief in the infallibility of the greatest teachers in the preceding generation . . . Learn from science that you must doubt the experts. As a matter of fact, I can also define science another way: Science is the belief in the ignorance of experts."

Professor Richard P. Feynman

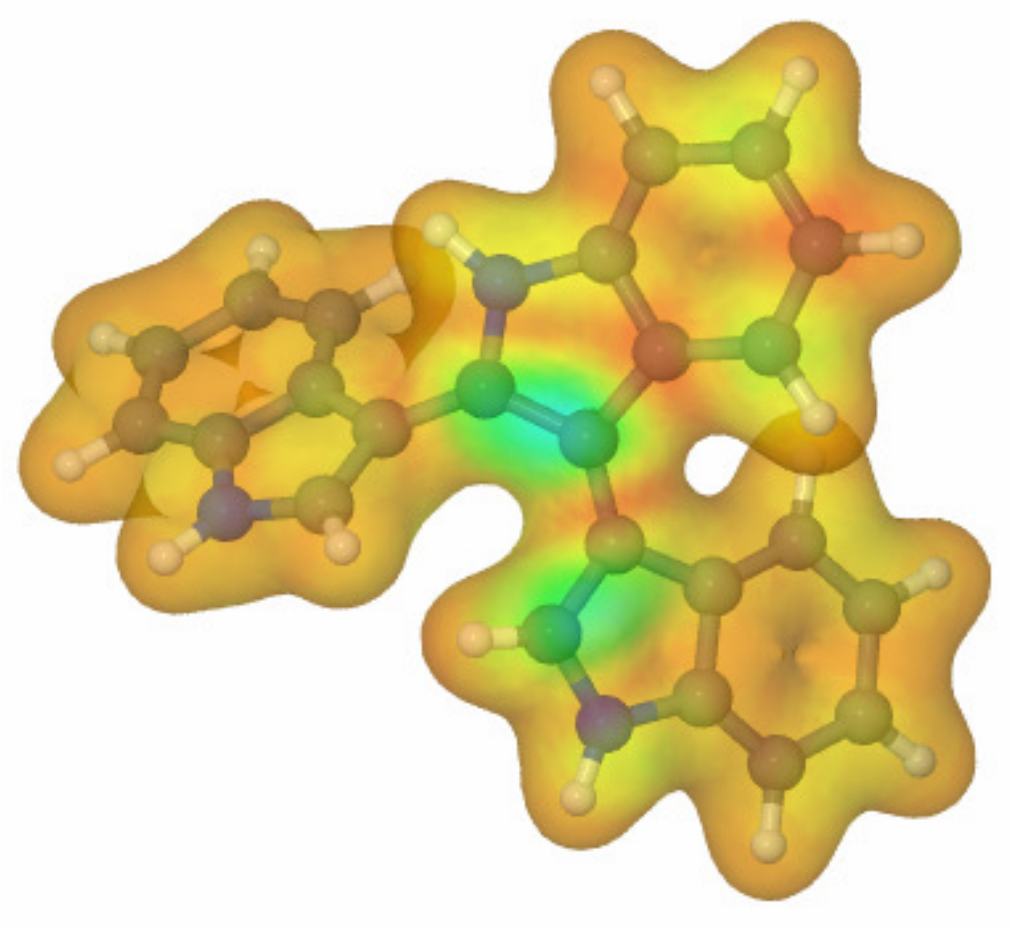

Abstract

The electropolymerisation of a range of indole derivatives results in the formation of redox active films. These redox films have been observed to be highly luminescent. Earlier studies have investigated electrochemical and photophysical properties, for potential applications such as fast response potentiometric sensors or novel materials for light emitting devices. The work in this thesis extends this approach to electrochemical and computational studies of a range of novel redox-active aromatic systems.

This work has exploited the continuing increase of computing power, employing powerful quantum computational models to complement and augment electrochemical methods. Density Functional Theory has been used to show that prediction of oxidation potentials in good agreement with experimental values is achievable for a wide range of aromatic systems. Calculation of the electron spin density of the radical cations has also helped to elucidate the likely coupling locations for the formation of electroactive layers. It is observed that the nature of substituents and additional hetero groups to the aromatic systems can have a profound effect on electron spin density distributions.

The redox-active species formed from indole dimers and 5-methylindolocarbazole have also been characterised. The species formed from electropolymerisation of 5-methylindolocarbazole has been found to be a mixture of three isomers of a 5-methylindolocarbazole dimer. Full characterisation of the product of the electropolymerisation of indole dimers was not possible; fluorescence work however suggests this to be a species with a greater degree of conjugation than either indole dimers or trimers. It is thought likely that this product is either a tetramer or longer chain polymer. This work demonstrates the applicability of a combination of computational and electrochemical methods to the characterisation of novel heteroaromatic systems.

Declaration

I hereby declare that the work presented in this thesis is my own unless otherwise stated by reference.

John B. Henry

April 2009

Acknowledgements

A great deal of gratitude is extended to the following people for their aid and encouragement for the duration of my post-graduate studies.

Firstly a great deal of thanks goes to my supervisor, Dr. Andrew Mount, for all his help, encouragement and ability to always discover just one more experiment to perform. Thanks also go to my second supervisor, Dr. Anita Jones, for her encouragement.

In the lab thanks go to Dilek Madenci for her training on the formation of electro-active films. Thanks also go to Mount group members past and present for advice and much needed lunch breaks, Helena Woodvine, Nathan Brockie, Louisa Reissig, Charlotte Brady, Dr. Elena Ferapontova, Dr. Nate Wittenberg, Dr. Ilenia Ciani and Dr.Chaker Tlili.

For the work on the characterisation of 5-MethylIC films in Chapter 5 thanks go to the Masters Project student Elanor Wood. And for the fluorescence spectra of benzothiophenes credit goes to the Masters Project student Becky Choules.

For stimulating weekly scientific discussion my gratitude goes to all who have attended the Mount/Pulham/Robertson/Yellowlees Materials Meetings over the past three years.

For their aid and discussions on the computational work in this thesis thanks goes to Dr. Andrew Turner and a particularly large thanks to Dr. Patricia Richardson for her continued help.

For their efforts, assistance and patience in attempting ESI-MS on the diindole products thanks goes to Dr. Bridgette Duncombe and Andrew Gray.

Gratitude is extended to that strange breed, the synthetic chemists named in Chapter 3, for their alchemical abilities in creating the aromatic systems studied in this thesis.

Acknowledgement goes to the University of Edinburgh for the funding of my post-graduate research.

Final thanks go to Danielle for providing a pleasant distraction during the writing of this thesis and to my parents and siblings for their support throughout the years.

Publications

1,4,5,8,9,12-Hexamethyltriphenylene. A Molecule with a Flipping Twist
Wang, Y.; Stretton, A. D.; McConnell, M. C.; Wood, P. A.; Parsons, S.; Henry, J. B.; Mount, A. R.; Galow, T. H.
J. Am. Chem. Soc.; **2007**; *129*(43); 13193-13200. DOI: 10.1021/ja074120j

The Production and Characterisation of Novel Conducting Redox-Active Oligomeric Thin Films From Electrooxidised Indolo[3,2,1-*jk*]carbazole
Wharton, S. I.; Henry, J. B.; McNab, H.; Mount, A. R.
Chem. Eur. J. *In Press.*

List of Chemical Abbreviations

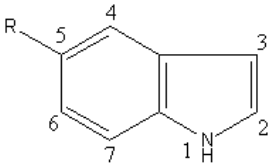

In – Indole

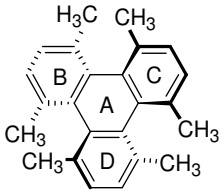

hmtp – 1,4,5,8,9,12-Hexamethyltriphenylene

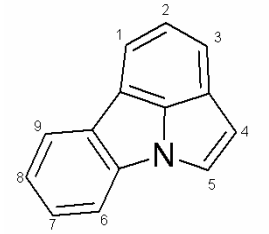

PC – Pyrrolo[3,2,1-jk]carbazole

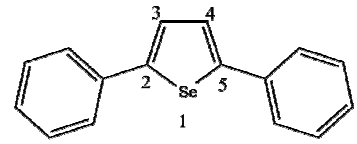

dbs – 2,5-dibenzoselenophene

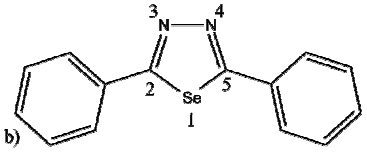

dbas – 2,5-dibenzo-3,4-diazaselenophene

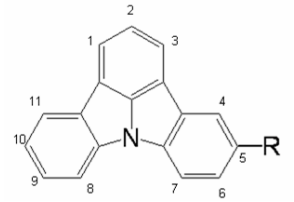

IC – indolo[3,2,1-jk]carbazole

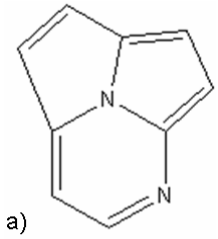

CZ – 1-azacycl[2,3,2]azine

Contents

Chapter 1: Introduction.

1.1 The Development of Novel Aromatic Materials.

The twentieth century witnessed the birth of macromolecular science through the synthesis of polymers; now at the start of the 21st century the field has matured into an incredibly active and diverse area of chemical research[1]. The field spans all aspects of chemistry, from biochemistry, where the polymeric helix of DNA is formed from natural nucleotide bases[2], through synthetic chemistry, where there is constant striving to form new macromolecules and to tune their properties, to physical chemistry, where the properties of polymers and plastics are investigated to probe the relationship between polymer structure and function. Of particular interest recently have been conducting conjugated polymers formed from aromatic monomers which provide an ideal basis for electrically conducting materials[3].

Communication between physical and synthetic chemists is particularly important in the development of novel materials with controlled properties. Polymeric materials are typically produced with a range of polymer chain lengths and structures. The resulting materials' properties are often determined by this chain length distribution, and the heterogeneity of the films formed from these polymer systems. Recently a new field of materials science has developed which uses the design and synthesis of novel small molecules and specific oligomers to form small molecular systems. These systems are typically able to form thin film materials with crystalline or homogeneous multilayers due to their uniform size enabling efficient packing. This increase in packing efficiency may lead to enhanced materials properties over polymers[4,5].

A vast range of synthetic methodologies exists for the production and functionalisation of aromatic molecules. The potential therefore exists to produce a novel aromatic with optimised properties designed for every novel materials application. However, the time and expense required for the synthesis and experimental screening of material properties for every aromatic molecule is

prohibitive. There is also the possibility that the determination of synthesis targets often drives synthesis development (where yields can be optimised with the environmental input and costs being minimised). Furthermore the understanding of structure property relationships can be used to efficiently explore the screening process. This thesis focuses on the development of an *in silico* screening method for aromatic systems to assess their potential for forming novel redox active luminescent materials, and the validation of this screening method through experimental measurement. This chapter will introduce the field of organic electro-active and luminescent materials and their applications; the development of computational methods to study the physicochemical properties of organic electro-active materials will then be discussed.

1.1.1 Aromatic Molecules: Pathways to Conducting Thin Film Materials.

1.1.1.1 Conducting Polymers.

It has long been known that conjugated polymers possessed electrical conductivity orders of magnitude higher than do other polymeric materials[6,7]. However, it was not until the final quarter of the last century that the study of these conducting polymer systems gained widespread interest.

The synthesis of highly conducting forms of polyacetylene[8,9] by Shirakawa, McDiarmid and Heeger in the late 1970's, for which they were awarded the Nobel Prize for Chemistry in 2000, led to an explosion of research into the field of conducting polymers. In this initial work it was discovered that, analogous to semi-conductors, polyacetylene could be made to be in *p* and *n*-doped forms via redox reaction, with conductivity ranging from metal-like electronic conductivity to fully insulating[10]. In conventional semi-conductors (e.g. Ge) such doping is achieved by the implantation of a small number of atoms of similar size into the lattice structure each with one less valence electrons (e.g. Ga) for p-doping or one more valence electron (e.g. As) for n-doping. p- and n- give the majority charge carrier, p- indicating positive holes and n- indicating negatively charged electrons. In conducting polymers the charge carriers are produced either through removal of

electrons (oxidation of the polymer) for p-doping or though addition of electrons (reduction of the polymer) for n-doping.

The doping of polyacetylene is achievable through chemical, electrochemical, photodoping or interfacial methods[11]. Chemical doping is achievable through redox reaction. Equation 1.1.1 illustrates p-type doping through reaction with I_2.

$$[polymer]_n + \frac{3}{2} nyI_2 \rightarrow [polymer^{+y}(I_3^-)_y]_n \quad \textbf{Equation 1.1.1}$$

Equation 1.1.2 illustrates n-type doping through reaction with sodium napthalenide ($Na^+C_{10}H_8^-$).

$$[polymer]_n + (Na^+C_{10}H_8^{\bullet -})_y \rightarrow [Na_y^+ polymer^{-y}]_n + yC_{10}H_8 \quad \textbf{Equation 1.1.2}$$

Photodoping is achieved by local oxidation and (nearby) reduction caused by photo-absorption and charge separation, electron-hole pair creation and separation into "free" carriers, as shown in Equation 1.1.3.

$$[polymer]_n + h\nu \rightarrow [polymer^{+y}\, polymer^{-y}]_n \quad \textbf{Equation 1.1.3}$$

y is the number of electron-hole pairs generated. Bulk and interfacial doping both involve electrochemical charge injection of electrons and/or holes through electrode contacts. In bulk doping the injected charge must be compensated by the incorporation of counter-ions to the polymer film, as shown in Equations 1.1.4 and 1.1.5 for p-type and n-type doping, respectively, in background electrolyte M^+X^-.

$$[polymer]_n + X^-_{sol'n} \xrightarrow{-nye^-} [polymer^{+y} X^-_y]_n \quad \textbf{Equation 1.1.4}$$

$$[polymer]_n + M^+_{sol'n} \xrightarrow{+nye^-} [polymer^{-y} M^+_y]_n \quad \textbf{Equation 1.1.5}$$

With interfacial charge injection there are no counter-ions available and reaction occurs as shown in Equations 1.1.6 and 1.1.7 for p-type and n-type doping respectively.

$$[polymer]_n - ye^- \rightarrow [polymer]_n^{+y} \quad \textbf{Equation 1.1.6}$$

$$[polymer]_n + ye^- \rightarrow [polymer]_n^{-y} \quad \textbf{Equation 1.1.7}$$

The distinction between bulk and interfacial electrochemical doping becomes clear when considering the charge injection in polymer light emitting diodes[12], where there are no counter-ions and an interfacial mechanism occurs, and in polymer light-

emitting electrochemical cells where bulk electrochemical doping with re-distribution of ions provides the mechanism for charge transfer[13].

Electrochemical doping introduces the ability to "switch" a formed film between a conducting, or semi-conducting, state and an insulating state through the application of an electric current. This ability to alter the properties of a material electrically, unlike conventional semiconductors, allows conducting polymers to be the active material in a wide range of "plastic" electronic and optoelectronic devices including lasers, high sensitivity plastic photodiodes and photovoltaic cells, ultrafast image processors (optical computers), thin-film transistors and all-polymer integrated circuits.[11] These electronic properties in combination with intrinsic polymer properties provides a potential route to light, inexpensive and flexible electronic devices.[4]

1.1.1.2 Electochemical Conducting Polymer Film Formation.

Heterocycles such as pyrrole[14,15] (Figure 1.1.1.a) were known to polymerise before the discovery of conducting polyacetylene formation by Heeger *et al*[8]. However it was not until after the discovery of highly conducting polyacetylene that interest in the polymerisation of aromatic molecules as a route to conducting materials was renewed. These heterocyclic polymers were of immense interest as not only were they found to be more stable, both chemically and thermally, than polyacetylene, but they also had monomer units that were far easier to derivatise and thus provide a broader base on which to study the polymerisation and tuning of electrical and physical properties of the formed films[16]. Polymerisation of pyrrole and thiophene involves the coupling of the heterocycles[17]; electrochemically this initially involves the oxidation of two monomer units to form radical cations. The accepted growth mechanism for these polymers through radical cation coupling is shown in Figure 1.1.2. After radical cation formation through oxidation of the monomer at, or above, the monomer oxidation potential, $E_{ox,M}$, coupling occurs between the positions of highest electron-spin density (the α- or 2, 5- positions on the monomer) to form a dimer[17]. The oxidation potential of this dimer ($E_{ox,D}$) is lower than that of the monomer and so further oxidation occurs readily at the electrode (as $E_{ox,D} < E_{ox,M}$) and coupling of dimer radical ($D^{\bullet+}$) and monomer radical ($M^{\bullet+}$) occurs to form a

trimer, coupling again occuring at the sites of greatest spin density. As the oligomer length (n) increases the oxidation potential of each oligomer decreases and this favours the coupling of oligomers to form a polymer, as the α-positions of each oligomer are the predominant coupling positions the formed polymer is generally a linear polymer with α-coupling along the majority of the polymer. Ready functionalisation of these polymers therefore may occur through the addition of substituents at the β-positions (or 3, 4-positions) in the monomers[16,18]. It is also possible to substitute at the N-position (or 1-position) in pyrrole[16], which although synthetically easier leads to a significant reduction in conductivity due to steric factors. As the coupling forms ever longer chain oligomers, greater electron-spin density can be found in the β-position of the radical cation and some coupling can also be found to occur through this position[19]. Films formed from such heterocycles have shown potential in a range of devices such as electrochemical sensors[16,20] and photoelectrochemical cells[21].

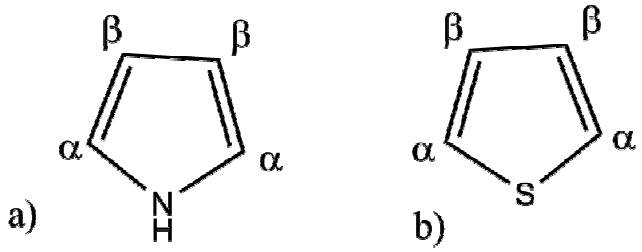

Figure 1.1.1. Structures of (a) pyrrole and (b) thiophene.

Aromatic conducting polymers have been formed from a range of monomer units. For example, aromatic monomers such as furan[22], phenylenes[23] and aniline[24] have been emplyed amongst others. For the most conducting materials it is desirable to have a high degree of chain alignment (to maximise polymer conductivity) and inter-chain ordering and structural homogeneity (to maximise interchain conductivity). In fact it is often the latter which determines film conductivity for the polymer systems. It is also desirable for these materials to be soluble and processible[11]. Interest has moved recently to the formation of electro-active and conducting materials formed from smaller heteroaromatic monomer and oligomer systems for which efficient packing and structural homogeneity should be more readily achievable.

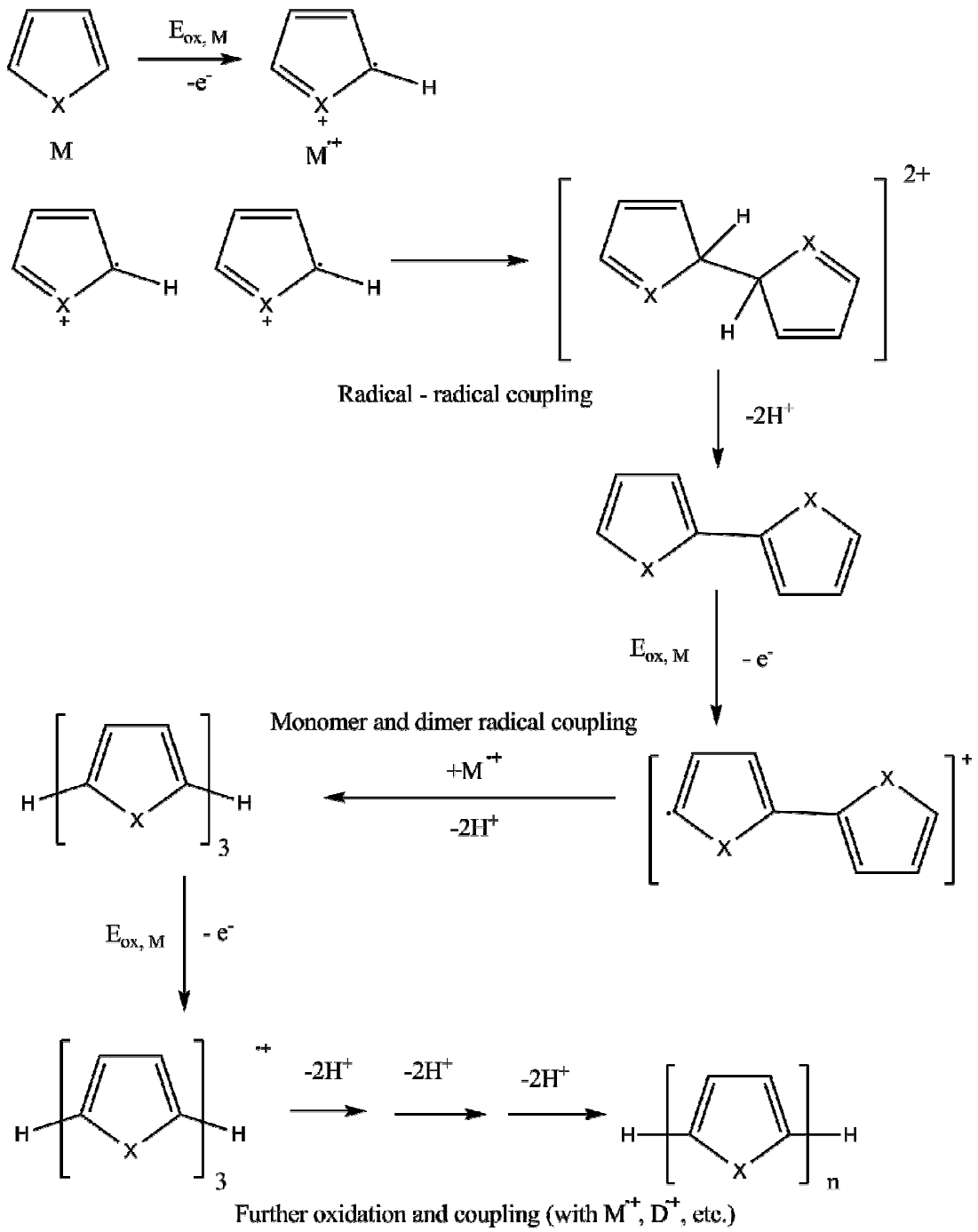

Figure 1.1.2. Accepted mechanism for heteroaromatic polymer growth by radical cation coupling.

1.1.1.3 Conjugated Organic Molecular Thin Films.

One of the major driving forces for the study of of conjugated organic materials was the discovery of the application of such materials in forming the emitting layer in light-emitting diodes[25]; as such the optimisation of luminescent and electrical properties is paramount. The field of light-emitting materials has largely been

divided into three major areas of interest, the conducting polymer systems discussed previously, small molecular materials[26] and conjugated molecules within dendrimers[27]. The systems referred to as molecular materials are typically conjugated organic systems, commonly doped with transition metal (such as Pt and Ir)[28,29] complexes to tune the electronic properties of these materials to optimise their use in devices. One approach is to produce novel conjugated organic materials for this application (classes of molecules which can be synthesised simply, with an ability to tune electronic and luminescent properties and with high processability). N-heteroaromatics represent such a class of molecules, with carbazole[30,31,32] and indolocarbazole[33,34,35] derivatives being reported as efficient hole transport materials with potential application in organic thin film transistors, while isoindoles[36] are highly fluorescent and have been investigated for light emitting devices.

Although such changes in the molecular composition of conducting polymers and molecular materials can be used to tune the electronic properties, they often also change the physical, and photophysical, properties of a material. For example increased electronic conduction and/or aggregation often lead to enhanced luminescence quenching in thin films. Dendrimers have been proposed as a good system to overcome the problem of luminescent quenching in light emitting materials[37]. Dendrimers are highly branched polymers surrounding a central core (a luminescent core, in this case). The highly branched nature of the dendrimer can then protect the luminescent core from aggregation and/or exposure to other quenchers. However, this protection of the luminescent properties of the core necessarily minimises aggregation (π-stacking) and reduces core electron transfer. This is therefore detrimental to the electronic properties of the molecule. Synthetic strategies for the formation of dendrimers are well understood with relatively high yields achievable[38]. However, the methods involved are complex and require a large number of steps, leading to appreciable cost in money and time. Such strategies still require the production and characterisation of molecules able to form luminescent and redox-active luminescent cores. Electrochemical formation of dendrimers is not possible currently and alternative strategies which maintain thin film luminescence are not well developed.

1.1.1.4 Indole Systems.

The term indole is derived from the indigo dyes which, in the form of indigotin (Figure 1.1.3.a), indoles form the major constituent[39]. Indole is also the at the core of a number of important biological molecules, such as the amino acid tryptophan (Figure 1.1.3.b), the neurotransmitter serotonin (Figure 1.1.3.c) and melatonin (Figure 1.1.3.d) which is important for skin pigmentation. The oxidation processes of these biological indoles is of interest in determining the role of these species inside living organisms and is a matter of some interest[40], understanding the electrochemical properties of indoles may aid this understanding.

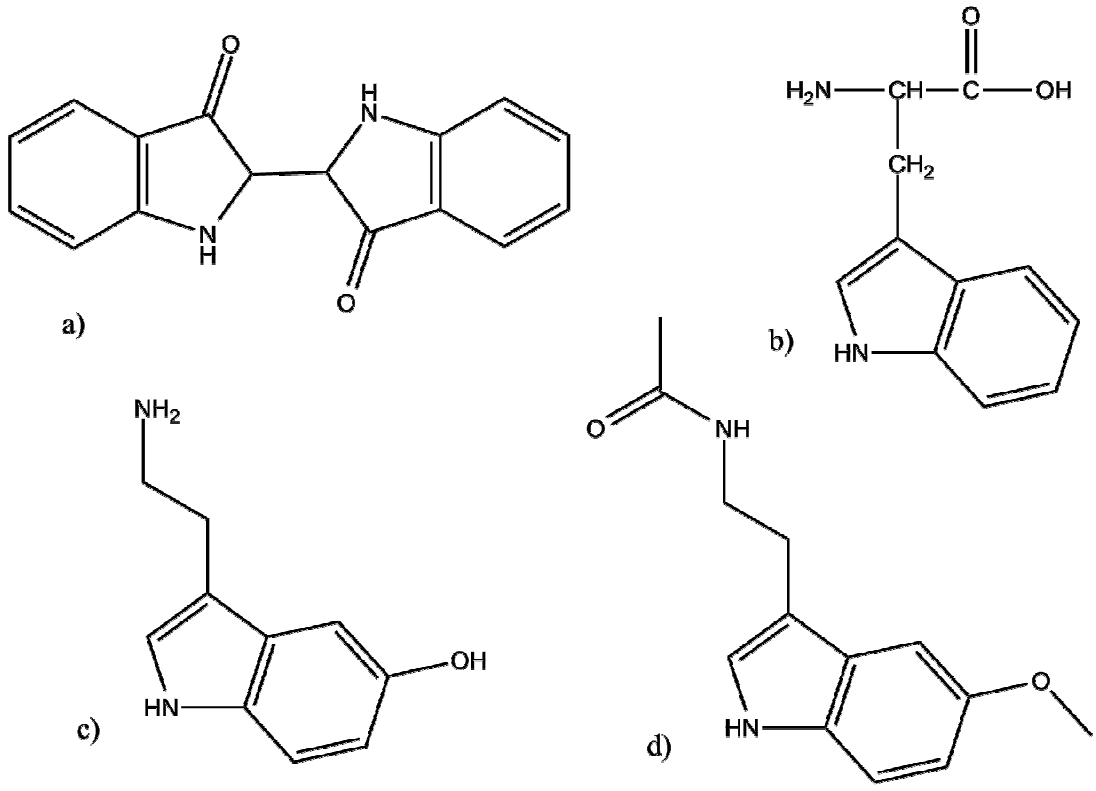

Figure 1.1.3. A range of important indole molecules containing indoles. a) Indigotin, b) tryptophan, c) serotonin and d) melatonin.

In the 1990s the Mount group showed that highly conducting electro-active films of asymmetric trimers of 5-substituted indoles can be formed electrochemically[41], forming reproducible and highly conducting π-stacked films, and proposed a mechanism for their formation (Figure 1.1.4). It was found that the choice of 5-

substituent introduced the ability to tune the electronic properties of the formed films[41] while leaving the fluorescent properties of the trimer chromophore unaffected[42] due to the characteristic fluorescence of the trimer core.

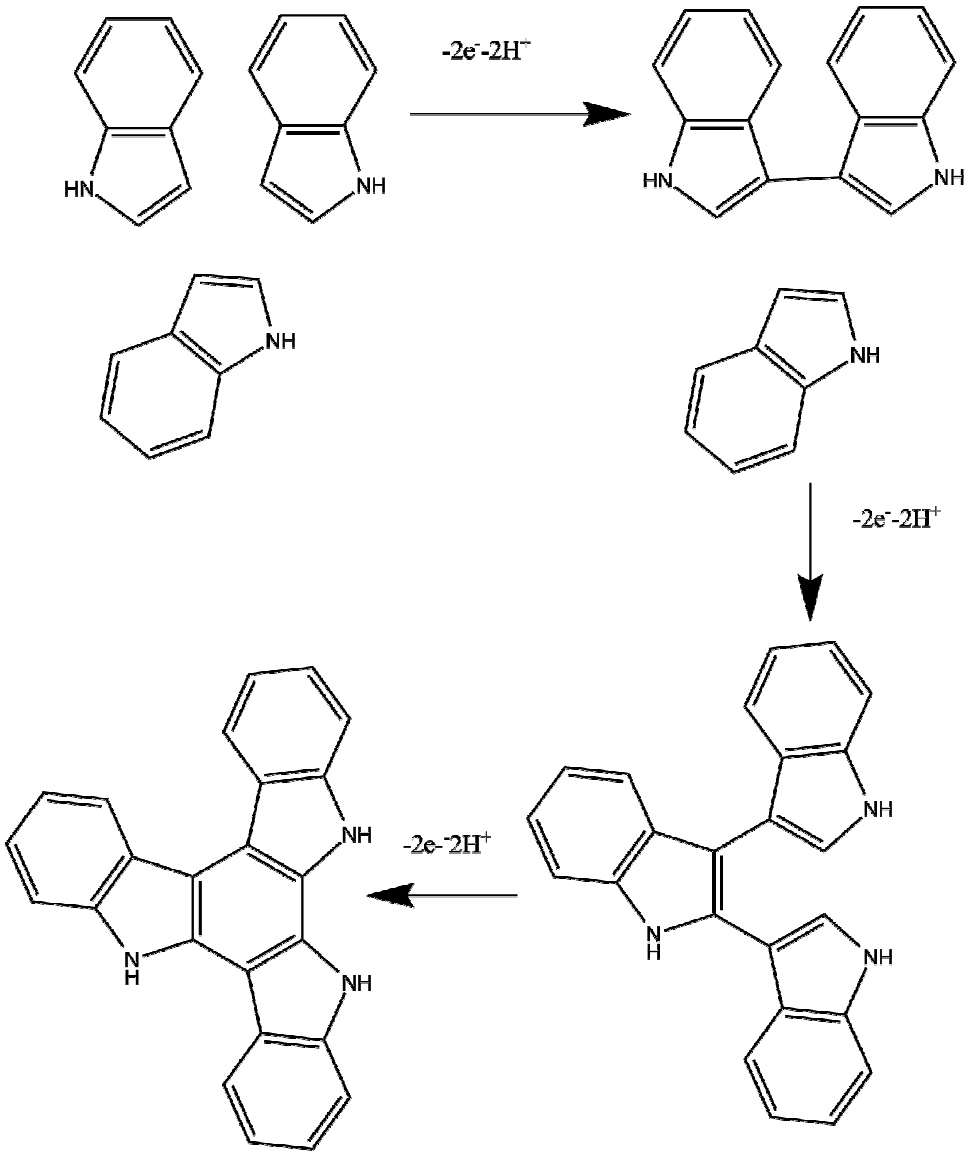

Figure 1.1.4. Proposed coupling mechanism of indole to form the asymmetric trimer product[41].

Electrochemically formed films of indole have been proposed as suitable for use in a range of devices. Bartlett *et al.*[43] proposed electropolymerised films of 5-carboxylic acid as fast response pH sensors as the formed films were sensitive to pH changes. Subsequent work in the Mount group[44] showed that films formed from 5-cyanoindole showed a rapid linear Nernstian response to pH in the range of pH 2 to 12. Bartlett

also described the use of indole-5-carboxylic acid films as mediators for the direct reduction and oxidation of cytochrome c[45], as binding between film and the protein was possible *via* the carboxylic acid groups and lysine residues on the protein surface, allowing electron transfer between the redox protein and the modified electrode. Tyrosinase[46] has been shown to be immobilised onto a film formed from indole-5-carboxylic acid allowing the formation of bioactive electrodes; while the oxidised films formed from indole-5-carboxylic acids have been shown to function as cathodes in aqueous rechargeable cells[47].

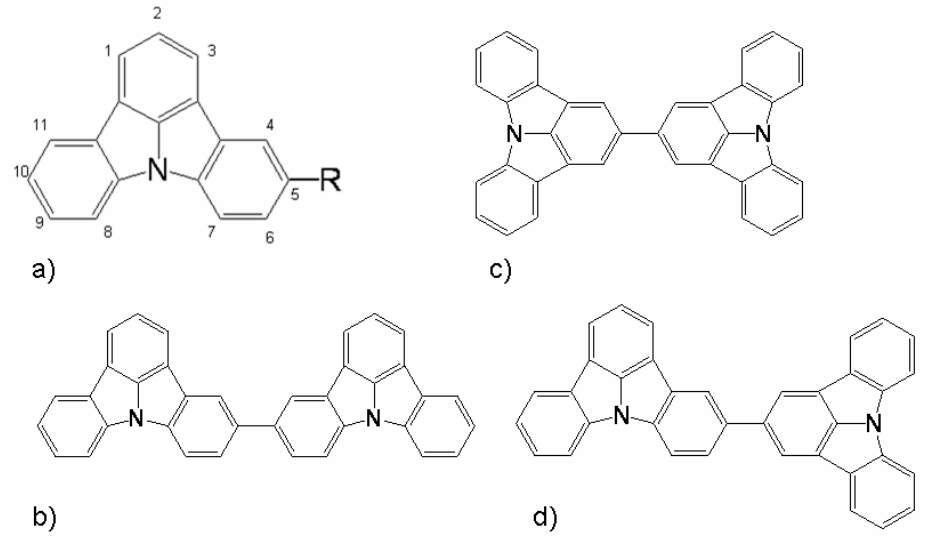

Figure 1.1.5. a) Structure and numbering system for 5-substituted indolo[3,2,1-jk]carbazoles. Structures of b) 5, 5'-IC dimer, c) 2, 2'-IC dimer and d) 2, 5-IC dimer.

Building on this indole work, recent experimental work on heterocycles containing indole units such as indolo[3,2,1-jk]carbazole[48] (Figure 1.1.5) has shown that upon electro-oxidation an oligomeric conducting film consisting of three dimers is formed. This introduces the possibility of the formation of oligomeric conducting films with enhanced packing efficiencies over polymers, with the possibility of selective direct electrochemical functionalisation. The ability to form electrochemically electro-active oligomer films under reproducible, mass transfer control raises the potential of developing a novel range of aromatic systems which can form electro-active and luminescent materials. A range of modifications to the indolo[3,2,1-jk]carbazole structure thorugh the addition of functional groups or the insertion of aza-groups into

the heterocycle system are possible[48]. These modifications may lead to a change in the electronic properties of the indolo[3,2,1-jk]carbazole structure while maintining the physical properties of the indolo[3,2,1-jk]carbazole unit and the dimer formed on electro-oxidation.

1.2 Modelling Physicochemical Properties of Aromatic Molecules.

The electrochemical and optical behaviours of aromatic molecules and conjugated oligomers and polymers originates from their chemical and electronic structures and properties. A proposed method for the study of such systems is the use of quantum mechanical calculations to calculate structure, properties and predict behaviour. Quantum chemical calculations can, in principle, provide a valuable complementary tool in predicting the nature of a large range of chemical processes and properties. Density Functional Theory (DFT) has been used to model some properties, such as the absorption and emission solvatochromic propeties[49] and to aid structural characterisation with NMR in solution[50] or powder[51]. This section will discuss work which is particularly relevant to the electronic and coupling mechanisms of organic aromatic systems.

1.2.1 Calculating Redox Potentials of Organic Molecules.

The thermodynamics of innumerable chemical and biological electron-transfer reactions[52] are fundamentally dependent on the relative redox potentials of the redox species involved, which measures the propensity of a species to donate or accept an electron. The ability to predict these redox properties accurately is therefore essential for the rational design of novel molecular systems[53]. Much of the previous work on the calculation of redox potentials has focussed on biologically important molecules (such as quinones[52,53,54,55,56] or in the design of DNA base analogues[57]). Some studies have focussed on environmentally important systems (such as hexachloroethane[58] and anilines[59]) and the calculation of redox potentials of indoles for the formation of electro-active films[60]. Others have attempted to predict the redox potentials of a range of organic[61,62,63,64] and inorganic[61,65] systems.

In general these approaches first compute gas-phase ionisation energies; approaches to the computation of these energies typically vary in the choice of either semi-empirical or DFT methodologies (the difference between these methodologies will be discussed in Chapter 2). Solvation energy terms are then calculated using either explicit solvation models (where the solvent molecules are explicitly included in the calculation with the species of study) or implicit solvation models (where solvation effects are modelled using an average interaction between a solvent continuum and the species). A more detailed description of an implicit solvation model is discussed in Chapter 2. In situations where there is a requirement to study strong and specific molecular interactions between the solvent and the species of interest, modelling the explicit solvation of molecules can be extremely important. Because such methods must include solvent molecules explicitly in the calculation they are computationally expensive. In general, where specific chemical bonding (for example hydrogen or covalent bonding) between individual solvent molecules and the species of interest is not present, the computationally less intensive implicit solvation methodologies are thought to provide a good approximation to enable the energetics of solvation to be calculated[66].

The computed redox potentials are then typically related to the free energy for the standard reaction of a common reference electrode, typically either the saturated calomel electrode (SCE), the standard hydrogen electrode (SHE), or the normal hydrogen electrode (NHE), as the calculation of the free energy of an electron in the metal of an electrode is fraught with difficulty, as the electron energy will depend on the electrical potential of the metal and may be affected by image effects of ions at the electrode surface. Intensive computational methods have been employed to model electron transfer from electrodes to ions[67] such techniques are, however computationally expensive. The calculated redox potentials are then compared to measured reported redox potentials from the literature. While this methodology should work well in principle, it has been reported[68] that caution should be exercised when comparing redox potentials measured in acetonitrile solutions with different reference electrodes due to a range of issues. One issue arises from the use of the SCE, historically one of the most frequently used reference electrodes in laboratories

due to the inconvenience of the SHE. The application of the SCE in nonaqueous media is limited however by water leakage into the nonaqueous phase and frequent incompatibility of KCl with those media, particularly when perchlorate ions are present[69]. The ferrocene/ferrocenium redox couple has been used as an internal standard recently, but this still raises difficulties due to the wide range of redox potentials that have been reported for this redox couple in acetonitrile solution[68]. Further issues can arise from the reporting of potentials with respect to the NHE electrode when the SHE is probably usually intended[68].

Previous studies[56,60] have shown that the calculation of redox potentials using a DFT method provides greater accuracy than semi-empirical methods, with reported errors within a few 10s of mV achievable using DFT methods as opposed to 100s of mV found for semi-empirical methods. One study by Baik and Friesner[61] compared the accuracy of calculating redox potentials for organic and inorganic systems. It was found that a good degree of accuracy was achievable for organic molecules, whereas metallocenes and a range of simple ligand systems gave deviations between calculated and experimental values of more than 100 mV, with the deviations being systematically offset from the expected values. Studies by Fu *et al.*[62] calculated the redox potentials of roughly 270 structurally unrelated organic molecules in acetonitrile and dimethyl sulphoxide (DMSO) solvent modelled via an implicit solvation model, and found an overall standard deviation of 170 mV in acetonitrile and 110 mV in DMSO when all the molecules were taken into consideration.

The study by Kettle *et al.*[60] employed a similar methodology, however, the calculated free energy of a standard redox couple (ferrocene/ferrocinium) was chosen as reference instead of through comparison to the free energy for the standard reaction of a common reference electrode and calculated redox potentials were compared with redox potentials measured as part of the work. This work reported calculated redox potentials for a range of 5-substituted indoles, reporting an error of 100 mV in the calculated potentials with respect to the measured potentials.

For the development of a screening method it is important to consider what level of accuracy is required. To assess the appropriate level of accuracy it is necessary to consider the aim of the screening method. If the objective of the screening method is only to identify substances that show oxidation within the solvent window of the electrolyte system being studied then a lower accuracy (a standard deviation of a hundred of mV or so) may be sufficient. If however the objective of the screening method is to identify species with specific electrochemical properties, to study the effects of substitution and to consider the thermodynamics of the system, a much higher degree of accuracy is required, of the order of 10s of mVs, or less. Such accuracy is not routinely achievable.

1.2.2 Modelling the Growth and Properties of Aromatic Conducting Materials.

There have been numerous calculations performed to model the growth of conducting polymers and oligomers[70,71,72,73,74,75,76,77]. The majority of these studies have focussed on the structure and conformations of these polymers. Initial calculations on the oxidation and growth mechanism of heterocyclic conducting polymers were performed on thiophene and pyrrole using a semi-empirical method[78]. These calculations showed a strong correlation between the sites of greatest calculated electron spin density on radical cations and the coupling sites for polymerisation of a range of monomers, such as pyrroles and thiophenes[79], but showed a poor agreement with the coupling positions of indoles[80]. This would be expected if polymer formation occurs through coupling of radical cations, as coupling of radical cations would be expected to occur by pairing of the radical spin from each radical cation to form a bond[60], with the assumptions that there is no, or little, perturbation of electron density on coupling and that there is no loss of protons from the radicals. When applied to oligomers the spin density became more delocalised and linkages involving the β-position were observed to be just as likely. Later studies employing more rigorous DFT methods were able to calculate the electron spin densities of pyrrole and thiophene monomers and oligomers with good correlation to experimental values obtained by electron paramagnetic resonance EPR[81].

Few calculations have been carried out on the electro-oxidation and coupling of indole. Most of these studies have used semi-empirical methodologies and assumed radical cation coupling to a neutral monomer[82,83,84], which give results inconsistent with the characterised products of indole electro-oxidation. The DFT study by Kettle[60] assumed a radical cation - radical cation coupling mechanism, with coupling at the sites of greatest electron spin density, and predicted the initial formation of a symmetric 3,3'-indole dimer. Further coupling of the indole dimer radical cation with a monomer radical cation was proposed as a route to the formation of the asymmetric trimer (Figure 1.1.4), the fully characterised product of indole electro-oxidation. However, the computational power was not available to establish this.

1.3 Aims of This Work.

In this thesis a range of electrochemical, spectroscopic and computational studies are reported. The primary aims of this research are to establish a robust computational method for the calculation of the redox, structural and growth properties of a range of aromatic molecules and to develop a screening mechanism to assess their suitability for the formation of novel electro-active materials. The formation and characterisation of novel electro-active materials and films will then be undertaken to assess the screening mechanism and validate its applicability by comparison to experiment.

The structure of this thesis is summarised below. Chapter 2 provides a summary of the theoretical aspects related to this work and Chapter 3 provides a brief summary of experimental details. Chapter 4 establishes a methodology for the calculation of redox potentials and properties for aromatic systems using a DFT method. This methodology is then applied to a range of aromatic systems and compared with experimental results. Calculations considering the polymerisation mechanism for indole are also contained within this chapter. Chapter 5 studies the electro-oxidation of 5-methylindolo[3,2,1-jk]carbazole and the characterisation of the resulting electro-oxidation products. The extension of the computational method to substituted indolo[3,2,1-jk]carbazole systems is also considered. In Chapter 6 the extension of the computational method to act as a screening method for a range of aromatic

molecules is discussed. Chapter 7 investigates the electrochemical behaviour of 2,3'-diindoles and studies films formed by their electro-oxidation. In Chapter 8 the conclusions of this research are discussed and the possibilities for future work considered.

1.4 References.

[1] Cowie, J. M. G. *"Polymers : chemistry and physics of modern materials*"; Stanley Thornes (Cheltenham), **1998**.

[2] Metzler, D. E. *"Biochemistry : The Chemical Reactions of Living Cells"*; Academic Press (USA), **2003**.

[3] Yang, C.-H.; Huang, L.-R.; Wen, T.-C.; Chung, S.-L.; Wang, T.-L. *J. Phys. Chem. C* **2007**, *111*, 9227.

[4] Briseno, A. L.; Mannsfeld, S. C. B.; Ling, M. M.; Liu, S.; Tseng, R. J.; Reese, C.; Roberts, M. E.; Yang, Y.; Wudl, F.; Bao, Z. *Nature* **2006**, *444*, 913.

[5] Briseno, A. L.; Tseng, R. J.; Ling, M. M.; Falcao, E. H. L.; Yang, Y.; Wudl, F.; Bao, Z. *Adv. Mater.* **2006**, *18*, 2320.

[6] Rose, J. D.; Stratham, E.S. *J. Chem. Soc.* **1950**, 69.

[7] Manefee, E.; Pao, Y. J. *J. Chem. Phys.* **1962**, *36***,** 3471.

[8] Shirakawa, H.; Louis, E. J.; MacDiarmid, A.G.; Chiang, C. K.; Heeger, A. J. *J. Chem. Soc., Chem. Comm.*, **1977**, 578.

[9] MacDiarmid, A.G. *Angew. Chem. Int. Ed.* **2001**, *40*, 2581.

[10] MacDiarmid, A.G. *Nobel Lecture,* **2000**, *December 8*. URL: http://nobelprize.org/nobel_prizes/chemistry/laureates/2000/heeger-lecture.pdf Accessed: 26 March 2009.

[11] Heeger, A. J. *Nobel Lecture,* **2000**, *December 8*. URL: http://nobelprize.org/nobel_prizes/chemistry/laureates/2000/macdiarmid-lecture.pdf Accessed: 26 March 2009.

[12] Burroughes, J. H.; Bradley, D. D. C.; Brown, A. R.; Marks, R. N.; Friend, R. H.; Burns, P. L.; Holmes, A. B. *Nature* **1990**, *347*, 539.

[13] Pei, Q.; Yu, G.; Zhang, C.; Yang, Y.; Heeger, A. J. *Science* **1995**, *269*, 1086.

[14] Angeli, A. *Gazz. Chim. Ital.*, **1916**, *46*, 279.

[15] Dall'Olio, A.; Dascola, G.; Varacca, V.; Bocche, U. *C.R. Acad. Sci.*, **1968**, *433*, 267C.

[16] McQuade, D. T.; Pullen, A. E.; Swager, T. M. *Chem. Rev.* **2000**, *100*, 2537.

[17] Schrebler, R.; Grez, P.; Cury, P.; Veas, C.; Merino, M.; Gomez, H.; Cordova, R.; del Valle, M. A. *J. Electroanal. Chem.* **1997**, *430*, 77.

[18] Higgins, S. J.; Pounds, T. J.; Christensen, P. A. *J. Mater. Chem.* **2001**, *11*, 2253.

[19] Roncali, J. *Chem. Rev.* **1992**, *92*, 711.

[20] Ramanavicius, A.; Ramanaviciene, A.; Malinauskas, A. *Electrochimica Acta* **2006**, *51*, 6025.

[21] Tsekouras, G.; Too, C. O.; Wallace, G. G. *Electrochimica Acta* **2005**, *50*, 3224.

[22] Gonzalez-Tejera, M. J.; Sanchez de la Blanca, E.; Carillo, I. *Synth. Met.* **2008**, *158*, 165.

[23] Grimsdale, A. C.; Mullen, K. *Macromol. Rapid. Commun.* **2007**, *28*, 1676.

[24] Trivedi, D. C. *J. Solid State Electrocehm.* **1998**, *2*, 85.

[25] Burroughes, J. H.; Bradley, D. D. C.; Brown, A. R.; Marks, R. N.; Mackay, K.; Friend, R. H.; Burn, P. L.; Holmes, A. B. *Nature*, **1990**, *347*, 539.

[26] Tang, C. W.; Van Slyke, S. A. *Appl. Phys. Lett.* **1987**, *51*, 913.

[27] Lo, S. C.; Burn, P. L. *Chem. Rev.* **2007**, *107*, 1097.

[28] Baldo, M. A.; O'Brien, D. F. O.; You, Y.; Shoustikov, A.; Sibley, S.; Thompson, M. E.; Forrest, S. R. *Nature*, **1998**, *395*, 151.

[29] Kondakova, M. E.; Pawlik, T. D.; Young, R. H.; Giesen, D. J.; Kondakov, D. Y.; Brown, C. T.; Deaton, J. C.; Lenhard, J. R.; Klubek, K. P. *J. Appl. Phys.* **2008**, *104*, 094501.

[30] Morin, J. F.; Drolet, N.; Tao, Y.; Leclerc, M. *Chem. Mater.,* **2004**, *16*, 4619.

[31] Li, J.; Dierschke, F.; Wu, J.; Grimsdale, A. C.; Mullen, K. J. *Mater. Chem.,* **2006**, *16*, 96.

[32] Drolet, N.; Morin, J. F.; Leclerc, N.; Wakim, S.; Tao, Y.; Leclerc, M. *Adv. Funct. Mater.,* **2005**, *15*, 1671.

[33] Wakim, S.; Bouchard, J.; Simard, M.; Drolet, N.; Tao, Y.; Leclerc, M. *Chem. Mater.,* **2004**, *16*, 4386.

[34] Li, Y.; Wu, Y.; Gardner, S.; Ong, B. S. *Adv. Mater.,* **2005**, *17*, 849.

[35] Wu, Y.; Li, Y.; Gardner, S.; Ong, B. S. *J. Am Chem. Soc.,* **2005**, *127*, 614.

[36] Mitsumori, T.; Bendikov, M.; Dautel, O.; Wudl, F.; Shioya, T.; Sato, H.; Sato, Y. *J. Am. Chem. Soc.,* **2004**, *126*, 16793.

[37] Pillow, J. N. G.; Halim, M.; Lupton, J. M.; Burn, P. L.; Samuel, I. D. W. *Macromolecules*, **1999**, *32*, 5985.

[38] Kivala, M.; Diederich, F. *Acc. Chem. Res.* **2009**, *42*, 235.

[39] Ferreira, E. S. B.; Hulme, A. N.; McNab, H.; Quye, A. *Chem. Soc. Rev.* **2004**, *33*, 329.

[40] Ferry, G.; Ubeaud, C.; Lambert, P.-H.; Bertin, S.; Coge, F.; Chomarat, P.; Delagrange, P.; Serkiz, B.; Bouchet, J.-P. Truscott, R. J. W.; Boutin, J. A. *Biochem. J.* **2005**, *388*, 202.

[41] Jennings, P.; Jones, A. C.; Mount, A. R.; Thomson, A. D. *J. Chem. Soc. Faraday Trans.* **1997**, *93*, 3791.

[42] Jennings, P.; Jones, A. C.; Mount, A. R. *J. Chem. Soc. Faraday Trans.* **1998**, *94*, 3619.

[43] Bartlett, P. N.; Farrington, J. *Bull. Electrochem.*, **1992**, *8*, 208.

[44] Mackintosh, J. G. *Ph. D. Thesis, "The Electropolymerisation of Novel Conducting Polymers.", University of Edinburgh* **1996**.

[45] Bartlett, P. N.; Farrington, J. *J. Electoanal. Chem.*, **1989**, *261*, 471.

[46] Biegunski, A. T.; Michoti, A.; Bukowska, J.; Jackowska, K. *Bioelectrochemistry*, **2005**, *69*, 41.

[47] Sivakkumar, S. R.; Angulakshmi, N.; Saraswathi, R. *J. Appl. Poly. Sci.*, **2005**, *98*, 917.

[48] Wharton, S. I. *Ph. D. Thesis, "Synthesis and Characterisation of Novel Conducting Films Based on Indolo[3,2,1-jk]carbazole Systems.", University of Edinburgh* **2005**.

[49] Han, W.-G.; Liu, T.; Himo, F.; Toutchkine, A.; Bashford, D.; Hahn, K. M.; Noodleman, L. *ChemPhysChem,* **2003**, *4*, 1084.

[50] Tait, K. M.; Parkinson, J. A.; Gibson, D. I.; Richardson, P. R.; Ebenezer, W. J.; Hutchings, M. G.; Jones, A. C. *Photochem. Photobiol. Sci.*, **2007**, *6*, 1010.

[51] Pickard, C. J.; Salager, E.; Pintacuda, G.; Elena, B.; Emsley, L. *J. Am. Chem. Soc.*, **2007**, *129*, 8932.

[52] Namazian, M.; Coote, M. L. *J. Phys. Chem.*, **2007**, *111*, 7227.

[53] Reynolds, C. A.; King, P. M.; Richards, W. G. *Nature*, **1988**, *334*, 80.

[54] Raymond, K. S.; Grafton, A. K.; Wheeler, R. A. *J. Phys. Chem. B*, **1997**, *101*, 623.

[55] Namazian, M.; Norouzi, P.; Ranjbar, R. *J. Mol. Struct. (THEOCHEM)*, **2003**, *625*, 235.

[56] Namazian, M. *J. Mol. Struct. (THEOCHEM)*, **2003**, *664-665*, 273.

[57] Baik, M-H.; Silverman, J. S.; Yang, I. V.; Ropp, P. A.; Szalai, V. A.; Yang, W.; Thorp, H. H. *J. Phys. Chem. B*, **2001**, *105*, 6437.

[58] Patterson, E. V.; Cramer, C. J.; Truhlar, D. G. *J. Am. Chem. Soc.*, **2001**, *123*, 2025.

[59] Winget, P.; Weber, E. J.; Cramer, C. J.; Truhlar, D. G. *Phys. Chem. Chem. Phys.*, **2000**, *2*, 1231.

[60] Kettle, L. J.; Bates, S. P.; Mount, A. R. *Phys. Chem. Chem. Phys.* **2000**, *2*, 195.

[61] Baik, M-H.; Friesner, R. A. *J. Phys. Chem. A*, **2002**, *106*, 7407.

[62] Fu, Y.; Liu, L.; Yu, H-Z.; Wang, Y-M.; Guo, Q-X. *J. Am. Chem. Soc*, **2005**, *127*, 7227.

[63] Fu, Y.; Liu, L.; Wang, Y-M.; Li, J-N.; Yu, T-Q.; Guo, Q-X. *J. Am. Chem. Soc.*, **2006**, *110*, 5874.

[64] Charles-Nicolas, O.; Lacroix, J. C.; Lacaze, P. C. *J. Chim. Phys.*, **1998**, *95*, 1457.

[65] Uedsemaa, M.; Tamm, T. *J. Phys. Chem. A*, **2003**, *107*, 9997.

[66] Mennucci, B.; Tomasi, J. *J. Chem. Phys.* **1997**, *106*, 5151.

[67] Reed, S. K.; Madden, P. A.; Papadopoulos, A. *J. Chem. Phys.* **2008**, *128*, 124701.

[68] Pavlishchuk, V. V.; Addison, A. W. *Inorg. Chim. Acta* **2000**, *298*, 97.

[69] Bond, A. M.; *"Modern Polarographic Methods in Analytical Chemistry"* Marcel Dekker (New York), **1980**.

[70] Bredas, J. L. *Synthetic Metals*, **1997**, *84*, 3.

[71] Kilic, G.; Toppare, L.; Yurtsever, E. *Synthetic Metals*, **1996**, *78*, 19.

[72] Audbert. P.; Catel, J-M.; Le Coustumer, G.; Duchenet, V.; Hapiot, P. *J. Phys. Chem.*, **1998**, *102*, 8661.

[73] DiCesare, N.; Belletete, M.; Marrano, C.; Leclerc, M.; Durocher, G. *J. Phys. Chem.*, **1998**, *102*, 5142.

[74] Lacroix, J.; Valente, R.; Maurel, F.; Lacaze, P. *Chem. Eur. J.*, **1998**, *4*, 1667.

[75] Milleifori, S.; Alparone, A. *J. Chem. Soc. Faraday Trans.*, **1998**, *94*, 25.

[76] Yurtsever, M.; Yurtsever, E. *Synthetic Metals*, **1999**, *98*, 221.

[77] Pinzino, C.; Angelone, R.; Benventi, F. *J. Polymer Science*, **1998**, *36*, 1901.

[78] Waltman, R. J.; Bargon, J. *Tetrahedron*, **1984**, *40*, 3963.

[79] Waltman, R. J.; Bargon, J. *Can. J. Chem.*, **1986**, *64*, 76.

[80] Waltman, R. J.; Diaz, A. F.; Bargon, J. *J. Phys. Chem.* **1984**, *88*, 4343.

[81] Smith, J. R.; Cox, P. A.; Campbell, S.; Ratcliff, N. M. *J. Chem. Soc. Faraday Trans.* **1995**, *91*, 2331.

[82] Berlin, A.; Canavesi, A.; Schiavon, G.; Seraglia, R.; Zecchin, S.; Zotti, G. *Tetrahedron*, **1996**, *23*, 7947.

[83] Talbi, H.; Monard, G.; Loos, M.; Billaud, D. *J. Molec. Struc.*, **1998**, *434*, 129.

[84] Talbi, H.; Monard, G.; Loos, M.; Billaud, D. *Synthetic Metals*, **1999**, *101*, 115.

Chapter 2: Theoretical Aspects.

The research presented in this thesis covers a wide range of electrochemical and computational methods. There is a great breadth and depth of information in the literature on these methods[1,2]. This chapter will therefore highlight the most important theoretical aspects on which the work in this thesis is based.

2.1 Electrochemical Methods.

2.1.1 Potential Sweep Voltammetry.

Potential sweep voltammetry methods are extremely powerful techniques that can provide a wealth of information for electrochemical systems; as such they are usually the first method deployed when studying new systems. Processes for which information can be obtained include: redox reactions of electroactive species in solution or on electrodes, the adsorption of species at an electrode, the kinetics and thermodynamics of reaction and the detection of soluble products generated at an electrode.

As potential sweep voltammetry studies in this thesis were performed in stagnant solutions, where transport of material to the electrode is predominantly diffusion controlled, this section will therefore focus on potential sweep voltammetry in stagnant solutions. Potential sweep voltammetry is best described as a class of dynamic techniques which involve the application of a potential to the working electrode which varies continuously with time. In linear sweep voltammetry (LSV), the potential of the electrode is first swept in one direction at a constant sweep rate, v. The potential of the electrode at any time can then be given by $E(t) = E_1 \pm vt$, where t is the time passed since the initiation of the sweep at the potential E_1. In LSV, upon reaching a chosen potential, E_2, the sweep is halted. It is possible however to reverse the sweep upon reaching E_2 and sweep the potential back to the initial potential E_1 at sweep rate -v. This method produces the first cycle of cyclic voltammetry (CV) and this cycling can be repeated a number of times. Figure 2.1.1 illustrates the potential time profile for the first cycle of such a CV experiment.

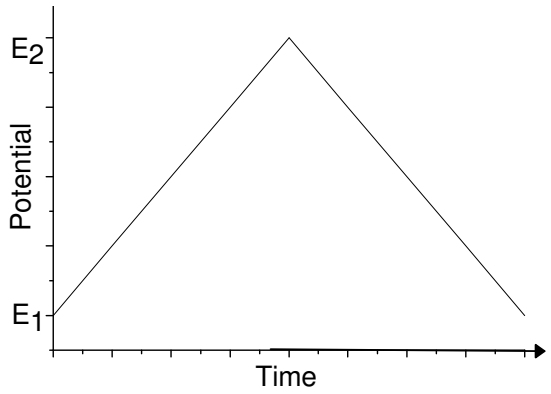

Figure 2.1.1. The potential time profile for the first cycle of a cyclic voltammetry experiment.

On considering an electrochemically reversible redox reaction $O + ne^- \leftrightarrow R$ the concentrations at the electrode surface are given by the Nernst equation:

$$E = E^{\theta'} + \frac{RT}{nF}\ln\frac{a_O}{a_R} = E^{\theta} + \frac{RT}{nF}\ln\frac{c_O}{c_R} \quad \textbf{Equation 2.1.1}$$

Where the standard reduction potential, $E^{\theta'}$, is related to the formal potential, E^{θ}, through the relation:

$$E^{\theta} = E^{\theta'} + \frac{RT}{nF}\ln\left(\frac{\gamma_O}{\gamma_R}\right) \quad \textbf{Equation 2.1.2}$$

As the activity coefficients in electrochemical reactions are almost always unknown the formal potential is commonly used in place of the standard oxidation potential. The terminology for the standard reduction potential and formal potential is interchangeable, for the rest of this thesis when standard potentials are discussed it will be the formal potential that is being considered. If initially only R is present in solution and $E_1 << E^{\theta}$ then initially no current will be observed as shown in Figure 2.1.2. As the potential approaches E^{θ} an increasing oxidation current, i, is observed as R is oxidised to form O, and the current passed increases exponentially as the electrode becomes more oxidising. Sweeping the potential further past E^{θ} then leads to a decrease in current as the surface concentration of species R decreases due to the diffusional limitation of mass transport of species R to the electrode surface. This results in the peaked voltammogram observed. For a reversible (Nernstian) system the peak potential is related to the half wave potential, $E_{1/2}$, by:

$$E_P - E_{1/2} = 1.09\frac{RT}{nF} = \frac{28.0}{n} \text{ mV at 298 K.}$$ **Equation 2.1.3**

A convenient diagnostic for a Nernstian peak is that:

$$E_P - E_{P/2} = 2.2\frac{RT}{nF} = \frac{56.5}{n} \text{ mV at 298 K.}$$ **Equation 2.1.4**

Where $E_{1/2}$ is related to E^{θ} by:

$$E_{1/2} = E^{\theta} + \frac{RT}{nF}\ln\frac{D_R^{1/2}}{D_O^{1/2}}$$ **Equation 2.1.5**

Where D_R and D_O are the diffusion co-efficients of the reduced and oxidised species, respectively.

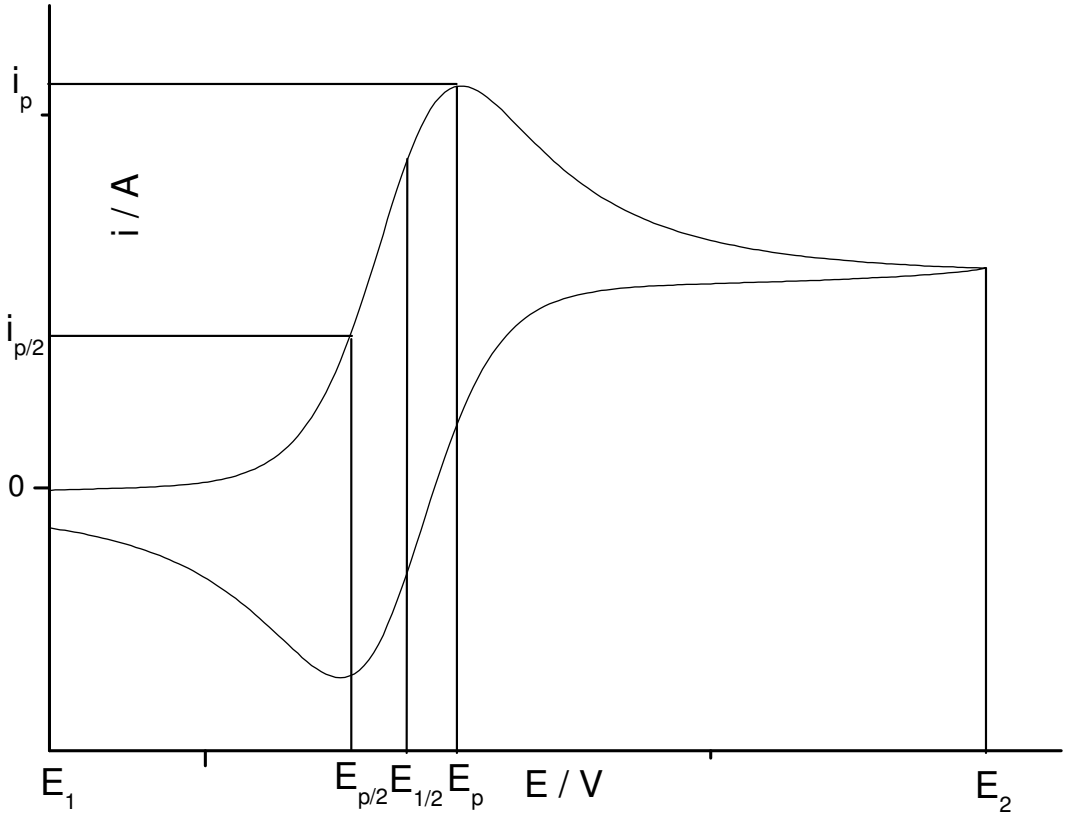

Figure 2.1.2. The typical current response for a cyclic voltammetry experiment.

For electrochemically reversible systems E_p is independent of sweep rate and i_p varies with the square root of the sweep rate, $v^{1/2}$, as:

$$i_p = (2.69x10^5)n^{3/2}AD_R^{1/2}v^{1/2}c_{R,\infty}$$ **Equation 2.1.6**

Where A is the electrode area (cm^2), D_R is the diffusion coefficient of R ($cm^2\ s^{-1}$) and $c_{R,\infty}$ is the bulk concentration of R (mol cm^{-3}). This relationship applies for reversible systems where the electrode kinetics are very facile.

Generally in controlled potential experiments the current-potential relationship can be characterised by:

$$i = nFAk^0\left[C_O(0,t)e^{-\alpha nf(E-E^\theta)} - C_R(0,t)e^{(1-\alpha)nf(E-E^\theta)}\right] \quad \textbf{Equation 2.1.7}$$

When k^0 is large the system is reversible and the electrode kinetics are fast. When k^0 is very small, the electrode kinetics are very sluggish, and the anodic and cathodic terms of Equation 2.1.7 are never simultaneously significant, or alternatively when a appreciable anodic current is flowing, the cathodic term is negligibly small. Such a system is known as a totally irreversible system. For totally irreversible systems i_p also varies with $v^{1/2}$, but with the relationship:

$$i_p = (2.99x10^5)n(\alpha n_a)^{1/2} AD_R^{1/2} v^{1/2} c_{R,\infty} \quad \textbf{Equation 2.1.8}$$

Where α is the activity of the species R. E_p is also dependent on sweep rate for totally irreversible systems, as the separation of E_p and $E_{1/2}$ increases as sweep rate increases.

For a redox active film adsorbed onto the electrode surface the CV will show a pair of peaks corresponding to the oxidation and reduction of the film. The reaction of the film is controlled by the charge transfer kinetics of the film, either in electron transfer from the electrode to the film surface or transfer of charge compensating counter-ions from solution into the film which can be more complicated than the problem of diffusion control and electron transfer in solution. The area under the peaks can provide information on the charge required for the electrochemical reaction and can show if the whole film is oxidised and reduced on each sweep.

2.1.2 Experiments at the Rotating Disc Electrode.

While CV provides a valuable amount of data on electrochemical systems the study of electrode reactions is complicated, electrochemical reactions occurring in stagnant solutions can give irreproducible time-dependent results as a result of convection gradients and depletion effects and there is no control of mass transport to the electrode. One of the best methods for overcoming these effects is to use a rotating disc electrode (RDE) to provide efficient mass transport and obtain reproducible time-independent results.

The RDE consists of a metal disc electrode surrounded by a coplanar insulating sheath of PTFE. The electrode is suspended in solution and rotated at a controllable rate, when it acts as a hydrodynamic pump as it is rotated as shown in Figure 2.1.3. The rotation of the electrode induces solution flow towards the electrode surface and then radially outwards across the disc.

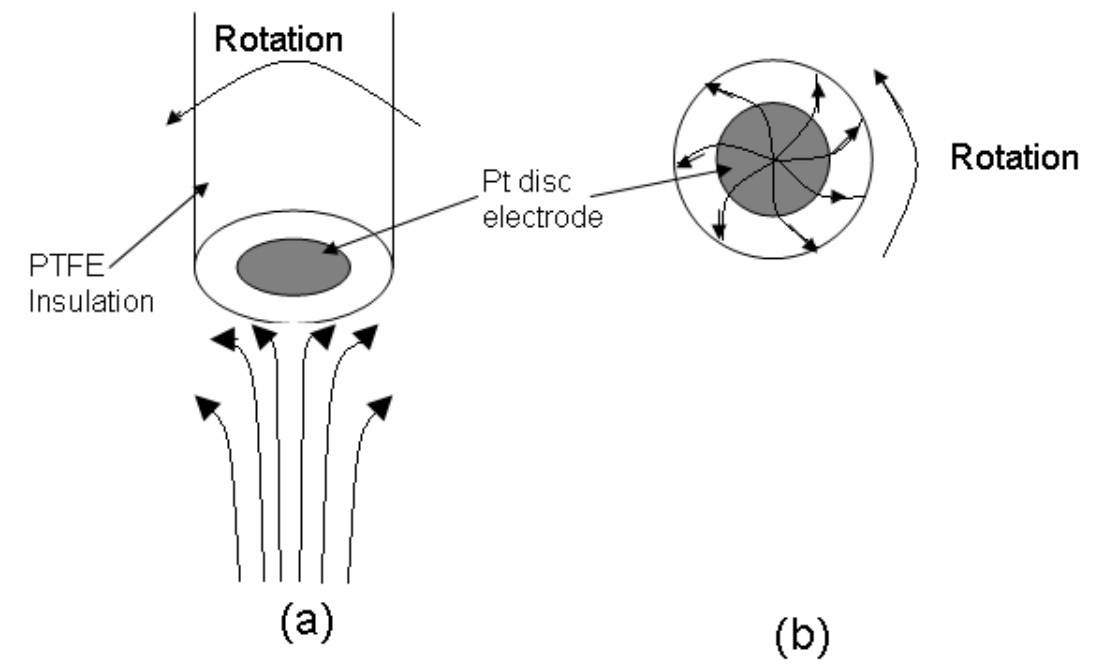

Figure 2.1.3. The rotating disc electrode construction and the hydrodynamic flow of solution (a) perpendicular to the rotating disc electrode and (b) across the surface.

Rotation in a large volume of solution produces a well defined flow pattern. In a system with background electrolyte, where there is no migration and transport is by convection and diffusion alone, the steady-state differential equation for transport can be obtained through inclusion of the fluid velocity flow to Fick's Law such that:

$$j = -D\nabla c + Vc \quad \textbf{Equation 2.1.9}$$

Where c is the concentration of the electroactive species (mol cm^{-3}), D is the diffusion coefficient ($cm^2\ s^{-1}$) and V is the fluid velocity of the electroactive species. The change in the concentration field with time can then be considered with the relation:

$$\frac{\partial c}{\partial t} + \nabla \cdot j = 0 \quad \textbf{Equation 2.1.10}$$

Under steady-state conditions $\frac{\partial c}{\partial t} = 0$, and Equation 2.1.10 becomes:

$$\nabla \cdot j = \nabla \cdot \left(-D\nabla c + Vc\right) = 0 \quad \textbf{Equation 2.1.11}$$

and so:

$$D\nabla^2 c = Vc \quad \textbf{Equation 2.1.12}$$

The steady-state differential equation for transport in the z-direction is then given by Equation 2.1.13.

$$D\frac{\delta^2 c}{\delta z^2} = V_z \frac{\delta c}{\delta z} \quad \textbf{Equation 2.1.13}$$

where V_z is the fluid velocity component in the z-direction (cm s^{-1}). Near the surface of the electrode V_z has the form:

$$V_z = -0.51\omega^{3/2}\upsilon^{-1/2}z^2 \quad \textbf{Equation 2.1.14}$$

Where ω is the rotation speed in (rad s^{-1}), and υ is the kinematic viscosity (cm^2 s^{-1}). The velocity then reaches a limiting velocity in the z-direction of:

$$U_0 = \lim_{z\to\infty} V_z = -0.88447(\omega\upsilon)^{1/2} \quad \textbf{Equation 2.1.15}$$

this creates a diffusion layer within the solution.

Integrating Equation 2.1.9 with boundary conditions that z=0, z→∞, c=c_0, c→c_∞ where c_∞ is the bulk concentration and c_0 is the concentration at the electrode surface of the redox substance and comparison with Fick's first law gives an expression for the flux, j (mol cm^{-2} s^{-1}) at the electrode:

$$\frac{j}{D} = -\left\{\frac{dc}{dz}\right\}_{z=0} = \frac{c_\infty - c_0}{z_D} \quad \textbf{Equation 2.1.16}$$

Where c_0 is the concentration at z = 0, j is the flux at the electrode (mol.$cm^{-2}s^{-1}$) and z_D is the diffusion layer thickness given by:

$$z_D = 0.643W^{-1/2}\upsilon^{1/6}D_R^{1/2} \quad \textbf{Equation 2.1.17}$$

Where W is the rotation speed (Hz). At distances of $z > z_D$ the solution is well stirred and transport is controlled by both diffusion and convection. For distances of $0 < z < z_D$ convection is negligible and transport in the z-direction is governed by diffusion, and this region is known as the Nernst diffusion layer. z_D results from the extrapolation of the concentration gradient from the electrode surface until the bulk concentration is obtained as shown in Figure 2.1.4.

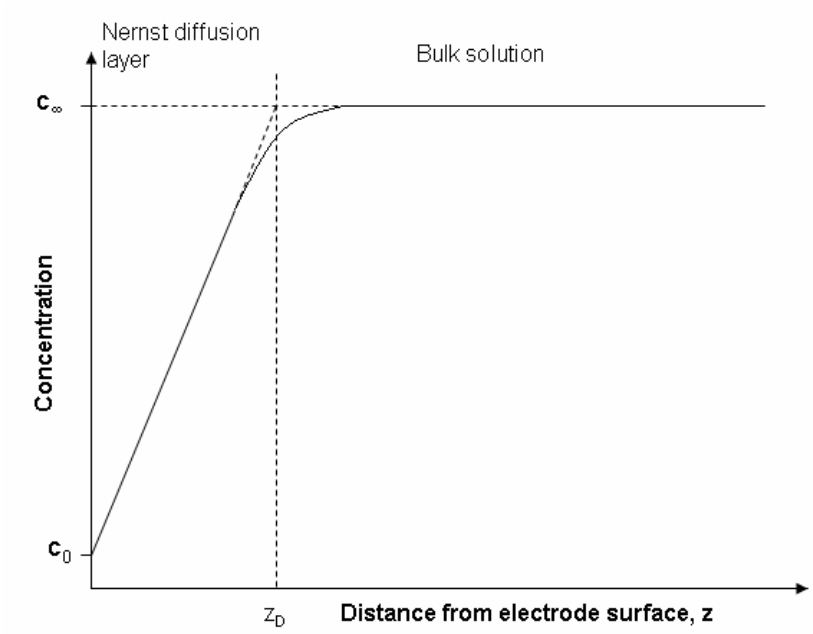

Figure 2.1.4. Variation of the concentration of active species normal to the RDE surface.

When there is a first order reaction at the electrode surface the flux at the electrode surface is $j = kc_0$. Substituting into Equation 2.1.15 gives:

$$\frac{-1}{j} = \frac{1}{kc_\infty} + \frac{1}{k_D c_\infty} = \frac{1}{c_\infty}\left[\frac{1}{k} + \frac{1}{k_D}\right] \quad \textbf{Equation 2.1.18}$$

Thus:

$$j = k_D(c_\infty - c_0) \quad \textbf{Equation 2.1.19}$$

Where k_D is the first order rate constant describing the mass transport of the electroactive species to the electrode surface, as $k_D = D/z_D$ ($cm.s^{-1}$). There are two limiting forms to Equation 2.1.18 depending on whether mass transport or surface reaction is the more dominant process.

If reaction at the electrode is slow then $1/k >> 1/k_D$ and $j \approx kc_\infty$, the surface reaction is rate limiting and only a small fraction of the species arriving at the electrode surface will react and the concentration at the electrode surface will be equal to the bulk solution. If, however, electrode reaction is fast then $1/k << 1/k_D$, $j = k_D c_\infty$, the surface concentration is zero; the reaction is under mass transport control and the transfer of reactant to the electrode determines the rate. The simplest mass transfer

independent reaction is the electrochemical reaction is given by Equation 2.1.20 but any first order process would satisfy this equation.

At the electrode surface the rate of the electrochemical reaction will typically depend on the electrode kinetics. For the redox reaction:

$$R \xrightarrow{-ne^-} O$$

The rate of the reaction at the electrode surface, k (cm s^{-1}), is controlled by:

$$k = k^{\theta} \exp(\alpha nF(E - E^{\theta})/RT) \quad \textbf{Equation 2.1.20}$$

where k^{θ} is the rate constant (cm s^{-1}) at $E = E^{\theta}$ and α is the transfer coefficient for oxidation[3].

All experiments at a RDE discussed within this thesis will be performed at a potential sufficient to ensure the surface electrochemical reaction is fast. The current observed in a system under mass transport control is known as the mass transport limiting current, i_L, and as $|i| = nFA|j|$, where A is the electrode area (cm^2) we obtain:

$$|i_L| = 1.554 nFAc_{\infty} D^{2/3} \nu^{-1/6} W^{1/2} \quad \textbf{Equation 2.1.21}$$

Equation 2.1.21 is known as the Levich equation and a plot of $|i_L|$ versus $W^{1/2}$ should produce a straight line through the origin. Such a plot is known as a Levich plot, more generally if both reaction rates are important the equation for $|i_L|$ becomes:

$$\frac{nFAc_{\infty}}{|i_L|} = \frac{0.643 D^{-2/3} \nu^{1/6}}{W^{1/2}} + \frac{1}{k} \quad \textbf{Equation 2.1.22}$$

Now a Levich plot will result in a line curving as W increases as k becomes rate limiting. A plot of i_L^{-1} versus $W^{1/2}$ will however result in a straight line, with an intercept which gives a value for k. This plot is known as a Koutecky-Levich plot.

The formation of a Levich plot assumes a fast electron transfer process at the electrode surface. In an electrochemical reaction a second process independent of the electron transfer process may be present, such that:

$$R \xrightarrow{k_i} R^* \xrightarrow{-ne^-, k_1} O$$

Here the observed rate constant, k, is defined as:

$$\frac{1}{k} = \frac{1}{k_i} + \frac{1}{k_{?1}} \quad \textbf{Equation 2.1.23}$$

Where k_i is again the rate constant for the mass transport independent step and the smaller of the two rate constants is again rate limiting and the equation for i_L becomes the Koutecky-Levich equation (Equation 2.1.22).

2.2 *Ab initio* Methods.

In recent years quantum chemical methods have begun to develop into a standard tool in the arsenal of experimental chemists and physicists for the *in silico* investigation of molecular systems. *Ab initio* (Latin: from the beginning) methods can provide information on the structure and properties of molecules, both providing an understanding of the chemical properties of molecular systems that have previously been studied, or providing insight into systems which cannot currently be studied experimentally. The experimentalist deploying these methods may not be an expert in the field of quantum mechanics, but it is important that such techniques are not used as "black boxes" generating solutions which may be unreliable. Currently there exist several standard *ab initio* methods which have been extensively tested on a significant range of molecular systems to demonstrate that they provide an acceptable level of reliability and accuracy. The following sections will discuss a range of these *ab initio* methods. All these methods share the aim of calculating from first principles the electronic structure and properties of chosen molecules. These methods differ in the level of theory applied to the problem and the consequential computational cost incurred in their calculations.

In general the level of theory in *ab initio* methods is determined by the degree to which the correlation energy is included or approximated in a calculation, and the completeness of the basis set used in the calculation. The degree to which electron correlation is included in an *ab initio* calculation places a fundamental limit on the accuracy that can be obtained via the method, irrespective of expansion of the basis set. The correlation problem, the importance of basis sets and the level of theory of

quantum chemical methods used in this research are discussed in the following sections.

2.2.1 Molecular Quantum Mechanics.

The aim of all quantum chemical methods is the solution of the non-relativistic, time-independent Schrödinger equation, specifically the electronic Schrödinger equation, to obtain information on the structure and properties of molecules and collections of molecules. Due to the quantum nature of electrons, as wavefunctions whose exact position and momentum can never be known, and the many-body problem[4] the most complex system for which the Schrödinger equation can be solved exactly is the hydrogen molecular ion (H_2^+), which is a simpler system than those that are most chemically interesting. Therefore to make progress in quantum chemistry certain approximations must be made.

The first approximation takes advantage of the disparity between the masses of electrons and nuclei; this is known as the Born-Oppenheimer approximation, which provides the foundation for modern quantum chemistry. Due to the fact that electrons are significantly lighter than nuclei, electrons are able to respond almost instantaneously to a change in the geometry of the nuclear framework of a molecule. This enables us to approximate that the electronic distribution is dependent only on the positions of the nuclei and not their momenta, or alternatively that the motions of the nuclei and electrons are separable.

This approximation allows the solution of the Schrödinger equation for a fixed set of nuclear positions. Then by performing a sequential procedure for a variety of nuclear geometries it is possible to map out the total molecular energy as a function of the molecular geometry. Whilst this approximation is valid in most situations problems may arise when the assumption of the separability of nuclear and electronic motions does not hold, in the case of large amplitude molecular vibrations or the motions of light nuclei for example.

Assuming the Born-Oppenheimer approximation, the time-independent, electronic Schrödinger equation for a fixed set of nuclear positions becomes:

$$\hat{H}\Psi(r:R) = E(R)\Psi(r:R) \quad \textbf{Equation 2.2.1}$$

Where E(R) is the electronic energy and Ψ(r:R) is the electronic wavefunction and r and R are the parameters denoting electronic and nuclear positions, respectively. The molecular Hamiltonian is then:

$$\hat{H} = \frac{-\hbar^2}{2m_e}\sum_{i}^{n}\nabla_i^2 - \sum_{i}^{n}\sum_{I}^{N}\frac{Z_I e^2}{4\pi\varepsilon_0 r_{iI}} + \frac{1}{2}\sum_{i,j}^{n}\frac{e^2}{4\pi\varepsilon_0 r_{ij}} \quad \textbf{Equation 2.2.2}$$

The first term in the Hamiltonian describes the kinetic energy of the system of n electrons, the second describes the nuclear-electron potential energy for the n electrons and N nuclei and the final term contains the electron-electron interactions. Conventionally the nuclear-nuclear repulsion energy is added as a classical term at the end of the calculation. The third term in the Hamiltonian causes the greatest problem in solving the electronic Schrödinger equation, as the motions of the electrons are coupled, which prevents the conversion of the many-body wavefunction into a simpler combination of one-electron functions. Two related effects give rise to the coupling of electronic motions; these are exchange and correlation.

The exchange effect is the origin of the Pauli exclusion principle and arises as a consequence of the indistinguishability of electrons. This indistinguishability introduces the requirement that the multi-electron wavefunction must be anti-symmetric with respect to the exchange of two electrons, which leads to the result that two electrons of the same spin are forbidden from occupying the same region of space. The exchange effect therefore acts to keep electrons of the same spin separated.

There are two origins for the correlation effect of electrons. Firstly, there is a correlation effect that arises electrostatically as a result of the motion of each electron in the charged cloud created by the n-1 other electrons in the system. The Coulombic repulsion between electrons means that the instantaneous motion of one electron affects the motion of every other electron in the system, acting to keep the electrons apart. Secondly, there is a spin correlation which arises from the exchange symmetry discussed previously. An exchange "hole" is created around electrons as a result of the necessity for electrons of the same spin to avoid each other, this exchange hole is

a space which is depleted of other electrons of the same spin. This exchange hole again acts to keep electrons of the same spin apart as it acts as a quasi-repulsive force analogous to the electrostatic correlation.

It is possible to include the exchange term in computational techniques by ensuring that the wavefunctions are suitably anti-symmetrised. The correlation effect is more complicated for inclusion into quantum chemical methods however and remains an ongoing problem. The following sections will discuss two methods for overcoming this problem.

2.2.2 Hartree-Fock.

The correlation effect is relatively small in magnitude compared to other terms in the electronic Schrödinger equation. It is therefore possible to think of a simple solution to the correlation problem by merely neglecting the coupling terms between the electrons and assuming that their motions are approximately independent, with only a "mean" repulsion from the other electrons in the system. This solution was first proposed by Hartree and then refined by Fock.

Hartree initially proposed a model in which one electron moves in a potential which is an average of the potential due to all the other electrons and nuclei in the system. This removes the instantaneous coupling due to correlation and individual electron motions can be said to be de-coupled. This simple method is remarkably successful for such an extreme simplification. Fock however highlighted the fact that Hartree's simplified method violated the Pauli exclusion principle as the wavefunctions generated were not properly anti-symmetric. This deficiency in Hartree's method can be rectified by anti-symmetrising Hartree's wavefunctions. This new Hartree-Fock formalism whilst still neglecting the electron correlation, now includes the exchange term explicitly.

By neglecting the correlation of the "real" multi-electron wavefunction it is possible to separate the wave function into a product of n one-electron functions, called spinorbitals, which are a product of a spatial orbital and a function describing the

electron spin. Each spinorbital can be described by a Hartree-Fock equation of the form:

$$\hat{f}_i\psi(i) = \varepsilon_i\psi(i) \quad \textbf{Equation 2.2.3}$$

Where ψ(i) is the spinorbital for electron i, and ε_i is the orbital energy of the spinorbital. $\hat{f}_i$ is the Fock operator given by:

$$\hat{f}_i = \hat{h}_i + \sum_u \left\{\hat{J}_u(i) - \hat{K}_u(i)\right\} \quad \textbf{Equation 2.2.4}$$

Where $\hat{h}_i$ is the core Hamiltonian for an electron i moving in the field of the bare nucleus. The summation is over all the spinorbitals, u, for the electron i. $\hat{J}$ is the Coulomb operator, accounting for the Coulombic interaction between electrons. $\hat{K}$ is the exchange operator, which takes account of the moderation of the energy as a result of the exchange symmetry. For an electron, 1, in a spinorbital ψ_a, the Coulomb and exchange operators can be defined by Equation 2.2.5 and Equation 2.2.6 respectively.

$$\hat{J}_u(1)\psi(1) = \left\{\int \psi_u^*(2)\left(\frac{e^2}{4\pi\varepsilon_0 r_{12}}\right)\psi_u(2)dx_2\right\}\psi_a(1) \quad \textbf{Equation 2.2.5}$$

$$\hat{K}_u(1)\psi(1) = \left\{\int \psi_u^*(2)\left(\frac{e^2}{4\pi\varepsilon_0 r_{12}}\right)\psi_a(2)dx_2\right\}\psi_u(1) \quad \textbf{Equation 2.2.6}$$

An issue with quantum chemical methods, regardless of the chosen calculation method, is the function or functions used to describe the spinorbitals or one-electron equations. The exact form of the spinorbitals required for the Hartree-Fock method (or any other method) is unknown. It is possible, however, to exactly model mathematically any unknown function, such as one describing a molecular orbital, by expanding a complete set of known basis functions:

$$\psi_i = \sum_{j=1}^{M} c_{ji}\phi_j \quad \textbf{Equation 2.2.7}$$

Each spinorbital, ψ_i, is expanded as a linear function of known basis functions, or expanded in a basis set of chosen functions. The requirement is then to calculate the expansion coefficients, c_{ij}, as opposed to having to calculate the wavefunctions

themselves. It is then possible to model any function or spin orbital through the use of a complete basis set. A complete basis set, however, requires the use of an infinite set of basis functions, which is currently precluded computationally. The necessity must therefore be to truncate the basis set expansion to a computationally tractable level. This unfortunately introduces an inherent error into any *ab initio* calculation. As a result of this, many *ab initio* methods can be described as having a 2-dimensional accuracy requirement, illustrated in Figure 2.2.1. The larger the basis set and the greater the level at which correlation is included the closer the method will be to yielding the "exact" solution. However, this is at a real cost in computational complexity and time.

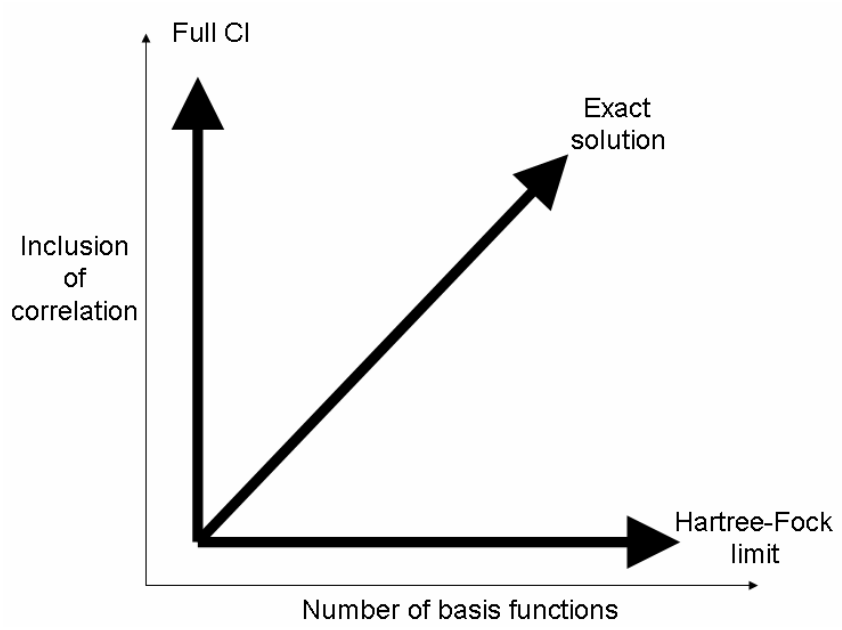

Figure 2.2.1. Representation of the 2-D accuracy requirement in *ab initio* calculations.

Substituting Equation 2.2.7 into the Hartree-Fock equation (Equation 2.2.3) and multiplication of both sides by the basis function ϕ_i^* leads to:

$$\sum_{j=1}^{M} F_{ij} c_{ja} = \varepsilon_a \sum_{j=1}^{M} S_{ij} c_{ja} \quad \textbf{Equation 2.2.8}$$

Where F_{ij} is defined as the Fock matrix, with elements:

$$F_{ij} = \int \phi_i^*(1) \hat{f}_1 \phi_j(1) dr \quad \textbf{Equation 2.2.9}$$

And S_{ij} is the overlap matrix with elements:

$$S_{ij} = \int \phi_i^*(1)\phi_j(1)dr \quad \textbf{Equation 2.2.10}$$

Equation 2.2.8 can be expressed in matrix form, the solution is then obtained from the determinantal equation:

$$\det|F - \varepsilon_a S| = 0 \qquad \textbf{Equation 2.2.11}$$

It may be apparent, however, that the solution to Equation 2.2.11 requires that to form the Fock operators to solve the Hartree-Fock equation we must first of all know the wavefunctions. This problem is a common feature in many *ab initio* methods. The problem may be tackled through the adoption of an iterative process towards the solution and halting the iteration once an answer has converged to within a suitable tolerance. This procedure is known as the Self-Consistent Field (SCF) method. For the Hartree-Fock method an initial estimate is made for the spinorbitals, which are then used to construct the Fock operator. Solution of the Hartree-Fock equations then provide a new set of spinorbitals which are used to construct a new Fock operator, and so on.

Once the optimised spinorbitals are obtained they are arranged in order of increasing energy, with the electrons occupying the n lowest. These are known as the occupied orbitals and form the Hartree-Fock ground-state wave function.

Whilst the contribution of the correlation energy to the total energy of a system is small, it is necessary that it is included to allow *ab initio* calculations to reach a level of accuracy required by experimentalists, the second axis on Figure 2.2.1. The inclusion of electron correlation is not simply needed to determine the energy of the molecular system, but is also needed to account for a wide range of chemical properties and fully describe the molecular potential energy surfaces.

There are many other methods which share a common feature of using Hartree-Fock spinorbitals as the basis for calculations. These methods have been widely used but suffer from scaling issues and the requirements to use large basis sets to perform accurate calculations. Density Functional Theory (DFT) methods take a conceptually

different approach, as they were initially developed by physicists to investigate solid state systems.

2.2.3 Density Functional Theory.

DFT is a formally exact method developed in the mid sixties by Hohenberg, Kohn and Sham. Hohenberg and Kohn[5] showed that the total electronic energy of a system of electrons can be written in terms of the electron probability density, ρ. For a system comprised of n electrons, ρ(r) denotes the total electron density at a particular point in space, r. The electronic energy E can be said to be a functional of the electron density, denoted by E[ρ], in that a given function ρ(r) has a single corresponding energy. The electron density uniquely determines the ground-state energy and all the other ground state electronic properties.

Kohn and Sham[6] developed the set of one electron equations from which, theoretically, the electron density ρ could be obtained. The exact ground state electronic energy E of a n-electron, N nuclei system may be written as:

$$E[\rho] = -\frac{\hbar^2}{2m_e}\sum_{i=1}^{n}\int \psi_i^*(r_1)\nabla_1^2\psi_i(r_1)dr_1 - \sum_{I=1}^{N}\int \frac{Z_I e^2}{4\pi\varepsilon_0 r_{I1}}\rho(r_1)dr_1 + \frac{1}{2}\iint \frac{\rho(r_1)\rho(r_2)e^2}{4\pi\varepsilon_0 r_{12}}dr_1 dr_2 + E_{XC}[\rho] \quad \textbf{Equation 2.2.12}$$

Where ψ_i are the Kohn-Sham orbitals. The first term describes the kinetic energy of the n electrons, the second term the electron-nuclear interactions, the third term represents the electron-electron Coulomb interaction and the final term is the exchange-correlation energy (with contributions as discussed previously). The exact analytical form of the exchange-correlation energy is unknown, only that since the total energy is a functional of the electron density, the exchange-correlation energy must also be some functional of the electron density.

The exact ground state charge density ρ at a point r is given by:

$$\rho(r) = \sum_{i=1}^{n}\left|\psi_i(r)\right|^2 \quad \textbf{Equation 2.2.13}$$

Where the summation is over all the occupied Kohn-Sham orbitals, ψ_i, with the Kohn-Sham orbitals being obtained from Equation 2.2.14.

$$\hat{h}\,\psi_i(r_i) = \varepsilon_i \psi_i(r_i)$$ **Equation 2.2.14**

Where $\hat{h}$ takes the form:

$$\hat{h} = \left\{ -\frac{\hbar^2}{2m_e}\sum_{i=1}^{n}\int \psi_i^*(r_1)\nabla_1^2\psi_i(r_1)dr_1 - \sum_{I=1}^{M}\int \frac{Z_I e^2}{4\pi\varepsilon_0 r_{I1}}\rho(r_1)dr_1 + \frac{1}{2}\int \frac{\rho(r_2)e^2}{4\pi\varepsilon_0 r_{12}}dr_2 + V_{XC}(r_1) \right\}$$

Equation 2.2.15

Which is derived from application of the variational method to the electron energy E[ρ], Equation 2.2.12, with the charge density as described in Equation 2.2.13. ε_i are the Kohn-Sham orbital energies and V_{xc} is the exchange-correlation potential defined by:

$$V_{XC}[\rho] = \frac{\delta E_{XC}[\rho]}{\delta\rho}$$ **Equation 2.2.16**

The Kohn-Sham equations are solved, essentially in the same manner as that at the heart of the Hartree-Fock method, through the application of a self-consistent method. An initial guess for the charge density ρ is made as a starting point. This is often a superposition of atomic densities for molecular systems. An approximate form of the functional dependence of E_{xc} on density is selected; this remains fixed throughout the iterative process (the choice of functional E_{xc} will be discussed later). This allows the calculation of V_{xc} as a function of r. Insertion of this into Equation 2.2.14 gives a solution to the set of Kohn-Sham equations and an initial set of Kohn-Sham orbitals is obtained. Using Equation 2.2.13 an improved density is computed from this set of Kohn-Sham orbitals. The process is then repeated iteratively until the density and the exchange-correlation energy converge to a set tolerance. The electronic energy can then be computed from Equation 2.2.12.

In contrast to Hartree-Fock methods (with their energy dependence on wavefunctions) DFT (with its energy dependence on electron density) is less reliant on the size of the basis set used for accuracy. Generally the main error in DFT calculations arises from the choice of functional used to model the exchange-correlation term.

Many different functionals for the exchange-correlation dependence have been developed. The simplest of these is based on the Local Density Approximation (LDA). The LDA is based on a system for which the exchange-correlation energy is known; this is the well studied system of a homogeneous electron gas (Jellium). In a molecule, where neither the positive nor negative charges are distributed homogeneously, this is clearly a large approximation. The approximation has, however, proven to be remarkably successful for periodic systems, but less so for molecular systems. To account for the inhomogeneity of true molecular electron densities, non-local or gradient, corrections are often added to the exchange-correlation energy. These terms are dependent on the derivatives of the density, as well as the electron density. Corrections have been developed by Perdew[7] and Becke[8] amongst many others, and are called generalised gradient approximations (GGAs.).

Hybrid models have also been developed in addition to these functionals. One of the most successful of these contains the Becke[8] (B) exact exchange functional and the Lee, Yang, Parr[9] (LYP) functional to account for correlation; this functional is called B3LYP. This functional has been shown to perform well for molecular systems and is used in the DFT calculations performed in this thesis.

2.2.4 Choice of Basis Set.

As mentioned in section 2.2.2 the choice of the appropriate basis set is critical and must be motivated by several considerations. A large enough basis set must be chosen to model the molecular orbitals accurately, but this must be balanced by the computational cost incurred by using such a large basis set. However, by carefully choosing the basis functions to be as similar as possible to the unknown function, fewer basis functions will be required, thus minimising computational cost.

There are two main types of functions used as basis functions in molecular quantum chemistry (excluding the use of numerical analysis); Slater type orbitals, STOs, and Gaussian type orbitals, GTOs.

2.2.4.5 Slater Type Orbitals.

STOs have the normalised form as shown for the 1s orbital:

$$\phi_{1s} = \left(\frac{\zeta_1^3}{\pi}\right) e^{(-\zeta_1 r)} \quad \textbf{Equation 2.2.17}$$

Where ζ are parameters describing the size of the orbitals. STOs provide a reasonable representation of atomic orbitals but, they are unsuitable for the evaluation of the many two-electron integrals required in most *ab initio* calculations due to their form.

2.2.4.6 Gaussian Type Orbitals.

An alternative choice of basis function is the Gaussian type function introduced by Boys in 1950. GTOs have the form:

$$g_s(\alpha, r) = \left(\frac{2\alpha}{\pi}\right)^{\frac{3}{4}} e^{\left(-\alpha r^2\right)} \quad \textbf{Equation 2.2.18}$$

where α is a constant determining the size, or radial extent, of the orbital. The main advantage of using the GTO functions is that the product of two Gaussian functions at two different centres is simply another Gaussian function centered at a point between the two centres. The complex two-electron integrals over three or four different centres are therefore reduced to integrals over two centres, making calculation much easier. There is, however, a large disadvantage to the use of Gaussian functions, in that they provide a less realistic description of atomic wavefunctions. The hydrogenic 1s orbital, and the STOs have a discontinuous derivative at the nucleus, whereas the GTO does not. Large basis sets of GTOs must therefore be used to model the behaviour of the atomic orbitals correctly near the nuclei. The problem can be solved in part by the use of linear combinations of primitive Gaussian functions centred on the nucleus, in a form known as the contracted Gaussian type function (CGTF). The optimised exponents for the contracted Gaussian functions are generally found through atomic SCF calculations.

2.2.4.7 Quality of the Basis Set.

The simplest type of basis set, called a minimal basis set, has one CGTF representing each of the atomic orbitals used. Hydrogen, in a minimal basis set, would have one CGTF representing the 1s orbital. 5 CGTFs would be needed to model the 1s, 2s and the three 2p basis sets in carbon, and so on. Minimal basis sets are generally only reserved for calculations on restrictively large systems or as a starting point for progressively more accurate calculations as they do not return very accurate energies or wavefunctions.

One improvement that can be made is to double the number of basis functions used. This is known as a double zeta basis set. Tripling the number of basis functions relative to the minimal basis set provides a triple zeta basis set. Double and triple zeta basis sets both involve a significantly increased computational cost over a singlet basis set, but have the advantage of significantly increasing accuracy. A compromise to the size/cost problem is to use a split-valence basis set.

The split valence set generally models the valence electrons, which are most chemically interesting, with several contracted functions. The core electrons, which are important energetically but less so chemically, are described by one contracted function. The restriction on the number of functions used to describe the core orbitals, which are generally not altered greatly with chemical bonding, provides a significant reduction in computational cost, and allows attention to be focused on the valence electrons.

The 6-31G basis set is an example of a split-valence basis set. The notation shows that the core orbitals are described by a contraction of 6 primitive GTOs (PGTOs), the inner part of the valence shell is modelled by a contraction of 3 PGTOs and the outer part of the valence shell is described by one PGTO.

So far an important issue has been ignored in the discussion of basis sets, that of the inclusion of polarisation and diffuse functions. The atomic orbitals centred on atoms are distorted when chemical bonds form in molecules. This distortion can be

modelled by including basis functions with higher angular momentum values, by adding d-type functions to describe the distortion of p-orbitals on carbon for example. With the inclusion of polarisation functions, the basis set is then called a double zeta with polarisation functions, for example, or in the case of a split valence set, 6-31G* or 6-31G(p). Polarisation functions improve the accuracy of the basis set in the description of ground or low lying excited states.

Diffuse functions are introduced to study higher excited states of systems with loosely bound functions. Diffuse functions are those which have a higher principal quantum number but the same value of angular momentum. In the case of carbon, for example, the highest occupied orbital is the 2p orbital, suitable diffuse functions to use would be the 3p or 4p. A d or + are generally added to the notation for the basis set to indicate the inclusion of diffuse functions, 6-31G(p,d) or 6-31G*+ for example.

2.2.5 Inclusion of Solvation Effects.

Having established the importance of the level of method and basis sets in quantum chemical methodologies there is another important consideration to take into account. The discussion, thus far, has assumed that the molecular systems we have been discussing have been *in vacuo*. The work of this thesis will aim to describe the properties of molecular systems in solution, to this end it is important to understand how solvent environments can be modelled, and to include solvation in these quantum chemical calculations.

When dealing with the evaluation of the energy of a process A ↔ B an accurate description of the electronic wavefunction and energy of both species is required. We have already discussed how an accurate description of the wavefunction and energy can be obtain *in vacuo*, however, when dealing with systems in solution an accurate description of both energetic terms, the energy of the solute and the solvation energy, are essential. There are many different methods for modelling solvation to a solute. This work utilises the integral equation formalism for the polarizable continuum model (IEF-PCM) used within the Gaussian 03 software.

2.2.5.1 The Polarizable Continuum Model.

Detailed descriptions of polarizable continuum model (PCM) methods can be found elsewhere[10,11,12,13], this section aims to provide a simple introduction to IEF-PCM. In order to take into account the energy of the solute in solution it is necessary to add a perturbation to the Hamiltonian. This is typically done through adding an interaction potential, $\hat{V}_{\text{int}}$, such that:

$$\hat{H}_0\Psi_0 = E_0\Psi_0 \quad \textbf{Equation 2.2.19}$$

in vacuo becomes:

$$\left[\hat{H}_0 + \hat{V}_{\text{int}}\right]\Psi = E\Psi \quad \textbf{Equation 2.2.20}$$

Where $\hat{H}_0$ is the Hamiltonian of the solute *in vacuo*, and Ψ_0 and Ψ are the solute wavefunctions *in vacuo* and in solution, respectively. In the polarizable continuum model, it is then possible to model $\hat{V}_{\text{int}}$ by modelling the solute molecule as forming a cavity within a continuous polarizable solvent. The cavity is considered to have a molecular shape, which is formed from the shape of the solute atoms or atomic groups.

The electrostatic potential, V, inside the cavity is described by a Poisson equation:

$$-\nabla^2 V = 4\pi\rho \quad \textbf{Equation 2.2.21}$$

Where ρ describes the solute electronic and nuclear charge density. In the bulk of the solvent, however, V follows the linearised Poisson-Boltzmann equation:

$$-\varepsilon\nabla^2 V + \varepsilon\kappa^2 V = 0 \quad \textbf{Equation 2.2.22}$$

Where ε is the solvent dielectric constant and κ is the inverse of the Debye length:

$$\kappa = \sqrt{\frac{8\pi I F}{\varepsilon RT}} \quad \textbf{Equation 2.2.23}$$

Where I is the ionic strength of the solution. The boundary conditions for the cavity are $V_e = V_i$ where the suffixes e, i refer to regions inside and outside the cavity respectively, and in addition:

$$\nabla V_e \cdot \hat{n} = \frac{1}{\varepsilon}\nabla V_i \cdot \hat{n} \quad \textbf{Equation 2.2.24}$$

Where $\hat{n}$ is the unit vector normal to the surface.

A solvent reaction field can then be described by a polarization charge appearing on the cavity surface. To achieve this, the surface is partitioned into small domains of known area, called tesserae. A set of apparent charges $\{q_i\}$ are univocally associated to these tesserae. The specific fitting of apparent charges is chosen to best model the net charge of the solute; explicit details of how this is achieved are found elsewhere[10].

The molecular free energy in the solution can then be written as the sum of four contributions:

$$G = G_{el} + G_{cav} + G_{dis} + G_{rep}$$

The electrostatic contribution, G_{el}, is given by:

$$G_{el} = \left\langle \Psi \middle| \hat{H}_0 \middle| \Psi \right\rangle + \frac{1}{2} \sum_{k}^{tesserae} q_k V_k$$

Where V_k is the electrostatic potential due to the solute nuclei and electrons and q_k is the polarization charge on tessera *k*.

G_{cav} corresponds to the work required to form a cavity in the solvent and is calculated by a classical hard sphere approach:

$$G_{cav} = \sum_{l}^{spheres} G_l^{HS} \frac{A_l}{4\pi R_l^2}$$

Where G_l^{HS} is the cavitation free energy for an isolated hard sphere of radius R_l, and A_l is the area of the sphere l exposed to the solvent and not buried by other spheres.

G_{dis} and G_{rep} are terms describing the solute-solvent dispersion and repulsion interactions, respectively; these are calculated classically using atom-atom interaction potentials. The inclusion of these terms into the calculations of molecular systems allows calculation of solvated molecular energies. Other more explicit solvation modelling is possible, but vastly more expensive computationally.

2.2.6 The Inclusion of temperature effects.

So far the discussion has emphasised the importance of basis set choice and the modelling of solvation for computational studies. Upon completion of a geometry

optimisation calculation the heat of formation, H_f can readily be obtained from Gaussian. However any real understanding of the thermodynamics of molecules in a closed system requires knowledge of their Gibbs free energies, G, which require the knowledge of the molecular entropy as shown in Equation 2.2.25.

$$G = H_f - TS \quad \textbf{Equation 2.2.25}$$

Where T is the temperature of the system, and S is the entropy of the molecule.

The entropy, and therefore the free energy, of a molecular system can be calculated in the Gaussian programme used in this work by carrying out a frequency calculation. In the frequency calculation the vibrational frequencies of the molecule at a specific temperature are obtained by computing the force constants. The force constants are determined analytically by double numeric differentiation. Once the force constants have been calculated the vibrational energies of the molecules can be calculated with a simple harmonic oscillator approximation. This approximation should be valid provided the potential energy well of the molecule can be reasonably modelled by the potential well of a simple harmonic oscillator, this should be possible in the case of inflexible molecules where the potential well is deep, for flexible molecules this approximation may be inaccurate. The permitted energy levels are then given by:

$$E_i = \left(i + \frac{1}{2}\right)\hbar\omega \qquad \omega = \left(\frac{k}{\mu}\right)^{\frac{1}{2}} \qquad i = 0,1,2,... \quad \textbf{Equation 2.2.26}$$

The thermodynamic total energy of the molecule can then be found from the solution of the partition function:

$$Z = \sum_i e^{-\frac{\left(i+\frac{1}{2}\right)\hbar\omega}{k_B T}} \quad \textbf{Equation 2.2.27}$$

The vibrational frequencies are then determined from the second derivatives of the energy with respect to the Cartesian nuclear coordinates and transformation to mass-weighted coordinates. Such a transformation is, however, only valid at a stationary

point on the potential energy surface of the molecule (for example the potential minimum of an optimised geometry).

Following a frequency calculation a thermochemistry analysis is performed and raw zero-point energies are given together with thermal corrections to the total energy, enthalpy and Gibbs free energy. The corresponding corrected energies are also provided.

2.3 References.

[1] Electrochemical Theory:

Bard, A. J.; Faulkner, L. R. "*Electrochemical Methods Fundamentals and Applications*"; John Wiley & Sons (USA) **2001**.

Fisher, A. C. "*Electrode Dynamics*" Oxford University Press (Oxford) **1996**.

[2] Computational Theory:

Hehre, W. J.; Radom, L.; Schleyer, P. v.R.; Pople, J. A. "*Ab initio Molecular Orbital Theory*" John Wiley & Sons (USA) **1986**.

Hirst, D. M. "*A Computational Approach To Chemistry*" Blackwell Scientific Publications (London) **1990**.

Carsky, P.; Urban, M. "*Ab initio Calculations. Methods and Applications in Chemistry*" Springer-Verlag (Berlin) **1980**.

Salem, L. "*Molecular Orbital Theory of Conjugated Systems*" W. A. Benjamin, Inc. (New York) **1966**.

Jensen F. "*Introduction to Computational Chemistry*" John Wiley & Sons (Chichester) **1999**.

Atkins, P. W.; Friedmen, R. S. "*Molecular Quantum Mechanics*" Oxford University Press (New York) **1997**.

Gaussian03, Online Manual, http://www.gaussian.com

[3] Bard, A. J.; Faulkner, L. R. "*Electrochemical Methods Fundamentals and Applications*"; John Wiley & Sons (USA) **2001**. "*Chapter 3: Kinetics of Electrode Reactions"* page 95.

[4] Tew, D. P.; Klopper, W.; Helgaker, T. *J. Comp. Chem.* **2007**, 28, *1307-1320.*

[5] Hohenberg, P.; Kohn, W. *Phys. Rev. B* **1964**, 136, *864-871.*

[6] Kohn, W.; Sham, L. J. *Phys. Rev. A* **1965**, 140, *1133-1138.*

[7] Perdue, J.; Wang, Y. *Phys. Rev. B* **1992**, 45, *13244-13249.*

[8] Becke, A. D. *Phys. Rev. A* **1988**, 38, *3098-3100.*

[9] Lee, C.; Yang, W.; Parr, R. G. *Phys. Rev. B* **1988**, 37, *785-789.*

[10] Mennucci, B.; Tomasi, J. *J. Chem. Phys.* **1997**, 106, *5151-5158.*

[11] Cancès, E.; Mennucci, B.; Tomasi, J. *J. Chem. Phys.* **1997**, 107, *3032-3041.*

[12] Cossi, M.; Barone, V.; Mennucci, B.; Tomasi, J. *Chem. Phys. Lett.* **1998**, 286, *253-260.*

[13] Tomasi, J.; Mennucci, B.; Cancès, E. *J. Molecular Structure: Theochem* **1999**, 464, *211-226.*

Chapter 3: Experimental.

3.1 Introduction.

In this chapter the reagents, experimental and computational methods used during the course of this research are outlined.

3.2 Chemicals.

3.2.1 Commercial Chemicals.

Lithium perchlorate (Aldrich, 99.99%) was dried in a vacuum oven for 24 hours prior to use. Silver perchlorate (Aldrich, 99.9%), ferrocene (Fluka AG >98%), indole (Aldrich, 99%), 2,3-benzofuran (Aldrich, 99%), thianaphthene (Aldrich, 99%) and benzo(b)selenophene (Acros, 97%) were all used as received.

3.2.2 Synthesised Chemicals.

3.2.2.1 Chapter 4.

1,4,5,8,9,12-Hexamethyltriphenylene was synthesised[1] by Dr. Trent Galow at the University of Edinburgh and used as received. 2,5-dibenzoselenophene and 2,5-dibenzo-3,4-diazaselenophene were synthesised by Dr. Guoxiong Hua within Prof. Derek Woollins' group at the University of St. Andrews and used as received. Synthesis occurred through reaction of Woollins' reagent[2] with 2,5-diones in refluxing toluene[3].

3.2.2.2 Chapter 5.

5-methylindolo[3,2,1-jk]carbazole was synthesised by Elanor Wood with the aid of Prof. Hamish McNab's group at the University of Edinburgh and used as received. Synthesis was through a similar flash vacuum pyrolysis (FVP) used in the synthesis of other 5-substituted indolo[3,2,1-jk]carbazoles[4].

3.2.2.3 Chapter 7.

The 2,3'-diindoles were synthesised by Rob Valentine within Dr. Neil Robertson's group at the University of Edinburgh and used as received.

3.2.3 Solvents.

Acetonitrile (MeCN, JT Baker, Ultra Low water), N, N-dimethylformamide (DMF, 99+% Acros), ethanol (analytical reagent grade, Fisher), d^6-dimethylsulfoxide (d^6-DMSO, Aldrich, 99.9%) and d^6-acetone (Aldrich, 99.9%) were used as received. Water was doubly deionised using a Millipore MilliQ water system.

3.3 Electrochemistry.

3.3.1 Circuitry.

Electrochemical studies were carried out using a modular potentiostat/galvanostat with combined waveform generator and voltage sources (PGSTAT12, Autolab) control, data collection and analysis carried out using the General Purpose Electrochemical System (GPES, Autolab) software on a PC. The rotating disc electrodes were controlled using a rotator and a motor controller (Oxford Electrodes Ltd.), this system is described elsewhere[5].

3.3.2 Electrodes.

The working electrode was a platinum rotating disc electrode, RDE, (Oxford Electrodes Ltd.), disc area 0.387 cm^2. This electrode was hand polished with a 3 μm alpha-alumina polish (Buehler Ltd.) in a water slurry, then washed with doubly deionised water. A 2 cm^2 platinum gauze was used as the counter electrode, this was cleaned by flame annealing with a Bunsen burner flame. The reference electrode (Bioanalytical Systems Inc.) consisted of a silver wire dipped in a 0.01 M solution of $AgClO_4$ in background electrolyte in a glass body with a VYCOR frit.

3.3.3 Experimental Details.

Peak oxidation potentials were measured using the normal cyclic voltammetry (staircase) method in GPES. This technique is detailed in Chapter 2 and elsewhere[6]. The standard potential, E^θ, for the Fc/Fc^+ redox couple was measured using the

normal cyclic voltammetry (staircase) method with the fit and simulation analysis in GPES.

Polymerisation studies at the RDE used the potential step chronoamperometry method in GPES. This method involved 2 potential steps, initially the electrode was held at a low potential, near 0 V, to prevent coupling, the potential was then stepped to a potential ≈100 mV higher than the measured monomer oxidation peak potential on Pt whilst rotating the RDE at speeds from 0 Hz to 16 Hz. After the required polymerisation time had passed the potential was stepped back to the initial potential. Specific potentials are reported in the relevant sections of the thesis.

All electrochemical measurements were performed in acetonitrile/background electrolye solutions. The background electrolyte used in this work was 0.1 M $LiClO_4$.

3.4 Spectroscopy.

3.4.1 UV/visible Absorption Spectroscopy.

UV/visible spectroscopic measurements were recorded using a Cary 300 Conc Spectrophotometer with a 1 cm path-length fused silica cuvette (Helma).

3.4.2 Fluorescence Spectroscopy.

Fluorescence experiments were recorded using a Spex Fluromax spectrometer with a 1 cm path-length fused silica cuvette (Helma).

3.4.3 ^{1}H Nuclear Magnetic Resonance Spectroscopy.

NMR experiments were recorded by K. Johnson at the University of Edinburgh. ^{1}H data were collected using a 250 MHz spectrometer (ARX250, Bruker) and a 360 MHz spectrometer (DPX360, Bruker) with fully deuterated d^1-chloroform or d^6-DMSO. ^{13}C spectra were recorded on a Bruker ARX250 (63 MHz) spectrometer. Chemical shifts (δ_H and δ_C) are quoted in ppm relative to tetramethylsilane, and all coupling constants are given in Hertz (Hz).

3.4.4 Mass Spectrometry.

Fast atom bombardment (FAB) mass spectra were recorded on a Kratos Profile instrument operated by Mr. A. T. Taylor at the University of Edinburgh.
Electron spray injection (ESI) mass spectra were recorded on a Finnigan LCQ Classic instrument.

3.5 Computational Details.

All calculations were carried out using the software package Gaussian 03[7] running on a SUSe 9.x Linux HPC cluster consisting of 68 AMD Opteron processing cores contained within EaStChem's Research Computing Facility's Hare cluster. Default convergence criteria were used for all calculations (maximum force = 0.00045, RMS force = 0.0003, maximum displacement = 0.0018 and RMS displacement = 0.0012). The computational method employed was the B3LYP method (discussed in Section 2.2.3), which is a hybrid functional method including a mixture of Hartree-Fock exchange with DFT exchange-correlation. The B3LYP method is a Becke Three Parameter Hybrid Functional which utilises the correlation functional of Lee, Yang and Parr (LYP) which includes both local and non-local terms. For calculations of the electron spin density the unrestricted method uB3LYP was employed. The basis set used in all calculations is 6-311+G(d,p) with acetonitrile solvation modeled with the polarizable continuum model (PCM)[8].

For all molecules a frequency calculation was performed on optimised geometries to ensure that a minimum in the potential energy hypersurface had been reached and to obtain calculated free energies for the molecules.

The spin density distribution was evaluated by generating cube files for electron density and electron spin. The spin density distribution plots were then made by mapping onto the 99% electron density map. Output was viewed using Jmol, an open-source Java viewer for chemical structures in 3D (http://www.jmol.org/) and rendered using the Persistence of Vision Raytracer (POV-Ray) freeware (http://www.povray.org).

3.6 References.

[1] Wang, Y.; Stretton, A. D.; McConnell, M. C.; Wood, P. A.; Parsons, S.; Henry, J. B.; Mount, A. R.; Galow, T. H. *J. Am. Chem. Soc.* **2007**, *129*, 13193-13200.

[2] Fitzmaurice, J. C.; Williams, D. J.; Wood, P. T.; Woollins, J. D. *J. Chem. Soc. Chem. Commun.* **1988**, 741.

[3] Paper in preparation.

[4] Wharton, S. I. *Ph. D. Thesis, "Synthesis and Characterisation of Novel Conducting Films Based On Indolo[3,2,1-jk]carbazole Systems.", University of Edinburgh* **2005**.

[5] Mount, A. R. *Ph. D. Thesis,"The Development of Modified Electrodes." , Imperial College London,* **1987**.

[6] Eco Chemie B. V. *Autolab. ModularElectrochemical Instruments* Utrecht, Netherlands, **2002**.

[7] Gaussian 03, Revision E.01, Frisch, M. J.; Trucks, G. W.; Schlegel, H. B.; Scuseria, G. E.; Robb, M. A.; Cheeseman, J. R.; Montgomery, Jr., J. A.; Vreven, T.; Kudin, K. N.; Burant, J. C.; Millam, J. M.; Iyengar, S. S.; Tomasi, J.; Barone, V.; Mennucci, B.; Cossi, M.; Scalmani, G.; Rega, N.; Petersson, G. A.; Nakatsuji, H.; Hada, M.; Ehara, M.; Toyota, K.; Fukuda, R.; Hasegawa, J.; Ishida, M.; Nakajima, T.; Honda, Y.; Kitao, O.; Nakai, H.; Klene, M.; Li, X.; Knox, J. E.; Hratchian, H. P.; Cross, J. B.; Bakken, V.; Adamo, C.; Jaramillo, J.; Gomperts, R.; Stratmann, R. E.; Yazyev, O.; Austin, A. J.; Cammi, R.; Pomelli, C.; Ochterski, J. W.; Ayala, P. Y.; Morokuma, K.; Voth, G. A.; Salvador, P.; Dannenberg, J. J.; Zakrzewski, V. G.; Dapprich, S.; Daniels, A. D.; Strain, M. C.; Farkas, O.; Malick, D. K.; Rabuck, A. D.; Raghavachari, K.; Foresman, J. B.; Ortiz, J. V.; Cui, Q.; Baboul, A. G.; Clifford, S.; Cioslowski, J.; Stefanov, B. B.; Liu, G.; Liashenko, A.; Piskorz, P.; Komaromi, I.; Martin, R. L.; Fox, D. J.; Keith, T.; Al-Laham, M. A.; Peng, C. Y.; Nanayakkara, A.; Challacombe, M.; Gill, P. M. W.; Johnson, B.; Chen, W.; Wong, M. W.; Gonzalez, C.; and Pople, J. A. Gaussian, Inc., Wallingford CT, 2004.

[8] Mennucci, B.; Tomasi, J. *J. Chem. Phys.* **1997**, 106, *5151-5158.*

Chapter 4: The Establishment of an Enhanced General Computational Method for Redox Active Aromatics.

4.1 Introduction.

Over the past 25 years, with computational power increasing rapidly (e.g. taking advantage of the number of transistors placed on a circuit board doubling every 18 – 24 months, in accordance with Moore's Law[1]), computational methods have been transformed from a crude technique for studying a limited number of systems to a valuable research resource allowing calculation of the structure, physical and electronic, and energies of chemical systems. It has been shown that computational methods can give reasonably accurate redox potentials for a wide range of organic molecules, with a standard deviation of 170 mV on a study of 270 molecules in acetonitrile[2]. Previously within the Mount[3,4] group, computational methods have been deployed to calculate the electronic structures of 5-substituted indoles (In**,** Figure 4.1.1) and predict their standard redox potentials $E^{\theta}(In^{+\bullet}/In)$ and the molecular properties of the radical cations formed by their electro-oxidation.

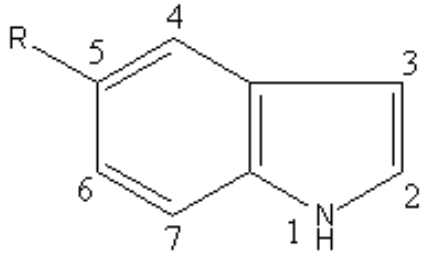

Figure 4.1.1. Structure of 5-substituted indoles.

Standard redox potentials were calculated computationally by calculating the free energy of reaction between indole and the ferrocene/ferrocinium (Fc/Fc^{+}) redox couple:

$$In^{+\bullet} + Fc \xrightarrow{\Delta G^{\theta}} In + Fc^{+}$$

as:

$$\Delta G^{\theta} = -nFE^{\theta}_{cell}$$

and:

$$E^{\theta}_{cell} = E^{\theta}(In^{+\bullet} / In) - E^{\theta}(Fc^{+} / Fc)$$

where $E^{\theta}(In^{+\bullet}/In)$ and $E^{\theta}(Fc^{+}/Fc)$ are the standard reduction potentials of $In^{+\bullet}/In$ and Fc^{+}/Fc respectively. This gives, E^{θ}_{cell}, which is the standard redox potential of $In^{+\bullet}/In$ relative to Fc^{+}/Fc. These values were then used to calculate the standard redox potential on any reference scale by using the experimentally measured value for $E^{\theta}(Fc^{+}/Fc)$ on that reference scale.

Consideration of the electronic structure of the indole radical cations enabled some insight into the most probable coupling positions for the radical cations in the formation of indole films. It had previously been proposed[3] that coupling of indole monomers occurred through the initial formation of a 3, 3'-dimer. This was then oxidised, and its radical cation coupled with another monomer radical cation to form the asymmetric trimer product as shown in Figure 1.1.4. Figure 4.1.2 shows the electron spin density distribution of a range of indoles. It can be observed that the highest electron spin density is located on the 3 position. It was proposed that as coupling of the radical cations occurs by pairing of the radical electron from each cation to form a bond, the most probable coupling site for bond formation would then be the site with the largest electron spin density in the radical cation. The electron spin density map therefore suggests that coupling is most likely to occur via initial 3, 3'-dimer formation.

Kettle[4] compared a density functional theory method (using the DMol[3] package, with a PW91 functional) with a semi-empirical approach (PM3) with a COSMO continuum solvation model. This showed that errors associated with semi-empirical methods were much greater in comparison to the DFT method, but the magnitude of the errors was counterbalanced to some extent by the lower computational time of the semi-empirical methods. At the time of this research such a compromise was important in making such calculations viable.

The aim of this chapter is to extend the use of computational methods to the calculation of the oxidation potentials and molecular properties of a range of novel heteroaromatics, to probe the generality of this approach to other heteroaromatics. This work applies a more powerful DFT method and takes advantage of the increased computing power now available, supplied by the EaSTCHEM Research Computing Facility

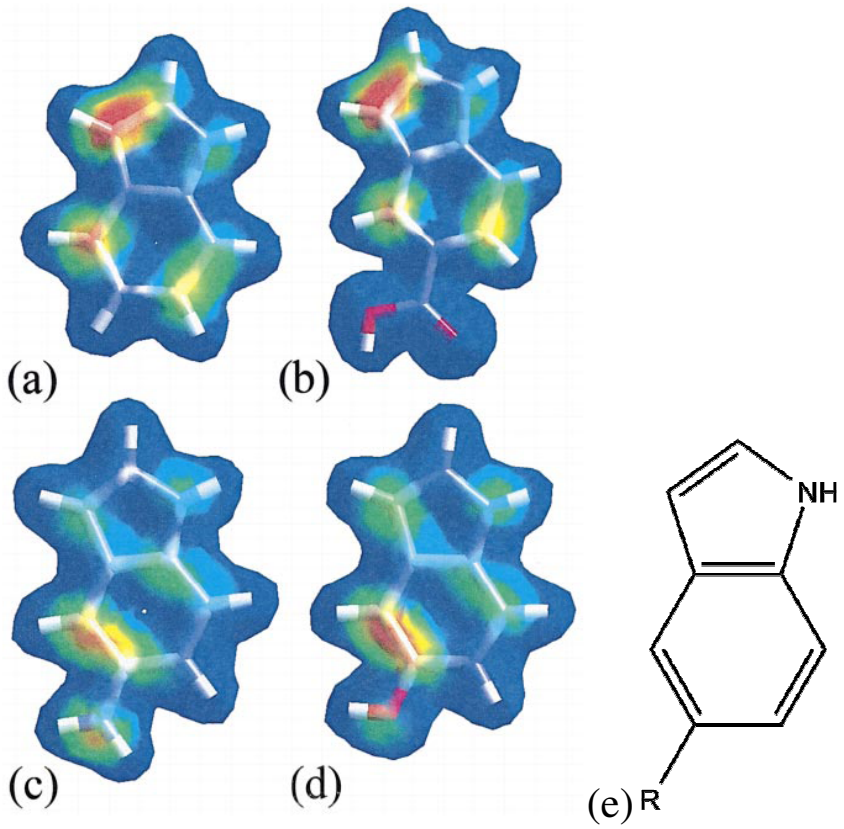

Figure 4.1.2. Taken from Reference 2. Spin density distribution mapped onto a 99% electron density isosurface for the radical cations of (a) indole, (b) 5-carboxylic acid indole, (c) 5-aminoindole, (d) 5-hydroxyindole. (The colouring is schematic as follows: red indicates a positive spin density whilst blue is zero. The same range of spin density was used for all 4 maps). (e) Structure showing orientation of indole units.

4.2 Visiting the Past: Reviewing Previous Indole Calculations.

This aim of the computational work in this thesis is to enhance the computational methods used previously within the Mount group; to achieve this goal it is necessary to review the previous work and establish which aspects of the methodology require improvement. This assessment uses the most comprehensive computational work

previously undertaken in the group, the computational studies on the electro-active behaviour of 5-substituted indoles by Kettle[4]. In this work Kettle assigned an error of 100 mV on all her calculated results. Re-analysis of the data and comparison of the error in the calculated values with respect to the experimentally measured values gives standard deviations of 42 and 96 mV respectively for PW91 and PM3 methods respectively. The error in the calculated values with respect to the experimentally observed errors was calculated with Equations 4.2.1-4.2.3, these errors will hereon be referred to as standard deviations for the calculated reduction potentials.

$$s = \sqrt{\frac{1}{N-1}((\sum_{i=1}^{N} x_i^2) - N\bar{x}^2)} \quad \textbf{Equation 4.2.1}$$

$$x_i = E_{calc,i} - E_{\exp tl,i} \quad \textbf{Equation 4.2.2}$$

$$\bar{x} = \frac{\sum_{i=1}^{N} \left| E_{calc,i} - E_{\exp tl,i} \right|}{N} \quad \textbf{Equation 4.2.3}$$

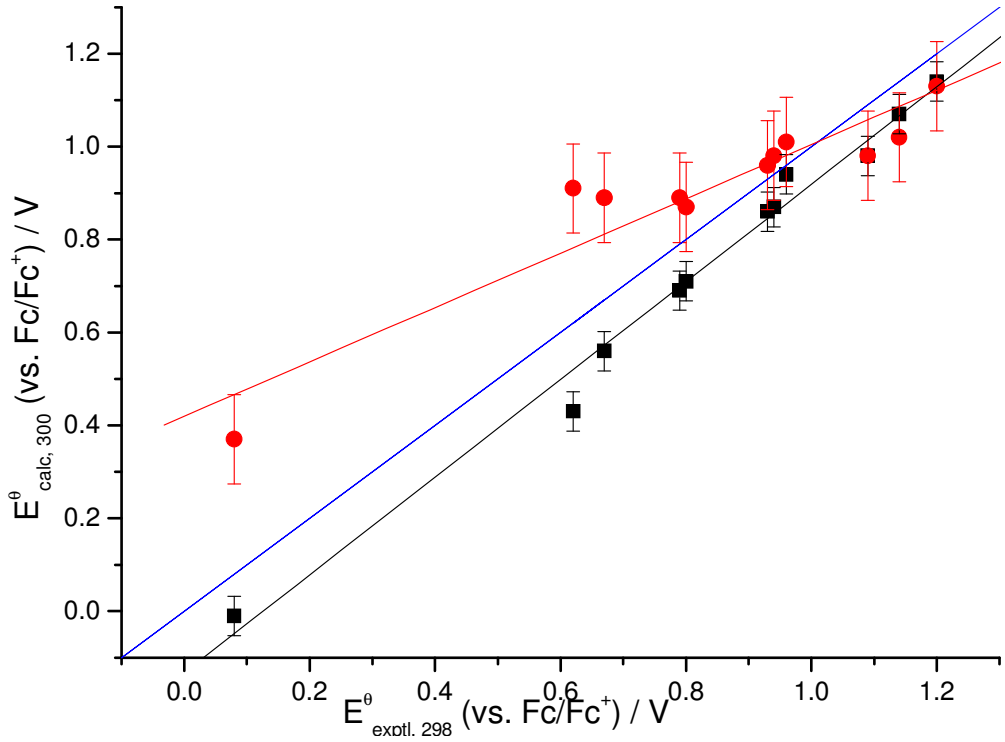

Figure 4.2.1. Plot of E^{θ}_{300}, c *vs.* E^{θ}_{298} for (●) semi-empirical method (PM3) and (■) DFT data (PW91) using data from reference 4. The blue line shows the expected relationship if the calculated and experimental data were equal.

Figure 4.2.1 shows a plot of the calculated redox potentials versus the experimentally measured redox potentials. For these data an ideal plot, with full agreement between calculated and experimental data, would show a line of unity gradient and zero intercept. It is clear that the PM3 calculations are markedly inferior to PW91 calculations, with a systematic overestimation of the redox potential for many of these indoles. In contrast, the PW91 calculations show much better correlation with a line of unity gradient within experimental error. However, there appears to be an offset in the intercept of the best fit line indicative of an error of roughly 100 mV in the $E^{\theta}(Fc^{+}/Fc)$ calculation. Not included on the plot are error bars for the measured oxidation potentials, the error in the measurement of a peak oxidation potential is less than 10 mV, error bars for this magnitude of error would be comparable in size to the width of the points in the plot.

Such a large error in the calculation of E^{θ} (Fc^{+}/Fc), with respect to the relatively small error in the distribution of the indole calculations, may be explained by the complexity involved with performing calculations on systems containing transition metals. A study on a range of organic and inorganic systems by Baik *et al.* showed that calculations of the redox potentials of metallocenes gave significantly larger errors than calculations of redox potentials for organic molecules[5]. The importance of the choice of basis set is discussed in section 2.2.4; the demands made by transition metal complexes on basis set choice are far greater than those by aromatic systems due to the importance of d-shell electrons in the bonding of most transition metal complexes. These d-shell electrons make the inclusion of diffuse and polarisation functions within the calculations vital. Kettle chose to use a STO basis set which included orbitals of double zeta quality and polarisation functions. The observed error in the calculation of $E^{\theta}(Fc^{+}/Fc)$ suggests that this basis set may not have been robust enough to enable high calculation accuracy.

The importance of the $E^{\theta}(Fc^{+}/Fc)$ calculation was further highlighted in computational work performed in the Mount group by Chapman[6]. Chapman repeated Kettle's calculations on three indole systems, using the Gaussian98 program with B3PW91 functional and calculated $E^{\theta}(Fc^{+}/Fc)$ with a relatively small 6-31G(d,p)

basis set. While Kettle's results showed a systematic underestimation of around 100 mV, Chapman's results showed an increase in the systematic underestimation to 190 mV, clearly highlighting the importance of basis set choice.

It is clear from this previous work that the greatest error in calculating the redox properties is likely to be due to the error in calculation of $E^{\theta}(Fc^{+}/Fc)$, evidenced by the systematic offsets of the calculated potentials. The close correlation of the indole calculations to their corresponding experimental value suggests, however, that the DFT approach with continuum solvation is appropriate for calculations on these organic systems.

4.3 Gaining Confidence: A New Approach to Indole Calculations.

An aim of this work is to establish a new methodology for calculating the redox properties that can be applied to a wide range of aromatic systems. Previous work showed that DFT functionals and continuum solvation yielded relatively accurate but imprecise results for the calculation of indole redox potentials. The source of the imprecision arose through the choice of the Fc^{+}/Fc redox couple as the reference reaction. Previously, calculations were performed on DMol[3] and Gaussian98 software. The choice of software in this work is Gaussian03 available on the EaStChem Research Computing Facility (RCF). However, the choice of software should have little effect on the overall methodology. In this new methodology, the use of DFT functionals and a continuum solvation model is retained. The B3LYP DFT functional has been suggested to be an appropriate method for the calculation of redox potentials for a wide range of organic molecules[2], while the choice of continuum solvation model was set by the software which utilises the Polarizable Continuum Model (PCM) discussed in Section 2.2.5. The computational power of the RCF removes many of the limitations on basis set size that restricted earlier calculations; therefore, the large basis set of 6-311+G(d,p) was selected for all the calculations in this work.

The largest alteration in the methodology between this work and previous work is through the choice of the reference. In an effort to overcome the systematic underestimation of redox potential observed in Kettle's PW91 calculations it was decided to use the $In/In^{+\bullet}$ peak oxidation potential as reference rather than the Fc/Fc^{+} couple used by Kettle. Although the Fc/Fc^{+} couple has the benefit of being a common reference redox couple in electrochemical studies, the electrochemistry of the $In/In^{+\bullet}$ oxidation has been studied extensively within the Mount group and is well understood. Comparison of all potentials to the indole oxidation potential should provide a robust methodological approach, these potentials can then be referred to the Fc/Fc^{+} couple as a common reference, by conversion using the experimentally measured value of E^{θ} ($In/In^{+\bullet}$) vs Fc/Fc^{+}.

Another difference in the methodology of this work to previous work is the choice of potential for comparison. Kettle and Chapman chose to use standard redox potentials, E^{θ}, as a comparison. As many of the molecules studied in this work display irreversible oxidation peaks, it can often be difficult to establish a precise E^{θ} from such peaks[2]. It is however possible to interconvert peak potentials and E^{θ} for electrochemically reversible systems. A good test of the electrochemical reversibility when there is chemical irreversibility is the separation of the peak potential and the half-peak potential. The methodology in this work will therefore compare peak oxidation potentials, provided that the separation between the peak-potential and half-peak potential meet the criteria for electrochemical reversibility.

The measured peak potentials, E_p, are related to the half-peak potentials, $E_{p/2}$, as $|E_p - E_{p/2}| = 57$ mV for a reversible one-electron redox reaction at 298K[7]. In this case, $E_{p/2}$ can be determined from E^{θ}, they are essentially equal when reactants and products have similar diffusion coefficients in solution as:

$$E_{\frac{p}{2}} = E^{\theta} + \frac{RT}{F}\left(1.09 + \ln\left(\frac{D_O}{D_R}\right)^{\frac{1}{2}}\right) \quad \textbf{Equation 4.3.1}$$

where D_O and D_R are the diffusion coefficients of the reduced and oxidised species in the redox reaction, respectively[7]. For example the measured value of $E_p - E_{P/2}$ for

$In^{+\bullet}$/In was found to be 63 mV at a sweep rate of 100 mV s^{-1}, suggesting that the assumption of electrochemical reversibility is reasonable. This method for interconversion of E_p and E^θ can then be justified.

The peak oxidation potential for any heteroaromatic molecule X can therefore be calculated with respect to indole by considering the redox reactions:

$$In^{+\bullet} + e^- \xleftrightarrow{\Delta G^\theta_{In}} In \qquad \Delta G^\theta_{In} = -FE^\theta\left(In^{+\bullet}/In\right) \quad \textbf{Equation 4.3.2}$$

$$X^{+\bullet} + e^- \xleftrightarrow{\Delta G^\theta_{X}} X \qquad \Delta G^\theta_{X} = -FE^\theta\left(X^{+\bullet}/X\right) \quad \textbf{Equation 4.3.3}$$

Which give the overall redox reaction:

$$X^{+\bullet} + In \xrightarrow{\Delta G^\theta} X + In^{+\bullet}$$

$$\Delta G^\theta = \Delta G^\theta_X - \Delta G^\theta_{In} = -(F)\left[E^\theta\left(X^{+\bullet}/X\right) - E^\theta\left(In^{+\bullet}/In\right)\right] \quad \textbf{Equation 4.3.4}$$

It is clear that by calculating free energies, ΔG^θ, a standard reduction potential of $X^{+\bullet}$/X relative to $In^{+\bullet}$/In can be readily obtained through Equation 4.3.4. If both reactions are electrochemically reversible, this is also the peak oxidation potential of X with respect to the peak oxidation potential of In. This can then be converted to a calculated peak oxidation potential for any reference scale by using the experimentally measured value of the indole peak oxidation potential on this reference scale.

Figure 4.3.1 shows the experimentally observed and calculated peak oxidation potentials, E_{pa}, for oxidation from the neutral (In) to the radical cation ($In^{+\bullet}$) in acetonitrile versus the Hammett substituent parameter σ^+. Again it is possible to make a comparison as in Figure 4.2.1 between the calculated and experimental data; this is shown in Figure 4.3.2 for the B3LYP calculations using the 6-311+G(d,p) and smaller 6-31G basis sets. Also included in Figure 4.3.2 is a reanalysis of Kettle's data using standard redox potentials calculated using In/$In^{+\bullet}$ as the reference calculation rather than the Fc/Fc^+ redox couple used by Kettle. It can be observed that the calculated values using both DFT methods no longer lie systematically below the ideal calculation line and lie closer, in general, to this line. This observation accounts for the lower standard deviations observed. As with Figure 4.2.1 it is possible to calculate a standard deviation between experimentally observed and calculated peak

oxidation potentials for these data. This was found to be 31 mV for the B3LYP method and 30 mV for the PW91 method. The 1 mV difference in standard deviation is negligible compared with the vast improvement on the 100 mV error previously quoted by Kettle. These standard deviations are also an improvement of around 10 mV on the standard deviation calculated for Kettle's calculations using Fc/Fc^+ as reference; this supports the hypothesis that the systematic error observed previously was due to the inaccurate calculation of $E^{\theta}(Fc/Fc^+)$, and provides justification for the new methodology. The calculation of oxidation potentials using the smaller 6-31G basis set gave a much larger standard deviation of 57 mV, highlighting the importance of the choice of basis set in quantum chemical calculations.

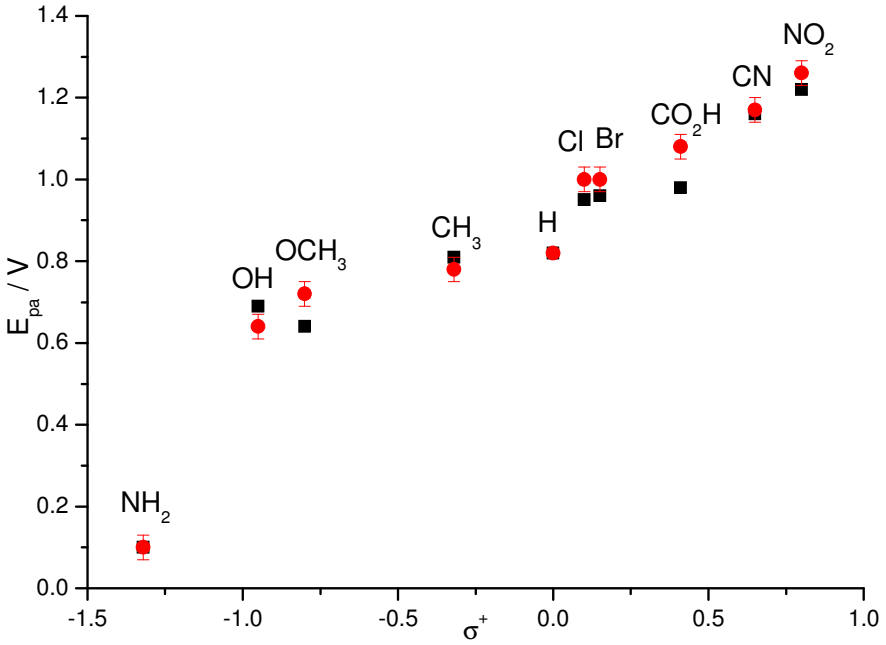

Figure 4.3.1. Plot of peak oxidation potentials for 5-substituted indoles *vs.* σ^+. (●) B3LYP calculations and (■) experimental.

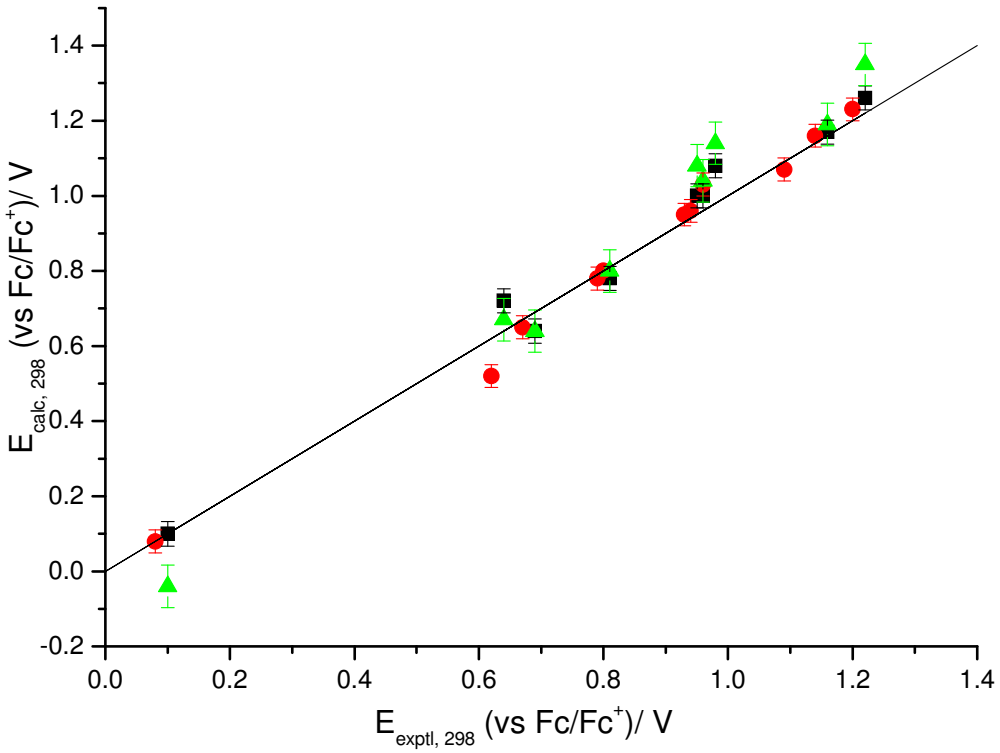

Figure 4.3.2. Plot of $E_{p,298,c}$ *vs.* $E_{p,298}$ for B3LYP calculated oxidation potentials of indoles with (■) 6-311+G(d,p) and (▲) 6-31G basis sets. (●) Corrected plot of $E^{\theta}_{300,c}$ *vs.* E^{θ}_{298} for PW91 calculated oxidation potentials of indoles, with calculated oxidation potentials compared to calculated indole E^{θ}. The line shows the relationship if the calculated and experimental data were equal.

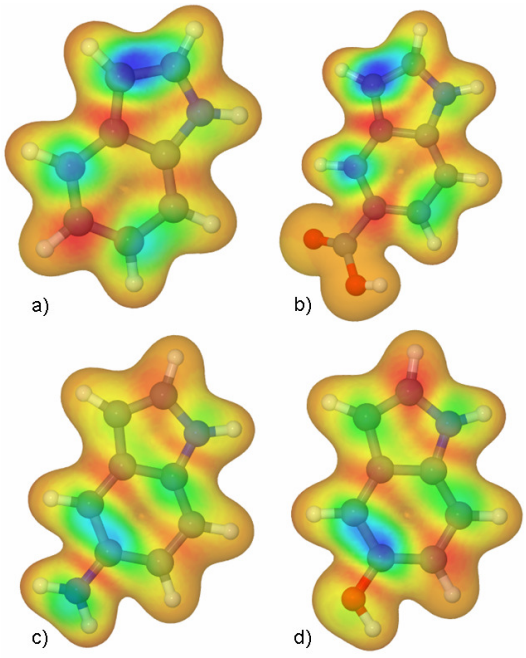

Figure 4.3.3. Spin density distribution mapped onto a 99% electron density isosurface for the radical cations of (a) indole, (b) 5-carboxylic acid indole, (c) 5-aminoindole, (d) 5-hydroxyindole. (The colouring is schematic as follows: blue indicates a positive spin density (0.005) whilst red is negative (-0.001). The same range of spin density was used for all 4 maps).

Figure 4.3.3 shows the electron spin density distribution for a range of 5-substituted indoles. By comparison with Figure 4.1.2 it is quite clear that the B3LYP method shows an excellent agreement with the results observed by Kettle using the PW91 method. These spin density maps again support the proposal that initial coupling within indoles should occur via the 3 positions to form a 3, 3' indole dimer.

It is now possible with the enhanced computing power available to extend the DFT calculations to calculate the oxidation potential and molecular properties of the 3, 3'-dimer of indole, the expected initial product of the coupling of these two indole radical cations. The calculated peak oxidation potential of the 3, 3'-dimer is -0.11 ± 0.03 V vs Fc/Fc^{+}, assuming the standard deviation for dimer oxidation potential calculation is the same as for monomer calculations. This is much lower than the indole peak oxidation potential (+0.82 V) and certainly lower than the electrode potential used to oxidise indole monomer. It is therefore highly likely that any dimer formed at the electrode surface would be readily oxidised and available for further

coupling to an indole monomer radical. Figure 4.3.4 shows the spin density distribution for the resulting 3, 3'-dimer radical cation. It can be seen that the greatest spin density can be observed in the 2 and 2'-positions; therefore any unreacted indole monomer radical in close proximity to the oxidised dimer is likely to undergo coupling via a 2-position on the dimer and the 3-position on the monomer to form the linear trimeric species shown in Figure 4.3.5.

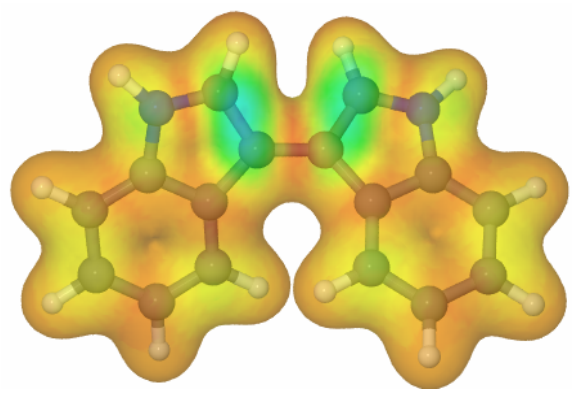

Figure 4.3.4. Spin density distribution mapped onto a 99% electron density isosurface for the radical cation of a 3, 3'-indole dimer. (The colouring is schematic as follows: blue indicates a positive spin density (0.005) whilst red is negative (-0.001). The same range of spin density was used for all 4 maps).

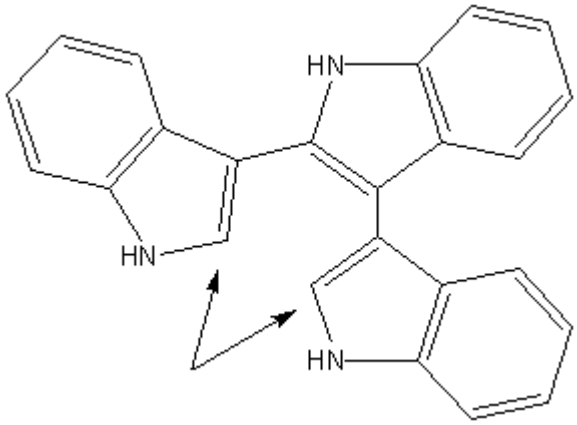

Figure 4.3.5. Schematic showing an indole coupled to a 3, 3'-indole dimer. Arrows indicate sites of further coupling for cyclisation to asymmetric trimer.

Calculations were then performed on the neutral and radical cation forms of the linear trimer shown in Figure 4.3.5 using the B3LYP method. Due to the large number of atoms in the trimer the basis set was limited to the smaller 6-31G. The calculated oxidation potential using this basis set was then found to be 0.12 ± 0.06 V

vs Fc/Fc^+. As with the calculated dimer oxidation potential this is much lower than the oxidation potential applied during formation of indole films, even allowing for the increased error associated with using this smaller basis set. This trimer would, therefore, again be expected to oxidise readily at the electrode surface. The calculated electron spin density for the trimer radical cation is shown in Figure 4.3.6. It is interesting to note that the highest electron spin density is located on only one of the unlinked 2-positions which is consistent with the lack of symmetry in the linear trimer. Cyclisation can then occur by a radical mechanism similar to that shown in Figure 4.3.7. The alternative mechanism, further oxidation to form the 2+ form of the trimer and intramolecular radical cation coupling is less likely for two reasons. First, the triplet form of the 2+ indole trimer is unlikely to be the lowest energy state making it unlikely that two radical electron would be present in the 2+ trimer. Secondly, the electrostatic repulsion within the 2+ trimer species would make cyclisation unfavourable.

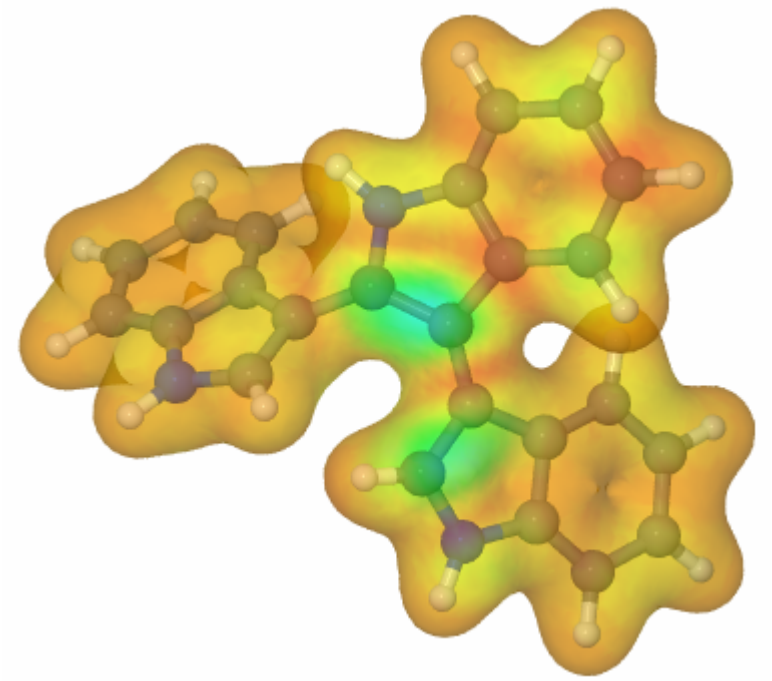

Figure 4.3.6. Spin density distribution mapped onto a 99% electron density isosurface for the radical cation of a linear indole trimer. (The colouring is schematic as follows: blue indicates a positive spin density (0.005) whilst red is negative (-0.001).

Not only does the enhanced computational methodology established in this section therefore give excellent agreement with measured redox processes, it also removes

the systematic underestimation of redox potentials observed in previous works while maintaining the small deviations between calculated and measured redox potentials which are a feature of DFT calculations with continuum solvation models[2,3]. It also provides a method for predicting the coupling reactions of these radical cations. Following the success of the calculations in modelling the redox properties of indoles this method will now be extended to study other related aromatic systems.

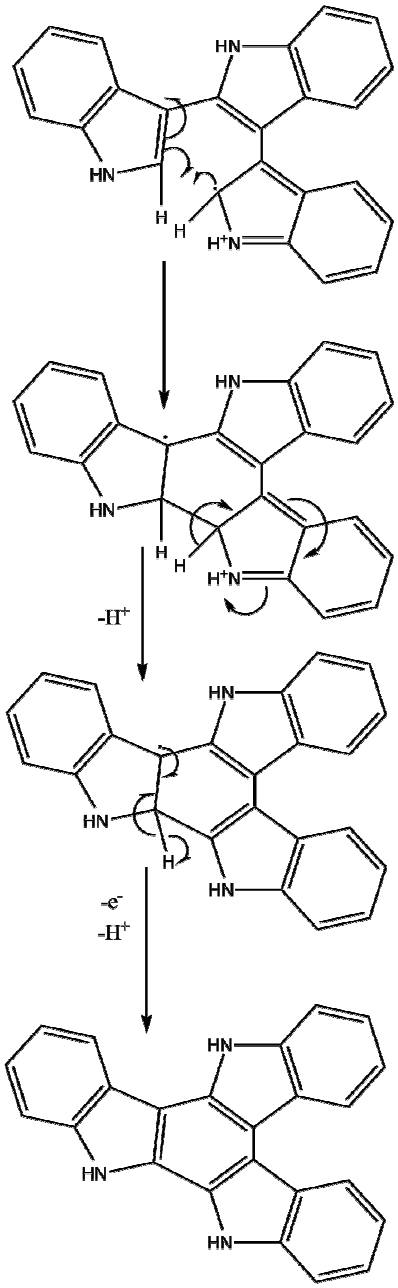

Figure 4.3.7. Suggested cyclisation method for linear trimer of indole.

4.4 Indole Analogues.

While the products of indole electro-polymerisation have been fully characterised,[8,9,10] little work has been performed on the films formed from indole analogues of the form shown in Figure 4.4.1.a. Most work on these systems propose a 2,3-linked polymer analogous to the indole product proposed by Berlin *et al.*[11]. However, given the coupling mechanism now established for indole, it is entirely possible that these molecules may couple in a similar fashion, yielding π-stacking conducting oligomeric films. In this work the oxidation potentials of three analogues of indole have been calculated, as well as the electron spin densities to enable the most probable coupling sites upon electro-oxidation and most probable products to be determined.

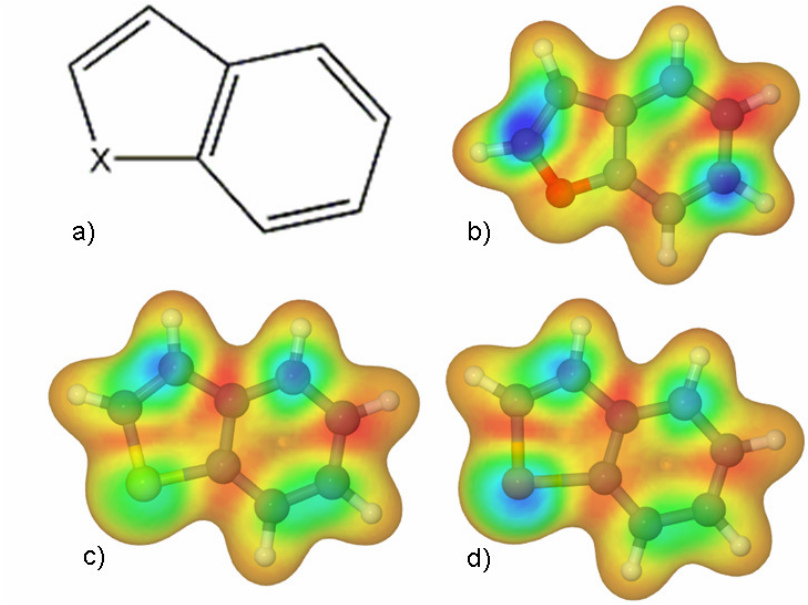

Figure 4.4.1. a) Structure of indole analogues. Spin density distribution mapped onto a 99% electron density isosurface for the radical cations of (b) benzo(b)furan, (c) benzo(b)thiophene, (d) benzo(b)selenophene. (The colouring is schematic as follows: blue indicates a positive spin density (0.005) whilst red is negative (-0.001). The same range of spin density was used for all 3 maps).

Table 4.4.1 shows the calculated and measured oxidation potentials for these indole analogues. If similar errors are applicable to these indole analogue systems as to 5-substituted indoles, this would give a standard deviation of 31 mV in these values. It is clear that the calculated values for the peak oxidation potentials of benzothiophene

and benzoselenophene are in excellent agreement with the experimentally observed values within this experimental error, whilst the benzofuran potential shows a reasonable agreement.

X	Measured peak oxidation potential (vs Fc/Fc^+) / V	Calculated peak oxidation potential (vs Fc/Fc^+) / V
O	1.47	1.38 ± 0.03
S	1.26	1.25 ± 0.03
Se	1.18	1.15 ± 0.03

Table 4.4.1. Measured and calculated oxidation potentials for indole analogues vs Fc/Fc^+. Measurement of oxidation potentials taken from 1 mM solutions in background electrolyte.

The spin density maps for benzothiophene (Figure 4.4.1.c) and benzoselenophene (Figure 4.4.1.d) show a remarkable similarity to the spin density map of indole, with the major difference being the increase in electron spin density on the X group as X is changed from NH to S to Se. Discarding the X group as an unlikely coupling position it can be observed that the largest spin density for each is in the 3-position, as with indole. It is therefore likely that on electro-oxidation benzothiophene and benzoselenophene would couple to form a 3, 3'-dimer analogous to indole.

The spin density map for benzofuran (Figure 4.4.1.b) displays an interesting diversion in behaviour from the other three indole-type systems, in that the region of highest spin density is moved from the 3-position to the 2-position. As with indole the region of highest spin density is likely to be the location of coupling. It is therefore likely that benzofuran will couple in the 2 position initially to form a 2, 2'-dimer.

As with indole it is possible to extend the DFT calculations to consider the oxidation potentials of the dimer species for these indole analogues. Table 4.4.2 shows the calculated peak oxidation potentials for the dimer forms predicted to form from the electro-oxidation of the three indole analogues. It is interesting to note that the oxidation potentials for all three analogues are very similar. As with indole, these

potentials are much less than the monomer oxidation potentials, and oxidation of these dimer species would be expected to rapidly occur at the electrode surface.

Dimer	**Calculated peak oxidation potential (vs Fc/Fc^+) / V**
2, 2'-dibenzofuran	+0.62 ± 0.03
3, 3'-dibenzothiophene	+0.69 ± 0.03
3, 3'-dibenzoselenophene	+0.66 ± 0.03

Table 4.4.2. Calculated oxidation potentials for predicted dimers.

Figure 4.4.2 shows the electron spin density maps of the radical cations of the predicted dimer structures for the three indole analogues. As observed with the 3, 3'-indole dimer the largest electron spin densities are in the uncoupled carbon position in each 5-membered ring. It is therefore likely that coupling of the dibenzo(b)thiophene and dibenzo(b)selenophene species will proceed in a similar manner to that observed within indole (Figure 1.1.4), leading to the formation of asymmetric trimer species. The proposed coupling mechanism for the 2, 2'-dibenzo(b)furan with further benzo(b)furan monomer is shown in Figure 4.4.3. It is interesting that as the 3, 3'-dimers and 2,2'-dimer both possess a symmetry across the dimer bond that the approach of a monomer unit to either dimer species will be predicted to yield the same asymmetric trimer product, as there is 2,2'- 3,3'- and 2,3' coupling present in this trimer, albeit through differing monomer coupling mechanisms.

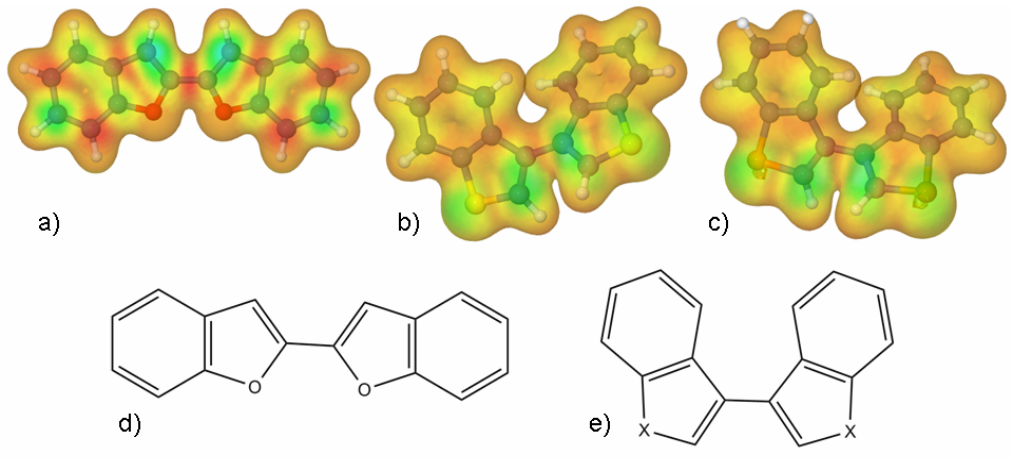

Figure 4.4.2. Spin density distribution mapped onto a 99% electron density isosurface for the radical cations of (a) 2, 2'-dibenzo(b)furan, (b) 3, 3'-dibenzo(b)thiophene, (c) 3, 3'-dibenzo(b)selenophene. (The colouring is schematic as follows: blue indicates a

positive spin density (0.005) whilst red is negative (-0.001). The same range of spin density was used for all 3 maps). Structural forms for (d) 2, 2'-dibenzo(b)furan and (e) 3 ,3'-dimers.

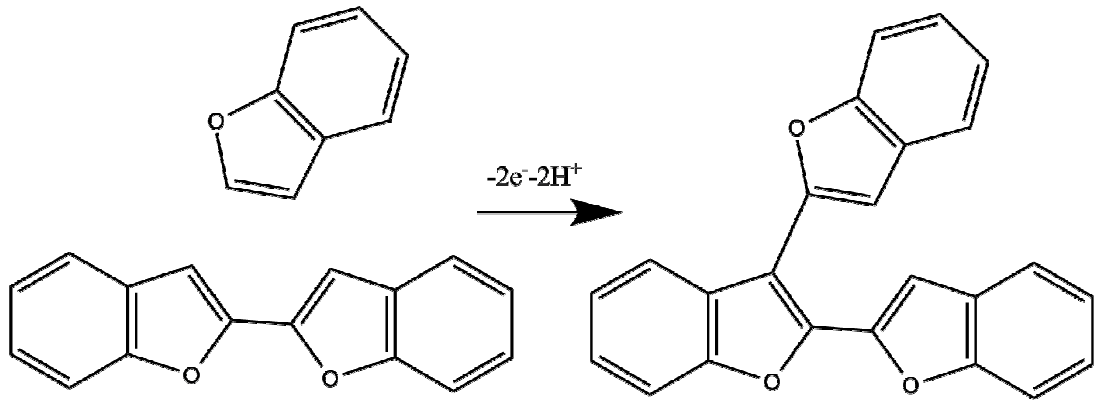

Figure 4.4.3. Proposed coupling reaction scheme of 2, 2'-dibenzo(b)furan with benzo(b)furan to form the linear benzo(b)furan trimer intermediate.

Calculations were then performed on the predicted linear trimer forms of the indole analogues, shown in Figure 4.4.4. As with the indole linear trimer the B3LYP method was again used with the basis set limited to the smaller 6-31G. Table 4.4.3 shows the calculated oxidation potentials for the indole analogues. It can be noted that all three trimer oxidation potentials are significantly lower than the monomer oxidation potential, again allowing for the increase in error associated with using the smaller basis set. These trimers would again be expected to oxidise readily at the electrode surface. It can be noticed for all the indole and indole analogue calculations that the calculated potential for monomer is always highest, with the monomeric species, a lower potential is then calculated for the dimer species as would be expected with the increase in conjugation length. It can be noted for all species that the calculated trimer oxidation potential are higher than the calculated oxidation potential for dimers. There are two possible explanations for this increase in oxidation potential, either it is an indicator of a real molecular property with the trimer being forced into a conformation where the effective conjugation length is reduced with respect to that of the dimer; or it is an artefact of the lower basis set and resulting decrease in accuracy of performing the trimer calculations.

Trimer	Calculated peak oxidation potential (vs Fc/Fc^{+}) / V
Benzofuran	+0.92 ± 0.06
Benzothiophene	+0.85 ± 0.06
Benzoselenophene	+0.89 ± 0.06

Table 4.4.3. Calculated oxidation potentials for predicted trimers.

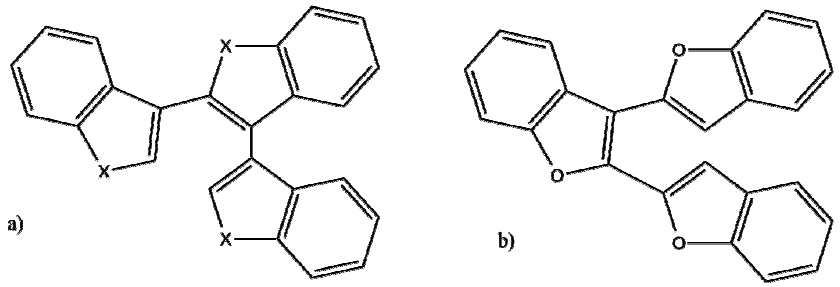

Figure 4.4.4. Predicted linear trimers for (a) benzo(b)thiophene, benzo(b)selenophene and (b) benzo(b)furan.

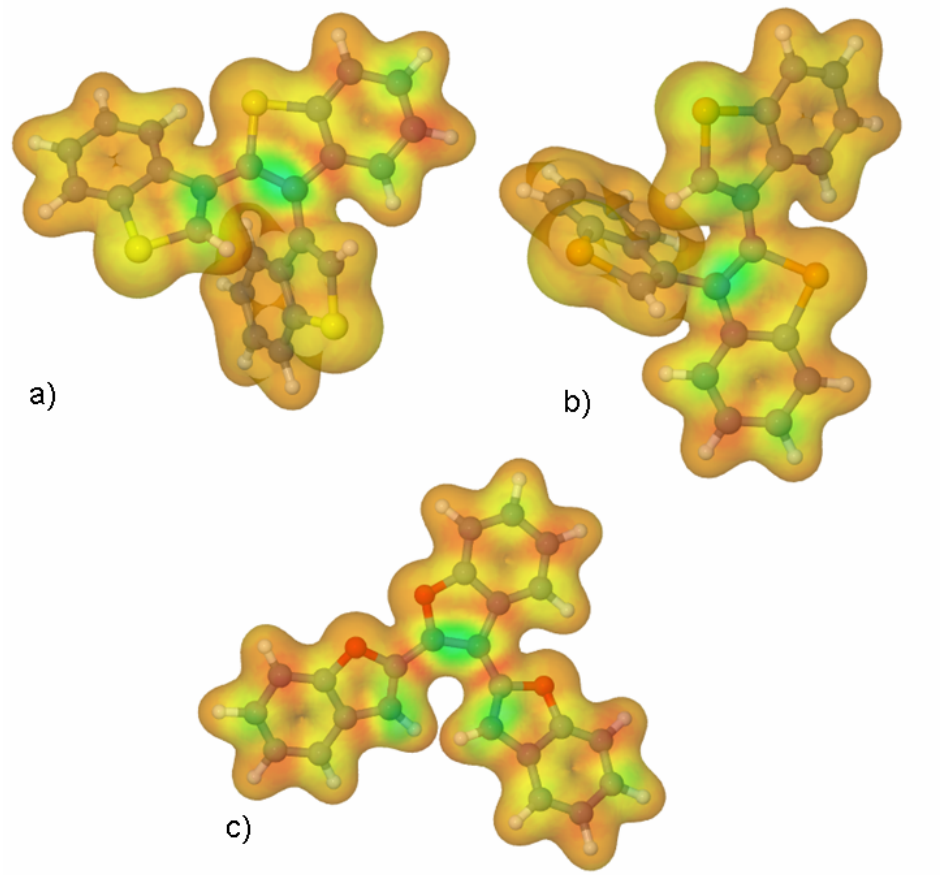

Figure 4.4.5. Spin density distribution mapped onto a 99% electron density isosurface for the radical cations of linear trimers of (a) benzo(b)thiophene, (b) benzo(b)selenophene and (c) benzo(b)furan. (The colouring is schematic as follows: blue indicates a positive spin density (0.005) whilst red is negative (-0.001). The same range of spin density was used for all 4 maps).

The calculated electron spin densities for the trimer radicals are shown in Figure 4.4.5. It is interesting to note that the electron spin density maps for benzo(b)thiophene and benzo(b)selenophene are similar to that observed for indole (Figure 4.3.6), which suggests that the method of cyclisation may be similar to that discussed previously for indole and shown in Figure 4.3.7. The electron spin density of the benzo(b)furan, however, shows the location of the spin density to be equally probable on either of the unlinked 3-positions. Cyclisation may then take place through one of the mechanisms shown in Figure 4.4.6. As with indole cyclisation could also occur through formation of the 2+ trimer radicals. Such cyclisation is not thought to be the most probable coupling mechanism as firstly, the triplet form of the 2+ trimers is unlikely to be the lowest energy state there is therefore little chance that two radical electrons would be present in the 2+ trimers. Secondly, the electrostatic repulsion within the 2+ trimer species would make its formation and therefore cyclisation unfavourable.

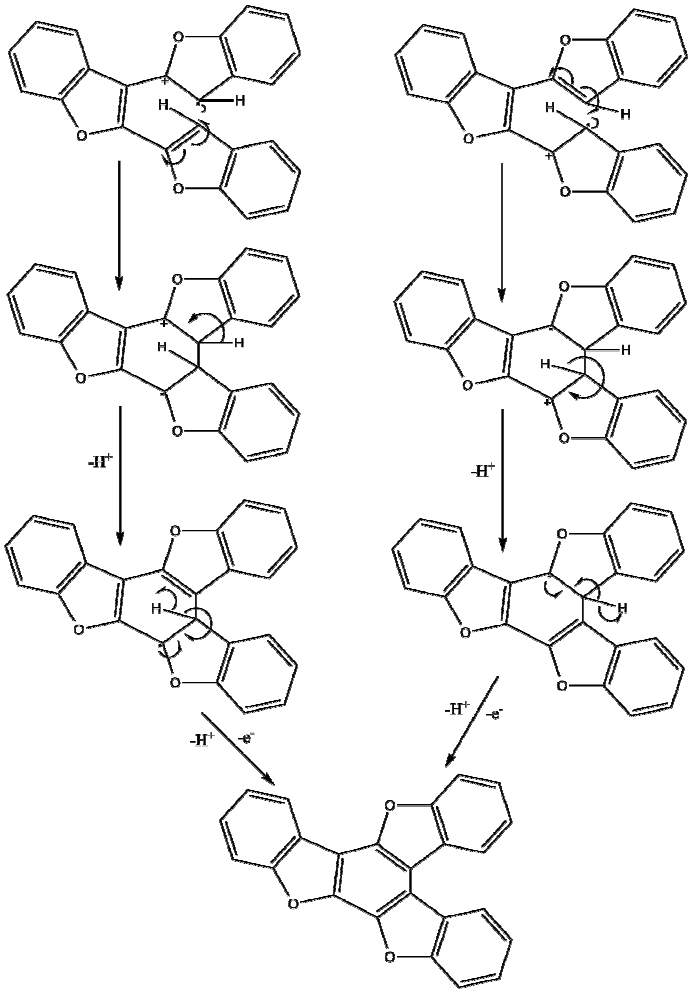

Figure 4.4.6. Proposed cyclisation mechanisms for benzo(b)furan.

It is therefore predicted that all three species will yield the asymmetric trimer product. Work carried out in conjunction with a Masters Project student, Becky Choules, on the electro-oxidation of indole and indole analogues has looked at the fluorescence spectra of benzo(b)thiophene, benzo(b)selenophene, indole, and films formed from their electro-oxidation. The excitation and emission spectra of the monomer and film of oxidised benzo(b)thiophene are shown in Figure 4.4.7, with corresponding spectra for benzo(b)selenophene in Figure 4.4.8 and indole in Figure 4.4.9. All spectra were recorded in ethanol at concentrations of around 10^{-6} M. It can be seen that the (0, 0) transitions of the dissolved film species (388 nm for benzo(b)thiophene, 403 nm for benzo(b)selenophene and 430 nm for indole) are significantly red-shifted from those of the monomers (297 nm for benzo(b)thiophene, 283 nm for benzo(b)selenophene and 293 nm for indole). This red-shifting of the

fluorescence spectra is consistent with an increase in electronic delocalisation in the product[12]. The red-shifitng of around 100 nm or more observed for each species is indicative that the three products have similar electronic conjugation lengths, consistent with the formation of trimer products for all species. The similarity in the patterns of the fluorescence excitation and emission spectra also provides a strong indication that a similar product is formed in each case. FAB mass spectrometry was performed on a sample produced by electro-oxidation of a 100 mM solution of benzo(b)thiophene. This showed a molecular ion peak at 369 Da, in exact agreement with the mass of a benzo(b)thiophene cyclic trimer product (369 Da).

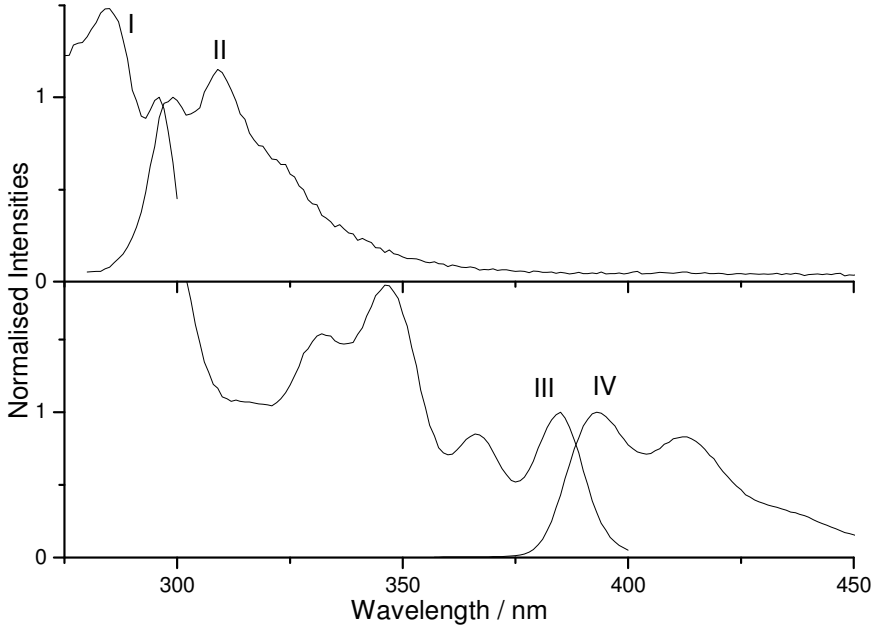

Figure 4.4.7. Excitation and emission spectra respectively for benzo(b)thiophene (I and II) and a film formed from benzo(b)thiophene electro-oxidation (III and IV) in ethanol. The emission wavelengths were 310 and 410 nm for I and III respectively, and the excitation wavelengths were 270 and 347 nm for II and IV respectively. Intensities were normalised to the peak intensities for the $S_0 \rightarrow S_1$ transition for excitation spectra, and the peak intensities for the $S_1 \rightarrow S_0$ transition for emission.

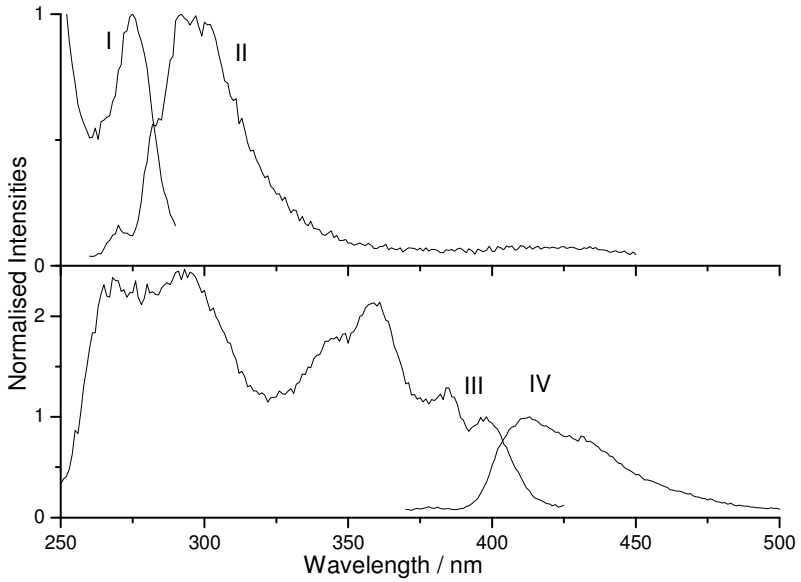

Figure 4.4.8. Excitation and emission spectra respectively for benzo(b)selenophene (I and II) and a film formed from benzo(b)selenophene electro-oxidation (III and IV) in ethanol. The emission wavelengths were 300 and 435 nm for I and III respectively, and the excitation wavelengths were 250 and 360 nm for II and IV respectively. Intensities were normalised to the peak intensities for the $S_0 \rightarrow S_1$ transition for excitation spectra, and the peak intensities for the $S_1 \rightarrow S_0$ transition for emission.

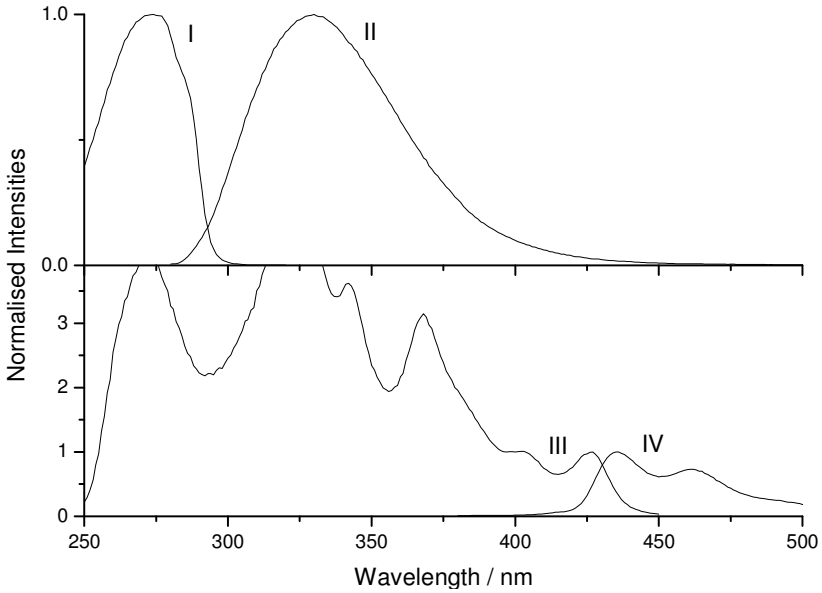

Figure 4.4.9. Excitation and emission spectra respectively for indole (I and II) and a film formed from indole electro-oxidation (III and IV) in ethanol. The emission wavelengths were 330 and 425 nm for I and III respectively, and the excitation wavelengths were 270 and 370 nm for II and IV respectively. Intensities were normalised to the peak intensities for the $S_0 \rightarrow S_1$ transition for excitation spectra, and the peak intensities for the $S_1 \rightarrow S_0$ transition for emission.

It can clearly be observed that the oxidation potential for these indole analogues can be calculated to a reasonable accuracy. Analysis of the electron spin densities of these molecules also suggests that the product formed by their electro-oxidation is likely to be similar to the product of indole electro-oxidation, albeit in the case of benzo(b)furan arising from a different coupling mechanism. It is now clear that the formation of a similar product is supported by initial fluorescence and mass spectroscopic data.

4.5 1,4,5,8,9,12-Hexamethyltriphenylene.

The next system to be studied computationally is 1,4,5,8,9,12-hexamethyltriphenylene (hmtp, Figure 4.5.1.a) synthesised by the Galow group[13] in the University of Edinburgh. This molecule is interesting due to the high steric strain in this aromatic system which leads to it being far more reactive than its non-strained cousins such as triphenylene (Figure 4.5.1.b), with this reactivity being driven by release of steric strain[14,15]. The electrochemical properties of hmtp were therefore calculated to further test the reliability of the B3LYP method with $In^{+\bullet}$/In again as the reference reaction for this heterocyclic system.

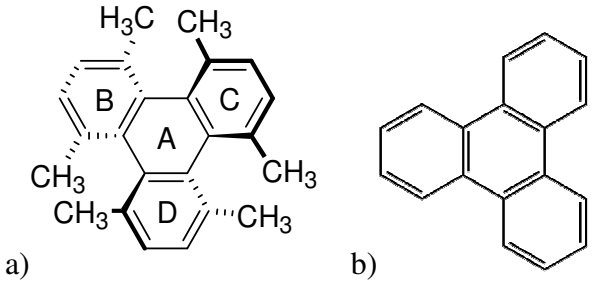

Figure 4.5.1. (a) Structure of hmtp showing ring assignments and non-planar geometry. (b) Structure of triphenylene.

Figure 4.5.2 shows the CV of hmtp, which shows a chemically irreversible one-electron oxidation wave (E_p = +1.01 V vs Fc/Fc^+, with $E_p - E_{1/2}$ = 79mV). Unsubstituted triphenylene shows an analogous irreversible one electron oxidation (E_p = +1.50 V vs Fc/Fc^+)[16]. The lower hmtp value is consistent with the electron-donating properties of the six methyl substituents and the increase in steric strain which destabilises the neutral molecule. Calculations of the oxidation potential of

hmtp gave a predicted oxidation potential of +1.06 ± 0.03 V vs Fc/Fc^+ which is in good agreement with the observed value, a part of the difference between the calculated and measured oxidation potential may be the assumption of electrochemically reversible electron transfer, as there is significant variation of $E_p - E_{1/2}$ from the reversible value of 57 mV.

The calculated structure of the hmtp radical cation shows an increased twist in the naphthalene substructure, with rings A and D exhibiting a 60° end-to-end twist compared to 53° in the neutral molecule. Figure 4.5.3 shows the electrostatic potential maps for these optimised geometries of the neutral and radical cation forms of hmtp. This shows a decrease in the π-bonding and delocalisation after oxidation at the A and D ring interface. This can be seen more clearly in Figure 4.5.4 which shows a bright blue region of the highest probability for the location of the unpaired electron at the interface of rings A and D. This decrease in electron density with respect to the neutral molecule in these positions leads to an increase in the importance of the steric repulsion in this section of the molecule. This is accompanied by a decrease in the bond strength which explains the increase in the end-to-end twist of the molecule.

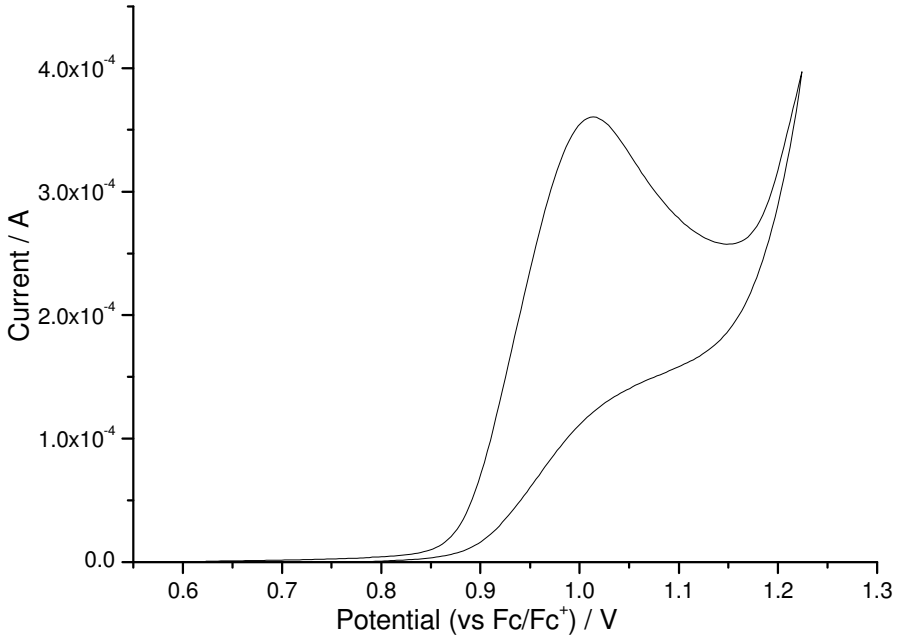

Figure 4.5.2. Cyclic voltammogram of hmtp at a concentration of 1 mM in background electrolyte with v = 100 mVs^{-1}.

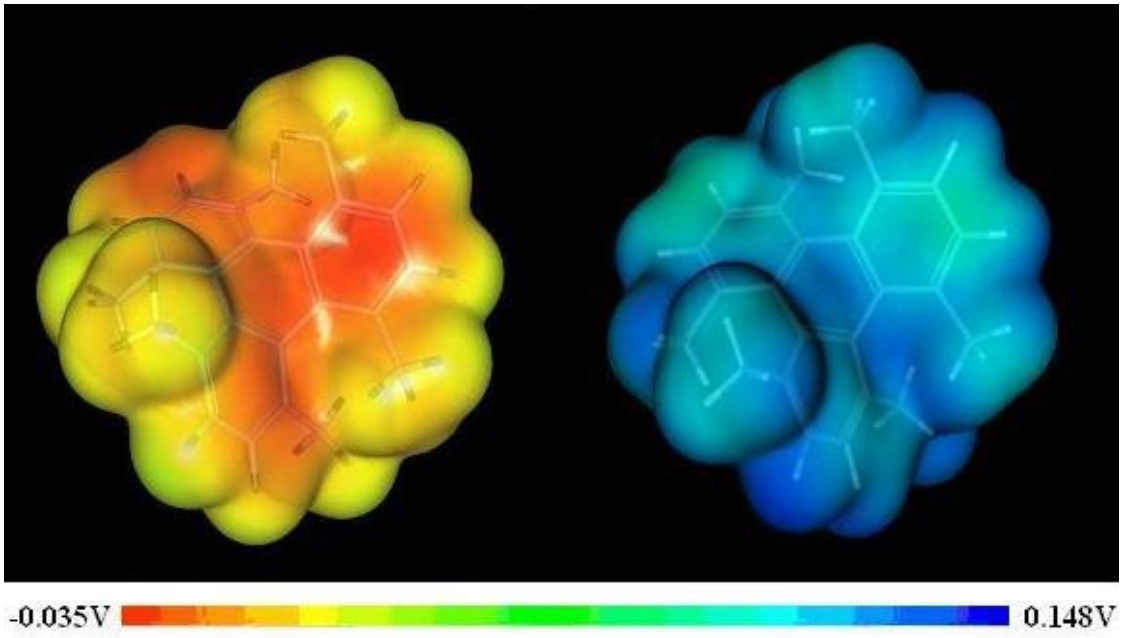

Figure 4.5.3. Electrostatic potential maps for the optimised geometries of hmtp and hmtp$^{+\bullet}$. Red is electron-rich, blue is electron-poor.

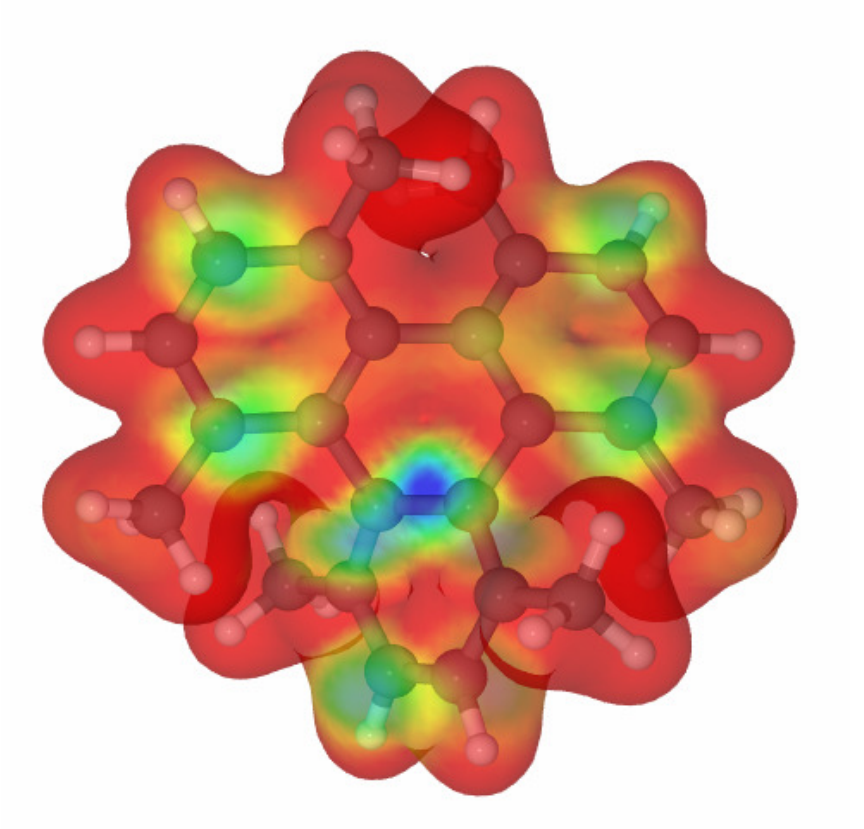

Figure 4.5.4. Spin density distribution mapped onto a 99% electron density isosurface for the radical cation of hmtp. (The colouring is schematic as follows: blue indicates a positive spin density (0.005) whilst red is zero.

4.6 Pyrrolo[3,2,1-jk]carbazole.

Pyrrolo[3,2,1-jk]carbazole (PC, Figure 4.6.1.a) has previously been the subject of a computational analysis within the Mount group. This study by Chapman[6] used the B3PW91 method with solvation modelled using the COSMO model and a Fc/Fc^+ reference. However, this method had a systematic error which underestimated the oxidation potentials of indoles by 190 mV. PC was therefore studied with the new methodology using $In^{+\bullet}/In$ as reference, which has already shown good agreement with experimentally observed data for a range of molecules.

The calculated peak oxidation potential for PC**,** using this new methodology is 1.07 ± 0.03 V vs. Fc/Fc^+. The reported[17] peak oxidation potential for PC is 0.98V vs Fc^+/Fc, which is in reasonable agreement with this calculated value. Due to poor solubility of the product formed from electro-oxidation of PC the product and coupling mechanism is thus far unknown. However, by consideration of the electron-spin density map a probable coupling mechanism may be proposed. Figure 4.6.1.b clearly shows that the greatest electron spin density is located on the PC 4-position, which is analogous to the 3-position on indoles. This suggests that if coupling occurs between radical cation pairs the most likely initial product will be a 4, 4'-dimer. This result was also predicted by Chapman's computational study of PC**.**

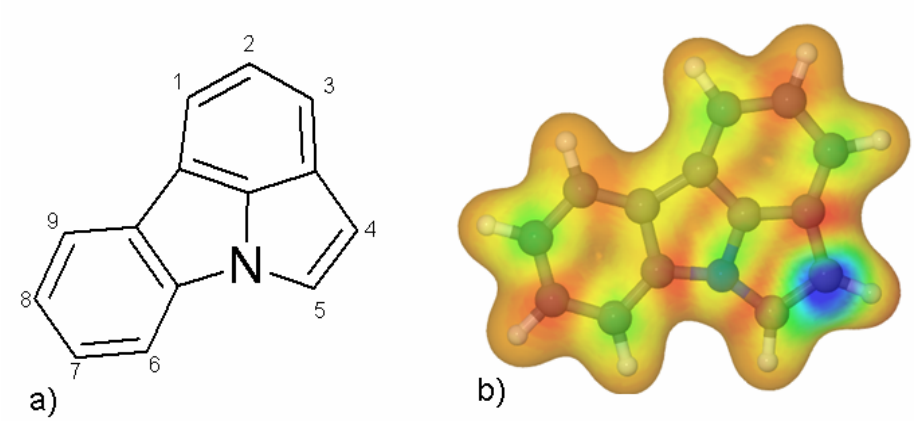

Figure 4.6.1. a) Structure and numbering system for PC. b) Spin density distribution mapped onto a 99% electron density isosurface for the radical cation of PC. (The colouring is schematic as follows: blue indicates a positive spin density (0.005) whilst red is negative (-0.001).

As with indole and its analogues, calculations can be performed on the predicted 4, 4'-PC dimer. The calculated peak oxidation potential for this dimer species is +0.34 V vs. Fc/Fc^{+}, this is significantly lower than the peak oxidation potential of the PC monomer, and any dimer formed would be expected to oxidise rapidly at the electrode surface after coupling. Once more, consideration of the location of the electron spin density of the dimer radical cation can indicate where, if at all, further coupling may be expected. Figure 4.6.2.a shows this data, with the greatest electron spin density at the unbonded 5-positions of the PC dimer, analogous to the 2-position on 3, 3'-diindole formed prior to trimerisation. This introduces the possibility of the formation of an asymmetric trimer of PC via the mechanism shown in Figure 4.6.3.

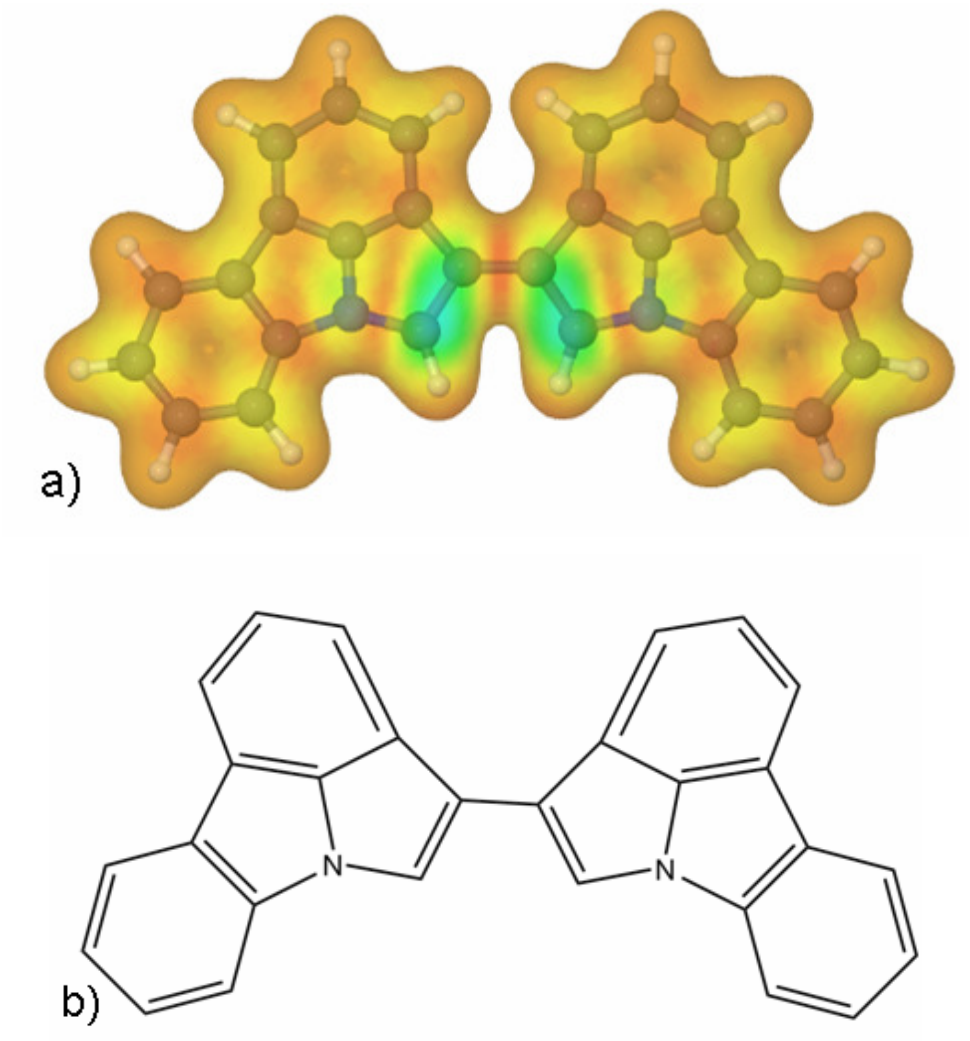

Figure 4.6.2. (a) Spin density distribution mapped onto a 99% electron density isosurface for the radical cation of 4, 4'-diPC. (The colouring is schematic as follows: blue indicates a positive spin density (0.005) whilst red is negative (-0.001). (b) Proposed structure of 4, 4'-diPC.

It is not clear whether formation of this timer is probable or would be restricted by steric clashing of the aromatic rings. A geometry optimisation calculation was therefore performed on an asymmetric trimer to observe to what effect the steric effects of the aromatic rings would have on the structure of a possible asymmetric trimer. This calculation used the B3LYP functional; due to the large number of nuclei in the molecule the basis set was restricted to the smaller 6-31G basis set to decrease computational time. The calculated geometry of the PC asymmetric trimer is shown in Figure 4.6.4. It is clear that the steric clashing of the aromatic rings would lead to a non-planar structure in the trimer. This result suggests that if PC trimer formation is possible the resulting trimer will be a strained aromatic heterocycle. Further experimental studies on the coupling of PC are planned to resolve the nature of this PC electro-oxidation product.

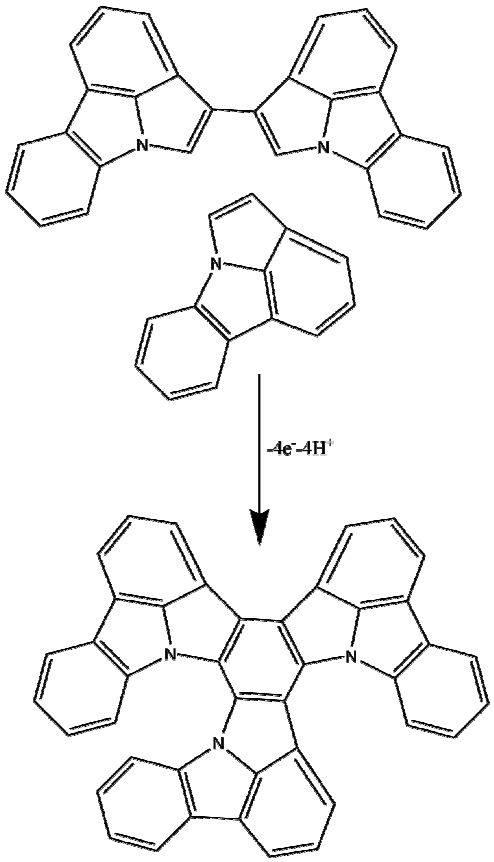

Figure 4.6.3. Possible mechanism for further coupling of PC dimer with further PC monomer.

a) 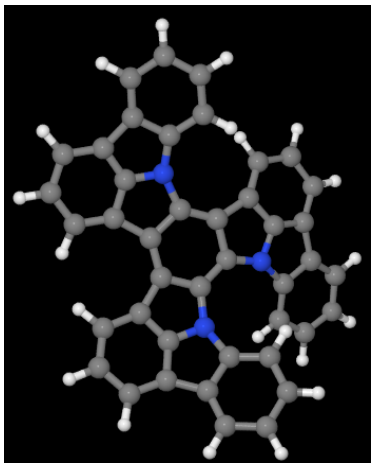 b) 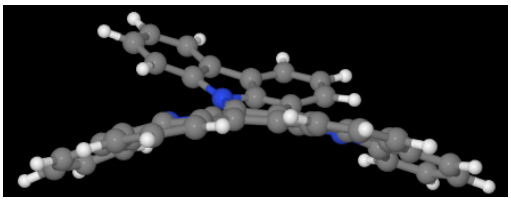

Figure 4.6.4. Possible geometry for an asymmetric trimer of PC. (a) "Top" view and (b) "side" view.

4.7 Dibenzoselenophenes.

The structures of 2,5–dibenzoselenophene (dbs) and 2,5–dibenzo–3,4-diazaselenophene (dbas) are shown in Figure 4.7.1. These molecules were synthesised in the Chemistry Department of the University of Saint Andrews by Professor Woollins' group. They were proposed as a possible species to act as a monomer for electrochemical polymerisation. It was thus decided to study these molecules electrochemically and submit them to calculations to assess their suitability for the formation of conducting polymers.

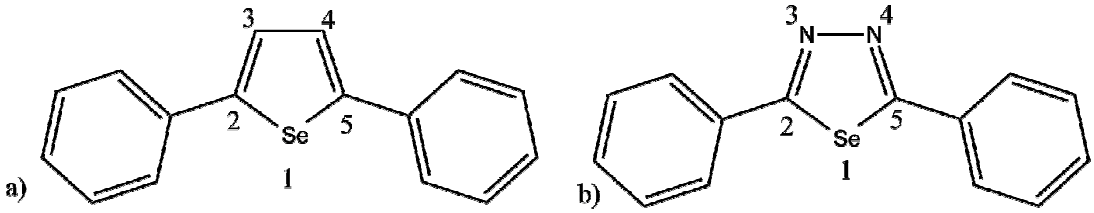

Figure 4.7.1. Structures of (a) 2,5-dibenzoselenophene and (b) 2,5-dibenzo-3,4-diazaselenophene.

CV's of dbs and dbas are shown in Figure 4.7.2 and Figure 4.7.3 respectively. It can be observed that dbs shows two oxidation processes with peak oxidation potentials of +0.82 V and + 0.98 V vs Fc/Fc^+. The CV of dbas does not show a distinct oxidation peak, but shows a broad oxidation feature around +1.4 to +1.6 V vs Fc/Fc^+. The oxidations of both species were chemically irreversible, and showed no evidence for

conducting film growth at any concentrations studied, although a non-conducting layer of material was formed on the Pt surface of the electrode.

The calculated first peak oxidation potentials were +0.80 ± 0.03 V and +1.54 ± 0.03 V vs Fc/Fc^+ for dbs and dbas respectively. The first oxidation potential for dbs is in good agreement with the measured oxidation potential, while the calculated peak oxidation potential for dbas coincides with the broad oxidation peak observed within the CV. Figure 4.7.4 shows the electron spin density maps for the radical cations of each species. It can be seen for both dibenzoselenophenes that the majority of the electron spin density is found on the 2 and 5 positions of the central selenophene ring and not delocalised on to the benzene rings. The location of the electron spin density on the central ring would make the cation-cation coupling observed with indoles and other heterocyclic species unlikely, which accounts for the lack of futher coupling. The formation of a non-conducting layer on the electrode surface does, however, suggest that some chemical reaction of radical cations may occur.

The calculations in combination with the electrochemical measurements suggest that these dibenzoselenophenes make poor candidates for the formation of conducting polymer films.

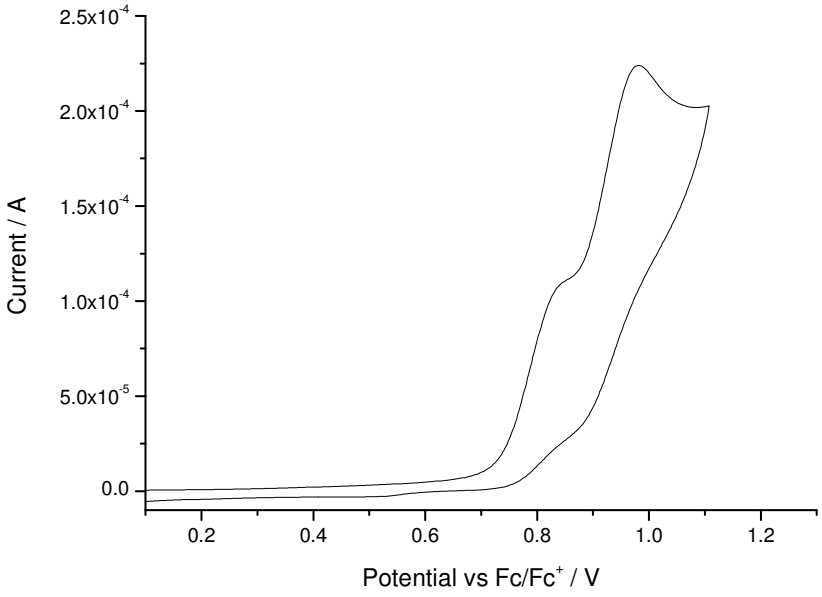

Figure 4.7.2. CV of 1 mM dbs in acetonitrile and background electrolyte. Sweep rate = 100 mVs^{-1}.

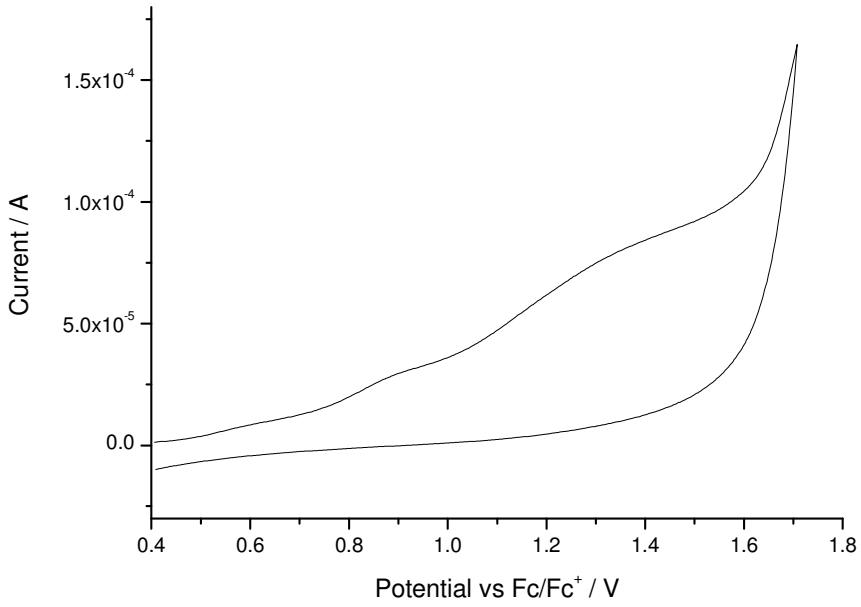

Figure 4.7.3. CV of 1.1 mM dbas in acetonitrile and background electrolyte. Sweep rate = 100 mVs^{-1}.

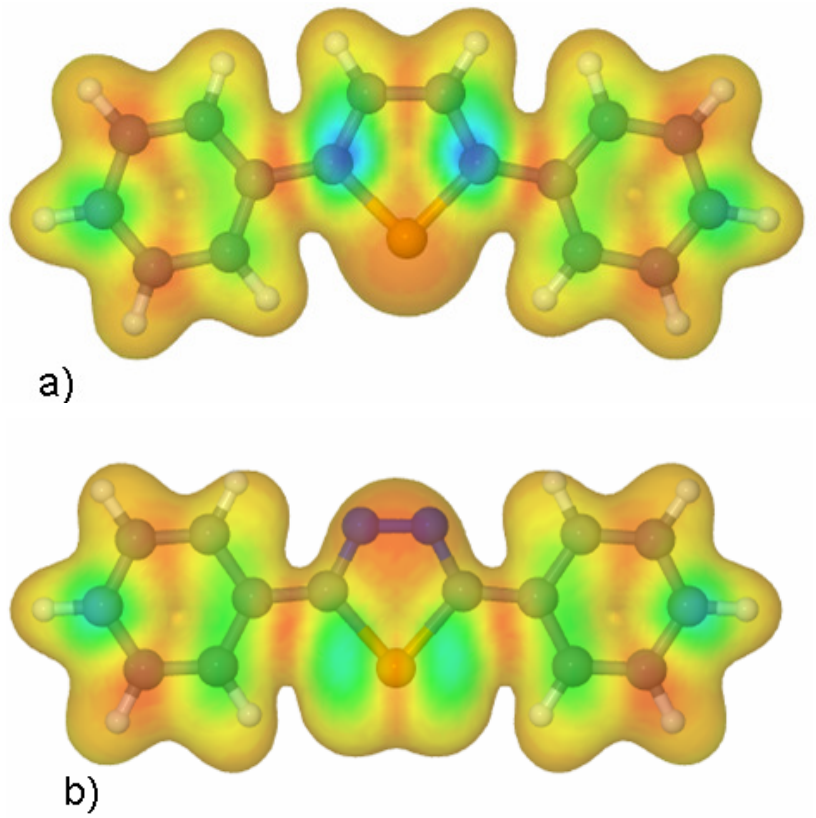

Figure 4.7.4. Spin density distribution mapped onto a 99% electron density isosurface for the radical cations of (a) dbs and (b) dbas. (The colouring is schematic as follows: blue indicates a positive spin density (0.004) whilst red is negative (-0.001).

4.8 Assessing the Quality of the General Computational Method.

As calculations have now been performed on a wide range of heteroaromatic molecules, it is therefore possible to discuss the quality of the calculations overall in calculating experimental results, extending the analysis performed on indole systems in Section 4.3. Figure 4.8.1 shows all calculated peak oxidation potentials plotted versus their experimentally measured peak oxidation potentials. Overall the peak oxidation potentials predicted from these DFT calculations show good agreement with the experimental data, with no significant systematic errors in the calculation and a calculated standard deviation of 32 mV. This is consistent with the error limits previously assigned to these calculations for indole alone, supporting the hypothesis that a similar error may apply to a range of heteroaromatics.

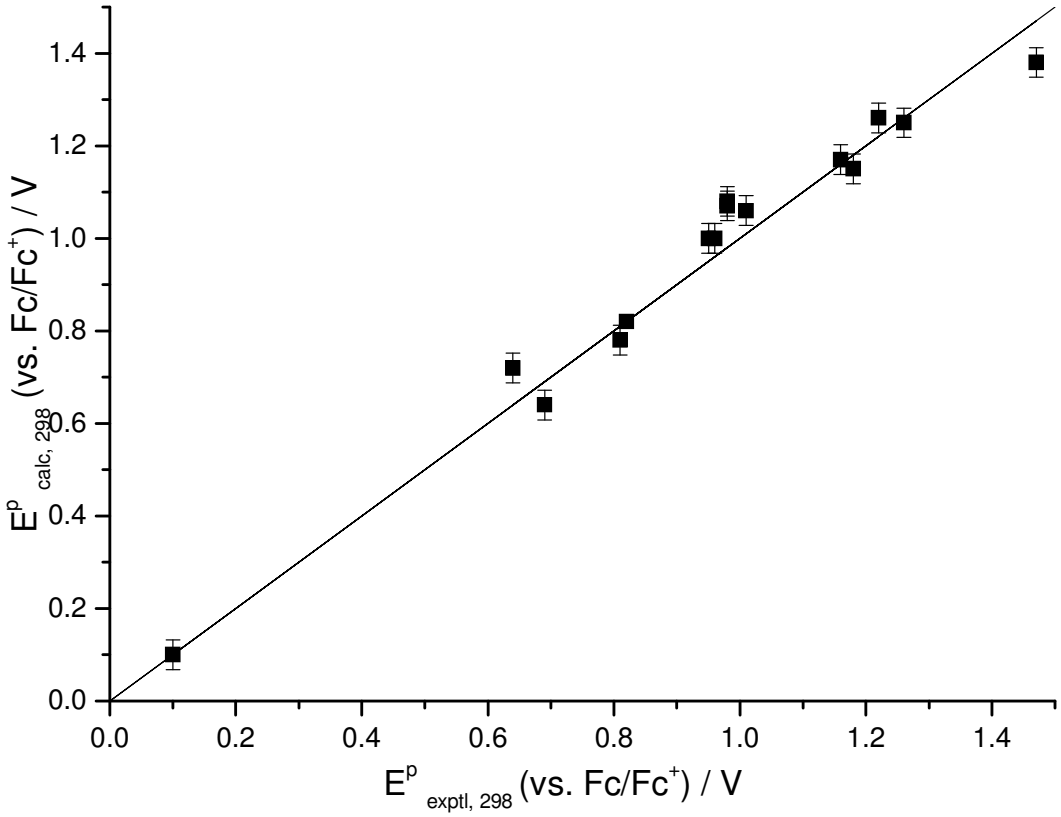

Figure 4.8.1. Plot of $E_{pa,298,c}$ *vs.* $E_{pa,293}$ for calculated peak oxidation potentials for all molecules discussed in this chapter. The line shows the relationship if the calculated and experimental data were equal.

4.9 Conclusions.

In this chapter a revised methodology for predicting the oxidation potentials for a range of heterocyclic species has been devised, using indole as a reference redox process as opposed to the Fc^+/Fc couple used previously. This methodology has proved to be extremely successful. Previous DFT calculations within the Mount group by Kettle and Chapman appeared to show a systematic underestimation of the redox potentials of heteroaromatic systems. Although these previous calculations differed from this work through their choice of DFT functional, basis set and solvation model, it is unlikely that either of these factors would account for the systematic errors observed. Where these methods differed greatly from this work was through the choice of the Fc^+/Fc redox couple as reference. It is probable that an under-calculation of this redox potential led to the systematic error observed, through inadequate functionals or basis sets for the calculation of energies of species containing a transition metal. It has also been shown again that consideration of the spin density distributions of radical cations can aid in the understanding of coupling between radical cations on electro-oxidation, can explain the observed change in structure of a highly strained heterocycle upon oxidation, predict the suitability of aromatic systems for formation of electro-active films and predict the likely products.

4.10 References.

[1] Moore, G. E. *Electronics* **1965**, *38*, Number 8.

[2] Fu, Y.; Liu, L.; Yu, H-Z.; Wang, Y-M.; Guo, Q-X. *J. Am. Chem. Soc*, **2005**, *127*, 7227.

[3] Kettle, L. J.; Bates, S. P.; Mount, A. R. *Phys. Chem. Chem. Phys.* **2000**, *2*, 195-201.

[4] Kettle, L. J. *Ph. D. Thesis, "A Computational and Electrochemical Study of Electropolymerised Indoles", University of Edinburgh* **2000**

[5] Baik, M-H.; Friesner, R. A. *J. Phys. Chem. A*, **2002**, *106*, 7407.

[6] Chapman, M. A. *Ph. D. Thesis, "The Electropolymerisation of Indolo[3,2,1-jk]carbazole and Pyrollo[3,2,1-jk]carbazole: An Electrochemical, Computational and Spectroscopic Study.", University of Edinburgh* **2003**.

[7] Bard, A. J.; Faulkner, L. R. "*Electrochemical Methods Fundamentals and Applications*"; John Wiley & Sons (USA) **2001**.

[8] Xu, J.; Nie, G.; Zhang, S.; Han, X.; Pu, S.; Shen, L.; Xiao, Q. *Eur. Polym. J.* **2005**, *41*, 1654-1661.

[9] Wang, F.; Shi, G.; Chen, F.; Xu, J.; Zhang, J. *J. Electroanal. Chem.* **2001**, *510*, 29-34.

[10] Xu, J; Shi, G.; Zahng, J.; Hong, X. *Macromol. Chem. Phys.* **2002**, *203*, 2385-2390.

[11] Berlin, A.; Canavesi, A.; Schiavon, G.; Zecchin, S.; Zotti, G. *Tetrahedron* **1996**, *52*, 7947.

[12] Jennings, P.; Jones, A. C.; Mount, A. R. *J. Chem. Soc. Faraday Trans.* **1998**, *94*, 3619.

[13] Wang, Y.; Stretton, A. D.; McConnell, M. C.; Wood, P. A.; Parsons, S.; Henry, J. B.; Mount, A. R.; Galow, T. H. *J. Am. Chem. Soc.* **2007**, *129*, 13193-13200.

[14] Tani, K.; Stoltz, B. M. *Nature* **2006**, *441*, 731-734.

[15] Shibata, K.; Kulkarni, A. A.; Ho, D. M.; Pascal R. A., Jr. *J. Org. Chem.* **1995**, *106*, 428-434.

[16] Nishinaga, T.; Inoue, R.; Matsuura, A.; Komatsu, K. *Org. Lett.* **2002**, *4*, 1435-1438.

[17] Wharton, S. I. *Ph. D. Thesis, "Synthesis and Characterisation of Novel Conducting Films Based On Indolo[3,2,1-jk]carbazole Systems.", University of Edinburgh* **2005**.

Chapter 5: Indolo[3,2,1-jk]carbazole Systems.

5.1 Introduction.

There has been recent interest in the chemical synthesis and characterisation of films formed from indolocarbazoles. For example, indolocarbazole derivatives have been reported as efficient hole transport materials, offering potential for organic thin film transistors[1,2,3], while indolo[2,3-a]carbazole has been investigated as a potential anion sensing material[4]. Previously the Mount group has reported on synthetic routes to indolo[3,2,1-jk]carbazole (IC) and a variety of 5-substituted derivatives[5, 6] (Figure 5.1.1). Films resulting from the electrooxidation of these ICs have been found to be highly conducting, redox active and luminescent. It was also observed that the IC formed films contained three specific dimer species (Figure 5.1.1.b-d) rather than polymers. Small molecules have the advantage of being able to produce, through their enhanced packing efficiency compared to polymers, homogeneous multilayers, often with enhanced materials properties. In reality small molecule thin film properties can be less desirable, due to the difficulty in obtaining optimum molecular ordering when depositing films from solution. Additionally, formation of dimers or more extended oligomers generally requires specific chemical synthesis, both for site specific coupling and also for monomer formation, which increases complexity and cost at a decreased yield. The formation of specific IC oligomers through electrochemical monomer oxidation and coupling overcomes both of these issues and allows selective direct electrochemical functionalisation (for example individual micro- or nanoelectrode elements in a sensor array). It also avoids the distribution of chain lengths typically found in most redox-active polymer films formed via electrooxidation of monomers, which can affect a materials performance. IC based films are, therefore, of great interest.

It has previously been observed with indoles that it is possible to control molecular properties through substitution in the indole 5-position[7]. In the previous chapter it was also shown that calculations on these species allow predictions of these

properties to a good level of accuracy. In this chapter a similar approach is used to investigate substituted-ICs. The electrochemical behaviour of 5-methylIC is presented and compared to experimental results for IC. Calculations of the peak oxidation potentials and radical cation spin densities of a range of 5-substituted ICs and related species are also presented in order to predict substituted-IC molecular properties. These calculations will be validated by comparison with values previously measured experimentally and those obtained for synthesised 5-methylIC species.

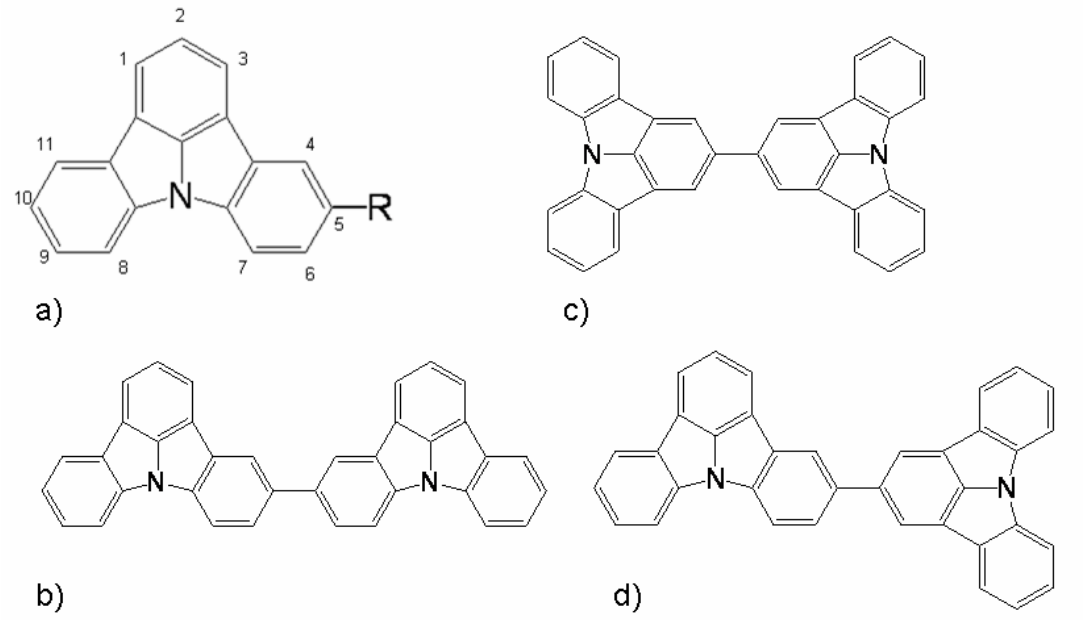

Figure 5.1.1. a) Structure and numbering system for 5-substituted indolo[3,2,1-jk]carbazoles. Structures of b) 5, 5'-IC dimer, c) 2, 2'-IC dimer and d) 2, 5-IC dimer.

5.2 Electrochemistry of 5-Methylindolo[3,2,1-jk]carbazole.

5.2.1 Cyclic Voltammetry of 5-Methylindolo[3,2,1-jk]carbazole.

The CVs resulting from the first three sweeps in a solution of 5-methylIC are shown in Figure 5.2.1. Cycle 1 shows an oxidation with a peak potential of +0.99 V vs Fc/Fc^+, with $E_p - E_{p/2}$ = 70 mV, which results in the deposition of a green film. On the reverse sweep a small reduction peak is observed around + 0.85 V. A similar peak is also observed with IC[5], but the reduction peak observed for 5-methylIC is larger than that observed for IC at the same sweep rate. The coupling mechanism for

IC is given by Scheme 5.2.1. These peaks can be attributed to the oxidation of IC and reduction of $IC^{+\bullet}$ respectively.

$$2IC \underset{+2e^-}{\overset{-2e^-}{\rightleftharpoons}} 2IC^{+\bullet} \xrightarrow{k} (IC)_2 + 2H^+$$

Scheme 5.2.1. Coupling mechanism for IC with coupling rate constant.

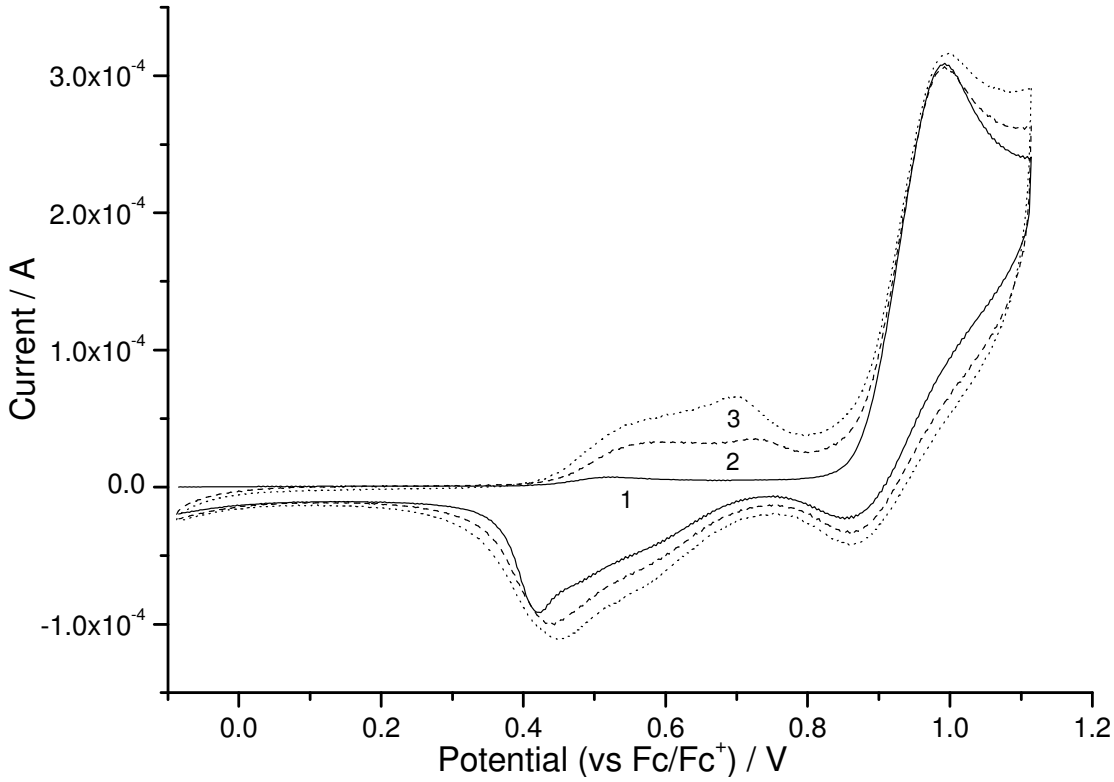

Figure 5.2.1. CVs of 1.25mM 5methylIC solution in background electrolyte. Sweep rate =100mV s^{-1}. Numbers indicate cycle numbers.

The larger reduction peak for the 5-methylIC radical cation therefore indicates that the coupling rate constant, k, is smaller than for the unsubstituted IC. This could either be due to a lower reactivity, the result of blocking a coupling site, or a combination of the two. Due to the similarity in peak potentials of 5-methylIC and IC (0.99 V and 1.01 V vs. Fc/Fc^+, respectively), the reactivity of the two is likely to be similar, suggesting the decrease in the coupling rate constant is due to the effects of blocking.

Continued cycling leads to a growth in two oxidation peaks around +0.60 V and +0.70 V and two associated reduction peaks around +0.55 V and +0.40 V. These peaks can be attributed to the redox oxidation and reduction of a surface film, which shows that appreciable coupling of monomer occurs upon oxidation at +1.00 V to create this electroactive film. This behaviour is similar to that observed for other ICs[5], but was not observed at such low concentrations for indoles[7], which follow a similar radical cation coupling mechanism[†]. The presence of an electroactive insoluble film was confirmed by removing the electrode from this solution, washing with background electrolyte and cycling this modified electrode in background electrolyte. The peaks observed were similar in height and identical in position as those observed in monomer solution.

The charge, Q, associated with the film redox process was found to be 31% of the monomer oxidation charge associated with coupling (given by the difference between the calculated charges from the IC oxidation and $IC^{+\bullet}$ reduction peaks ($Q_{IC+\bullet,\,ox} - Q_{IC+\bullet,\,red}$). This is comparable to the charges obtained on film formation in IC[5] indicating that the coupling and redox reactions observed with 5-methylIC are similar to those observed for IC.

Figure 5.2.2 shows CVs of varying sweep rate, v, for 5-methylIC. As discussed in section 2.1.1, for monomer oxidation the peak current, i_p, should be proportional to $v^{1/2}$ consistent with a system undergoing electron transfer under diffusion control in solution. It is clear (Figure 5.2.3) that the data shown in Figure 5.2.2 follow this relationship.

[†] As indole coupling leads to formation of an asymmetric cyclic trimer requiring coupling of three monomer radical cations it may be expected that indole coupling would occur only at higher concentrations, if similar coupling rates are observed in each case.

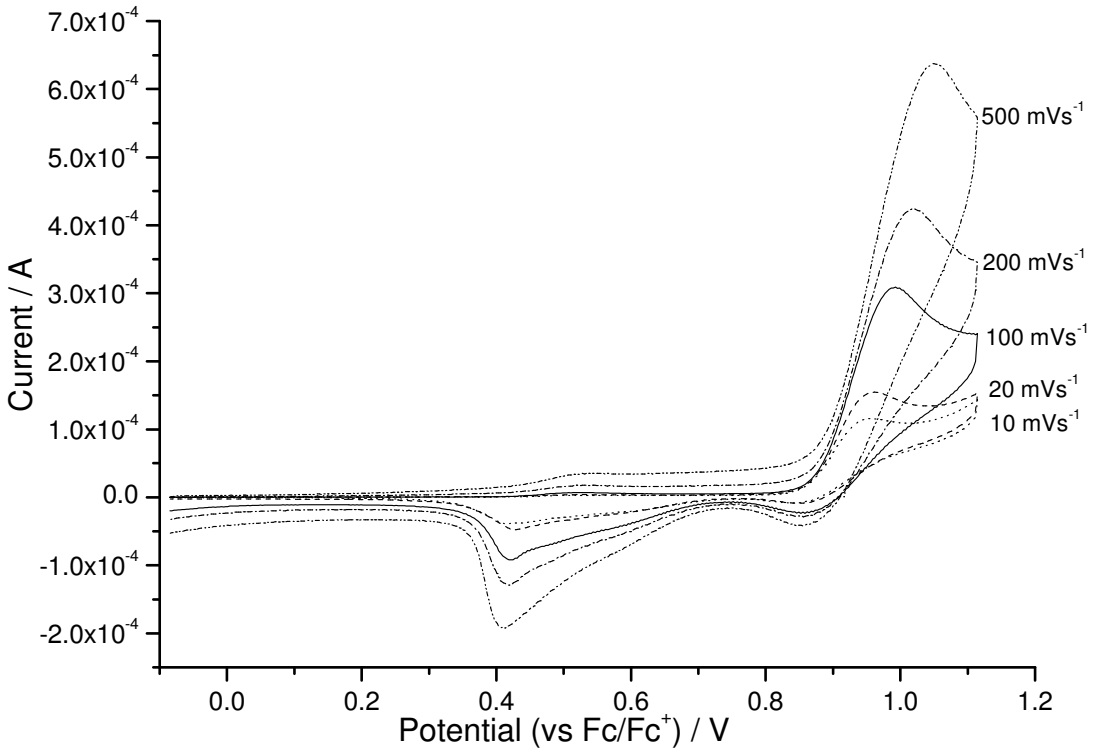

Figure 5.2.2. First cycleCVs of 1.25mM 5-methylIC solution at varying sweep rates.

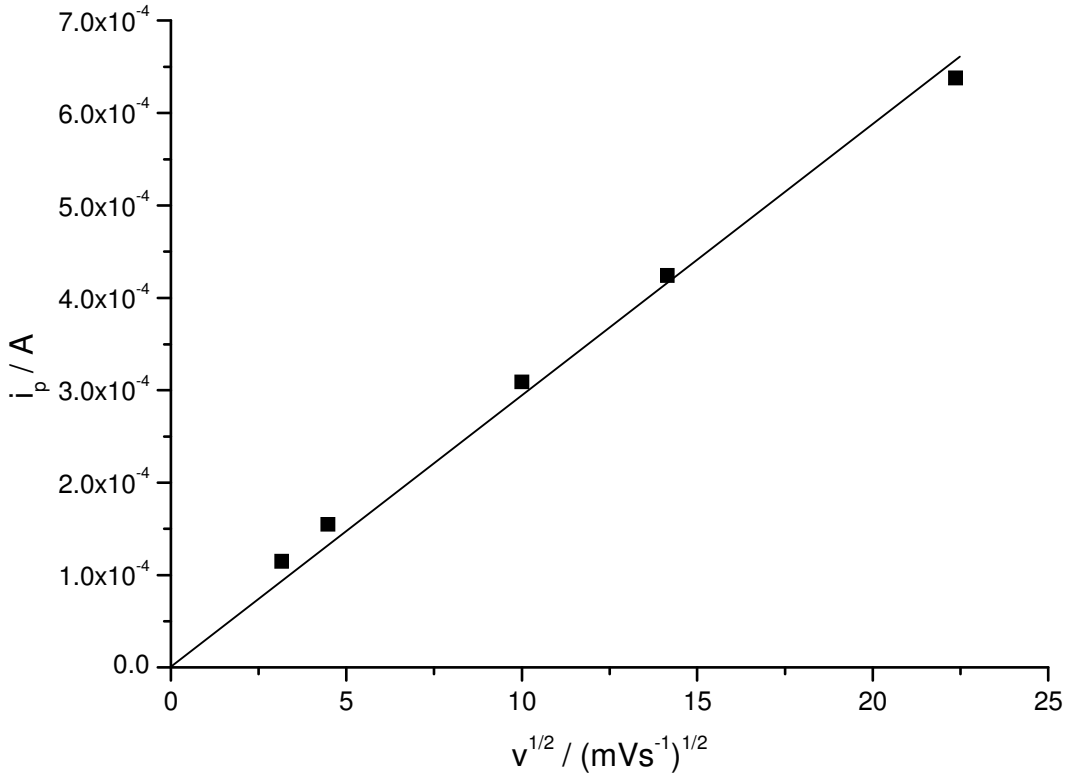

Figure 5.2.3. Plot of peak current vs the square root of sweep rate, for the electro-oxidation of 5-methylIC.

5.2.2 Electro-oxidation of 5-methylindolo[3,2,1-jk]carbazole by chronoamperometry at a rotating disc electrode.

As discussed previously (section 2.1.2), chronoamperometry performed at a rotating disc electrode (RDE) is a valuable method for obtaining quantitative information on the electrode kinetics of a reaction. The potential for monomer electrooxidation was selected such that the reaction was not under electrochemical control, as changes in electrode reactivity during film formation should then not affect the observed current. For this reason the potential selected for electro-oxidation studies on 5-methylIC was +1.100 V vs Fc/Fc^+; this potential is 100 mV greater than the peak oxidation potential on platinum.

The electro-oxidation of 5-methylIC was studied at a platinum RDE using chronoamperometry over a range of bulk concentrations (c_∞ = 1-10 mM) and rotation speeds (W = 1-16 Hz). For an RDE in acetonitrile background electrolyte if the time for steady-state currents to be achieved is due to the onset of steady-state hydrodynamic flow, the current should be within 1% of its steady-state[8] value at a time τ when: $\tau \geq \frac{2.1}{W}$, for all solvents. For rotation speeds in the range 1-16 Hz such conditions should be obtained within a few seconds. A typical current/time transient for the electro-oxidation of a 10 mM solution of 5-methylIC at a rotation speed of 4Hz is shown in Figure 5.2.4. During these electro-oxidations it was observed that a dark green film was deposited on the electrode surface, and that the solution went from being clear and colourless to clear with a light indigo colour. On applying +1.100 V, the transient shows a jump to a relatively high current before relaxing to a steady-state current. Transients of this form have been observed previously for indole[7] and IC[5] systems; this initial period is of the same timescale as the onset of steady state conditions but slightly larger; it is thought to correspond to the time taken for complete coverage of the electrode surface by the conducting 5-methylIC film, after which steady-state currents are observed. These steady-state currents are passed for minutes, showing the steady-state growth of an electro-active conducting film of increasing thickness on the surface.

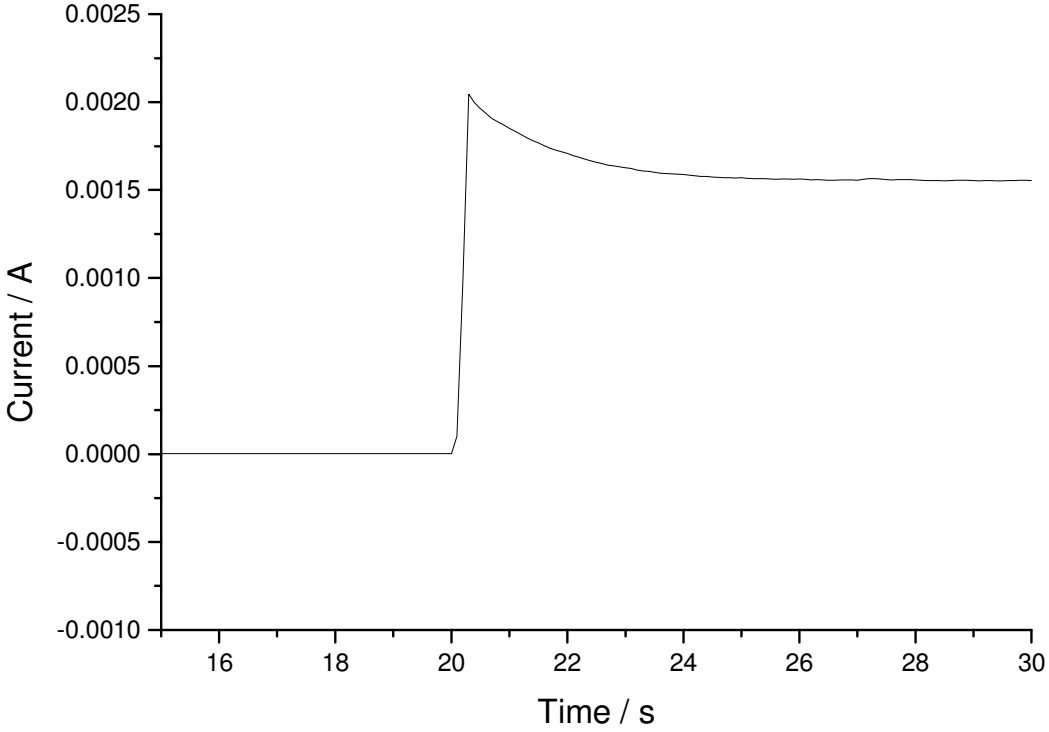

Figure 5.2.4. Current/time transient for the electro-oxidation of a 10mM solution of 5methylIC at a rotation speed of 4Hz. Potential stepped from 0.000 V to +1.100 V vs Fc/Fc+ at t = 20 s to initiate film growth.

The films produced through this potential step method were again analysed by cyclic voltammetry in background electrolyte solution, after being washed with a small amount of the background electrolyte solution to remove any unreacted monomer. CVs were then recoded at a variety of sweep rates (Figure 5.2.5). When film kinetics are fast with respect to sweep rate, the whole film will be oxidised and reduced on each sweep. Consequentially, i_p will be proportional to v. If however film kinetics are slow with respect to v, then the whole film will not be oxidised and reduced on each sweep. Where slower film kinetics are observed, i_p will vary with $v^{1/2}$ if the reaction of the film redox centres is diffusion limited. Figure 5.2.6 shows a linear relationship between peak current and sweep rate at low sweep rates. At higher sweep rates (>100 mVs^{-1}) this relationship breaks down, suggesting the film is not able to respond sufficiently quickly at high sweep rates, as the charge transfer processes in the film become rate determining. The peaks can also be observed to separate on the potential axis with increasing sweep rate (Figure 5.2.5), as film kinetics become important.

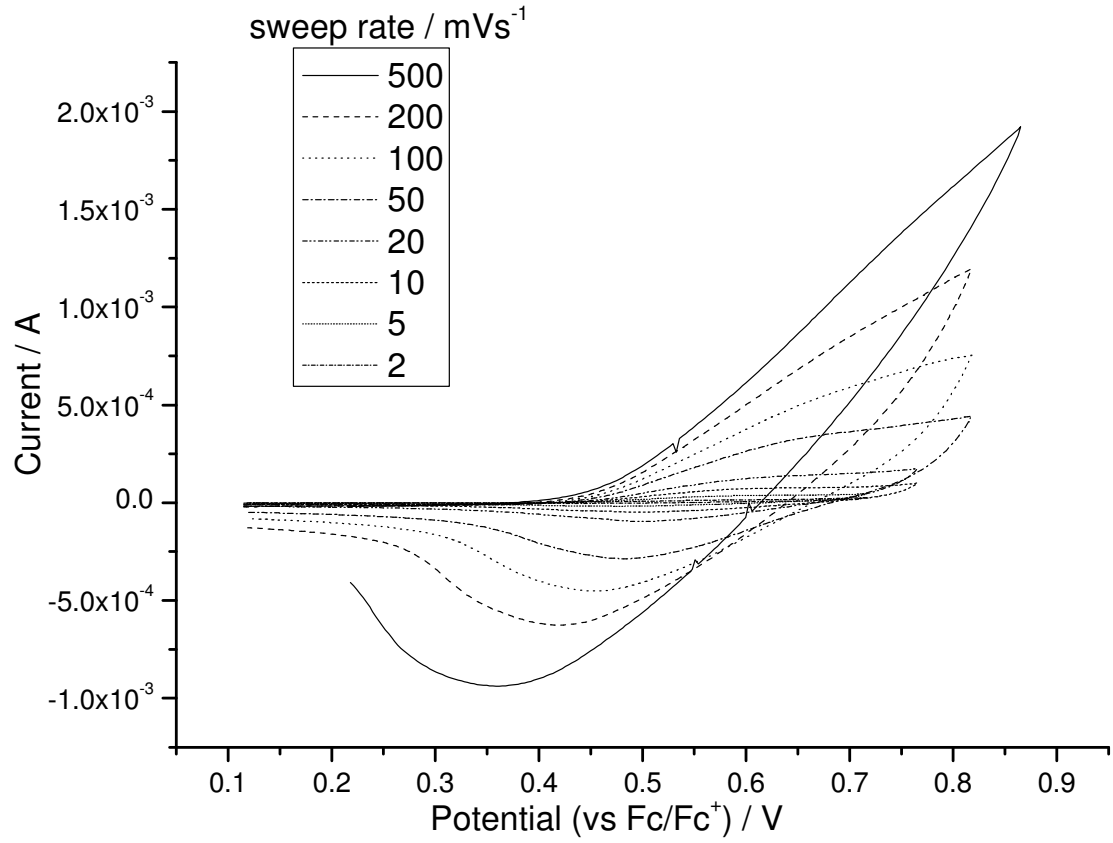

Figure 5.2.5. Variation of first cycle CVs with sweep rate for a 5-methylIC film formed from 10mM monomer solution at a potential of 1.1V vs Fc/Fc^+ and a rotation speed of 4Hz (for 10s).

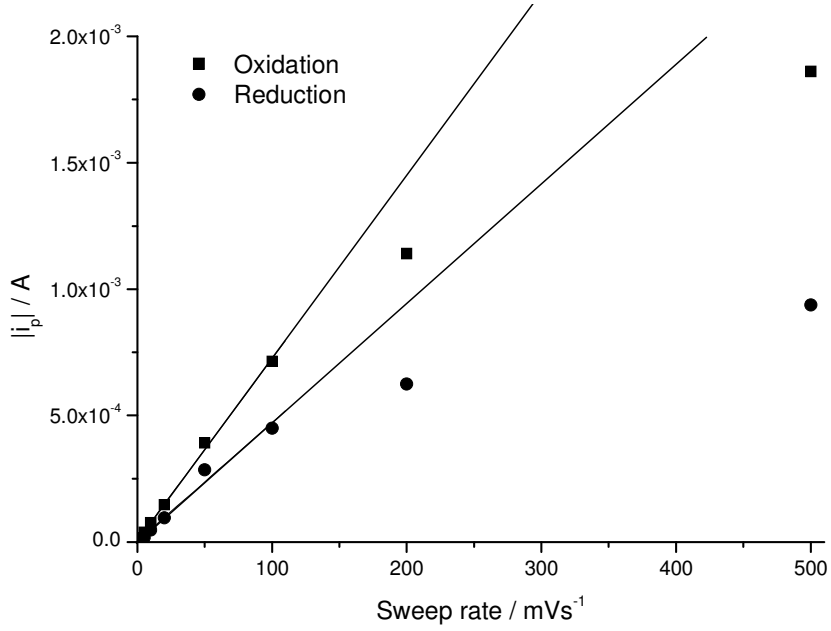

Figure 5.2.6. A plot of peak oxidation and reduction currents against sweep rate for the 5-methylIC film from Fig. 5.2.5.

For low sweep rates, where the film kinetics are sufficiently rapid that the whole film is oxidised and reduced, the area under the redox peaks gives the total redox charge. This charge can be compared to the charge passed during film formation. Comparison shows the percentage of redox charge for monomer concentrations of 1.25, 2.5, 5 and 10 mM are 12.8, 13.9, 16.4 and 20.9% respectively for films formed at a rotation speed of 4 Hz and a electro-oxidation time of 30 seconds. Under these conditions results vary from IC[5] and CVs of 5-methylIC at low concentrations, where the redox charge is 33% of the polymerisation charge. The most likely cause of this difference from IC is the slower coupling rate observed for 5-methylIC. If the decrease in coupling rate previously observed with CV (section 5.2.1) is sufficiently slow then significant coupling will occur away from the electrode and the amount of film formation will be decreased. Another less probable cause for the decrease is that film undergoes further coupling on the electrode surface to form a more polymeric film as observed with indoles[7], this is unlikely due to the absence of a second (irreversible) oxidation peak for the 5-methylIC film below the potential chosen for film formation as is observed for indoles where further coupoling of trimer centres is observed. The first of these causes is also the most probable as there is a significant colouring of the monomer solution after periods of film formation which was not reported during formation of IC films. It is also consistent with the observed percentage increasing with increase in monomer concentration as the coupling rate is given by $k_{coupling}[IC^{+\bullet}]^2$, while the diffusion rate is equal to $k_{MT}[IC^{+\bullet}]$. Increasing $[IC^{+\bullet}]$ should therefore lead to an increase in surface coupling compared to diffusion and hence increase the amount of formed film observed on the electrode surface. Another possible cause for the decrease in redox charge compared with the theoretically ideal value is that there is enhanced solubility of the dimer product with the addition of methyl groups, but this is highly unlikely as cycling of the film in acetonitrile/background electrolyte solution showed no decrease in film redox charge with increased cycling.

A powerful technique for the analysis of the electrode kinetics of a reaction is through analysis of the relationship between the current passed during

electrooxidation and the rotation speed of the RDE, over a range of concentrations. To this end, the RDE was rotated at 1Hz and the potential was stepped from 0.00 V to +1.10 V vs Fc/Fc^+. Once steady-state currents were obtained the rotation speed was stepped up and repeated until data for rotation speeds of 1, 2, 4, 9 and 16 Hz were recorded (forward run). The process was then reversed (reverse run), by stepping down through the same sequence, until 1 Hz was reached again (Figure 5.2.7). The equivalent currents on the reverse run of this method show currents larger than those of the forward run. This can be attributed to progressive increase in electrode area as conducting film growth occurs. Further evidence for this is shown by the fact that the difference in currents for the 1 Hz measurements increase as bulk concentration increases. For this reason only the data for the forward run were used for analysis using the Koutecky-Levich equation, as the effective area could then be approximated to the initial electrode area of bare platinum.

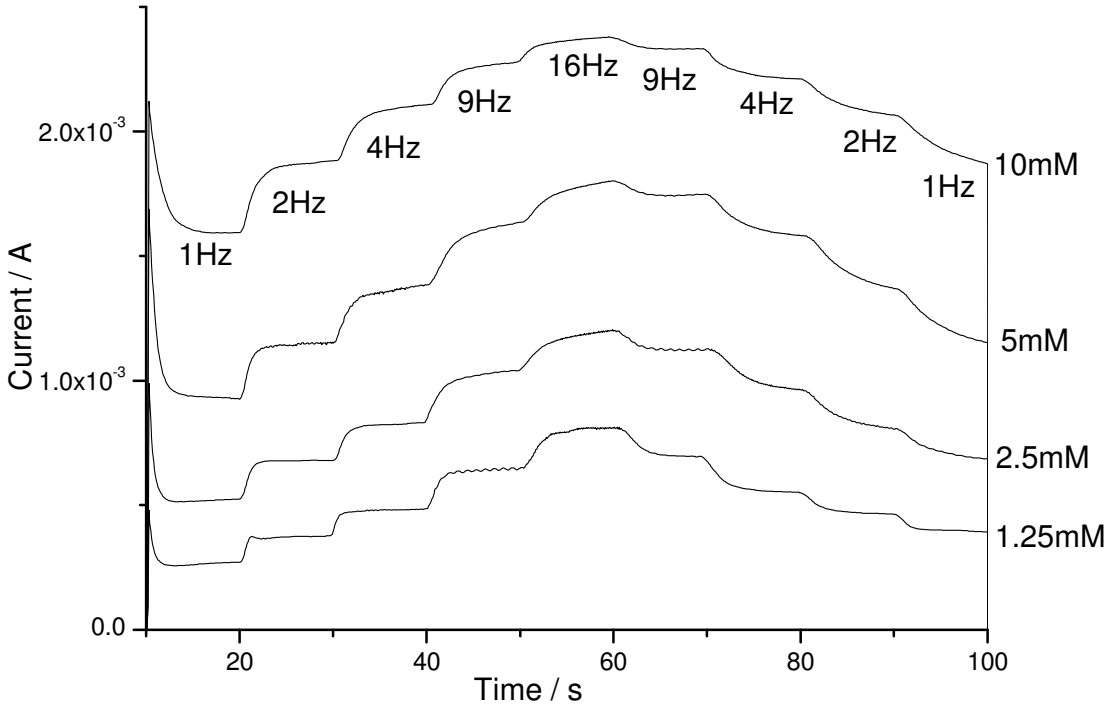

Figure 5.2.7. Current-time transient for the electro-oxidation of 5-methylIC at 1.1V vs Fc/Fc^+ at rotation speeds of 1, 2, 4, 9 and 16Hz for varying concentrations.

Analysis using the Koutecky-Levich equation (see section 2.1.2) assumes first-order kinetics and predicts a linear relationship between the inverse of the observed current (1/i) and the inverse of the square root of the rotation speed ($1/W^{1/2}$). It is assumed

that the electro-oxidation mechanism for 5-methylIC is similar to that observed for IC (Scheme 5.2.1); the redox behaviour for such a formed film is shown in Scheme 5.2.2, where three electrons will be required to couple the monomer units and form an oxidised dimer film on the electrode surface, giving a value for n of 1.5 per monomer unit.

$$2IC \xrightarrow{-2e^- -2H^+} IC_2 \underset{+e^-}{\overset{-e^-}{\rightleftharpoons}} IC_2^+$$

Scheme 5.2.2. Proposed film formation and redox reaction mechanism for IC.

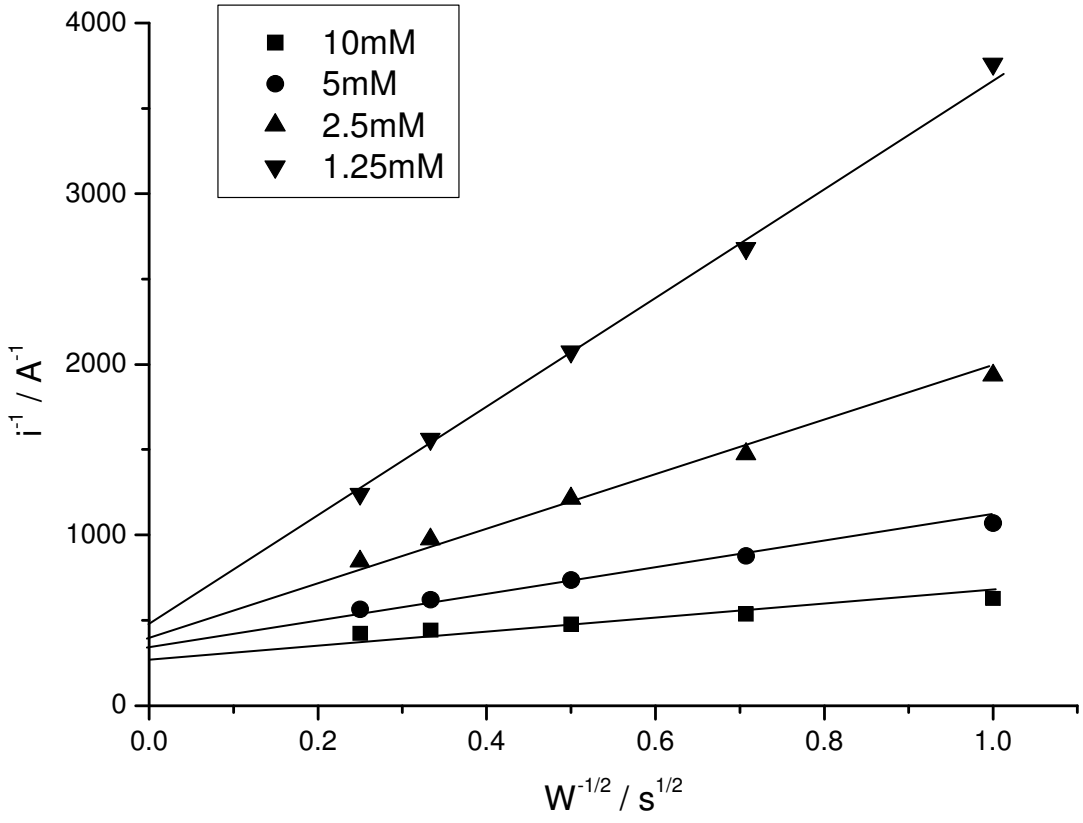

Figure 5.2.8. Koutecky-Levich plots for 1.25, 2.5, 5 and 10 mM solutions of 5-methylIC. The lines shown are lines with a theoretical gradient calculated using D=4x10^{-5} cm^2 s^{-1}.

Analysis using a Koutecky-Levich plot (Figure 5.2.8) shows that data for each concentration gives a straight line. This indicates that monomer oxidation and coupling obeys 1st order kinetics as this is an assumption of the Koutecky-Levich equation (section 2.1.2) which is suggestive of a surface process[9]. The data were

globally analysed by fitting all the data to Equation 2.1.22. From the slope if n = 1.5 a global monomer diffusion coefficient of D = (4.0 ± 0.9) x 10^{-5} cm^2s^{-1} can be calculated. This is a reasonable value for an organic molecule of this size in acetonitrile background electrolyte when compared to a diffusion coefficient of 1.5 x 10^{-5} cm^2s^{-1} for 5-aminoindole[10]. The diffusion co-efficient can also be estimated with the Einstein relation for diffusion:

$$D = \frac{k_B T}{6\pi\eta r}$$ **Equation 5.2.1**

where η is the viscosity of acetonitrile (3.45 x 10^{-4} Pa.s) and r is the approximate radius of the molecule modelled as a sphere (5 Å), this relation gives an estimate of the diffusion coefficient of 1.26 x 10^{-5} cm^2s^{-1} which again is reasonable when compared to the value calculated from the Koutecky-Levich data.

Monomer concentration (mM)	**i_∞ / mA**
1.25	2.0 ± 0.1
2.5	2.5 ± 0.1
5	3.0 ± 0.1
10	3.6 ± 0.2

Table 5.2.1. Mass transport independent currents for 5-methylIC electro-oxidation.

The intercepts of the Koutecky-Levich plots give the mass transport independent current (i_∞), when mass transport is highly efficient and the reaction is surface controlled (since as W → ∞, the concentration at the electrode surface, $c_0 \rightarrow c_\infty$). These values are presented in Table 5.2.1. Typically the intercepts of a Koutecky-Levich analysis, i_∞, would be expected to vary linearly with c_∞ as they are first order processes. This is not observed in this work, here the value of i_∞ increases with c_∞ but not linearly. The most probable cause of this behaviour is an adsorption during the electro-oxidation process as reported with indoles[9], as the Koutecky-Levich equation becomes:

$$1/i_\infty = 1/(nFAk_{ads}c_\infty) + 1/(nFAk)$$ **Equation 5.2.2**

where k_{ads} is the rate constant for adsorption to the electrode surface. When there is total surface coverage of the electrode the second term in Equation 5.2.1 dominates

and a constant i_∞ value would be expected. Where total surface concentration has not been established i_∞ will show a dependence on the bulk concentration, as is observed here. The values for i_∞ observed for 5-methylIC are lower than the corresponding values observed for equivalent concentrations of IC; again this is indicative of a lower coupling for 5-methylIC, as the Koutecky-Levich analysis was performed on IC and 5-methylIC at potentials that ensured the formation of highly reactive radicals. The decrease in coupling is likely to be due to the blocking of a coupling position.

5.3 Characterisation of film formed from electro-oxidation of 5-methylindolocarbazole.

It has previously been shown that films formed from IC consist of three distinct dimers[5]. Up to this point it has been found that a similar coupling mechanism is likely to occur in 5-methylIC, which would be expected to yield similar products. This section contains a spectroscopic characterisation of the electro-active film formed upon electro-oxidation of the 5-methylIC monomer to determine the nature of the film products.

5.3.1 FAB mass spectrometry

FAB mass spectroscopy was performed on a sample produced by electro-oxidation of a 10mM monomer solution with a rotation speed of 4Hz.. The resultant mass spectrum showed a parent ion peak at 508 Da. This is consistent with dimer formation as it is the mass of the coupling of two monomer units of mass 255 Da accompanied by the loss of two protons.

5.3.2 Fluorescence spectroscopy.

ICs are strongly luminescent. The fluorescence quantum yield, Φ_F, was estimated by comparing the ratios of the total intensities of fluorescent emission with the absorption at the excitation wavelength:

$$\Phi_F \approx \left(\frac{\sum I}{A_{ex}} \right) \quad \textbf{Equation 5.3.1}$$

The Φ_F for ICs can then be related to Φ_F for indole by the relation:

$$\frac{\Phi_{F,IC}}{\Phi_{F,indole}} = \frac{\left(\frac{\sum I_{IC}}{A_{ex,IC}}\right)}{\left(\frac{\sum I_{indole}}{A_{ex,indole}}\right)} \quad \textbf{Equation 5.3.2}$$

Using this method Φ_F values of 41% and 31% were calculated for IC and 5-methylIC respectively. IC showed a peak fluorescence emission at 375 nm. The dimer products of IC were also found to be highly fluorescent with a red-shifted peak emission of 405 nm.

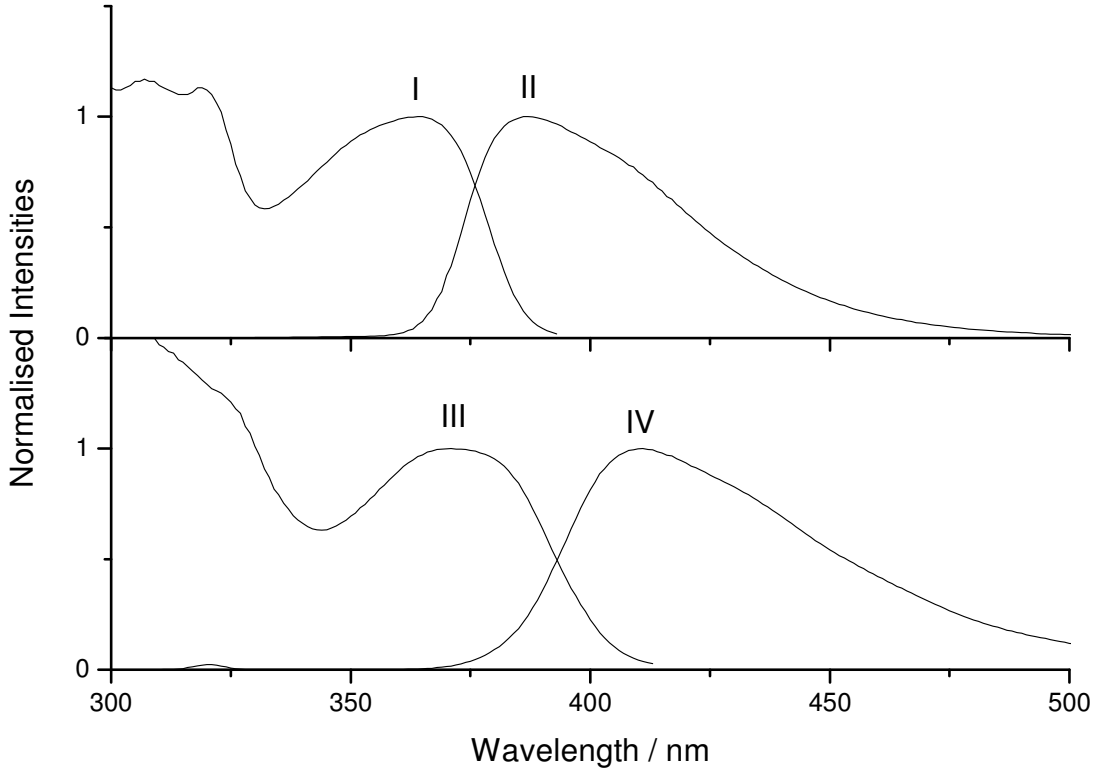

Figure 5.3.1. Excitation and emission spectra respectively for 5-methylIC (I and II) and the film formed from IC electro-oxidation (III and IV) in DMF. The emission wavelengths were 405 and 433 nm for I and III respectively, and the excitation wavelengths were 320 nm for II and IV. Intensities were normalised to the peak intensities for the $S_0 \rightarrow S_1$ transition for excitation spectra, and the peak intensities for the $S_1 \rightarrow S_0$ transition for emission.

The excitation and emission spectra for 5-methylIC and of the film are shown in Figure 5.3.1. All spectra were recorded in DMF at concentrations around 10^{-6} M. It

can be seen that the peak emission of the dissolved film species (410 nm) is red-shifted from that of the monomer (385 nm). The position of the (0, 0) transition exhibits similar behaviour, shifting from 376 nm to 392 nm. This red-shifting of the fluorescence spectra is consistent with an increase in the delocalisation of the π-molecular orbitals around the product units[11]. This is similar to the result observed for IC and consistent with the products formed from electro-oxidation being dimers.

The red shifting of the excitation spectra may also account for the colouring of the solution during film formation, as the dimer absorbs light within the visible range of whereas the monomer does not. As more dimer product is formed and diffuses into the solution an increase change of the solution colour from clear and colourless to coloured may be expected.

5.3.3 NMR spectroscopy.

A sample of film was produced for NMR analysis and dissolved in a mixture of deuterated d^6-DMSO and d^6-acetone. Film solubility in this mixture was limited, which in turn limits the accuracy in determining the ratios of products. 1H NMR (Figure 5.3.2), COSY (Figure 5.3.3) and HSQC (Figure 5.3.4) spectra were obtained. The COSY spectrum shows that the signals at 8.58ppm arise from two protons as doublets which couple to 2 protons as doublets at 8.55ppm, whilst HSQC shows that each proton is coupled to a different carbon. The HSQC data also shows 2 additional singlet protons coupled to two other carbons. These signals are very weak and of the same intensity as the peaks at 8.73 ppm. Through analogy with the NMR spectra observed by Wharton for IC[5] the only dimer with peaks in both of these regions is the 2, 10-linked dimer (Figure 5.3.5.A).

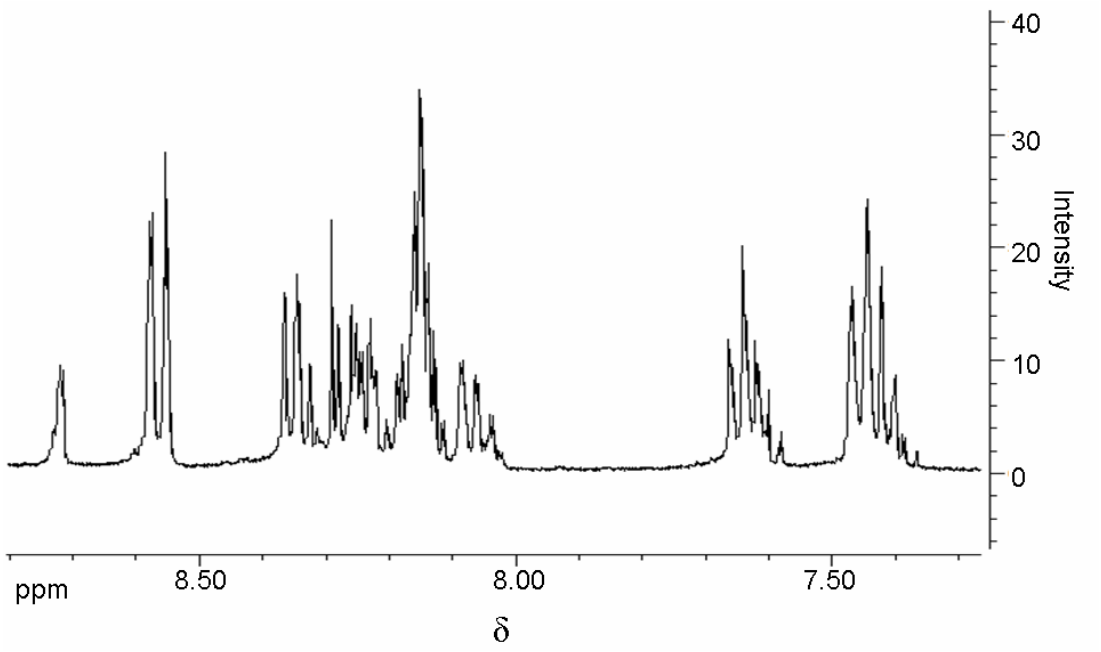

Figure 5.3.2. 360MHz 1H NMR spectrum of 5-methylIC film.

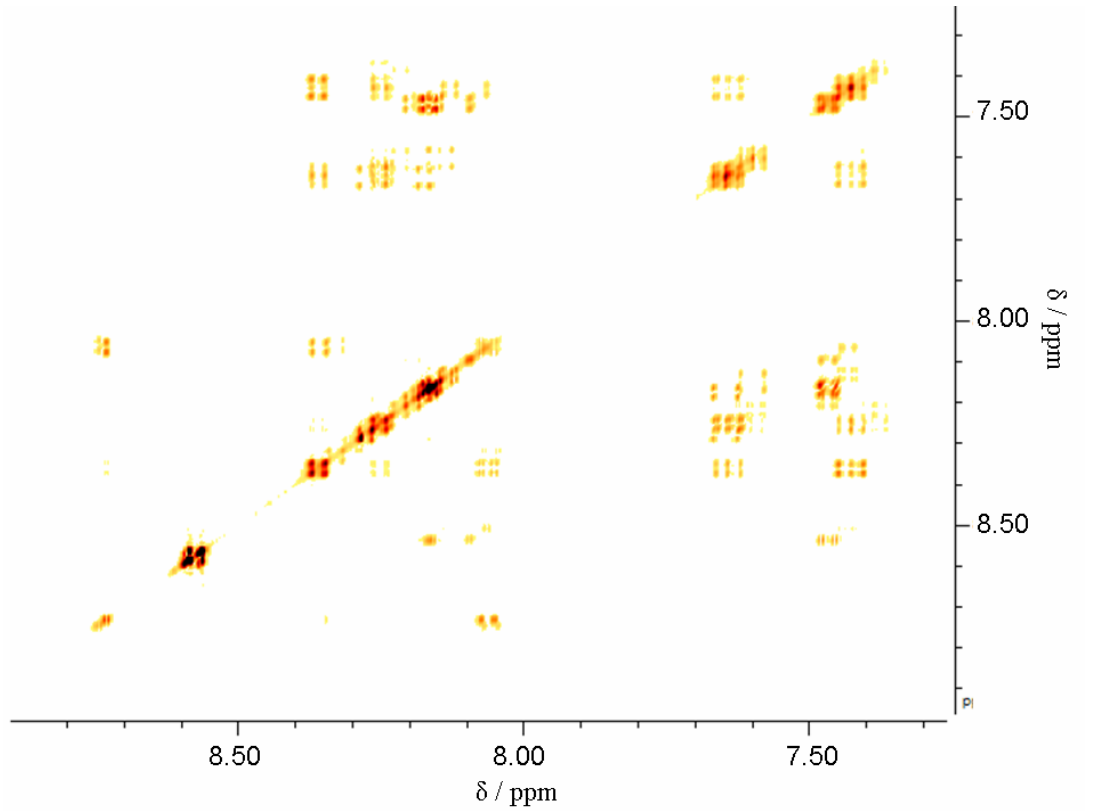

Figure 5.3.3. 360MHz 2D-COSY spectrum of 5-methylIC film.

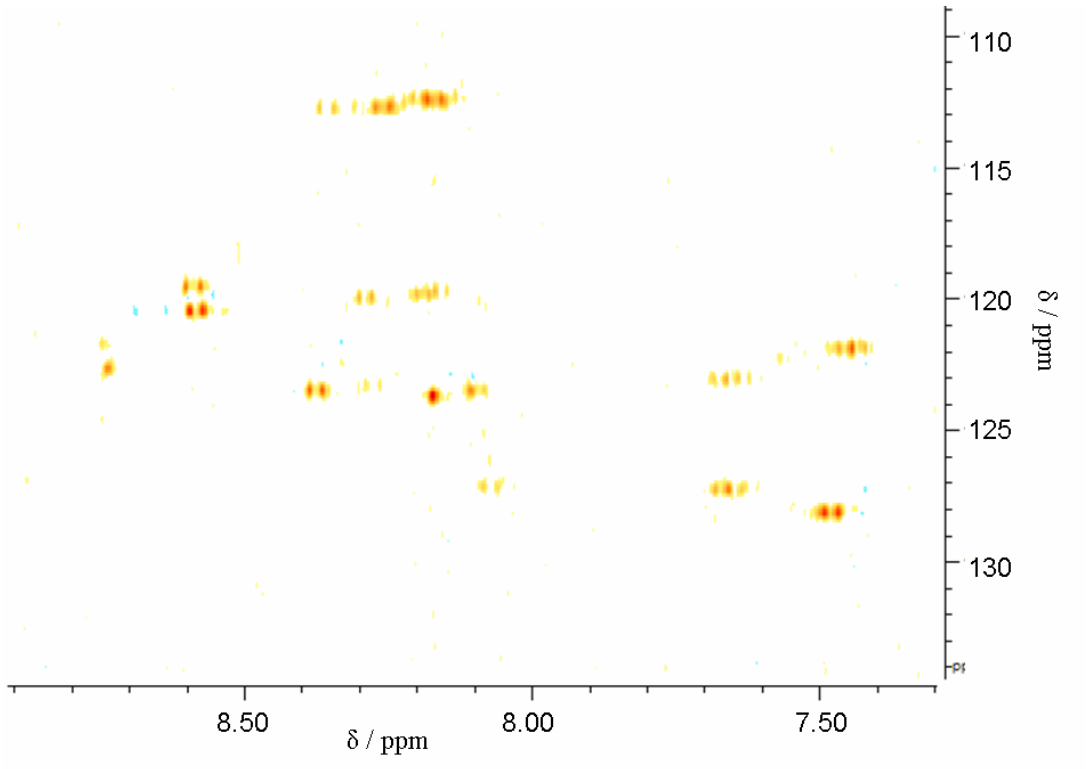

Figure 5.3.4. 360MHz 1H/13C HSQC spectrum of 5-methylIC film.

Through further comparison with Wharton's results we can assign the next highest chemical shift, 8.72ppm, to the 10, 10'-linked dimer (Figure 5.3.5.B); this product would not show any peaks in the 8.55 to 8.60ppm range. The peak at 8.72ppm shows coupling to a peak at 8.06ppm, which then couples to a proton at 8.37ppm. These peaks are all of high intensity, showing a significant proportion of this dimer. The remaining peaks at 8.55 and 8.58ppm can therefore be attributed to the 2, 2'-linked dimer (Figure 5.3.5.C). This assignment of dimers is through analogy with the products observed by Wharton[5], however given the thoroughness of Wharton's NMR analysis (with retro-synthesis and NMR-spiking) this provides confidence that these three dimers are the products of the IC electro-oxidation. Due to solubility issues it is difficult to quantify the relative amounts of each dimer formed.

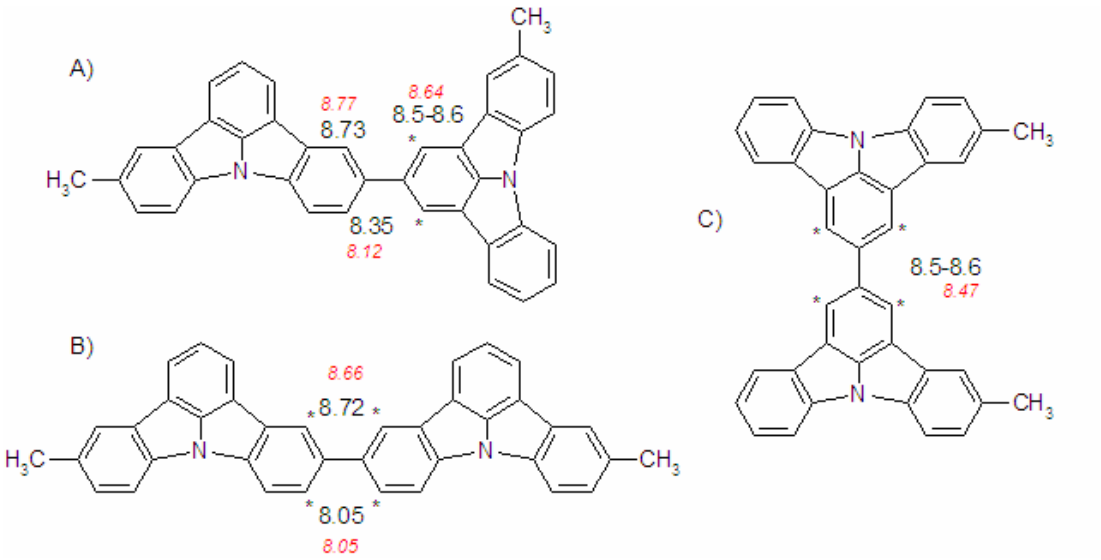

Figure 5.3.5. A) 2, 10-coupling, B) 10, 10'-coupling, and C) 2, 2'-coupling. Assignments are given for the relevant protons are in black, and assignments in red are these determined for the unsubstituted dimers[3].

5.4 Calculations on 5-substituted indolo[3,2,1-jk]carbazoles and related systems.

Previously, the oxidation potentials of four 5-substituted ICs have been reported[5] (Table 5.4.1), and these results show some correlation with the Hammett constant, σ^+, of the substituent, as has previously been observed for indoles[8]. Previous calculations have been useful in indicating probable coupling sites for IC[6], but a systematic error in calculation of oxidation potentials led to poor agreement with observed experimental values. It was hoped that the enhanced method for calculating oxidation potentials (Chapter 4) would provide a better correlation between experimental and calculated values; this is tested in this work.

Calculated oxidation potentials were obtained for a range of 5-substituted ICs using the method described in section 4.3, again using the B3LYP method with indole as reference. These calculated values are shown[‡] in Table 5.4.2 and compared to the

[‡] Extending the statistical analysis for the deviation of calculated peak potentials from experimentally observed peak potentials (used in Chapter 4); it is found that, when the standard deviation is extended to include all molecules studied in Chapter 4 and the ICs which have been measured experimentally, the standard deviation is 36 mV.

experimental values in Figure 5.4.1, which also show the relationship of the calculated and measured oxidation potentials to the Hammett substituent constant, σ^+. It can be seen that the calculated and experimental oxidation potentials generally follow a linear relationship with σ^+, indicating that substituents in the 5-position are effectively conjugated into the aromatic system. It is interesting that this plot has a gradient similar to that observed for 5-substituted indoles and that the amino substituent shows a systematic deviation from the line.

Substituent	**Measured peak oxidation potential (vs Fc/Fc^+) / V**
5-NH_2[§]	+0.36
5-CH_3[**]	+0.99
5-H[§]	+1.01
5-Br[§]	+1.12
5-CN[§]	+1.20

Table 5.4.1. Oxidation potential of various IC monomers at concentrations of 1mM.

As observed previously with indole (sections 4.2-4.3) it is possible to directly compare these values to the experimental data. Figure 5.4.2 shows the relationship between the calculated and measured potentials. If the calculations agree perfectly with the experimental data a slope with a gradient of 1 and zero intercept should be observed. It can be seen that the calculated values provide a good level of agreement with the experimentally observed values within experimental error. This quality of agreement between calculation and experimentally observed values is especially notable given that the calculations do not take into account specific adsorption of molecules at the electrode surface or specific solvation effects.

[§] From reference 3.
[**] This work.

Substituent	Calculated peak oxidation potential (vs Fc/Fc^+) / V
5-NH_2	+0.23 ± 0.04
5-CH_3	+0.91 ± 0.04
5-H	+1.01 ± 0.04
5-Br	+1.06 ± 0.04
5-CN	+1.25 ± 0.04
5-Cl	+1.06 ± 0.04
5-CO_2	+1.18 ± 0.04
5-OH	+0.69 ± 0.04
5-OCH_3	+0.71 ± 0.04
5-NO_2	+1.34 ± 0.04

Table 5.4.2. Calculated oxidation potentials for 5-substituted ICs vs Fc/Fc^+.

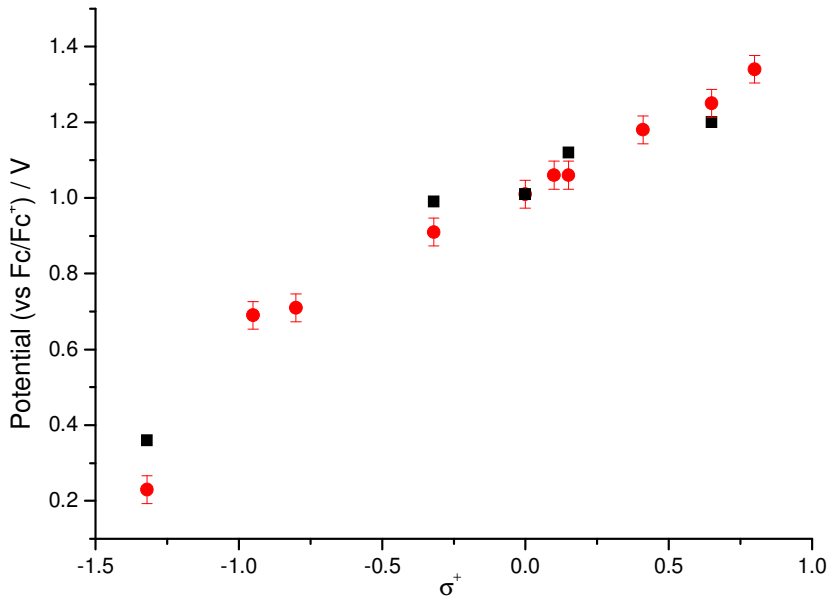

Figure 5.4.1. Calculated (■) and measured (●) oxidation potentials for 5-substituted ICs vs Hammett substituent constant.

One property of the IC molecules which is of great interest is the location of the electron spin density in the radical cation. It has been shown for indoles that the location of highest electron spin density in calculations is in agreement with the position of radical cation coupling in the formation of indole trimer films. This is to be expected if coupling of the radical cations occurs by localised pairing of this

radical spin from each cation to form a bond and radical spin density remains localised during coupling, when coupling should occur at the positions of highest electron spin density. Figure 5.4.3 shows the electron spin density mapped onto the 99% electron density isosurface of the radical cations for a range of 5-substituted ICs. Areas of high electron spin density are indicated as blue, with the darkest areas having the highest spin density. On the unsubstituted IC the highest spin density is observed in the 2, 5, 7, 8 and 10 positions. Coupling at the 7 and 8 positions can be discounted due to steric factors, which suggests that coupling is most probable at the 2, 5 and 10 positions. This coupling is indeed what has previously been confirmed experimentally by Wharton[5].

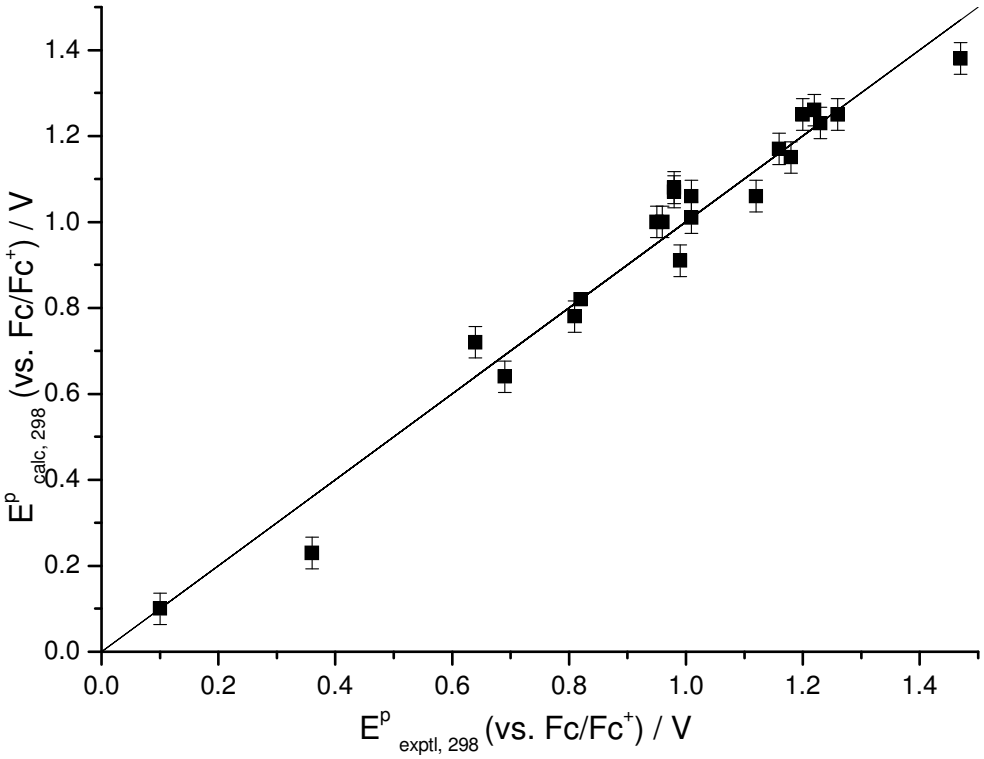

Figure 5.4.2. Plot of calculated vs measured oxidation potentials. The line shows the relationship expected if the calculated and experimental data were equal.

It is clear that for the majority of substituents the electron-spin density is not affected by the nature of the substituent, with the spin density being located in the same positions as observed for the unsubstituted IC. Coupling in these substituted ICs would therefore be expected to occur in a similar fashion to that observed with unsubstituted IC, albeit with no coupling at the 5-position due to the blocking effect

of the substituent. It is interesting that the only substituent with a significant change in the electron spin density distribution in the radical cation is the NH_2 substituent. It can also be seen (Figure 5.4.1) that this is the substituent that does not appear to follow the linear relationship between oxidation potential and σ^+, which suggests that the amino substituent significantly perturbs the electronic distribution in the molecule.

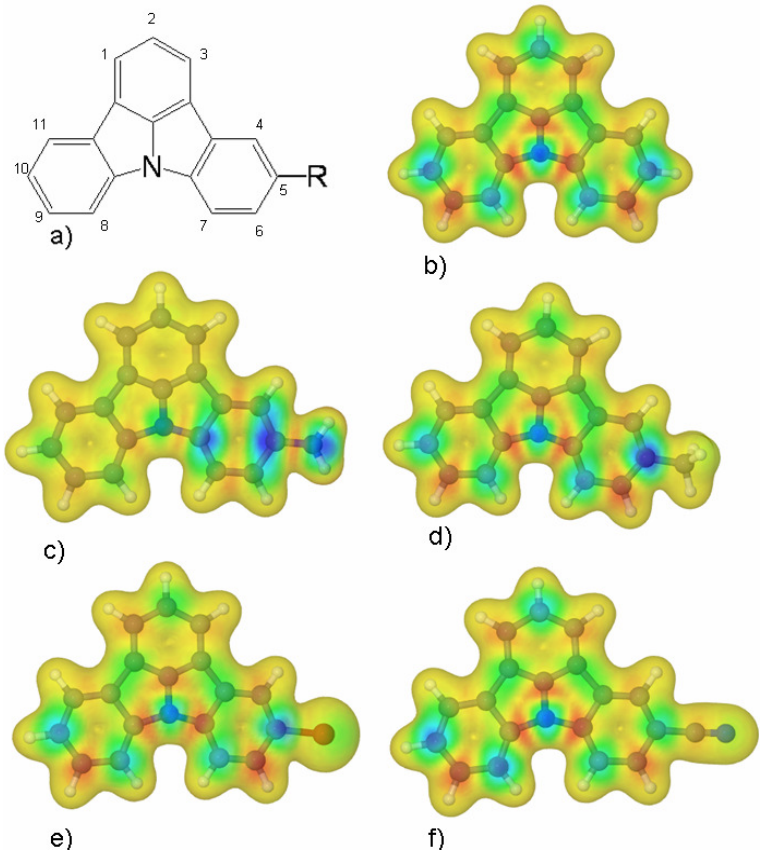

Figure 5.4.3. Electron spin density maps for radical cations of 5-substituted ICs, the darkest blue areas show the regions of highest spin density. (a) Skeleton structure for 5-substituted ICs. (b) unsubstituted IC. (c) 5-NH_2 IC. (d) 5-CH_3 IC. (e) 5-Br IC. (f) 5-CN IC. (The colouring is schematic as follows: blue indicates a positive spin density (0.003) whilst red is negative (-0.001). The same range of spin density was used for all 5 maps).

5.5 Conclusions.

It has been shown that 5-methylIC can be electro-oxidised to form an electro-active film at an electrode surface. Characterisation of this formed film has shown that the film consists of three dimers of 5-methylIC. The oxidation potentials for a range of 5-substituted ICs have been calculated and are in good agreement with

experimentally observed values. Analysis of the regions of high electron spin density within the radical cations of these species has highlighted the correlation between sites of high radical spin density and site specific coupling to form products, as has previously been observed with indoles.

5.6 References.

[1] Wakim, S.; Bouchard, J.; Simard, M.; Drolet, N.; Tao, Y.; Leclerc, M. *Chem. Mater.***2004**, *16,* 4386.

[2] Li, Y.; Wu, Y.; Gardner, S.; Ong, B. S. *Adv. Mater.* **2005**, *17,* 849.

[3] Wu, Y.; Li, Y.; Gardener, S.; Ong, B. S. *J. Am. Chem. Soc.* **2005**, *127,* 614.

[4] Curiel, D.; Cowley, A.; Beer, P. D. *Chem. Commun.* **2005**, 236.

[5] Wharton, S. I. *Ph. D. Thesis, "Synthesis and Characterisation of Novel Conducting Films Based on Indolo[3,2,1-jk]carbazole Systems.", University of Edinburgh* **2005**.

[6] Chapman, M. A. *Ph. D. Thesis, "The Electropolymerisation of Indolo[3,2,1-jk]carbazole and Pyrrolo[3,2,1-jk]carbazole: An Electrochemical, Computational and Spectroscopic Study.", University of Edinburgh* **2003**.

[7] Mackintosh, J. G. *Ph. D. Thesis, "The Electropolymerisation of Novel Conducting Polymers.", University of Edinburgh* **1996**.

[8] Bard, A. J.; Faulkner, L.R. Methods Involving Forced Convection-Hydrodynamic Methods *Electrochemical Methods Fundamentals and Applications*, Second Edition; John Wiley & Sons, Inc. **2001**; p*354*.

[9] Mackintosh, J. G.; Wright, S. J.; Langridge-Smith, P. R. R.; Mount, A. R. *J. Chem. Soc., Faraday Trans.* **1996**, *92*, 4109.

[10] Jennings, P.; Jones, A. C.; Mount, A. R.; Thomson, A. D. *J. Chem. Soc. Faraday Trans.* **1997**, *93*, 3791.

[11] Jennings, P.; Jones, A. C.; Mount, A. R. *J. Chem. Soc. Faraday Trans.* **1998**, *94*, 3619.

Chapter 6: Using the General Computational Method to Screen Novel Heteroaromatics.

6.1 Introduction.

In the previous two chapters a general computational method has been established for studying molecular properties (e.g. the peak oxidation potential and electron spin densities) for small aromatic systems. Up until now these results have been compared with electrochemical measurements and with the analysis of formed films to show that the computational method can provide a generally reliable method for calculating experimental peak oxidation potentials within a few tens of mVs, as well as adequately predicting the likely coupling positions for a range of heteroaromatic systems for which coupling occurs through radical cation formation.

In this chapter this general computational method will be applied to a range of systems that, with the exception of one molecule, have not been studied electrochemically thus far. The aim of this chapter is to assess the potential for applying this method as a predictive tool for screening novel heteroaromatic sytems to assess their suitability for forming new oligomeric materials. This chapter will also assess the extension of the general computational screening method to the computation of the acid/base properties of aromatic systems through the calculation of pKa's.

6.2 Azaindolocarbazoles.

The first novel system to be considered is a modification to the indolo[3,2,1-j,k]carbazole (IC) systems discussed in Chapter 5. The modification is the introduction of a pyridine type nitrogen into the IC structure to form azaICs. The inclusion of the ring nitrogen introduces two main opportunities; firstly it introduces the possibility of tuning molecular properties by the changing of this ring atom from C to N. Secondly the presence of a ring nitrogen could lead to other potential applications, for example in sensing technologies. It is well known that pyridine-type

rings can chelate metals such as nickel and copper[1], so it is possible that some azaICs may also act as ligands. Any such chelation should lead to a measurable change in the electrochemical characteristics of the corresponding azaIC film. Protonation can also take place at the lone pair of electrons on a pyridine nitrogen, as they are located in the σ-orbital in the plane of the ring rather than delocalised within the ring. Protonation of the film should also lead to a measurable electrochemical response which suggests that conducting azaIC films could act as a fast-response pH sensor.

Three such azaICs were synthesised by Wharton[2] and are shown in Figure 6.2.1. Only the azaIC with the Nitrogen in the 7-position has been studied electrochemically. The 7-azaIC was found to have a peak oxidation potential of +1.23 V vs. Fc/Fc^+ and formed an electroactive film consisting of three dimers with 2, 2'-, 2, 10'- and 10, 10'-linking. Wharton[2] found that a formed 7-azaIC film showed a potential response with pH in the range pH 1 – 5.5 with a potential slope of 53 ± 1 mV in this region, and a slope similar to IC, which shows no pH response, above this pH (Figure 6.2.2).

The calculated peak oxidation potentials for the azaICs are shown in Table 6.2.1 The value for 7-azaIC is in excellent agreement with the experimentally measured value, and was included in the assessment of the applicability of the general computational method to all molecules that have been studied theoretically and computationally in this work (Section 5.4: Figure 5.4.2). IC is included in Table 6.2.1 for easy comparison. One interesting trend in the introduction of the aza-groups to the IC system is the apparent increase in oxidation potential of the order of 200 mV for the addition of each aza-group. The predicted potentials all lie within the solvent window for acetonitrile with background electrolyte systems, and so should not cause a problem for the future electro-oxidation of these systems using similar methods as the previous IC studies[2].

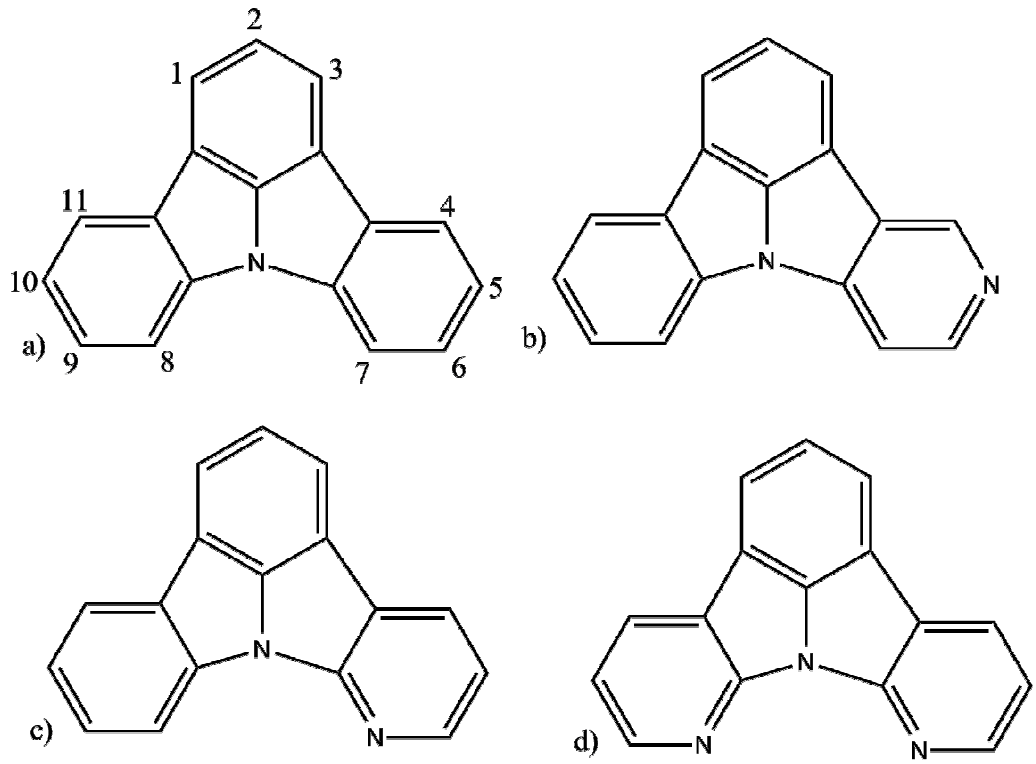

Figure 6.2.1. (a) Structure and numbering of IC. Structures of (b) 5-azaIC, (c) 7-azaIC and (d) 7, 8-diazaIC.

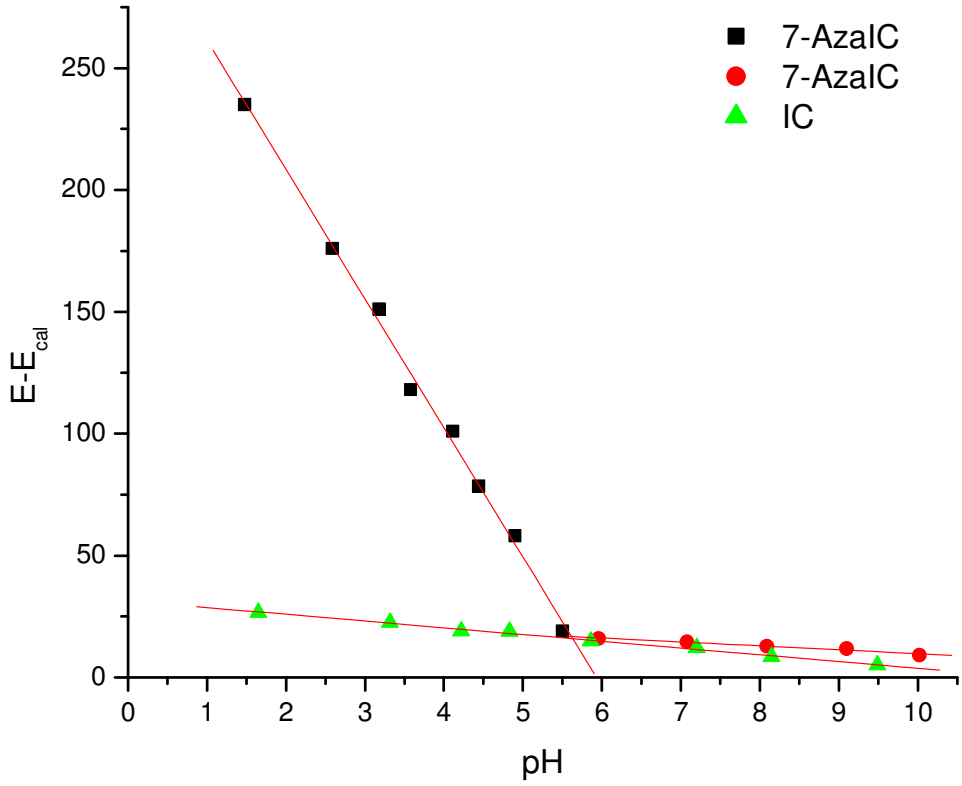

Figure 6.2.2. Potential response of a 7-azaIC and an IC film versus pH. From Reference 2.

Indolocarbazole	Calculated peak oxidation potential (vs Fc/Fc^+) / V	Experimental peak oxidation potential (vs Fc/Fc^+) / V
IC	+1.01 ± 0.04	+1.01[2]
5-azaIC	+1.28 ± 0.04	-
7-azaIC	+1.23 ± 0.04	+1.23[2]
7,9-diazaIC	+1.47 ± 0.04	-

Table 6.2.1. Calculated oxidation potentials of IC and three azaICs vs Fc/Fc^+.

Figure 6.2.3 shows the electron spin density maps of the three azaIC radical cation systems with IC included for reference. Again, it should be possible by analogy to consider the distribution of electron spin densities within these azaIC systems as determining the likely coupling positions of the radical cations upon electro-oxidation. In all three cases it is clear that electron spin density is greatly reduced in the benzene rings containing the aza-group. It may be noticed that the greatest spin densities for 7-azaIC, discounting the sterically hindered 9-position, are in the 2 and 10-positions. These are the coupling positions favoured in 5-methylIC coupling, as discussed previously (Chapter 5:) which upon coupling would produce the three dimers observed by Wharton[2] and discussed in Chapter 5: for 5-methylIC.

The greatest electron spin density in the 5-azaIC radical cation is calculated to be in the 2 position, and the spin density in the 10 position is decreased relative to IC. Electrooxidation of 5-azaIC may therefore lead to a greater proportion of 2, 2'-dimer than observed from the 7-azaIC, although coupling in the 10 position may still be possible producing the 2, 10'- and 10, 10'-dimers. For 7, 9-diazaIC spin density in the 5 and 10-positions is drastically reduced in comparison with IC, while there is a great deal of electron spin density in the 2-position. In this case coupling in the 2-position is the most likely outcome to form 2, 2'-dimer, with the formation of appreciable amounts of the other dimers much less likely. The introduction of two aza-groups into the IC structure therefore opens an intriguing route to the control of coupling and the formation of single dimer products.

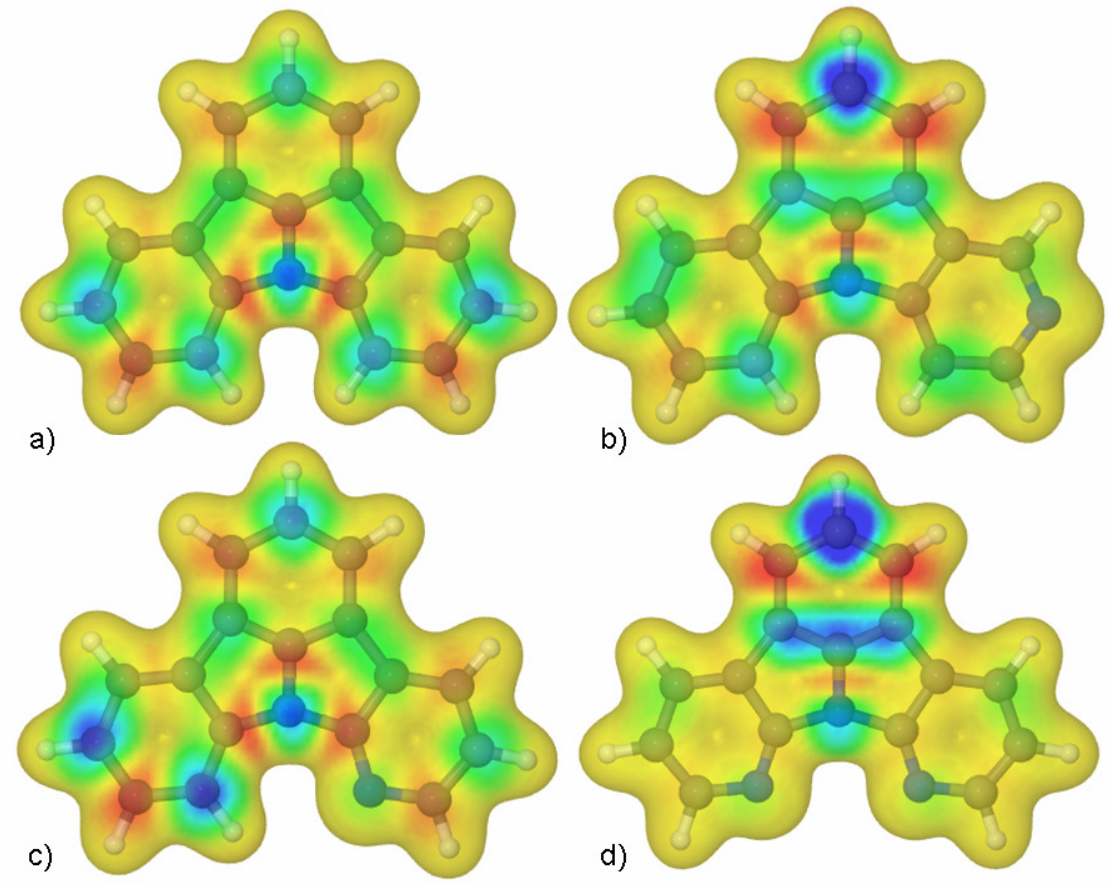

Figure 6.2.3. Electron spin density maps for radical cations of modified ICs, the darkest blue areas show the regions of highest spin density. (a) IC, (b) 5-azaIC, (c) 7-azaIC and (d) 7, 8-diazaIC. (The colouring is schematic as follows: blue indicates a positive spin density (0.003) whilst red shows a negative spin density (-0.001). The same range of spin density was used for all 4 maps).

6.3 Calculation of pKa for Heteroaromatics.

As mentioned previously, there is a potential for azaIC films to act as pH sensing films. Previous calculations on carboxylic acids have shown some potential for calculating pKa values[3], albeit utilising computationally expensive Complete Basis Set Methods. Considering the acid/base properties of oligomeric materials through the protonation/deprotonation properties of the oligomer constituent may lead to a method of screening molecules with preferential acid/base characteristics, offering routes to desired devices, such as fast-response pH sensors. Development of a method for calculating pKa values for azaIC systems may provide some indication of the pH sensing capabilities of these systems and assess the pH range over which a pH response could be observed for these films. The possibility of extending the general

calculation method without Complete Basis Set Methods used in this work to the calculation of pKa's using the carboxylic acids studied by Liptak and Shields[3] as an example system will therefore be considered.

By analogy with the calculation of peak oxidiation potentials with respect to a reference redox species, discussed in Section 4.3, it is possible in principle to calculate the pKa of a molecule with respect to a reference acid/base system. To calculate the pKa of a molecule X, pKa_x, against that of a reference molecule Y, pKa_Y, the acid dissociation constants for both species must be considered:

$$XH^+(aq) + H_2O \xrightarrow{\Delta G_X} X_{(aq)} + H_3O^+(aq) \quad \textbf{Reaction 6.3.1}$$

$$YH^+(aq) + H_2O \xrightarrow{\Delta G_Y} Y_{(aq)} + H_3O^+(aq) \quad \textbf{Reaction 6.3.2}$$

Combining Equation 6.3.1 and Equation 6.3.2 gives:

$$YH^+(aq) + X_{(aq)} \xrightarrow{\Delta G_{calc}} Y_{(aq)} + XH^+(aq) \quad \textbf{Reaction 6.3.3}$$

Where

$$\Delta G_{calc} = \Delta G_Y - \Delta G_X \quad \textbf{Equation 6.3.1}$$

Noting that $pKa_?$ and $\Delta G_?$ are related by:

$$pKa_? = \frac{\Delta G_?}{2.303RT} = -\log_{10} Ka_? \quad \textbf{Equation 6.3.2}$$

pKa_x can then be calculated from a known value of pKa_Y by combining Equation 6.3.1 and Equation 6.3.2 to give:

$$pKa_X = pKa_Y - \frac{\Delta G_{calc}}{2.303RT} \quad \textbf{Equation 6.3.3}$$

Where ΔG_{calc} can in principle be calculated from the energies of the constituent species in the reaction, as:

$$\Delta G_{calc} = G_Y + G_{XH^+} - G_{YH^+} - G_X \quad \textbf{Equation 6.3.4}$$

This method avoids the need to accurately calculate the energy of the H_3O^+ species, which, like the calculation of the energy of a free electron in the redox reaction, is fraught with difficulty and a matter of contention as to whether the energy of the H_3O^+ species or the free proton in solution provides the best model for the deprotonation reaction of an acid species[3]. There is a further potential advantage in terms of molecular solvation if X and Y are chosen to be chemically similar. If they

have similar acidic groups, then errors in the calculated solvated energies of G_Y, G_{YH+}, G_X and G_{XH+} due to implicit solvation may cancel, increasing accuracy.

The calculation of pKa's is highly sensitive to errors, with an error of 1.36 kcal/mol in ΔG_{calc} corresponding to an error of 1 pKa unit at 298 K from Equation 6.3.2. If the error in the calculation of $\Delta G_?$ is similar to the error of 40 mV observed in the calculation of redox potentials then a standard deviation of 0.68 pKa units would be expected from these dissociation calculations. However, these calculations use water solvation rather than acetonitrile and so the errors may well be different.

Table 6.3.1 shows the observed and calculated pKa's for the range of carboxylic acids studied by Liptak and Shields[3], for which they reported the ability to calculate pKa's to an accuracy of less than half a pKa unit using Complete Basis Set Methods (CBSM). This data is summarised in Figure 6.3.1, with the error bars showing the estimated error of 0.68 pKa units. It can clearly be observed that the differences in pKa's using the simplified and computationally less expensive methodology in this work calculates the differences in pKa's between the carboxylic acids poorly, with the error in the calculated pKa differences being much greater than the 0.68 pKa units expected if the error in the calculation was simply of the same magnitude as that observed in the calculation of redox potentials.

Acid, X **Y = cyanoacetic acid**	**Experimental[3]**		**Calculated this work**	**Calculated CBSM[3]**	
	pKa_X	**$\Delta pKa = pKa_X - pKa_Y$**	**$\Delta pKa = pKa_X - pKa_Y$**	**pKa_X**	**$\Delta pKa = pKa_X - pKa_Y$**
Cyanoacetic acid	2.45	-	-	2.34	-
Chloroacetic acid	2.85	0.4	0.73	3.36	0.51
Formic acid	3.75	1.3	2.52	3.53	1.19
Acetic acid	4.75	2.3	5.33	5.19	2.85
Pivalic acid	5.03	2.58	6.75	5.19	2.85

Table 6.3.1. Comparison of observed[3] and calculated pKa's for a range of carboxylic acids.

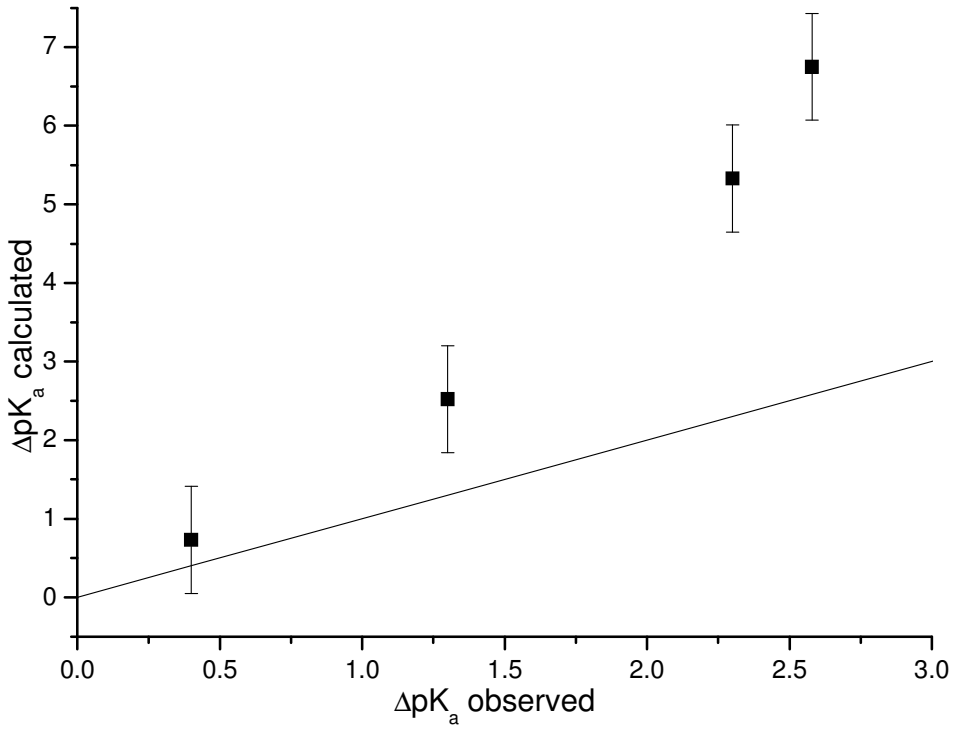

Figure 6.3.1. Plot of calculated vs. observed pKa values for the calculations shown in Table 6.3.1. The line shows the relationship expected if calculated and observed data were equal.

The aim of these pKa calculations was to see if the B3LYP method and 6-311+G(d,p) basis set could provide a reasonable estimation of the acid/base properties of a species without resorting to the more sophisticated and computationally more expensive methods used by others[3]. The most accurate of those methods had a maximum error of 0.5 pKa units. If the error in the pKa calculations had been similar to the error observed in calculating oxidation potentials in nonaqueous solutions then the calculations would have been of the same order of accuracy as the more sophisticated methods. It is clear that the error in calculating the pKa's of acids in aqueous solutions is far larger than this. This study on carboxylic acids suggests that the errors in the energies calculated using the B3LYP method with 6-311+G(d,p) basis set and PCM solvation are too large to calculate pKa's to any useful accuracy and that the calculation of acid/base properties is currently restricted to methods which are computationally more expensive. For these reasons and due to the lack of a suitable reference molecule it was decided that the

calculation of pKa to estimate the working range for a potential azaIC pH sensor was beyond the scope of the general calculation method of this thesis.

6.4 Other Substituted Indolocarbazoles.

The calculations in section 6.2 predict that through judicious positioning of aza-groups within the ring structures of ICs it may be possible to form single dimer products. Another potential route to single dimer products could be achieved by blocking probable coupling positions with substituents. Wharton[2] showed that the mono-bromination of IC is possible with N-bromosuccinamide yielding 2- and 5-bromoIC. The redox behaviour of 5-substituted ICs is discussed in Chapter 5. In this section the calculated redox behaviour of 2-bromoIC and two di-bromoICs will be considered, these represent a group of substituted ICs which may be possible synthetic goals following successive bromination, 2, 5- and 5, 10-dibromoIC.

Figure 6.4.1 show the structures of the three brominated ICs. The calculated peak oxidation potentials for these molecules are summarised in Table 6.4.1 with 5-bromoIC included as a reference. As discussed in Chapter 5, the peak oxidation potentials of 5-substituted-ICs show a linear relationship with Hammett substituent constant, σ^+. 5-bromoIC correspondingly has a higher oxidation potential than IC. It is interesting to note that the predicted peak oxidation potential for 2-bromoIC is the same as that for 5-bromoIC suggesting that substitution in the 2 and 5 positions has a similar effect on the reactivity of the IC substrate. As with the addition of additional aza-groups discussed in Section 6.2 the addition of additional bromo-groups is predicted to have the effect of increasing the peak oxidation potentials, but to a lesser extent than the effect of aza-group addition. The predicted peak oxidation potentials for all bromoICs are in the potential window of acetonitrile/background electrolyte systems; and so electrochemical studies of all these species should therefore be possible.

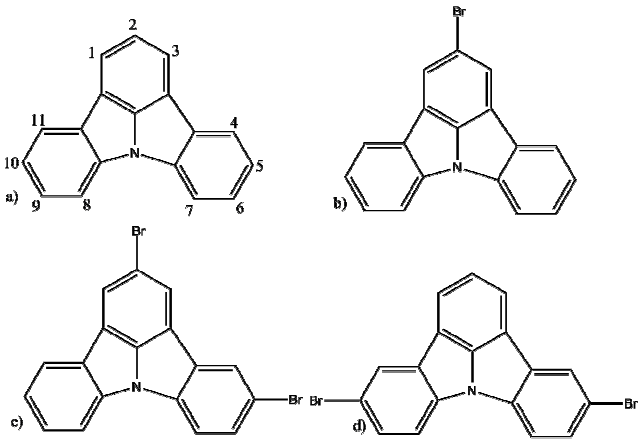

Figure 6.4.1. (a) Structure and numbering of IC. Structures of (b) 2-bromoIC, (c) 2, 5-dibromoIC and (d) 5, 10-dibromoIC.

Indolocarbazole	Calculated peak oxidation potential (vs Fc/Fc^+) / V	Experimental peak oxidation potential (vs Fc/Fc^+) / V
IC	+1.01 ± 0.04	+1.01[2]
5-bromo	+1.06 ± 0.04	+1.12[2]
2-bromo	+1.06 ± 0.04	-
2, 5-dibromo	+1.11 ± 0.04	-
5, 10-dibromo	+1.09 ± 0.04	-

Table 6.4.1. Calculated oxidation potentials of four bromoICs vs Fc/Fc^+.

Figure 6.4.2 shows the electron spin density maps of the three bromoIC radical cations, with 5-bromoIC included for reference. For the 2-bromoIC it is clear that the greatest electron spin density is located in the 5 and 10-positions, the likely product from the coupling of two 2-bromoIC radical cations would therefore be 5, 5'-di-2-bromoIC due to the symmetry of the molecule. The greatest electron spin density on the 2, 5-dibromoIC radical cation can be found in the 10 position, indicating that coupling of two radical cations of this dibromoIC would lead to the formation of a single 10, 10'-dimer product. The highest electron spin density for the 5, 10-dibromoIC in a position which would not be sterically hindered for coupling is in the 2-position, the electron spin density in this position is, however, relatively low. Coupling of this dibromoIC would lead to a single 2, 2'-dimer product, due to the relatively low electron spin density on this 2 position it is possible that the coupling rate may be reduced. Such a reduction in the coupling rate would be observed

experimentally by an increase in the peak reduction current in the CV of this dibromoIC. The calculations in this section suggest that selective blocking of IC coupling positions may provide a route to single oligomeric properties compared to the three dimer products observed on 5-substituted IC coupling.

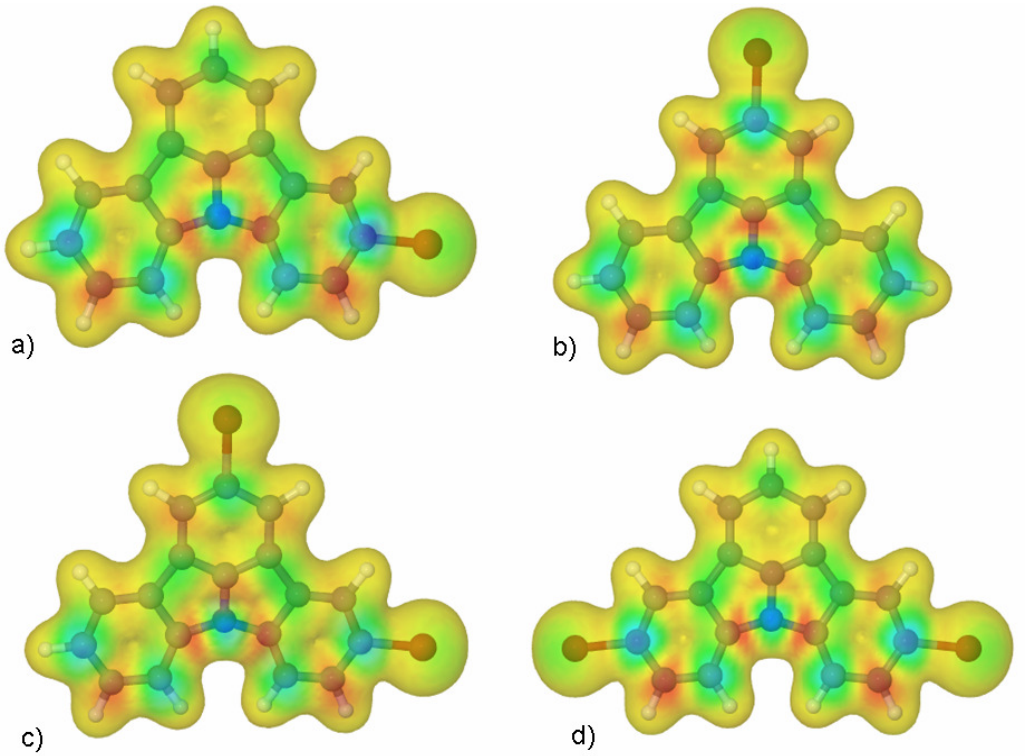

Figure 6.4.2. Electron spin density maps for radical cations of modified ICs, the darkest blue areas show the regions of highest spin density. (a) 5-bromoIC, (b) 2-bromoIC, (c) 2, 5-dibromoIC and (d) 5, 10-dibromoIC. (The colouring is schematic as follows: blue indicates a positive spin density (0.003) whilst red is negative (-0.001). The same range of spin density was used for all 4 maps).

6.5 Azapyrrolocarbazoles.

The next system to be considered is the modification of the pyrolo[3,2,1-jk]carbazole system discussed in Section 4.6. This modification will again be the introduction of a pyridine type nitrogen into the PC structure to form azaPCs. As with azaICs it is possible that films formed from the electrooxidation may be able to form the basis of sensing devices for metal through chelation to metals, or through protonation to act as a fast response pH sensor. Wharton[2] also found that he was unable to characterise the product formed from electrooxidation of PC and attributed this to the poor

solubility of the formed product. Wharton also found that the dimeric products of azaIC electrooxidation were more soluble than the dimeric products of IC electrooxidation, and suggested that the products of azaPC electrooxidation would be more soluble which would aid in the characterisation of azaPC electrooxidation products. Figure 6.5.1 shows the structures of two azaPCs to which Wharton was able to find synthetic routes.

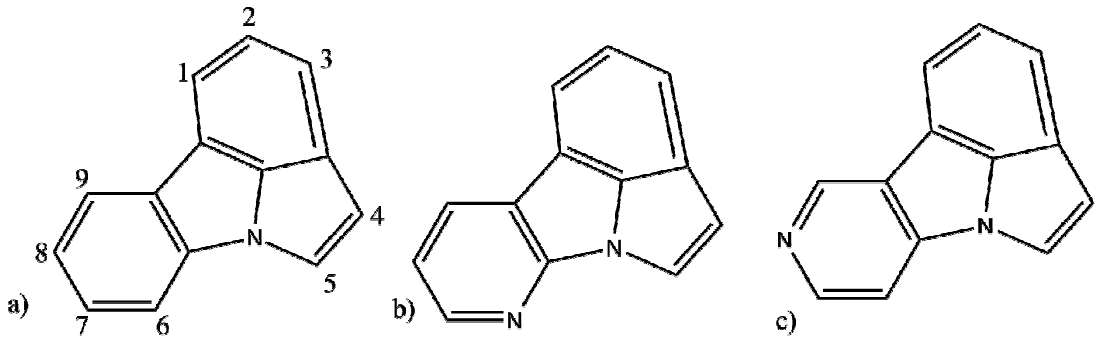

Figure 6.5.1. (a) Stucture and numbering of PC. Structures of (b) 6-azaPC and (c) 8-azaPC.

Table 6.5.1 shows the predicted peak oxidation potentials for these azaPCs with the calculated peak oxidation potential of PC for comparison. As previously observed for azaICs the introduction of the pyridine type nitrogen into the ring system of PC has the effect of raising the oxidation potential relative to the unmodified PC**.** Again the calculated peak oxidation potentials are well within the solvent window of the preferred background electrolyte systems used within the group for studies on the electrooxidation of heteroaromatics. It was assumed by Wharton that azaPCs upon electrooxidation would yield a similar product to that formed by PC after electrooxidation. To see if this is likely to be the case it is necessary to discuss whether the electron spin density distributions of the azaPCs radical cations are similar to that of the PC radical cation.

Pyrrolocarbazole	**Calculated peak oxidation potential (vs Fc/Fc^+) / V**
PC	+1.01 ± 0.04
6-azaPC	+1.27 ± 0.04
8-azaPC	+1.32 ± 0.04

Table 6.5.1. Calculated oxidation potentials of PC and two azaPCs vs Fc/Fc^+.

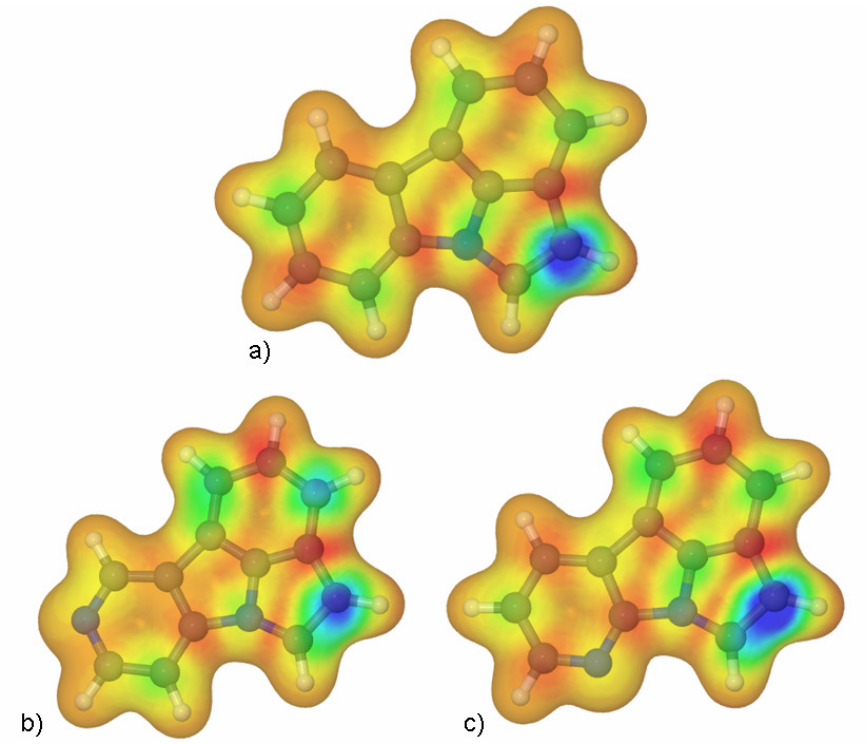

Figure 6.5.2. Electron spin density maps for radical cations of modified PCs, the darkest blue areas show the regions of highest spin density. (a) PC, (b) 8-azaPC and (c) 6-azaPC. (The colouring is schematic as follows: blue indicates a positive spin density (0.005) whilst red is negative (-0.001). The same range of spin density was used for all 3 maps).

Figure 6.5.2 shows the electron spin density distributions of PC and the two azaPCs for comparative purposes. It is clear that the electron spin density maps for all three molecules are very similar, with the only real difference being a decrease in electron spin density around the inserted aza-nitrogens. The greatest electron spin density in each of the azaPCs is clearly in the 4-position, the likely first product of electrooxidation is the 4, 4'-azaPC dimer. As the azaPCs are so similar to PC, it is likely that as calculated for PC these dimers will have an oxidation potential such that they will be readily oxidised at the electrode where they may be able to further couple with a monomer radical cation to form a trimer, as discussed for PC. Due to the size of these azaPC dimers and constraints on time it has not been possible to perform calculations on these dimers to support this hypothesis.

6.6 1-azacycl[2,3,2]azine.

Cyclazines are tricyclic systems containing a completely conjugated perimeter of sp^2 hybrlidized carbon atoms held planar by a centrally lying nitrogen atom. Initial studies on cycl[3,2,2]azines was inspired by the requirements for aromaticity in aromatic systems[4]. Subsequent studies on these systems have either focussed on simpler synthetic routes[5] or on the distribution of electron spins within anions[6], the only electrochemical study of a cycl[3,2,2]azine system involves the incorporation of a unit onto thiophene prior to polymerisation of the thiophene[7]. Figure 6.6.1.a shows the structure of 1-azacycl[2,3,2]azine (CZ), which has been synthesised by James Montgomery in the McNab group at the University of Edinburgh and is currently being purified. The only mention of CZ in the literature is when discussing specific nomenclature for cyclazines[8] and for calculations on the structures of cyclazines[9]. As there appear to have been no previous studies on the electrochemistry of cyclazine systems they make an interesting candidate for the new general computational method, to assess the potential electrochemical properties of CZ.

The peak oxidation potential for CZ was calculated to be +1.05 ± 0.04 V vs. Fc/Fc^+. As with the other species discussed thus far this potential is within the potential window of the acetonitrile solvent limit. The electron spin density distribution (Figure 6.6.1.b) shows the greatest electron spin density (discounting sterically hindered sites) in the 4 and 7-positions. Coupling of radical cations in these positions would be likely to yield, initially, three CZ dimers with 4, 4'-, 4, 7'- and 7, 7'-coupling.

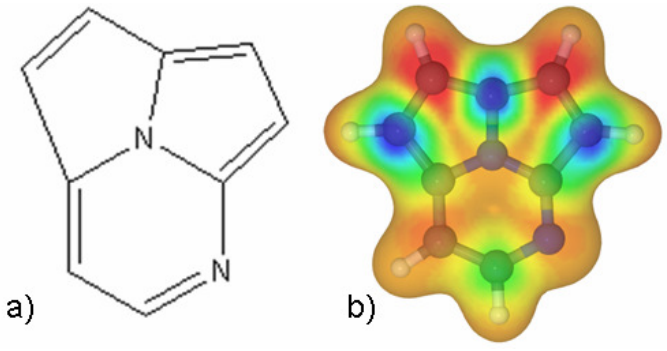

Figure 6.6.1. Electron spin density maps for radical cation of CZ, the darkest blue areas show the regions of highest spin density. (The colouring is schematic as follows: blue indicates a positive spin density (0.005) whilst red is negative (-0.001)).

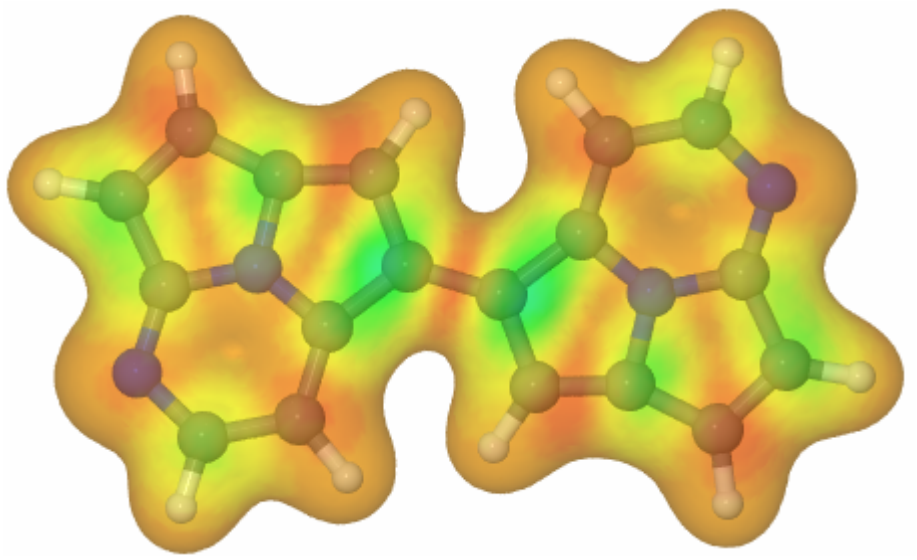

Figure 6.6.2. Electron spin density maps for radical cation of the 4,4'-dimer of CZ, the darkest blue areas show the regions of highest spin density. (The colouring is schematic as follows: blue indicates a positive spin density (0.005) whilst red is negative (-0.001)).

The 4, 4'-dimer was selected for further study to ascertain the properties that may be expected from an electrochemically formed dimer of CZ. The oxidation potential of this dimer is calculated to be +0.42 ± 0.04 V vs Fc/Fc^{+}. This is significantly lower than the oxidation potential of CZ and any dimer that is formed at the electrode surface is therefore likely to be oxidised rapidly at the potentials used for CZ oxidation. Figure 6.6.2 shows the electron spin density map for the radical cation of the resulting 4, 4'-dimer. The largest electron spin density can be observed in the 4 and 4'-positions, where further coupling is exceedingly unlikely as it would result in a loss of aromaticity. The next largest electron spin density is observed in the 7 and 7'-positions, and there is therefore a possibility that further coupling could take place in these positions, to CZ units or other dimer units. Such coupling could lead to the formation of a linear CZ oligomer and/or polymer with linking between monomer units from the 4 and 7-positions.

The possibility of forming a novel conducting polymer from cyclazine suggests that such systems make intriguing candidates for future electrochemical studies.

6.7 Conclusion.

We have extended our general computational method established in Chapters 4 and 5 to a range of novel aromatic heterocyclic systems. Calculations suggest that all of the molecules studied should be oxidizable within the potential window of a suitable background electrolyte such as 0.1 M $LiClO_4$ in acetonitrile. The electron spin density maps of radical cations suggests that the formed radical cations may couple in a way to produce a range of novel electroactive films, of stacked oligomers similar to indole trimer and IC films, and linear polymeric films similar to polypyrrole. The application of this approach may provide useful insight into how heteroaromatic molecules couple, as well as providing motivation for synthesis and experimental study of novel heteroaromatics. Discussion of these results with the relevant synthetic groups in preparation of future work is planned.

6.8 References.

[1] Rodgers, M. T.; Stanley, J. R.; Amunugama, R. *J. Am. Chem. Soc.,* **2000**, *122*, 10969.

[2] Wharton, S. I. *Ph. D. Thesis, "Synthesis and Characterisation of Novel Conducting Films Based On Indolo[3,2,1-jk]carbazole Systems.", University of Edinburgh* **2005**.

[3] Liptak, M. D.; Shields, G. C. *J. Am. Chem. Soc.* **2001**, *123*, 7314.

[4] Windgassen, R. J.; Saunders, W. H.; Boekelheide, V. *J. Am. Chem. Soc.* **1959**, *81*, 1459.

[5] Jessep, M. A.; Leaver, D. *Chem. Comm.* **1979**, 790.

[6] Atherton, N. M.; Gerson, F.; Murrell, J. N. *Mol. Phys.* **1963**, *6*, 265.

[7] Behroozi, S. J.; Mandal, B. K. *Synth. Met.* **1999**, *107*, 93.

[8] Ceder, O.; Beijer, B. *J. Heterocycl. Chem.* **1976**, *13*, 1029.

[9] Sabljic, A.; Trinajstic, N. *J. Mol. Struct.* **1978**, *49*, 415.

Chapter 7: Studies on 2,3'-diindoles.

7.1 Introduction.

As discussed in Chapter 4, the electrooxidation of indole was found to yield an electroactive film consisting of an asymmetric indole trimer. This has been fully characterised using mass spectrometry and NMR spectroscopy (Figure 7.1.b).[1] It has been proposed by others, however, that electrooxidation of indole leads to formation of a linear conducting polymer, with linkage of the monomer units occurring via the 2 and 3 positions (Figure 7.1.c).[2,3] The characterisation of the "polymers" in most of these studies is largely limited to IR spectroscopy which shows a decrease in the intensity of the peaks associated with the C-H stretch assigned to the 2 and 3 positions of the indole. This would also be found with the formation of asymmetric trimer. Only one other study[4] utilises NMR in the characterisation of the proposed linear "polymer". The NMR spectra in this paper are however identical to those published by Mackintosh et al[5,6] which demonstated cyclic trimer formation. As with the IR spectra these NMR results show coupling in the 2 and 3 position of the indole but this 1D-NMR does not yield the detailed coupling assignment provided by the COSY and NOESY techniques deployed by Mackintosh *et al.*[7] to enable cyclic trimer structure to be unambiguously determined. Therefore an open question remains as to whether linear indole oligomers or polymer can be formed from monomer with 2,3-coupling and once formed, how they would polymerise and what their properties would be. Previous work on coupling of indoles via bromination shows a route to the formation of a symmetric trimer displaying 2,3'-coupling[8], it is, however, extremely unlikely that the product of dimer coupling will be a trimer.

Previous work on pyrrole and thiophene, which couple to form linear polymers, employed dimers and larger oligomers as a means for producing linear polymeric films[9] and to attempt to lower the oxidation potential at which polythiophene films can be formed so that polymerisation can take place in aqueous solutions[10] with more controlled coat morphologies. Therefore, a range of 2,3'-dimers of 5-substituted

indoles (Figure 7.1.d) have been synthesised by Rob Valentine of the Robertson group at the University of Edinburgh. This chapter will report a study of the electrochemical properties of these dimers and the electroactive films formed upon their electrooxidation, and will discuss the attempts made to characterise the products of these films. The computational method established within this thesis will also be extended to these systems and the applicability of this extension will be discussed.

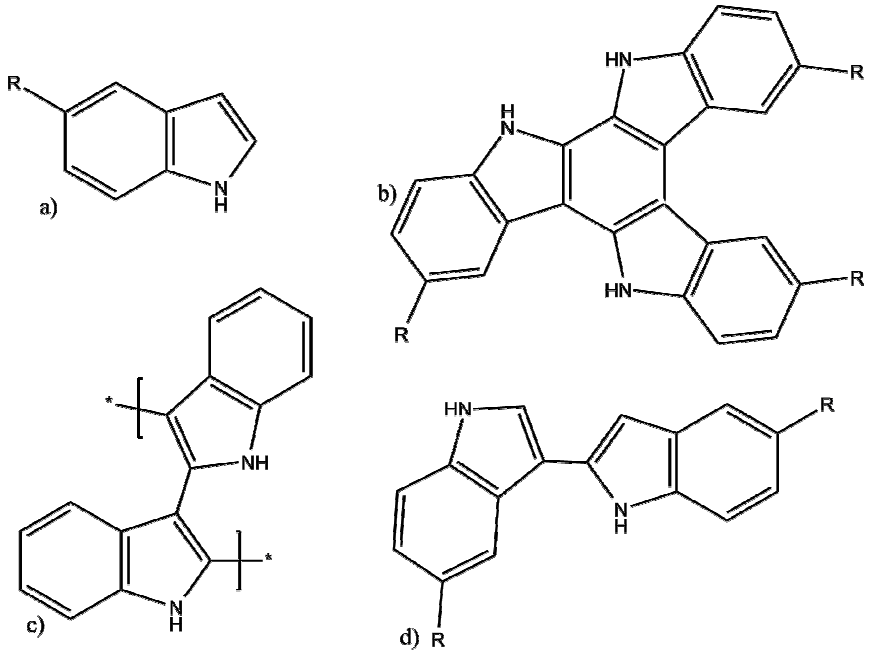

Figure 7.1.1. Various 5-substituted indole forms. a) 5-substituted indole, b) 5-substituted indole asymmetric trimer, c) suggested form for linear indole polymer and d) 2,3'-di-5-substituted indoles.

7.2 Electrochemistry of 2,3'-dimers of 5-substituted Indoles.

7.2.1 Cyclic Voltammetry of 2,3'-dimers of 5-substituted Indoles.

The CVs of four 2,3'-dimers of 5-substituted indoles are shown in Figures 7.2.1-4, the form of each of these CVs is similar and comparison of the four dimers will provide a basis to study two of the dimers in further detail in the following sections. All the CVs show an initial peak in the range of +0.4 to +0.45 V followed by a shoulder or peak near +0.6 V before an increase in current at potentials above +0.8 V. For each dimer, repeated cycling leads to the formation of a very thin film on the electrode surface.

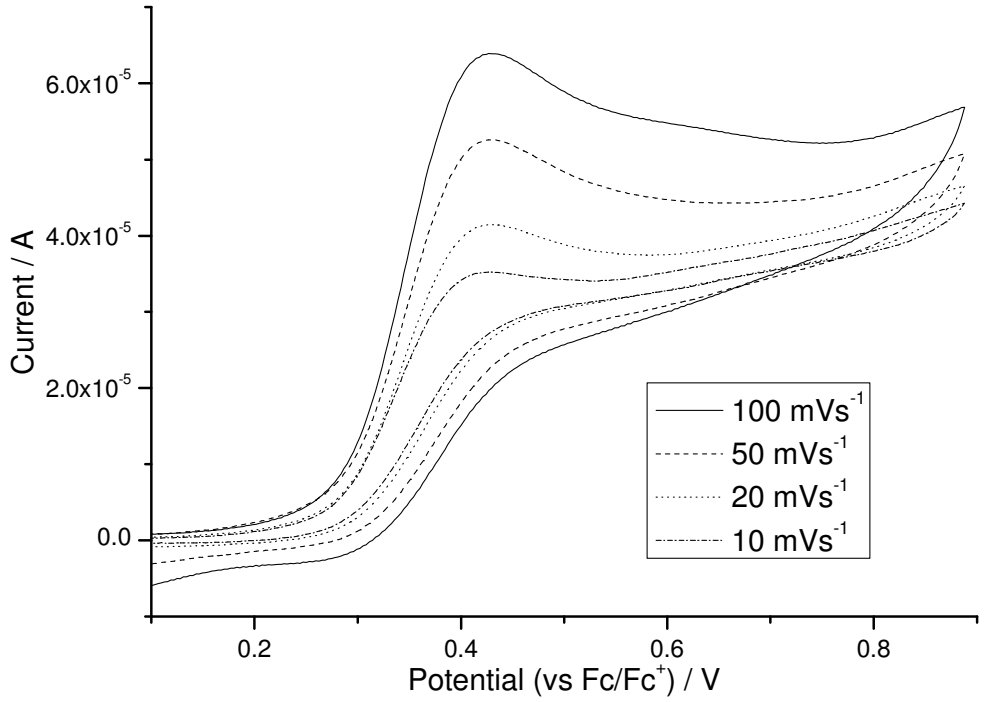

Figure 7.2.1. CVs of 0.9 mM 2,3'-diindole solution in background electrolyte with varying sweep rates.

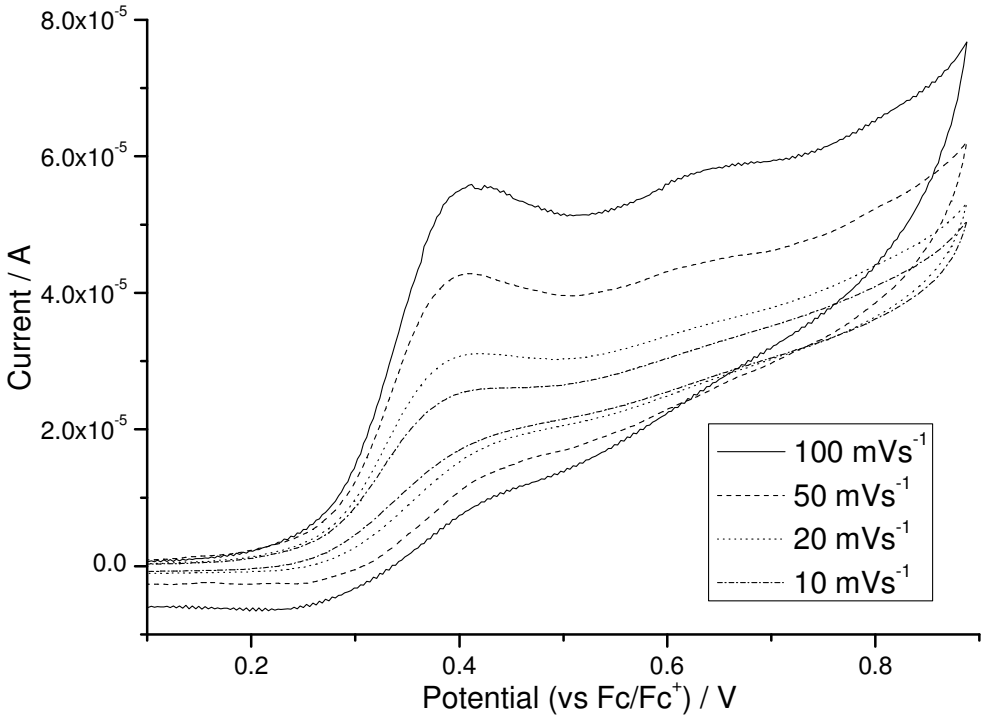

Figure 7.2.2. CVs of 0.9 mM 2,3'-di-5-methoxyindole solution in background electrolyte with varying sweep rates.

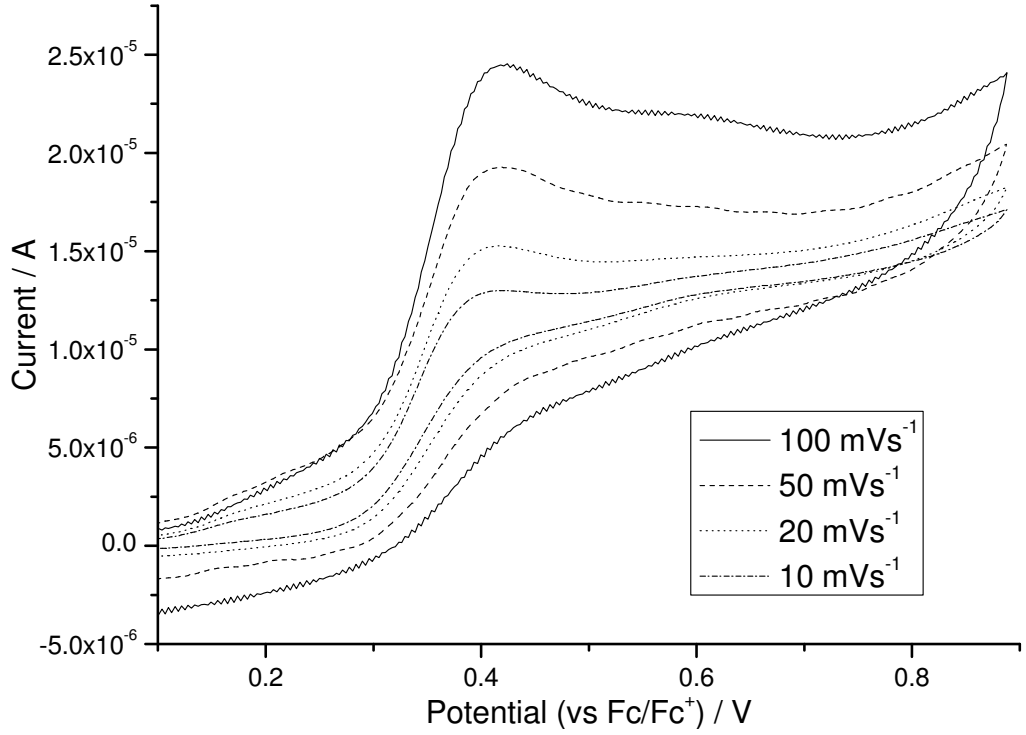

Figure 7.2.3. CVs of 1 mM 2,3'-di-5-methylindole solution in background electrolyte with varying sweep rates.

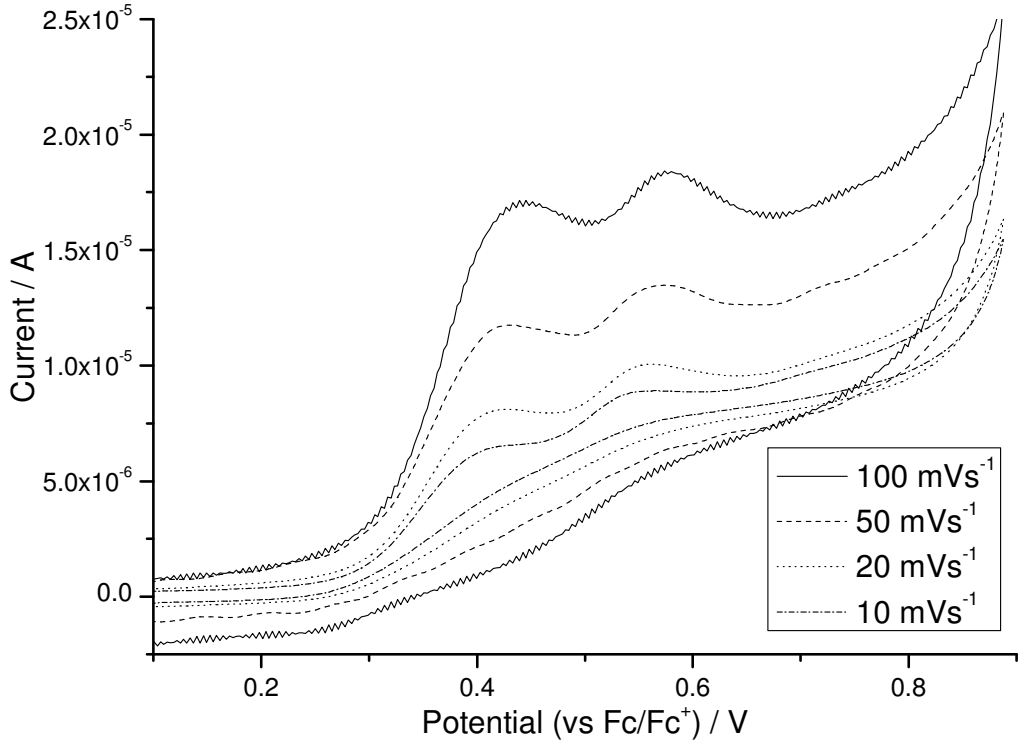

Figure 7.2.4. CVs of 1 mM 2,3'-diindole-5-carboxylic acid solution in background electrolyte with varying sweep rates.

Table 7.2.1 summarises the peak oxidation potentials observed for the dimers. The difference between the peak potential, E_P, and the half-wave potential, $E_{P/2}$, is between 80 and 90 mV for all dimers. This difference is significantly larger than the 56.5/n mV splitting that would be expected for fully reversible one electron systems, suggesting that this peak is the result of an irreversible one electron oxidation.

R group	E_P / V	$E_{P/2}$ / V	$E_P - E_{P/2}$ / mV
H	+0.427	+0.339	88
OCH_3	+0.412	+0.330	82
CH_3	+0.418	+0.337	81
CO_2H	+0.442	+0.357	85

Table 7.2.1. Peak potential, half-wave-potential and differences for 2,3'-indole dimers at v = 100 mVs^{-1}.

The cause of the shoulders between +0.6 and +0.8 V is not clear. The most likely cause is either the presence of a small amount of impurity present in the sample which may be a by-product of the synthesis, or it may arise from the possibility of having two rotamers of the indole dimers as shown in Figure 7.2.5, with each rotamer having a different oxidation potential or oxidation of a product formed from coupling. The possibility of the existence of the two rotamers and the possible effects on oxidation potentials will be discussed further in Section 7.4.

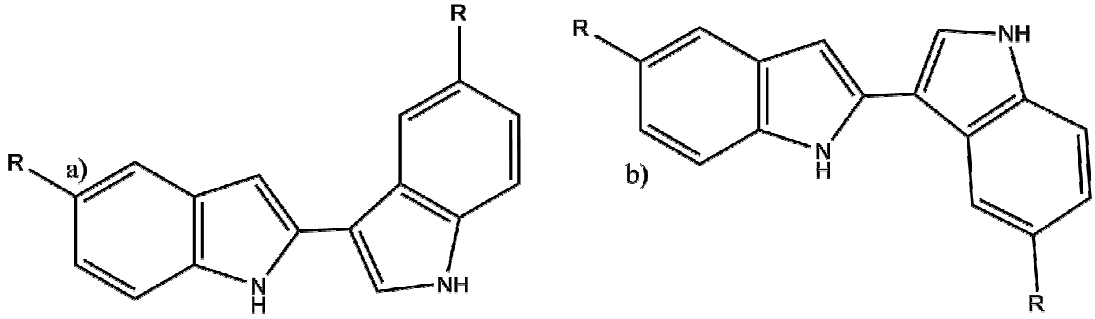

Figure 7.2.5. Possible rotamers for 2,3'-diindoles. a) "cis" and b) "trans" conformations.

As the oxidation is in solution it is anticipated that the peak current is proportional to the square root of the sweep rate, $v^{1/2}$. It is clear that the data shown in Figure 7.2.6 follow this relationship. It is expected, however, that this relationship should also have a zero intercept, but this is not observed in any of these plots except perhaps for

the 2,3'-diindole-5-carboxylic acid. A non-zero intercept could arise where there is convection of material to the electrode surface. In these CV experiments the rotating disc was stationary and there was no source of stirring within the solution to cause significant convection so this is unlikely to be the cause. At low sweep rates, 10 mVs^{-1}, it can be seen that the peaks begin to approach a potential wave, rather than forming a peak; this behaviour has not been observed for similar systems that have been studied electrochemically in this manner (such as indoles[1], indolocarbazoles[11] or pyrrolocarbazole[11]). The greatest difference between the other heterocyclic species and the indole dimer species is the very poor solubility of the dimer systems in acetonitrile compared to the other mentioned systems. It is possible that this poor solubility may lead to the deposition of a thin layer of surface adsorbed molecules prior to electrochemical cycling, leading to an alteration of the surface properties of the electrode.

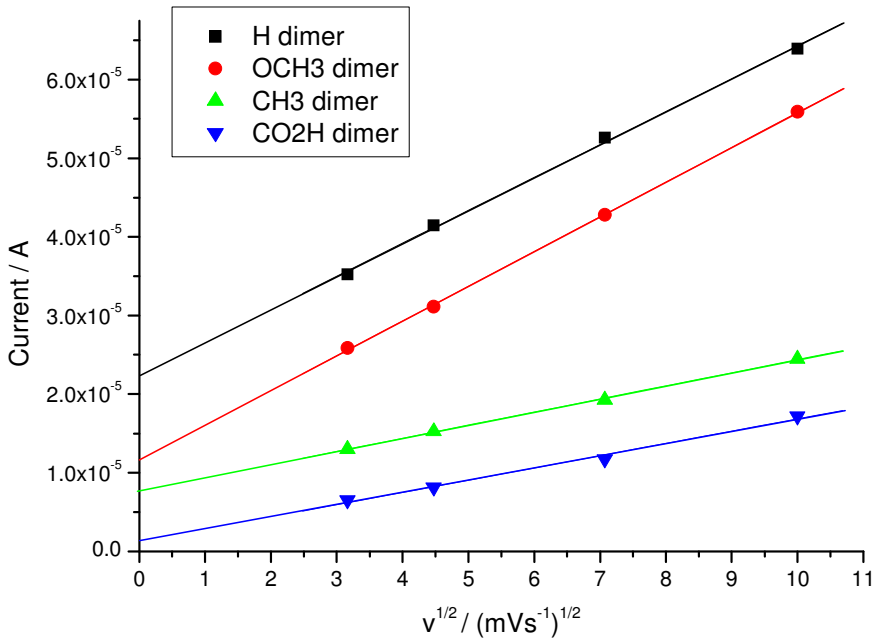

Figure 7.2.6. Peak current *vs.* the square root of sweep rate for the electro-oxidation of (■) 2,3'-diindoles, (●) 2,3'-di-5-methoxyindole, (▲) 2,3'-di-5-methylindole and (▼) 2,3'diindole-5-carboxylic acid.

The CVs resulting from the first three sweeps for solutions of 2,3'-diindole and 2,3'-di-5-methoxyindole are shown in Figures 7.2.7 and 7.2.8 respectively. While repeated cycling forms a thin yellow coloured film on the electrode surface there is

no obvious growth of peaks associated with the redox properties of a formed film, as was observed for 5-methylIC in Section 5.2. The formed film is clearly not insulating, as continued electrode activity is observed with continued sweeps. If the formed film was insulating in character the electrode surface would rapidly become unreactive. The absence of clear redox peaks from the formed film and the thinness of the film suggest that film formation is a very inefficient process.

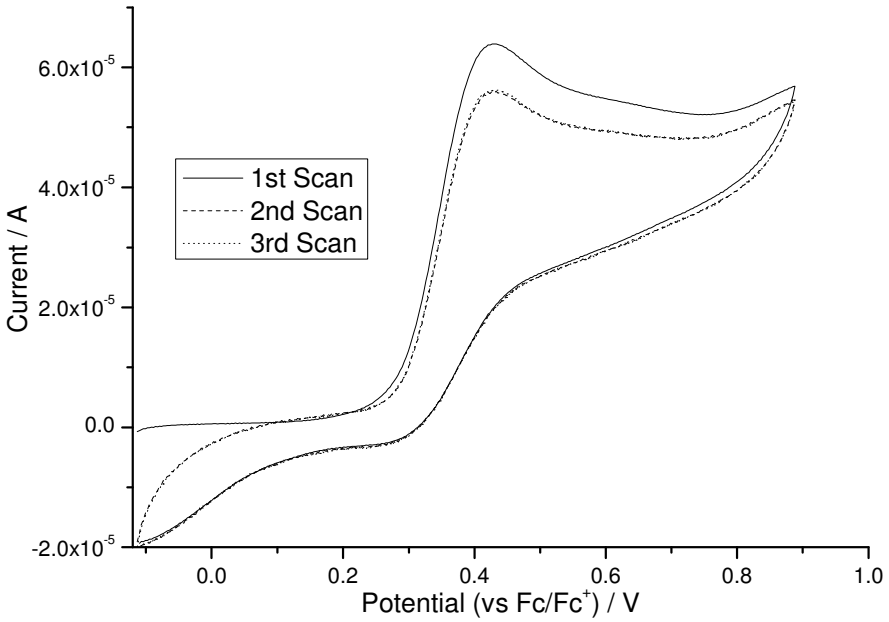

Figure 7.2.7. CVs of 0.9 mM 2,3'-diindole in background electrolyte. Sweep rate = 100 mVs^{-1}.

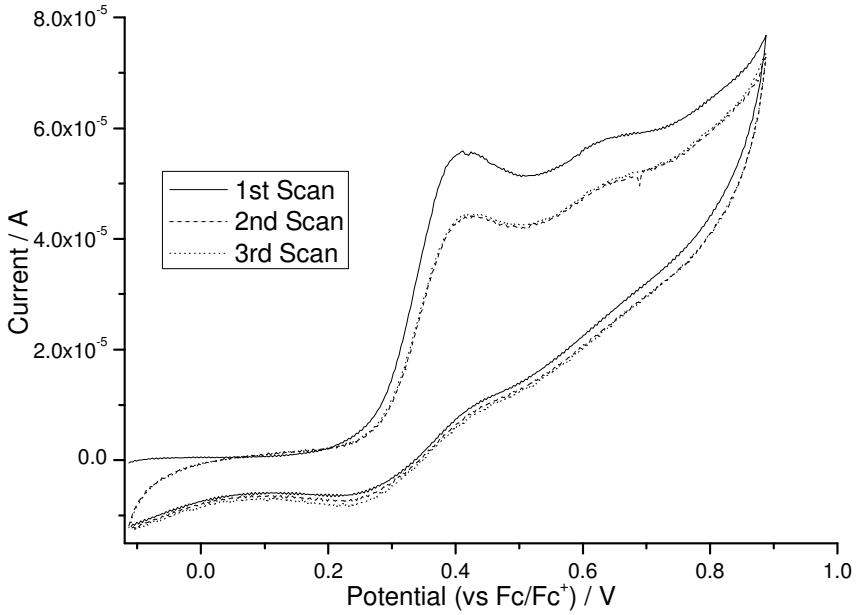

Figure 7.2.7. CVs of 0.9 mM 2,3'-di-5-methoxyindole in background electrolyte. Sweep rate = 100 mVs^{-1}.

7.2.2 Electro-oxidation of 2,3'-diindole and 2,3'-di-5-methoxyindole by Chronoamperometry at a Rotating Disc Electrode.

Due to the poor solubility of the indole dimers only the 2 dimers with the greatest solubility in acetonitrile solutions were selected for further study; these were the 2,3'-diindole and 2,3'-di-5-methoxyindole which were soluble up to 5 mM but insoluble at 10 mM concentrations. Typical current-time transients for the electro-oxidation of the diindoles are shown in Figure 7.2.8. Both diindoles show a similar response with an initial sharp peak upon stepping to an oxidising potential, consistent with the immediate oxidation of molecules at the electrode surface. A steady-state current is then observed and maintained for a long period of time, showing that the electrode surface remains active over the course of the experiment. Upon application of a reducing potential a negative peak is observed as charge is removed from the film formed at the electrode surface, the presence of a film on the electrode surface can be confirmed visually, while the charge observed during the reduction can be confirmed to be due to the redox-activity of the formed film through comparison to the charge passed at a bare platinum electrode in the absence of diindole.

CVs of films formed from 2,3'-diindole and 2,3'-di-5-methoxyindole are shown in Figures 7.2.9 and 7.2.10 respectively. The charge passed during the oxidation and reduction of these films in background electrolyte was found to be roughly equal to the reduction charge observed after film formations (Figure 7.2.8). The peak currents for the oxidation of the films with varying sweep rates are shown in Figures 7.2.11 and 7.2.12. For both films it can be observed that the peak currents are directly proportional to the sweep rate. This indicates that the film is fully oxidised on each sweep and charge transfer through the film is rapid; this would be expected for such electroactive thin films. It is worth noting that the oxidation peak for the formed film occurs at a similar potential to the oxidation peak of the dimer in solution; this may account for the failure to observe film formation *via* the growth of redox film peaks during cyclic voltammetry as commonly observed for formation of electroactive films.

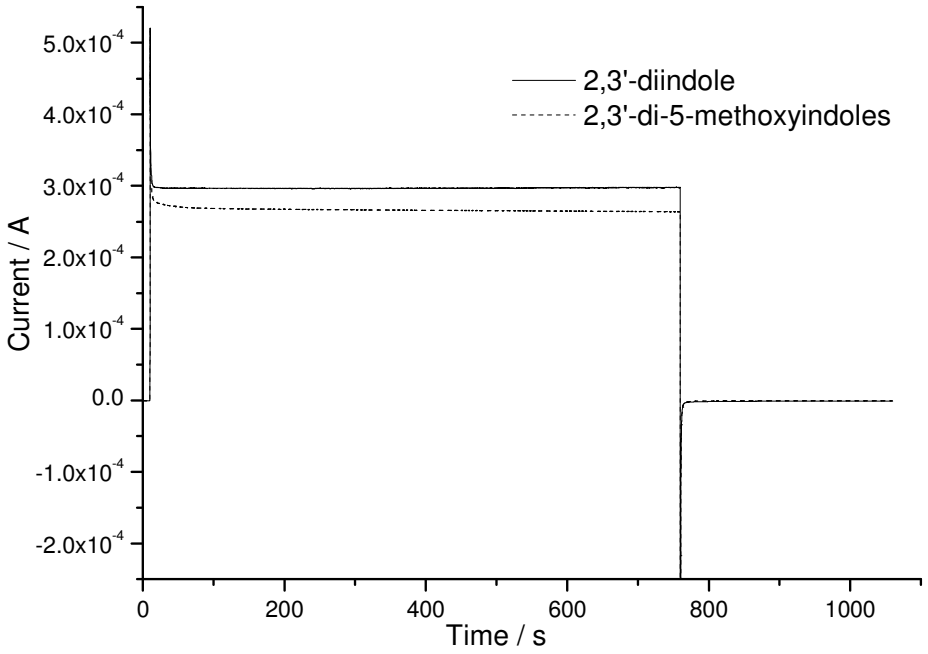

Figure 7.2.8. Current-time transients for the electro-oxidation of 5 mM solutions of 2,3'-diindole and 2,3'di-5-methoxyindole with background electrolyte. The electro-oxidation consisted of three potential steps one initial step of –0.113 V for 10 s, one step of +0.587 V for 750 s and a final step of –0.113 V for 300 s. All Potentials are with respect to Fc/Fc^+. Rotation speed of electrode was 1 Hz.

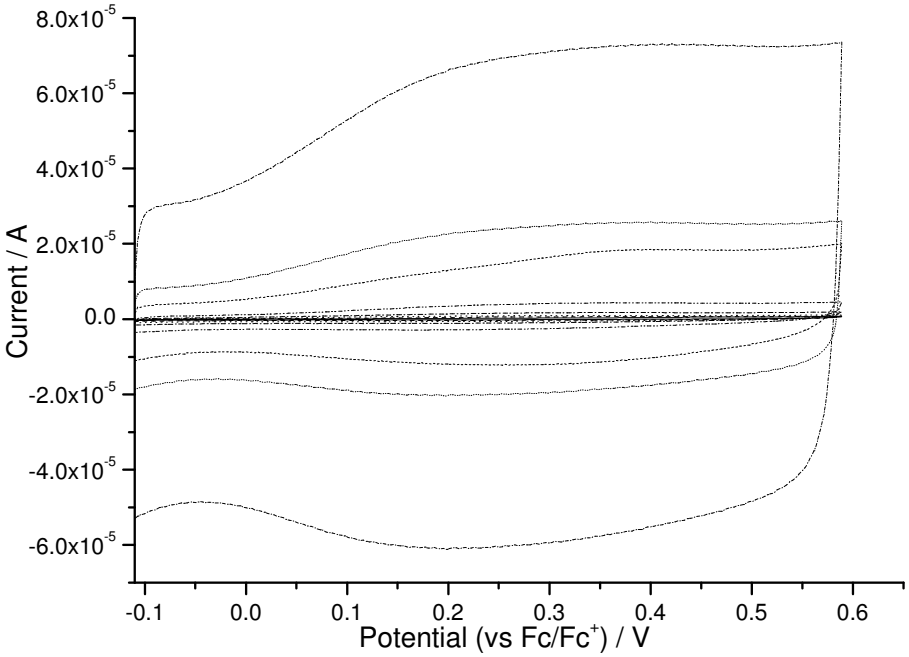

Figure 7.2.9. Variation of CVs with sweep rate for a film formed from 5 mM 2,3'-diindole solution over 750 s at a potential of +0.587 V vs Fc/Fc^+ and a rotation speed of 4 Hz. Film cycled in monomer-free background electrolyte solution at a range of sweep rates between 5 and 500 mVs^{-1}.

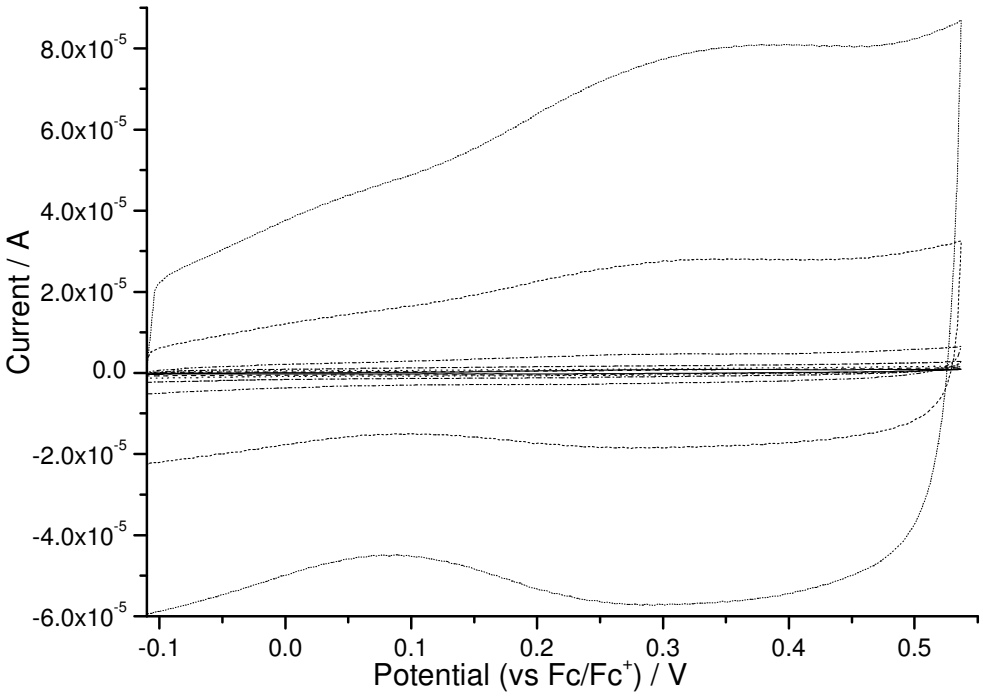

Figure 7.2.10. Variation of CVs with sweep rate for a film formed from 5 mM 2,3'-di-5-methoxyindole solution over 750 s at a potential of +0.587 V vs Fc/Fc^+ and a rotation speed of 4 Hz. Film cycled in monomer-free background electrolyte solution at a range of sweep rates between 5 and 500 mVs^{-1}.

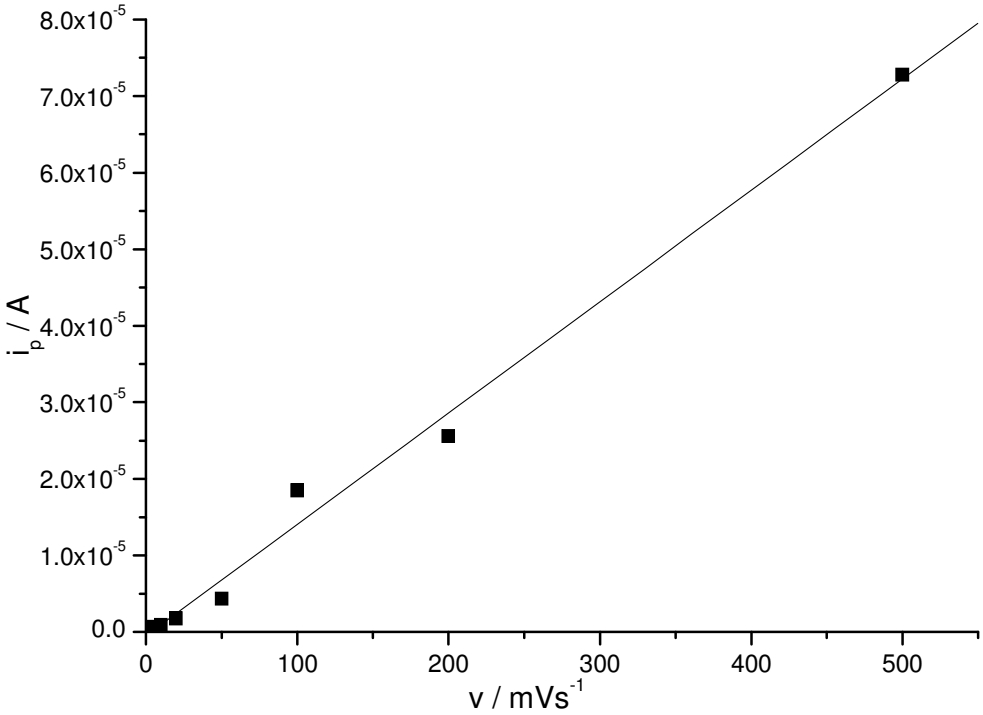

Figure 7.2.11. A Plot of peak oxidation current vs sweep rate of a film formed from the electro-oxidation of 2,3'-diindole.

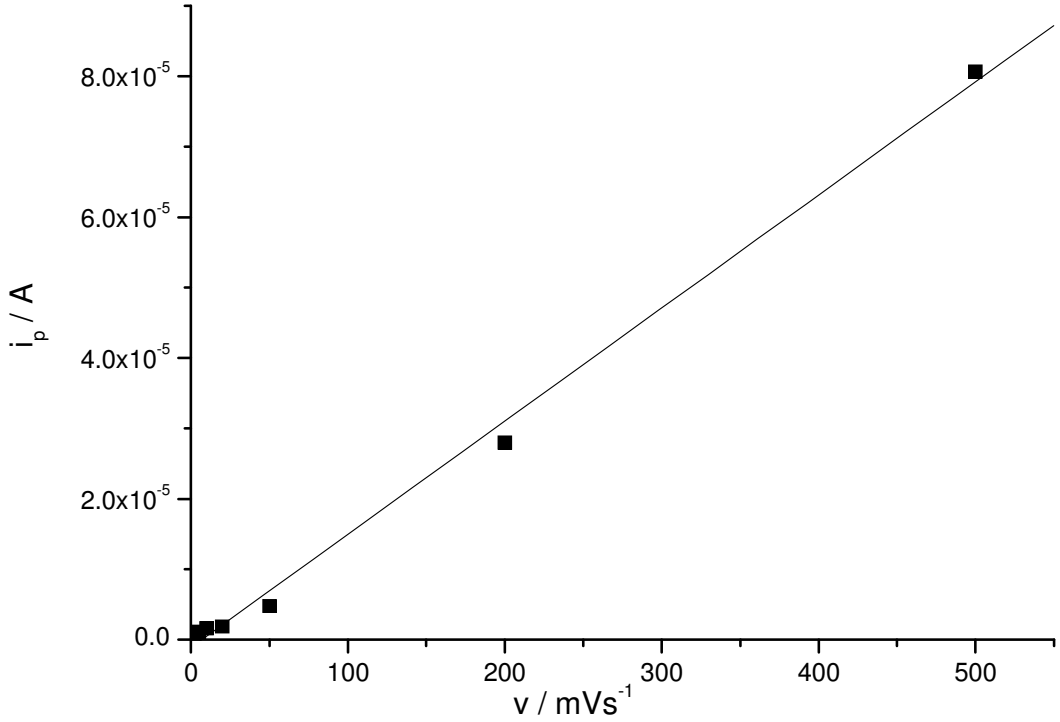

Figure 7.2.12. A Plot of peak oxidation current vs sweep rate of a film formed from the electro-oxidation of 2,3'-di-5-methoxyindole.

Comparison of the reduction charge of a formed film to the charge passed during the film formation can often yield information on the mechanism of film formation as in the cases of indoles[1] and indolocarbazoles[11].[††] These are summarised in Table 7.2.2. It can quickly be seen that all percentages are less than 0.5 % and significantly less than that expected for indole dimer, trimer or polymer film formation. This indicates that only a small amount of the oxidised dimer couples at the electrode surface to form a film. Upon continued electrooxidation it was found that a precipitate forms in solution; this precipitate may again indicate that coupling of diindole may occur away from the electrode surface and not contribute to film formation.

[††] Theoretical percentages of (reduction charge/oxidation charge) for indole trimer and indolocarbazole dimer film formations are 14% and 33% respectively[1,11]. For pyrrole and other linear polymers it is often found that there is one redox-active electron passed during film formation for every four monomer units, this would give a theoretical percentage of (reduction charge/oxidation charge) of 11% following film formation.

As previously discussed in Section 5.2.2, a powerful technique for the analysis of the electrode kinetics of a reaction is through analysis of the relationship between the current passed during electrooxidation and the rotation speed of the RDE, over a range of concentrations. To this end, the RDE was rotated at 1Hz and the potential was stepped from -0.113 V to +0.587 V vs Fc/Fc^{+}. Once steady-state currents were obtained the rotation speed was stepped up and repeated until data for rotation speeds of 1, 2, 4, 9 and 16 Hz were recorded (forward run). The process was then reversed (reverse run), by stepping down through the same sequence, until 1 Hz was reached again (Figures 7.2.13 and 7.2.14 for 2,3'-diindole and 2,3'-di-5-methoxyindole, respectively). The currents on the reverse run of this method generally show similar currents to those of the forward run. This can be attributed to a negligible increase in electrode area as conducting film growth occurs.

	Rotation Speed / Hz	**(Reduction Charge / Oxidation Charge) / %**		
		1.25 mM	**2.5 mM**	**5 mM**
2,3'-diindole	**1**	**0.42**	**0.42**	**0.36**
	4	**0.25**	**0.32**	**0.25**
	16	**0.28**	**0.34**	**0.42**
2,3'-di-5-methoxyindole	**1**	**0.48**	**0.39**	**0.25**
	4	**0.28**	**0.15**	**0.09**
	16	**0.23**	**0.11**	**0.07**

Table 7.2.2. Summary of the reduction charges of formed diindole films as a percentage of the oxidation charge passed during film formation at a range of concentrations and rotation speeds.

Analysis for both dimers using Koutecky-Levich plots (Figures 7.2.15 and 7.2.16 of 2,3'-diindole and 2,3'-di-5-methoxyindole respectively) shows that the data for each concentration gives a straight line. This indicates that the dimer oxidation and coupling obey 1st order kinetics as this is an assumption of the Koutecky-Levich equation (Section 2.1.2); this is indicative of a surface process[12]. The data were analysed by fitting all data to Equation 2.1.22, with n=1 and a global dimer diffusion coefficient of D = (2.0 ± 0.3) x 10^{-5} cm^2s^{-1} and (1.6 ± 0.3) x 10^{-5} cm^2s^{-1} for 2,3'diindole and 2,3'-di-5-methoxyindole, respectively. This diffusion co-efficient is

consistent with the previously reported diffusion co-efficients of 5 substituted indoles which range from 1.5 x 10^{-5} cm^2s^{-1} to 3.0 x 10^{-5} cm^2s^{-1}.[13]

The chosen value of n = 1 is consistent with coupling involving the linkage of two dimer molecules to form an indole tetramer, either on the electrode surface or in solution. The low redox charges compared to film formation charges also indicated a low coupling efficiency on the electrode surface, and a decrease in charge with increasing rotation speed suggest appreciable product solubility. All this indicates a very different indole film product than that observed when electro-oxidising indole monomer.

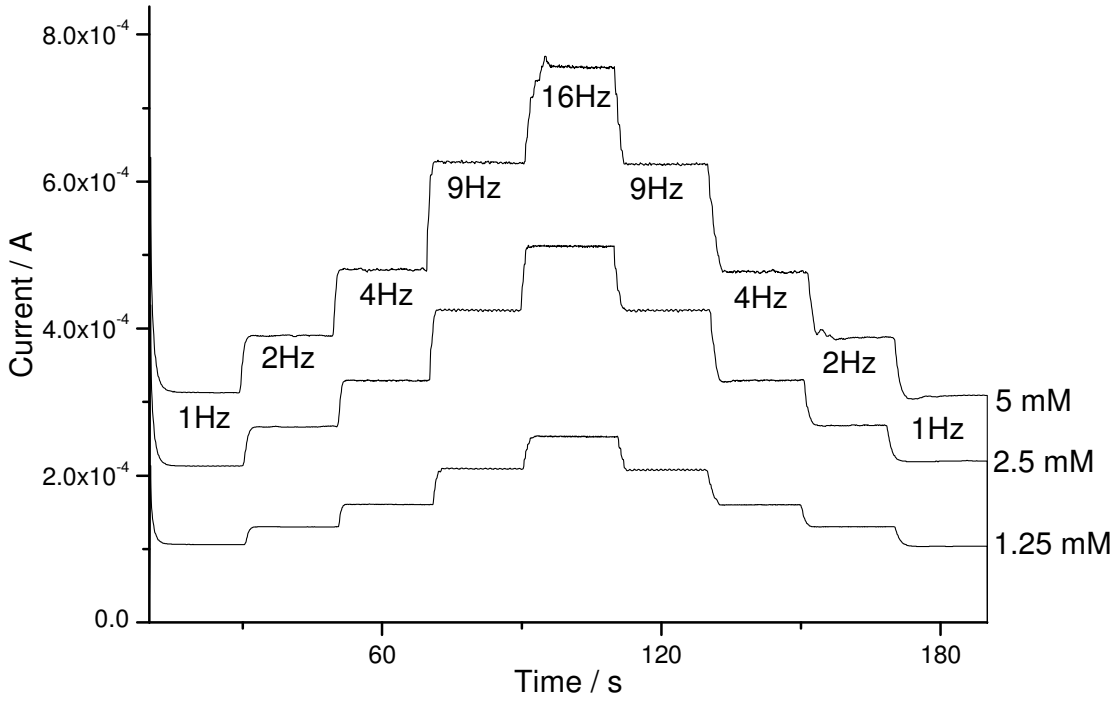

Figure 7.2.13. Current-time transient for the electro-oxidation of 2,3'-diindole solution at +0.587 V vs Fc/Fc^+ at rotation speed of 1, 2, 4, 9 and 16 Hz for varying concentrations.

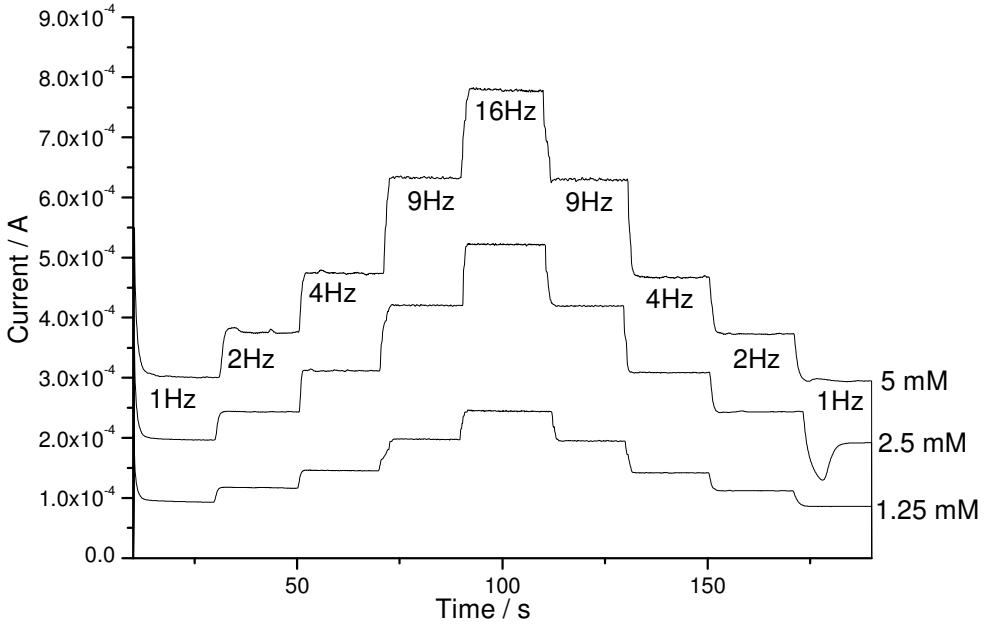

Figure 7.2.14. Current-time transient for the electro-oxidation of 2,3'-di-5-methoxyindole solution at +0.587 V vs Fc/Fc^{+} at rotation speed of 1, 2, 4, 9 and 16 Hz for varying concentrations.

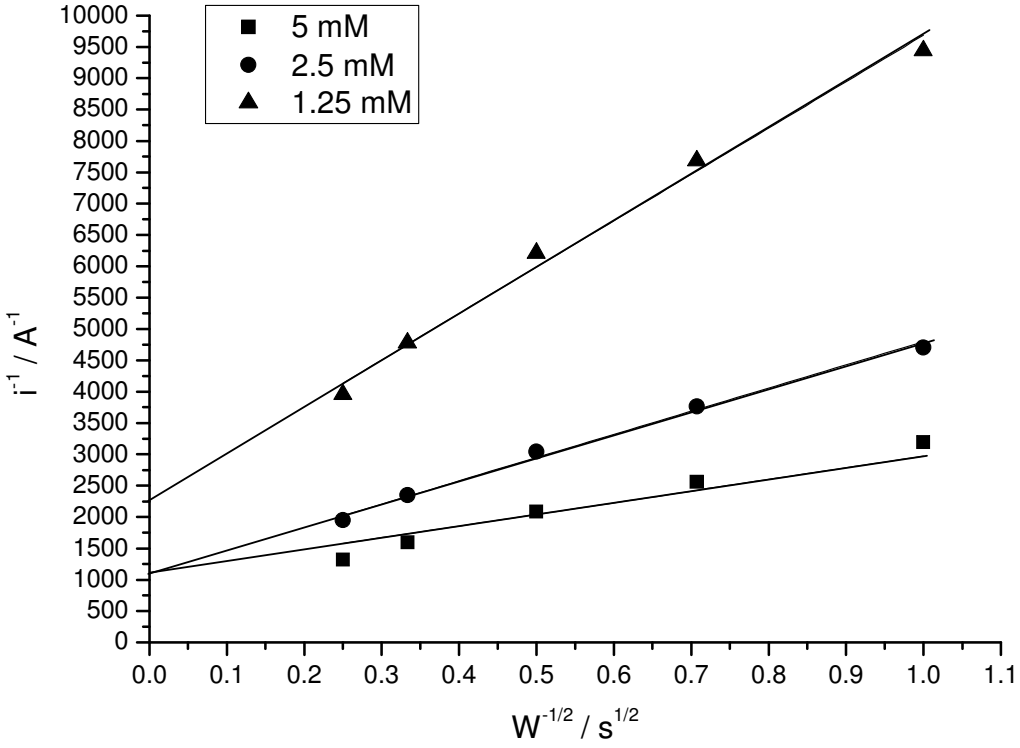

Figure 7.2.15. Koutecky-Levich plots for 1.25, 2.5 and 5 mM solutions of 2,3'-diindole. The lines shown are lines with a theoretical gradient calculated using D = 2 x 10^{-5} cm^2s^{-1}.

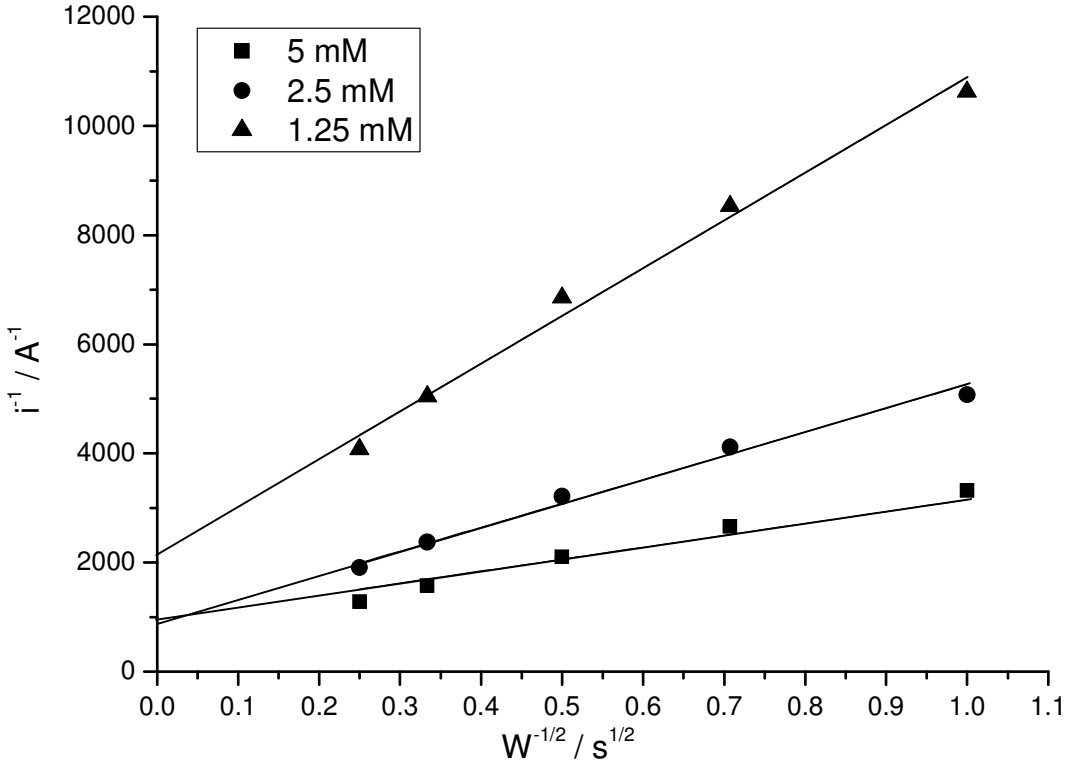

Figure 7.2.16. Koutecky-Levich plots for 1.25, 2.5 and 5 mM solutions of 2,3'-di-5-methoxyindole. The lines shown are lines with a theoretical gradient calculated using $D = 2 \times 10^{-5}$ cm^2s^{-1}.

7.3 Attempts to Characterise Films Formed From the Electro-oxidation of 2,3'-diindole and 2,3'-di-5-methoxyindole.

In section 7.2.2 fitting of data to Koutecky-Levich plots raised the hypothesis that coupling of diindole will yield an indole tetramer product. In this section the efforts to characterise the nature of the electro-active films formed from the electro-oxidation of 2,3'-diindole and 2,3'-di-5-methoxyindole will be discussed.

7.3.1. Fluorescence Spectroscopy.

5-substituted indoles are highly luminescent molecules, with indole having a fluorescence quantum yield (Φ_F) of 40% in ethanol solution[14]. The trimer products formed from electro-oxidation of 5-substituted indoles were also found to be highly luminescent, with a red-shifted emission when compared to the indole monomer[15]. 2,3'-diindole and 2,3'-di-5-methoxyindole and their formed films were studied to

discover if their emissive properties could provide some sign of the nature of the electroactive film formed upon electro-oxidation of the dimers.

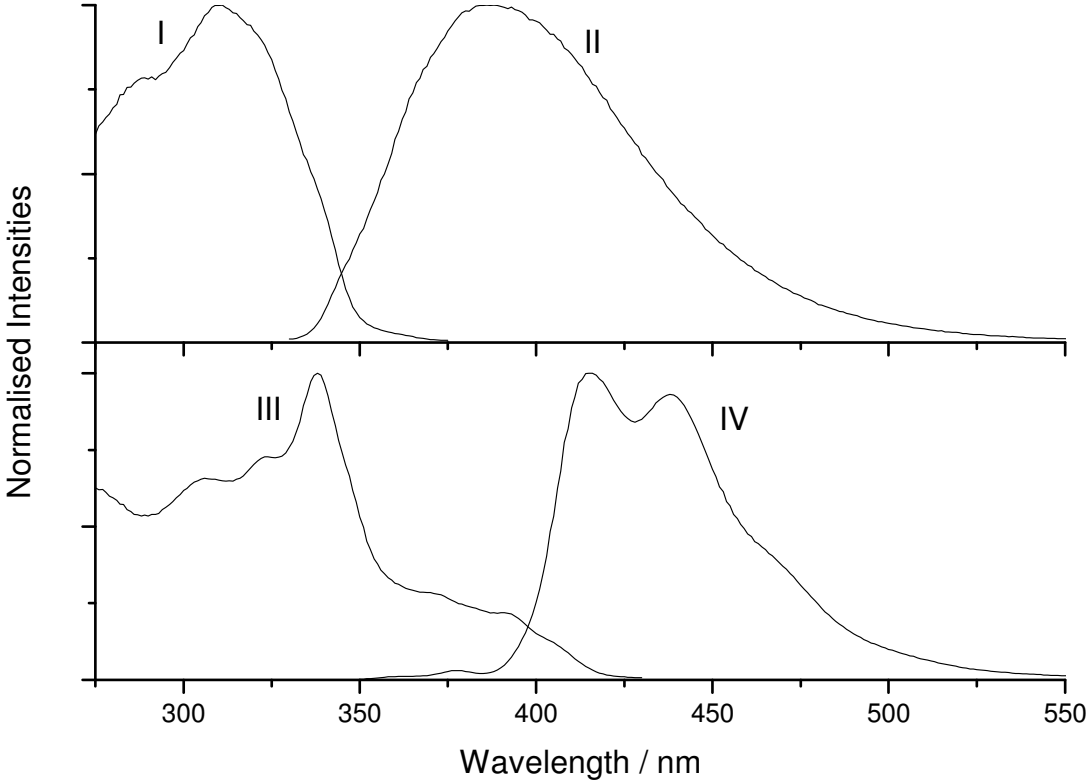

Figure 7.3.1. Excitation and emission spectra respectively for 2,3'-diindole (I and II) and the film formed from electro-oxidation (III and IV) in DMF. Emission wavelengths were 385 and 440 nm for I and III respectively, excitation wavelengths were 320 and 345 nm for II and IV respectively. Intensities were normalised to the most intense peaks for excitation spectra, and the peak intensities for the $S_1 \rightarrow S_0$ transition for emission.

The emission spectra of 2,3'-diindole and 2,3'di-5-methoxyindole, and the films formed from the electro-oxidation of both, are shown in Figures 7.3.1 and 7.3.2 respectively. All spectra were recorded in ethanol at μM concentrations. The change in spectra between the dimer and electrooxidised film is similar for both diindoles, with the position of the (0, 0) transition being red-shifted for the film products relative to the dimers, similar to the behaviour observed previously for 5-methylIC (Section 5.3.2). Again such red-shifting is indicative of a greater delocalisation in the product. Fluorescence spectra of the product precipitate collected from the reaction

vessel displayed peak emissions consistent with the formed film plus a small amount of dimer fluorescence.

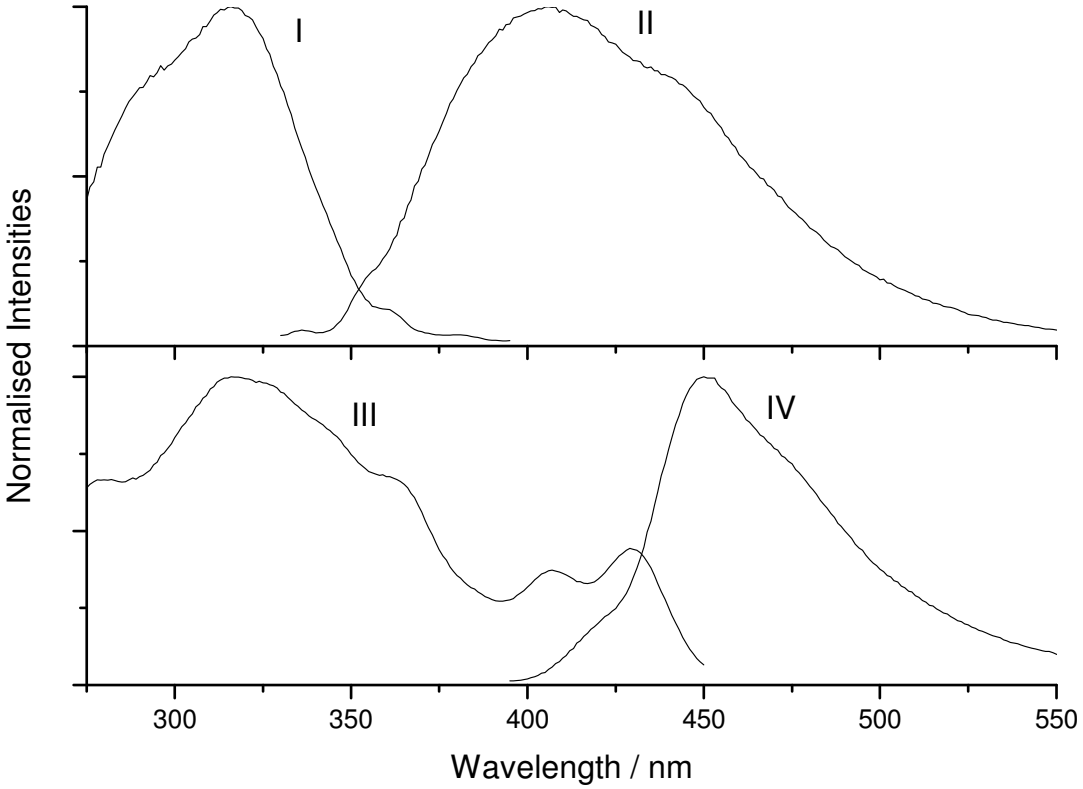

Figure 7.3.2. Excitation and emission spectra respectively for di-5-methoxyindole (I and II) and the film formed from electro-oxidation (III and IV) in DMF. Emission wavelengths were 385 and 460 nm for I and III respectively, excitation wavelengths were 320 and 385 nm for II and IV respectively. Intensities were normalised to the most intense peaks for excitation spectra, and the peak intensities for the $S_1 \rightarrow S_0$ transition for emission.

While this indicates that the film product has a greater delocalisation than the dimer, it does not provide any indication of the exact nature of the film product. Figure 7.3.3 displays the emission spectra for a series of 5-methoxyindole species. It has been shown that the products of the electro-oxidation of 5-substituted indoles are asymmetric trimers; it is therefore possible to compare the successive spectra of increasing the number of indole units from one to two to three as a progression from 5-methoxyindole, to the 2,3'-di-5-methoxyindole studied in this work to an asymmetric trimer of 5-methoxyindole. It can be observed that as the number of indole units is increased the emission spectra are increasingly red-shifted. It can also

be seen that the emission spectrum of the product formed from dimer electro-oxidation is red-shifted with respect to the asymmetric trimer, consistent with the hypothesis that the product is a tetramer of 5-methoxyindole. However, a longer chain conjugated polymer would also be expected to show a red-shifting with respect to the trimer species. The fluorescence data are therefore consistent with the formation of a tetramer but they do not provide conclusive evidence. For conclusive evidence further techniques such as mass spectrometry and NMR are required.

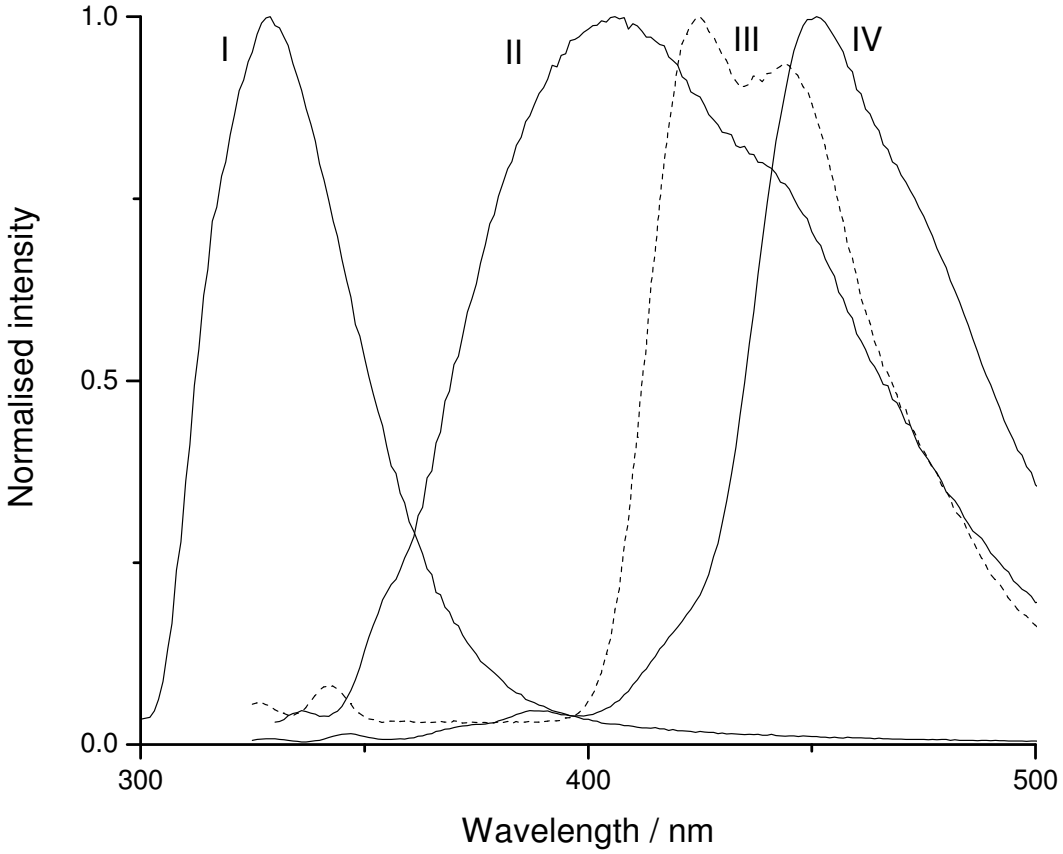

Figure 7.3.3. Solution steady-state emission spectra for a range of methoxyindole species. (I) 5-methoxyindole (excitation 285 nm); (II) 2,3'-di-5-methoxyindole (excitation 320 nm); (III) asymmetric trimer of 5-methoxyindole (excitation 320 nm) and (IV) product formed from electro-oxidation of 2,3'-di-5-methoxyindole (excitation 320 nm).

7.3.1 ESI Mass Spectrometry.

Mass spectroscopy and ^{1}H NMR spectroscopy have previously proven to be valuable techniques in the characterisation of electro-active oligomer films. ^{1}H NMR spectroscopy was attempted on the products of diindole electro-oxidation. Repeated

attempts, however, failed to provide clear spectra for analysis due to poor solubility of the formed film. The FAB method of ionisation for mass spectroscopy, used in the characterisation of indolocarbazole films, also failed to produce a clear spectrum for analysis. Attempts were also made to characterise the products of the diindole electro-oxidations using the electro-spray injection (ESI) method of ionisation for mass spectroscopy, for which only μM concentrations are typically necessary. Characterisation with ESI-MS was not possible as no peaks were observed/ This may be indicative that the product is a long chain molecule and/or extremely cross-linked.

7.4 Calculations on 2,3'-diindole Systems.

In previous chapters a computational method for the calculation of the redox properties of heterocyclic systems was developed. In this section we will consider the extension of this computational method to the heterocyclic 2,3'-diindole systems. The measured and calculated peak oxidation potentials of the diindoles are summarised in Table 7.4.1. It is clear that there is not a good correlation between the calculated and measured oxidation potentials within the expected error limits of 37 mV, and that they are clearly systematically low. It is possible that different rotamers might show different oxidation potentials, with the lower energy "trans"-conformation having the lowest oxidation potential. It should be noted that the electrochemical study of the diindoles suggested that there is an absorption process associated with oxidation, whereas the computational method does not take into account specific adsorption of molecules at the electrode or the effects of specific solvation. Solution oxidation via this adsorbed layer could also give rise to a higher oxidation potential, if the adsorbed film had a higher oxidation potential than in solution. Reasons for the observed higher oxidation potentials could be that the reduced form is stabilised by adsorption as a result of changing the geometry and/or solvation of the absorbed species.

While these calculations cannot accurately predict observed the peak oxidation potentials of the diindoles, consideration of the electron spin density maps may still provide some insight into the potential coupling positions of diindoles and provide an explanation for the observed solution coupling. Figure 7.4.1 shows the electron spin

density maps for three of the 5-substituted diindoles. The primary feature of note is that the electron spin density is concentrated on one indole unit and not delocalised through the whole molecule as it is in larger heterocycles such as indolocarbazole. The largest electron spin density is located in the unlinked 3-position of the 2,3'-diindoles If coupling of the diindoles follows a radical-radical coupling mechanism similar to that observed with indoles and indolocarbazoles then coupling would be most likely to occur between the unlinked 3-positions initially forming an indole tetramer. Reaction of the diindoles at the electrode surface may then be limited either by the diindoles being less reactive than the associated indole monomers, thermodynamics, or through steric hindrance between the reacting diindoles, kinetics. The coupling reaction may then primarily occur between dimers in solution away from the electrode surface resulting in the observed precipitate.

Substituent	**Measured peak oxidation potential (vs Fc/Fc^+) / V**	**Calculatated peak oxidation potential (vs Fc/Fc^+) / V**	
		"trans"	**"cis"**
-H	+0.43	+0.20 ± 0.04	+0.25 ± 0.04
$-OCH_3$	+0.41	+0.18 ± 0.04	+0.28 ± 0.04
$-CO_2H$	+0.44	+0.50 ± 0.04	+0.53 ± 0.04
$-CH_3$	+0.42	+0.17 ± 0.04	+0.19 ± 0.04

Table 7.4.1. Measure and calculated peak oxidation potentials for four 5-substituted 2,3' diindoles.

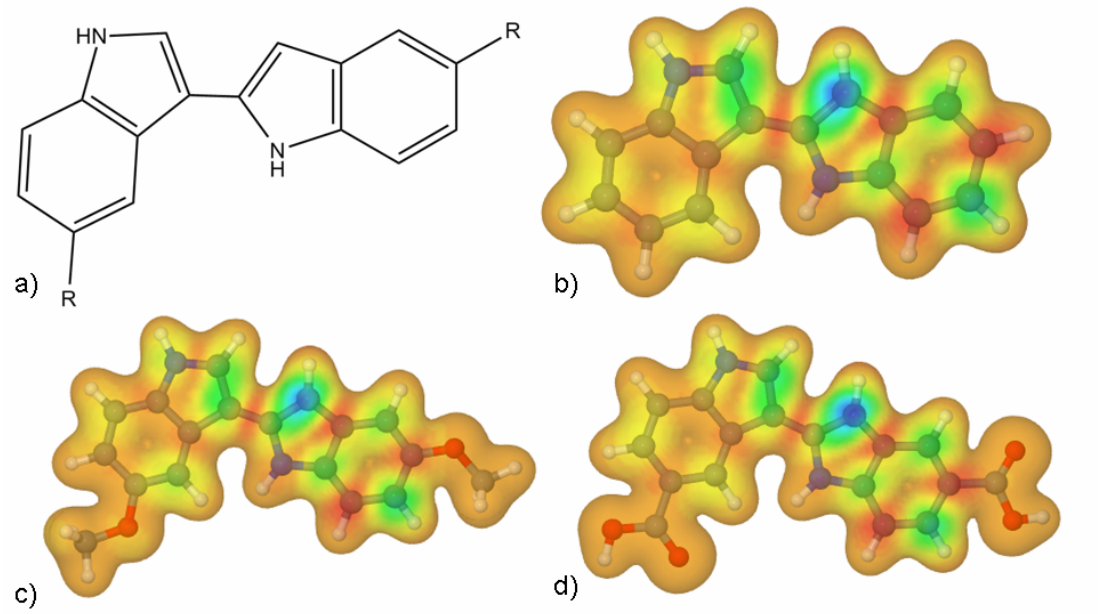

Figure 7.4.1. a) Structure of 5-substituted 2,3'-diindoles. Spin density distribution mapped onto a 99% electron density isosurface for the radical cations of (b) 2,3'-diindole, (c) 2,3'-di-5-methoxyindole and (d) 2,3'diindole-5-carboxylic acid. (The colouring is schematic as follows: blue indicates a positive spin density (0.005) whilst red is negative (-0.001). The same range of spin density was used for all 3 maps).

7.5 Conclusions.

Electro-oxidation of 5-substituted diindoles is an intriguing electrochemical process which appears to exhibit an electrode adsorption process as a step in the oxidation, as evidenced by the non-zero intercepts in Levich plots and plots of peak oxidation currents *vs*. sweep rates. The adsorption step highlights a weakness in the established computational method in that there is no modelling of electrode processes. For previously discussed heterocycles where redox processes occur initially in solution this was a reasonable approximation. The work with diindoles shows, however, that in redox processes that have a direct interaction with the electrode surface, the approximate model shows poor correlation with experimentally observed results, in situations such as this a far more powerful computational method which includes an electrode model must be included. It is also interesting to note that the calculations predict that there should be a dependence of the oxidation potential on the nature of the substituent, but no such dependence is observed experimentally.

7.6 References.

[1] Mackintosh, J. G. *Ph. D. Thesis, "The Electropolymerisation of Novel Conducting Polymers.", University of Edinburgh* **1996**.

[2] Berlin, A.; Canavesi, A.; Schiavon, G.; Zecchin, S.; Zotti, G. *Tetrahedron* **1996**, *52*, 7947.

[3] Talbi, H.; Billaud, D.; Louarn, G.; Pron, A. *Spectrochim. Acta A*, **2001**, *57*, 423.

[4] Xu, J.; Hou, J.; Zhou, W.; Nie, G.; Pu, S.; Zhang, S. *Spectrochim. Acta A* **2006**, *63*, 723.

[5] Mackintosh, J. G.; Redpath, C. R.; Jones, A. C.; Langridge-Smith, P. R. R.; Reed, D.; Mount, A. R. *J. Electroanal. Chem.* **1994**, *375*, 163.

[6] Mackintosh, J. G.; Redpath, C. R.; Jones, A. C.; Langridge-Smith, P. R. R.; Mount, A. R. *J. Electroanal. Chem.* **1995**, *388*, 179.

[7] Mackintosh, J. G.; Mount, A. R.; Reed, D. *Magn. Reson. Chem.* **1994**, *32*, 559.

[8] Robertson, N.; Parsons, S.; MacLean, E. J.; Coxall, R. A.; Mount, A. R. *J. Mater. Chem.* **2000**, *10*, 2043.

[9] Guyard, L.; Hapiot, P.; Neta, P. *J. Phys. Chem. B* **1997**, *101*, 5698.

[10] Hapiot, P.; Lagrost, C.; Aeiyach, S. Jouini, M.; Lacroix, J-C. *J. Phys. Chem. B*, **2002**, *106*, 3622.

[11] Wharton, S. I. *Ph. D. Thesis, "Synthesis and Characterisation of Novel Conducting Films Based on Indolo[3,2,1-jk]carbazole Systems.", University of Edinburgh* **2005**.

[12] Mackintosh, J. G.; Wright, S. J.; Langridge-Smith, P. R. R.; Mount, A. R. *J. Chem. Soc., Faraday Trans.* **1996**, *92*, 4109.

[13] Jennings, P.; Jones, A. C.; Mount, A. R.; Thomson, A. D. *J. Chem. Soc. Faraday Trans.* **1997**, *93*, 3791.

[14] Kirby, E. P.; Steiner, R. F. *J. Phys. Chem.* **1970**, *74*, 4480.

[15] Jennings, P.; Jones, A. C.; Mount, A. R. *J. Chem. Soc. Faraday Trans.* **1998**, *94*, 3619.

Chapter 8: Conclusions and Scope for Future Work.

Through this work and a re-evaluation of the previous results obtained by Kettle[1] it has been shown that it is possible to use DFT calculations to calculate the oxidation potentials accurately for a range of aromatic systems. It is likely that this method can be used to predict the oxidation potentials of a range of aromatic systems, introducing a method of screening to aid and motivate synthesis of a range of new heterocycles with desirable properties. Initial screening work has been presented in Chapter 6 where a number of potentially interesting systems are considered. Further study of the electrochemical behaviour of these species is strongly recommended, and may yield a number of novel interesting and useful thin-film materials.

In this thesis computational methods have been developed and combined with electrochemical techniques in the study of redox-active aromatics. For 5-substituted indoles, this work is found to be in excellent agreement with the initial work of Kettle[1], but now with enhanced accuracy and precision as shown by the absence of a systematic offset of the calculated potentials from the experimentally measured values. Furthermore, application of this computational method to the study of indole oxidation and coupling has given thermodynamic support to the entire coupling mechanism. Extension of the calculations to the postulated linear indole trimer intermediate establishes a plausible mechanism to explain the cyclisation of trimer observed experimentally. Extension of this work to chemical analogues of indole suggests an electrochemical route to a range of similar trimeric species which may be achievable. Initial work on formation of films from these indole analogues has been encouraging. Further work on the formation and characterisation of such films is already planned and underway.

Indolocarbazole systems have also been studied using a combination of computational and electrochemical results. As with the work on 5-substituted indoles this work has established good quantitative agreement with previous experimental

work. The calculation of the electronic structures of the radical cations of these species formed on oxidation has shown that a radical cation – radical cation coupling mechanism would explain the selective product formation found in these films. Furthermore the thermodynamics of this reaction have been shown to be favourable. The electro-active films formed from 5-methylIC have also been studied. The film formed from 5-methylIC was found to consist of 3 dimers of 5-methylIC. This work shows that films formed from 5-substituted ICs form similar products to unsubstituted IC, and that selective functionalisation of IC films through selective substitution is possible.

Extension of this method to the hexamethyltriphenylene (hmtp) system suggests that this system makes a poor candidate for the formation of electro-active thin film materials, as the staggered conformation of the hmtp molecule will inhibit π-stacking and therefore affects the conductive properties of an hmtp film. However, this, like dendrimers, should lead to enhanced thin film fluorescence. An initial study of thin film fluorescence of these films has shown such enhanced fluorescence. Electro-oxidation of hmtp has also been calculated and experimentally shown not to lead to the formation of any new redox- active oligomeric film species. The cause of this enhanced fluorescence is the same property that inhibits the use of this film as a redox-active layer. It is thought that the inhibition of the π-stacking within the film decreases the rate of quenching of the excited state and results in enhanced film fluorescence properties.

There are, however, some limitations to this computational method. This is highlighted by the marked difference between the experimental values of the oxidation potentials of diindoles shown in Chapter 7, where the calculated oxidation potentials were systematically lower than those measured experimentally. The error in the calculation of the thermodynamics of the diindole system introduces doubt on the quantum chemical properties of the diindole systems and their predicted properties, such as their growth mechanisms. This shows that where electro-oxidation involves a strong interaction with the electrode or a large conformational change of the system the simple model of the redox process of the molecules in

solution becomes insufficient and an accurate prediction of the oxidation potential may require a far more complex and computationally expensive method for accurate results to be achievable. This highlights the importance of validating calculated properties with experimentally observations before applying the methods as a predictive tool.

The computational method was also found to be inadequate when extended to the calculation of pKa's of a range of acids. Whilst the general order of acidity was found the error in calculated pKa's was too large to provide a useful predictive method, due to the limitations of the B3LYP method and 6-311+G(d,p) basis set with PCM solvation. The calculation of pKa's therefore appears to be limited currently to computationally more expensive methods.

These results give fresh motivation for the future work, which may concentrate on electrochemical studies of the systems screened in Chapter 6, and the indole analogue systems. Furthermore, as computational power continues to increase it is hoped that this computational method can be utilised with larger basis sets and more complex solvation models. This should lead to the accurate calculation of pK_as, and the determination of larger molecular systems.

8.1 References.

[1] Kettle, L. J. *Ph. D. Thesis, "A Computational and Electrochemical Study of Electropolymerised Indoles", University of Edinburgh* **2000**.

Appendix 1: Molecular Energies and Coordinates.

Chapter 4:

Indole neutral solvated species: HF -363.928717 a.u.

C	-0.981547	1.427178	-0.000025
C	0.248688	0.749322	-0.000207
C	0.247181	-0.671986	-0.000159
C	-0.934762	-1.416850	-0.000073
C	-2.133761	-0.717405	0.000115
C	-2.156833	0.691335	0.000081
C	1.623767	1.165681	-0.000155
C	2.388646	0.031371	0.000286
N	1.566098	-1.080366	0.000062
H	-1.010422	2.511396	0.000021
H	-0.919958	-2.501427	0.000114
H	-3.069384	-1.264981	0.000276
H	-3.111823	1.204514	0.000233
H	1.997306	2.177736	-0.000111
H	3.461463	-0.081229	0.000909
H	1.881861	-2.035321	-0.001061

Indole cation solvated species: HF -363.725068 a.u.

C	-1.021850	1.418551	0.000112
C	0.229442	0.753302	-0.000002
C	0.260692	-0.670699	-0.000057
C	-0.876287	-1.436830	-0.000046
C	-2.116748	-0.743139	0.000026
C	-2.184345	0.650916	0.000105
C	1.560394	1.202324	-0.000144
C	2.386981	0.045155	0.000199
N	1.617799	-1.045514	-0.000170
H	-1.068637	2.501051	0.000120
H	-0.852720	-2.520009	-0.000097
H	-3.032516	-1.322047	0.000023
H	-3.151140	1.137630	0.000136
H	1.922215	2.219569	-0.000154
H	3.465372	-0.017771	0.000323
H	1.963160	-1.997300	-0.000311

5-aminoindole neutral solvated species: HF -419.308193 a.u.

C	-0.816495	-1.127891	-0.005859
C	0.525161	-0.700484	-0.003500

C	0.812948	0.691273	-0.000320
C	-0.205867	1.647878	0.000753
C	-1.520449	1.202492	-0.005478
C	-1.839023	-0.180561	-0.007907
C	1.790611	-1.382180	0.001003
C	2.768706	-0.414666	0.005765
N	2.189143	0.832732	0.005609
N	-3.191278	-0.574376	-0.080666
H	-1.058498	-2.189079	-0.007163
H	0.017973	2.712049	0.006485
H	-2.332370	1.926556	-0.009100
H	1.957115	-2.451477	0.000483
H	2.697239	1.718039	0.005643
H	3.846654	-0.517197	0.008843
H	-3.838041	0.088997	0.339707
H	-3.368677	-1.511543	0.273753

5-aminoindole cation solvated species: HF -419.130849 a.u.

C	0.777681	-1.160942	-0.000395
C	-0.526819	-0.716593	-0.000317
C	-0.789795	0.696108	-0.000122
C	0.244778	1.661765	-0.000138
C	1.537828	1.217779	-0.000213
C	1.829320	-0.190575	-0.000135
C	-1.813616	-1.374682	-0.000082
C	-2.756184	-0.390726	0.000336
N	-2.129520	0.855387	0.000279
N	3.102486	-0.600451	0.000548
H	1.027431	-2.220649	-0.000281
H	0.013962	2.724539	-0.000064
H	2.369008	1.919083	-0.000252
H	-1.996510	-2.441218	-0.000149
H	-2.622852	1.757444	-0.000096
H	-3.837291	-0.450941	0.000569
H	3.874936	0.068084	0.000844
H	3.341399	-1.593696	0.000026

5-bromoindole neutral solvated species: HF -2937.472921 a.u.

C	-0.097658	-0.948998	-0.000025
C	-1.478790	-0.680519	-0.000018
C	-1.925213	0.672439	0.000003
C	-1.033573	1.748738	-0.000017
C	0.327407	1.468672	-0.000049
C	0.765826	0.131812	-0.000035
C	-2.652563	-1.506738	-0.000007
C	-3.732963	-0.659103	-0.000014
N	-3.300750	0.649162	0.000036
BR	2.672198	-0.199626	0.000016

H	0.273965	-1.969468	-0.000021
H	-1.385588	2.777413	-0.000008
H	1.048953	2.279146	-0.000050
H	-2.690761	-2.588026	-0.000018
H	-3.910782	1.469323	0.000221
H	-4.792310	-0.883428	0.000036

5-bromoindole cation solvated species: HF -2937.262617 a.u.

C	-0.086150	-0.954822	-0.000253
C	-1.467496	-0.680510	-0.000401
C	-1.920817	0.665680	-0.000376
C	-1.062401	1.735144	0.000469
C	0.324625	1.450679	0.000485
C	0.786131	0.135556	0.000031
C	-2.611572	-1.506513	0.000735
C	-3.742717	-0.634272	0.000101
N	-3.326127	0.624456	-0.000585
BR	2.670522	-0.190706	-0.000066
H	0.280773	-1.978426	-0.000308
H	-1.411951	2.765291	0.000823
H	1.030757	2.276730	0.000775
H	-2.656851	-2.590471	0.001649
H	-3.946977	1.452562	-0.001320
H	-4.798747	-0.887821	0.000036

Indole-5-carboxylic acid neutral solvated species: HF -552.573496 a.u.

C	-0.224340	-0.988335	0.057283
C	1.137943	-0.677151	0.053933
C	1.535984	0.690026	-0.047964
C	0.604124	1.729937	-0.139078
C	-0.739515	1.394550	-0.115701
C	-1.162539	0.044774	-0.014361
C	2.343570	-1.456642	0.127034
C	3.389018	-0.572905	0.066634
N	2.905418	0.717564	-0.038632
C	-2.598539	-0.329784	-0.025147
O	-3.007646	-1.427253	-0.356975
O	-3.513623	0.598881	0.335827
H	-0.561076	-2.018621	0.124734
H	0.920209	2.765694	-0.232653
H	-1.472464	2.193117	-0.205517
H	2.421250	-2.532579	0.211068
H	4.456508	-0.752991	0.089635
H	3.485680	1.557648	-0.100581
H	-3.132122	1.384938	0.777129

Indole-5-carboxylic acid cation solvated species: HF -552.360343 a.u.

C	-0.240304	-0.992473	0.096697

C	1.127868	-0.677332	0.080277
C	1.535384	0.679898	-0.061639
C	0.642422	1.713467	-0.175290
C	-0.731253	1.377687	-0.133268
C	-1.168053	0.054320	0.003742
C	2.299288	-1.457105	0.165935
C	3.398309	-0.550697	0.071933
N	2.939090	0.687465	-0.060670
C	-2.621078	-0.308295	-0.033708
O	-3.005970	-1.359246	-0.497483
O	-3.517879	0.574511	0.429461
H	-0.575693	-2.023140	0.182805
H	0.957623	2.747671	-0.293743
H	-1.453978	2.186037	-0.230185
H	2.383211	-2.532897	0.279182
H	4.462880	-0.765784	0.095931
H	3.531828	1.531382	-0.151697
H	-3.144203	1.285541	0.998507

5-chloroindole neutral solvated species: HF -823.552982 a.u.

C	-0.502878	-1.026556	-0.000148
C	0.863221	-0.691295	-0.000241
C	1.242646	0.682065	-0.000105
C	0.299155	1.713290	-0.000377
C	-1.045946	1.366471	-0.000309
C	-1.418051	0.010161	-0.000087
C	2.076122	-1.458567	-0.000335
C	3.113772	-0.558847	0.000219
N	2.618032	0.726398	0.000291
CL	-3.152523	-0.379134	0.000274
H	-0.829358	-2.062610	-0.000011
H	0.600468	2.757877	-0.000436
H	-1.810286	2.137134	-0.000327
H	2.167557	-2.536659	-0.000583
H	3.187197	1.575305	0.002422
H	4.182857	-0.730882	0.000529

5-chloroindole cation solvated species: HF -823.342724 a.u.

C	0.516026	-1.030579	-0.000398
C	-0.850008	-0.691501	-0.001030
C	-1.239451	0.674603	-0.000971
C	-0.331940	1.702936	0.000065
C	1.039323	1.353481	0.000474
C	1.437355	0.017816	0.000055
C	-2.031231	-1.462821	0.000271
C	-3.120581	-0.538329	0.000929
N	-2.645345	0.699191	-0.000832
CL	3.149818	-0.361061	0.000142

H	0.839812	-2.068845	-0.000270
H	-0.633007	2.748215	0.000712
H	1.788325	2.141194	0.001014
H	-2.127315	-2.543453	0.001557
H	-3.226928	1.555203	0.002292
H	-4.187332	-0.742246	0.001738

5-cyanoindole neutral solvated species: HF -456.206211 a.u.

C	-0.615482	-1.035999	0.000023
C	0.742414	-0.705321	-0.000023
C	1.121920	0.671750	-0.000047
C	0.181120	1.708985	-0.000015
C	-1.158490	1.365132	0.000025
C	-1.555226	0.000751	0.000043
C	1.957180	-1.472145	-0.000001
C	2.990758	-0.572332	0.000045
N	2.490110	0.715249	-0.000143
C	-2.945932	-0.315362	0.000118
N	-4.076607	-0.567529	-0.000105
H	-0.941764	-2.073012	0.000048
H	0.489726	2.751291	-0.000046
H	-1.920383	2.139204	0.000036
H	2.048439	-2.550234	0.000042
H	3.059303	1.565509	0.000688
H	4.060590	-0.739554	-0.000044

5-cyanoindole cation solvated species: HF -455.989734 a.u.

C	-0.631929	-1.041934	-0.000029
C	0.731483	-0.706577	0.000055
C	1.122099	0.663265	0.000090
C	0.220317	1.697459	0.000079
C	-1.146678	1.350883	0.000066
C	-1.562739	0.006794	-0.000006
C	1.911350	-1.476762	0.000127
C	3.000414	-0.550603	-0.000058
N	2.525894	0.687456	0.000051
C	-2.961655	-0.293054	-0.000084
N	-4.091216	-0.534627	-0.000269
H	-0.956590	-2.080625	-0.000065
H	0.527831	2.740840	0.000087
H	-1.894060	2.141239	0.000067
H	2.008572	-2.557559	0.000126
H	3.107885	1.544403	0.000030
H	4.067639	-0.754930	-0.000154

5-hydroxyindole neutral solvated species: HF -439.182851 a.u.

C	0.810770	-1.152172	0.000006
C	-0.523074	-0.703899	0.000020

C	-0.789159	0.694245	-0.000168
C	0.240187	1.637790	-0.000135
C	1.550344	1.173717	-0.000242
C	1.829874	-0.210196	-0.000288
C	-1.797729	-1.366296	-0.000284
C	-2.759942	-0.383955	0.000179
N	-2.161701	0.854916	0.000266
O	3.127215	-0.676256	0.000378
H	1.052953	-2.211937	0.000461
H	0.031478	2.704830	0.000179
H	2.377713	1.880773	-0.000026
H	-1.979767	-2.432970	-0.000706
H	-3.839388	-0.469537	0.000193
H	-2.657198	1.747710	0.000566
H	3.760770	0.071365	-0.000075

5-hydroxyindole cation solvated species: HF -438.985716 a.u.

C	0.767662	-1.177179	-0.000054
C	-0.525750	-0.717075	-0.000285
C	-0.766599	0.697482	-0.000134
C	0.280826	1.649574	-0.000021
C	1.573645	1.185735	0.000114
C	1.828516	-0.211201	0.000214
C	-1.828281	-1.357320	0.000031
C	-2.753913	-0.358489	0.000282
N	-2.099939	0.875038	-0.000131
O	3.052961	-0.713325	-0.000091
H	1.020989	-2.235467	0.000143
H	0.064385	2.715862	-0.000149
H	2.416703	1.873653	0.000085
H	-2.026630	-2.421528	-0.000227
H	-3.836039	-0.395592	0.000484
H	-2.579809	1.788440	-0.000009
H	3.759642	-0.013206	0.000448

5-methoxyindole neutral solvated species: HF -478.484681 a.u.

C	0.628742	-0.826312	0.000268
C	-0.773239	-0.658776	0.000299
C	-1.324909	0.649243	0.000191
C	-0.512263	1.788688	0.000229
C	0.860643	1.606485	0.000174
C	1.427842	0.309139	-0.000007
C	-1.878970	-1.574195	0.000021
C	-3.026640	-0.815851	-0.000261
N	-2.699606	0.520477	-0.000081
O	2.805105	0.287933	-0.000744
C	3.457550	-0.978371	0.000151
H	1.049122	-1.825035	0.000186

H	-0.938846	2.788805	0.000257
H	1.531371	2.461196	0.000110
H	-1.832753	-2.655379	0.000013
H	-4.064243	-1.125138	-0.000607
H	-3.370738	1.290243	-0.000947
H	3.202130	-1.557503	0.894164
H	4.525770	-0.765465	-0.000066
H	3.202057	-1.558824	-0.892983

5-methoxyindole cation solvated species: HF -478.284615 a.u.

C	-0.598048	-0.859692	-0.000372
C	0.764911	-0.679079	-0.000139
C	1.310465	0.655603	0.000009
C	0.489349	1.813788	-0.000288
C	-0.862866	1.628958	-0.000446
C	-1.419977	0.307157	-0.000054
C	1.896694	-1.586513	-0.000370
C	3.013613	-0.815624	0.000072
N	2.644365	0.539827	0.000746
O	-2.741617	0.270232	0.000256
C	-3.461641	-0.984244	0.000409
H	-1.024267	-1.857090	-0.000901
H	0.928298	2.808920	-0.000150
H	-1.553861	2.467361	-0.000528
H	1.857127	-2.668169	-0.000630
H	4.062307	-1.085559	0.000313
H	3.312662	1.325413	0.000686
H	-3.222082	-1.554236	-0.899079
H	-4.511823	-0.704681	0.000900
H	-3.220975	-1.554717	0.899199

5-methylindole neutral solvated species: HF -403.254822 a.u.

C	-0.810215	-1.109640	0.000066
C	0.538000	-0.701649	0.000100
C	0.836852	0.688053	0.000086
C	-0.171902	1.657618	0.000077
C	-1.488742	1.218521	0.000064
C	-1.825010	-0.158998	-0.000043
C	1.796725	-1.395564	0.000022
C	2.781723	-0.437785	-0.000082
N	2.209973	0.816371	0.000051
C	-3.279936	-0.572305	-0.000118
H	-1.056776	-2.169629	0.000047
H	0.065319	2.718927	0.000018
H	-2.289241	1.955267	0.000028
H	1.953020	-2.466453	0.000113
H	3.858957	-0.546794	-0.000287
H	2.726109	1.697578	-0.000928

H	-3.381966	-1.659788	-0.001589
H	-3.805373	-0.185343	-0.879603
H	-3.804824	-0.187866	0.880807

5-methylindole cation solvated species: HF -403.052495 a.u.

C	-0.826987	-1.111973	-0.001403
C	0.526174	-0.704607	-0.000407
C	0.839953	0.680777	0.000315
C	-0.129168	1.651020	0.000098
C	-1.475496	1.212759	-0.000811
C	-1.837198	-0.143610	-0.001176
C	1.746085	-1.406476	0.000234
C	2.784131	-0.425247	0.000569
N	2.242493	0.786420	0.000396
C	-3.293327	-0.539988	0.001317
H	-1.073225	-2.172085	-0.002497
H	0.109930	2.712119	0.000116
H	-2.257382	1.969820	-0.001460
H	1.903006	-2.479660	-0.000078
H	3.860089	-0.570657	0.000933
H	2.773979	1.672610	-0.000579
H	-3.406920	-1.624469	-0.036625
H	-3.816844	-0.111630	-0.858152
H	-3.795086	-0.176920	0.903152

5-nitroindole neutral solvated species: HF -568.504772 a.u.

C	0.259790	-0.991106	-0.001217
C	-1.099222	-0.678673	0.000256
C	-1.500850	0.693933	-0.001762
C	-0.573241	1.745420	-0.002981
C	0.769700	1.422322	-0.002074
C	1.167216	0.066270	-0.001430
C	-2.302298	-1.464840	0.003844
C	-3.347906	-0.581522	0.002526
N	-2.865064	0.715579	-0.000794
N	2.587929	-0.239483	0.000319
O	2.943141	-1.421564	-0.007263
O	3.395133	0.694222	0.009845
H	0.607169	-2.018374	-0.000100
H	-0.896427	2.783098	-0.004153
H	1.522944	2.200690	-0.002013
H	-2.375896	-2.544289	0.005943
H	-3.447868	1.557602	-0.003712
H	-4.415313	-0.763489	0.003731

5-nitroindole cation solvated species: HF -568.284936 a.u.

C	0.276550	-1.000516	-0.000802
C	-1.090796	-0.681765	0.000809

C	-1.500449	0.683675	-0.003114
C	-0.612211	1.730485	-0.005345
C	0.758877	1.402676	-0.003713
C	1.169024	0.066775	-0.001976
C	-2.259237	-1.468503	0.006665
C	-3.360694	-0.556313	0.004068
N	-2.903075	0.688365	-0.001823
N	2.613982	-0.225625	0.000684
O	2.959591	-1.400853	-0.013784
O	3.391911	0.720236	0.017271
H	0.621455	-2.030636	0.000914
H	-0.933059	2.769760	-0.007543
H	1.500817	2.195234	-0.003982
H	-2.341484	-2.550650	0.011100
H	-3.497132	1.537722	-0.005701
H	-4.425347	-0.774756	0.005724

3,3'-diindole neutral solvated species: HF -726.646018 a.u.

C	-1.634847	-1.413354	-0.527568
C	-1.686244	-0.086984	-0.075052
C	-2.951137	0.469560	0.226815
C	-4.137840	-0.243347	0.146272
C	-4.050352	-1.571498	-0.271195
C	-2.817853	-2.141396	-0.615210
C	-0.708103	0.976715	0.075036
C	-1.447523	2.126082	0.442936
N	-2.749077	1.816572	0.545204
C	1.635052	-1.413164	0.528119
C	1.686279	-0.086902	0.075262
C	2.951058	0.469610	-0.227147
C	4.137782	-0.243296	-0.146931
C	4.050436	-1.571390	0.270753
C	2.818076	-2.141217	0.615389
C	0.708088	0.976765	-0.074470
C	1.447352	2.126132	-0.442682
N	2.748875	1.816637	-0.545430
H	-0.700074	-1.866877	-0.827028
H	-5.093700	0.208653	0.382601
H	-4.953363	-2.164833	-0.345408
H	-2.786563	-3.166933	-0.961966
H	-1.089759	3.115864	0.681299
H	-3.473515	2.460538	0.831148
H	0.700395	-1.866538	0.828172
H	5.093571	0.208679	-0.383592
H	4.953472	-2.164721	0.344693
H	2.786930	-3.166685	0.962360
H	1.089528	3.115971	-0.680712
H	3.473140	2.460535	-0.831962

3,3'-diindole cation solvated species: HF -726.476450 a.u.

C	-1.634847	-1.413354	-0.527568
C	-1.686244	-0.086984	-0.075052
C	-2.951137	0.469560	0.226815
C	-4.137840	-0.243347	0.146272
C	-4.050352	-1.571498	-0.271195
C	-2.817853	-2.141396	-0.615210
C	-0.708103	0.976715	0.075036
C	-1.447523	2.126082	0.442936
N	-2.749077	1.816572	0.545204
C	1.635052	-1.413164	0.528119
C	1.686279	-0.086902	0.075262
C	2.951058	0.469610	-0.227147
C	4.137782	-0.243296	-0.146931
C	4.050436	-1.571390	0.270753
C	2.818076	-2.141217	0.615389
C	0.708088	0.976765	-0.074470
C	1.447352	2.126132	-0.442682
N	2.748875	1.816637	-0.545430
H	-0.700074	-1.866877	-0.827028
H	-5.093700	0.208653	0.382601
H	-4.953363	-2.164833	-0.345408
H	-2.786563	-3.166933	-0.961966
H	-1.089759	3.115864	0.681299
H	-3.473515	2.460538	0.831148
H	0.700395	-1.866538	0.828172
H	5.093571	0.208679	-0.383592
H	4.953472	-2.164721	0.344693
H	2.786930	-3.166685	0.962360
H	1.089528	3.115971	-0.680712
H	3.473140	2.460535	-0.831962

Linear indole trimer neutral solvated species: HF -1088.843685 a.u.

C	0.306346	2.224955	1.260941
C	1.287980	1.973638	0.284592
C	2.117077	3.049359	-0.151253
C	1.980020	4.350439	0.349863
C	0.993932	4.570588	1.310479
C	0.167433	3.517087	1.763617
C	1.712503	0.778991	-0.431229
C	2.761136	1.168779	-1.243725
N	3.006872	2.530588	-1.083547
C	3.403944	-1.957990	0.145683
C	2.022367	-1.760119	-0.034321
C	1.149062	-2.882043	0.063443
C	1.619382	-4.177411	0.308662
C	2.995237	-4.346273	0.466589

C	3.877993	-3.245506	0.391162
C	1.205757	-0.589239	-0.291347
C	-0.118195	-1.023790	-0.345298
N	-0.141078	-2.407729	-0.117342
C	-3.203309	-1.564427	0.780617
C	-2.686100	-0.620037	-0.128019
C	-3.581202	0.325605	-0.711963
C	-4.953667	0.329571	-0.436897
C	-5.438023	-0.630628	0.450134
C	-4.569420	-1.564415	1.057194
C	-1.354556	-0.316977	-0.634969
C	-1.492379	0.773396	-1.474261
N	-2.823140	1.160612	-1.523581
H	-0.329780	1.421280	1.614177
H	2.620384	5.158360	0.008690
H	0.861641	5.566928	1.720635
H	-0.585374	3.721162	2.518489
H	3.342676	0.577050	-1.933139
H	3.727477	3.049252	-1.555326
H	4.086495	-1.115542	0.099742
H	0.940130	-5.021707	0.377323
H	3.393096	-5.338311	0.655732
H	4.942077	-3.408748	0.531264
H	-0.966550	-2.975227	-0.208537
H	-2.547538	-2.267636	1.283823
H	-5.618454	1.056981	-0.892403
H	-6.497208	-0.655345	0.684828
H	-4.973823	-2.287230	1.758525
H	-0.736161	1.294572	-2.037360
H	-3.177556	1.938553	-2.053333

Linear indole trimer radical cation solvated species: HF -1088.673052 a.u.

C	-3.390504	-0.408825	1.099654
C	-2.588593	-1.087786	0.165599
C	-2.907019	-2.439775	-0.131084
C	-4.002393	-3.108159	0.412363
C	-4.803683	-2.394517	1.309026
C	-4.490811	-1.067457	1.656654
C	-1.342141	-0.769342	-0.548190
C	-0.974203	-1.960203	-1.211534
N	-1.904112	-2.925040	-0.983670
C	-2.537065	2.290066	-0.497131
C	-1.221237	1.795680	-0.405826
C	-0.161716	2.722895	-0.235166
C	-0.361756	4.092656	-0.098522
C	-1.684106	4.553106	-0.155216
C	-2.754508	3.663529	-0.365434
C	-0.634714	0.472309	-0.564090

C	0.803891	0.669112	-0.552832
N	1.033679	1.998032	-0.303208
C	3.428954	0.482520	1.411774
C	3.107855	-0.197214	0.221911
C	4.033527	-1.138232	-0.305120
C	5.264424	-1.406607	0.302522
C	5.565514	-0.706129	1.469619
C	4.656393	0.224151	2.019616
C	1.938442	-0.216900	-0.653693
C	2.215303	-1.138081	-1.661810
N	3.458543	-1.682541	-1.455437
H	-3.162839	0.605537	1.400085
H	-4.219408	-4.141753	0.166089
H	-5.667242	-2.876286	1.753038
H	-5.113232	-0.546057	2.375060
H	-0.131091	-2.151785	-1.848402
H	-1.878213	-3.855538	-1.372615
H	-3.369760	1.624213	-0.685264
H	0.465348	4.781406	0.032293
H	-1.881955	5.613975	-0.051910
H	-3.763716	4.052983	-0.434346
H	1.959502	2.398452	-0.266164
H	2.733903	1.183319	1.862428
H	5.957072	-2.131258	-0.111350
H	6.511708	-0.883546	1.968169
H	4.918631	0.741622	2.935683
H	1.659279	-1.362508	-2.557775
H	3.906126	-2.346703	-2.067343

Benzo(b)furan neutral solvated species: HF -383.782582 a.u.

C	-0.964781	1.439569	-0.000066
C	0.258520	0.752479	-0.000046
C	0.246809	-0.653160	-0.000039
C	-0.912715	-1.416221	0.000102
C	-2.116386	-0.712523	0.000056
C	-2.140491	0.695068	-0.000074
C	1.654134	1.127774	0.000060
C	2.355811	-0.029528	0.000178
O	1.531571	-1.133859	-0.000178
H	-0.993523	2.526444	-0.000163
H	-0.880022	-2.502527	0.000197
H	-3.053775	-1.262638	0.000123
H	-3.099085	1.207638	-0.000142
H	2.072052	2.126522	0.000103
H	3.416379	-0.245310	0.000280

Benzo(b)furan cation solvated species: HF -383.558276 a.u.

C	1.012273	1.433213	0.000100

C	-0.243572	0.757484	0.000037
C	-0.264668	-0.662288	-0.000056
C	0.849616	-1.444484	0.000018
C	2.085707	-0.743599	0.000034
C	2.159188	0.662820	0.000062
C	-1.578756	1.170437	0.000061
C	-2.342002	-0.009850	-0.000148
O	-1.583530	-1.100461	-0.000111
H	1.051697	2.520283	0.000172
H	0.808388	-2.531180	0.000003
H	3.006947	-1.323047	0.000023
H	3.135331	1.139990	0.000076
H	-1.981917	2.178173	0.000158
H	-3.418927	-0.162926	-0.000192

Benzo(b)thiophene neutral solvated species: HF -706.766056 a.u.

C	1.416370	1.375119	0.000099
C	0.110186	0.851085	0.000053
C	-0.060247	-0.555030	-0.000010
C	1.031304	-1.428894	0.000008
C	2.310241	-0.884432	0.000082
C	2.501016	0.509964	0.000094
C	-1.151286	1.548940	-0.000006
C	-2.219051	0.712385	-0.000029
S	-1.766020	-0.980576	-0.000127
H	1.566711	2.452405	0.000108
H	0.885606	-2.506251	0.000001
H	3.172820	-1.545902	0.000122
H	3.511278	0.911098	0.000127
H	-1.239455	2.631429	-0.000004
H	-3.271838	0.971616	-0.000069

Benzo(b)thiophene cation solvated species: HF -706.546746 a.u.

C	1.443389	1.361860	0.000096
C	0.125737	0.848895	0.000115
C	-0.067465	-0.555427	0.000071
C	0.986664	-1.438332	0.000156
C	2.302707	-0.899302	0.000130
C	2.522788	0.473148	0.000074
C	-1.097633	1.554954	0.000157
C	-2.205697	0.700572	-0.000129
S	-1.796800	-0.944265	-0.000272
H	1.606076	2.438089	0.000060
H	0.836592	-2.515999	0.000119
H	3.145867	-1.586181	0.000102
H	3.538339	0.859185	0.000003
H	-1.189005	2.638841	0.000255
H	-3.252006	0.996096	-0.000202

Benzo(b)selenophene neutral solvated species: HF -2710.094301 a.u.

C	2.068414	1.242016	0.000112
C	0.692149	0.947156	0.000039
C	0.291050	-0.410200	0.000053
C	1.222484	-1.450950	0.000090
C	2.576884	-1.131247	0.000055
C	2.996819	0.209949	0.000087
C	-0.404655	1.888457	-0.000066
C	-1.640651	1.338616	-0.000098
SE	-1.607339	-0.556549	-0.000050
H	2.395891	2.279426	0.000144
H	0.900856	-2.489401	0.000038
H	3.315388	-1.928956	0.000003
H	4.059319	0.439446	0.000104
H	-0.243171	2.963935	-0.000076
H	-2.593717	1.855445	-0.000140

Benzo(b)selenophene cation solvated species: HF -2709.878510 a.u.

C	-2.072963	1.240973	-0.001971
C	-0.698930	0.940007	-0.000458
C	-0.296581	-0.415027	0.000241
C	-1.205068	-1.450262	0.001830
C	-2.587049	-1.124339	0.001589
C	-3.009618	0.196702	-0.001011
C	0.382224	1.868617	0.001171
C	1.645324	1.296902	0.003389
SE	1.614739	-0.540593	-0.001046
H	-2.399705	2.279801	-0.003694
H	-0.889060	-2.491800	0.003625
H	-3.315728	-1.932040	0.003215
H	-4.071795	0.428124	-0.001904
H	0.236391	2.948398	0.001041
H	2.594726	1.826232	0.004600

2,2'-dibenzo(b)furan neutral solvated species: HF -766.364484 a.u.

C	-4.213680	1.302410	-0.000176
C	-2.892502	0.790391	-0.000062
C	-2.693314	-0.615118	0.000083
C	-3.721225	-1.533536	0.000171
C	-5.011288	-0.998055	0.000117
C	-5.252775	0.396929	-0.000056
C	-1.608169	1.360878	-0.000123
C	-0.701941	0.290970	-0.000034
O	-1.354684	-0.902853	0.000079
C	4.213679	1.302411	0.000188
C	2.892501	0.790391	0.000062

C	2.693315	-0.615118	-0.000086
C	3.721225	-1.533536	-0.000169
C	5.011289	-0.998054	-0.000104
C	5.252775	0.396929	0.000074
C	1.608169	1.360877	0.000101
C	0.701942	0.290967	0.000038
O	1.354683	-0.902854	-0.000099
H	-4.394816	2.369960	-0.000342
H	-3.538980	-2.599955	0.000271
H	-5.857568	-1.674718	0.000194
H	-6.276330	0.749892	-0.000095
H	4.394814	2.369960	0.000355
H	3.538982	-2.599955	-0.000276
H	5.857569	-1.674716	-0.000181
H	6.276330	0.749893	0.000116
H	-1.348829	2.408442	-0.000270
H	1.348827	2.408440	0.000238

2,2'-dibenzo(b)furan cation solvated species: HF -766.168274 a.u.

C	-4.213680	1.302410	-0.000176
C	-2.892502	0.790391	-0.000062
C	-2.693314	-0.615118	0.000083
C	-3.721225	-1.533536	0.000171
C	-5.011288	-0.998055	0.000117
C	-5.252775	0.396929	-0.000056
C	-1.608169	1.360878	-0.000123
C	-0.701941	0.290970	-0.000034
O	-1.354684	-0.902853	0.000079
C	4.213679	1.302411	0.000188
C	2.892501	0.790391	0.000062
C	2.693315	-0.615118	-0.000086
C	3.721225	-1.533536	-0.000169
C	5.011289	-0.998054	-0.000104
C	5.252775	0.396929	0.000074
C	1.608169	1.360877	0.000101
C	0.701942	0.290967	0.000038
O	1.354683	-0.902854	-0.000099
H	-4.394816	2.369960	-0.000342
H	-3.538980	-2.599955	0.000271
H	-5.857568	-1.674718	0.000194
H	-6.276330	0.749892	-0.000095
H	4.394814	2.369960	0.000355
H	3.538982	-2.599955	-0.000276
H	5.857569	-1.674716	-0.000181
H	6.276330	0.749893	0.000116
H	-1.348829	2.408442	-0.000270
H	1.348827	2.408440	0.000238

3,3'-dibenzo(b)thiophene neutral solvated species: HF -1412.319727 a.u.

C	-1.450687	1.489755	0.799273
C	-1.655472	0.244798	0.180568
C	-2.978437	-0.117617	-0.159619
C	-4.065032	0.720268	0.054479
C	-3.825285	1.964272	0.640847
C	-2.532277	2.335842	1.020707
C	-0.716645	-0.833274	-0.083665
C	-1.378891	-1.968237	-0.564344
S	-3.051376	-1.766180	-0.786918
C	1.450686	1.489755	-0.799272
C	1.655472	0.244798	-0.180567
C	2.978437	-0.117617	0.159618
C	4.065032	0.720268	-0.054481
C	3.825284	1.964273	-0.640849
C	2.532276	2.335842	-1.020706
C	0.716645	-0.833274	0.083667
C	1.378892	-1.968237	0.564345
S	3.051377	-1.766180	0.786917
H	-0.460772	1.789661	1.117219
H	-5.070654	0.418258	-0.211392
H	-4.654765	2.638240	0.816620
H	-2.370004	3.293956	1.498883
H	-0.914588	-2.896081	-0.866387
H	0.460771	1.789663	-1.117216
H	5.070654	0.418258	0.211389
H	4.654764	2.638241	-0.816622
H	2.370003	3.293957	-1.498882
H	0.914589	-2.896081	0.866389

3,3'-dibenzo(b)thiophene cation solvated species: HF -1412.121001 a.u.

C	-1.450687	1.489755	0.799273
C	-1.655472	0.244798	0.180568
C	-2.978437	-0.117617	-0.159619
C	-4.065032	0.720268	0.054479
C	-3.825285	1.964272	0.640847
C	-2.532277	2.335842	1.020707
C	-0.716645	-0.833274	-0.083665
C	-1.378891	-1.968237	-0.564344
S	-3.051376	-1.766180	-0.786918
C	1.450686	1.489755	-0.799272
C	1.655472	0.244798	-0.180567
C	2.978437	-0.117617	0.159618
C	4.065032	0.720268	-0.054481
C	3.825284	1.964273	-0.640849
C	2.532276	2.335842	-1.020706
C	0.716645	-0.833274	0.083667
C	1.378892	-1.968237	0.564345

S	3.051377	-1.766180	0.786917
H	-0.460772	1.789661	1.117219
H	-5.070654	0.418258	-0.211392
H	-4.654765	2.638240	0.816620
H	-2.370004	3.293956	1.498883
H	-0.914588	-2.896081	-0.866387
H	0.460771	1.789663	-1.117216
H	5.070654	0.418258	0.211389
H	4.654764	2.638241	-0.816622
H	2.370003	3.293957	-1.498882
H	0.914589	-2.896081	0.866389

3,3'-dibenzo(b)selenophene neutral solvated species: HF -5418.975946 a.u.

C	-1.300038	1.785894	1.006883
C	-1.620369	0.589357	0.343589
C	-2.984175	0.318425	0.096690
C	-3.998210	1.200740	0.442652
C	-3.645130	2.396825	1.071845
C	-2.308034	2.677009	1.361368
C	-0.724812	-0.497648	-0.037890
C	-1.392896	-1.619475	-0.518412
SE	-3.218424	-1.419619	-0.657268
C	1.300038	1.785893	-1.006884
C	1.620369	0.589356	-0.343589
C	2.984175	0.318425	-0.096690
C	3.998210	1.200740	-0.442652
C	3.645130	2.396825	-1.071845
C	2.308033	2.677009	-1.361367
C	0.724812	-0.497648	0.037891
C	1.392896	-1.619475	0.518413
SE	3.218425	-1.419619	0.657267
H	-0.271459	2.015143	1.253832
H	-5.038324	0.970559	0.246424
H	-4.419350	3.101471	1.350118
H	-2.051231	3.596621	1.872632
H	-0.922315	-2.523506	-0.877189
H	0.271458	2.015142	-1.253833
H	5.038324	0.970560	-0.246424
H	4.419349	3.101472	-1.350117
H	2.051231	3.596621	-1.872631
H	0.922315	-2.523506	0.877191

3,3'-dibenzo(b)thiophene cation solvated species: HF -5418.778127 a.u.

C	-1.300038	1.785894	1.006883
C	-1.620369	0.589357	0.343589
C	-2.984175	0.318425	0.096690
C	-3.998210	1.200740	0.442652
C	-3.645130	2.396825	1.071845

C	-2.308034	2.677009	1.361368
C	-0.724812	-0.497648	-0.037890
C	-1.392896	-1.619475	-0.518412
SE	-3.218424	-1.419619	-0.657268
C	1.300038	1.785893	-1.006884
C	1.620369	0.589356	-0.343589
C	2.984175	0.318425	-0.096690
C	3.998210	1.200740	-0.442652
C	3.645130	2.396825	-1.071845
C	2.308033	2.677009	-1.361367
C	0.724812	-0.497648	0.037891
C	1.392896	-1.619475	0.518413
SE	3.218425	-1.419619	0.657267
H	-0.271459	2.015143	1.253832
H	-5.038324	0.970559	0.246424
H	-4.419350	3.101471	1.350118
H	-2.051231	3.596621	1.872632
H	-0.922315	-2.523506	-0.877189
H	0.271458	2.015142	-1.253833
H	5.038324	0.970560	-0.246424
H	4.419349	3.101472	-1.350117
H	2.051231	3.596621	-1.872631
H	0.922315	-2.523506	0.877191

Linear benzo(b)furan trimer neutral solvated species: HF -1148.357893 a.u.

C	-4.221600	-2.417306	-0.595655
C	-3.405379	-1.299622	-0.340408
C	-4.004138	-0.122043	0.159743
C	-5.362444	0.006021	0.422951
C	-6.152796	-1.118253	0.164198
C	-5.588719	-2.311678	-0.338864
C	-1.999143	-1.013509	-0.471637
C	-1.804194	0.281873	-0.058294
O	-3.031726	0.859285	0.339123
C	2.670225	-3.719862	0.658801
C	2.331281	-2.384119	0.376806
C	3.310611	-1.544674	-0.196319
C	4.600134	-1.955672	-0.508436
C	4.913655	-3.288669	-0.221359
C	3.960919	-4.156151	0.355048
C	1.147104	-1.575241	0.537482
C	1.432603	-0.317535	0.070139
O	2.776189	-0.270317	-0.389131
C	2.652756	2.733612	-0.033544
C	1.330484	2.253203	-0.016934
C	0.276320	3.184794	0.015639
C	0.450581	4.563130	0.033578
C	1.771332	5.019399	0.013724

C	2.854324	4.114477	-0.019057
C	0.714533	0.931378	-0.000947
C	-0.657113	1.139162	0.011012
O	-0.945182	2.515283	0.033475
H	-5.777813	0.929745	0.806045
H	-7.220094	-1.072071	0.352625
H	-6.235597	-3.161884	-0.528648
H	1.946952	-4.395860	1.102482
H	5.318826	-1.276336	-0.950101
H	5.907424	-3.661281	-0.445722
H	4.241041	-5.183210	0.565130
H	3.486043	2.045030	-0.065849
H	-0.396840	5.236576	0.060701
H	1.966259	6.086522	0.022937
H	3.867146	4.503436	-0.034254
H	-3.799369	-3.338291	-0.983412
H	-1.238935	-1.676303	-0.851481
H	0.212711	-1.886364	0.975807

Linear benzo(b)furan trimer radical cation solvated species:
HF -1148.166160 a.u.

C	-4.189015	-2.395143	-0.650203
C	-3.377817	-1.275560	-0.343877
C	-3.991001	-0.101447	0.170984
C	-5.350337	0.021748	0.408153
C	-6.126957	-1.102274	0.101414
C	-5.554147	-2.291312	-0.420505
C	-1.986857	-0.998878	-0.436352
C	-1.792064	0.309131	0.017346
O	-3.021600	0.876759	0.386098
C	2.597696	-3.729811	0.682558
C	2.285540	-2.384592	0.375285
C	3.290176	-1.560598	-0.194698
C	4.572501	-1.992357	-0.488694
C	4.852777	-3.330142	-0.179722
C	3.879912	-4.183657	0.398132
C	1.122236	-1.573677	0.509530
C	1.433525	-0.302061	0.026882
O	2.776205	-0.276790	-0.399032
C	2.668940	2.724375	-0.187361
C	1.345799	2.246826	-0.070292
C	0.301182	3.181810	0.079682
C	0.473395	4.552053	0.123712
C	1.796252	5.004168	-0.000229
C	2.872372	4.103131	-0.153330
C	0.741624	0.933427	-0.018447
C	-0.666479	1.152091	0.084850
O	-0.927753	2.506745	0.181557

H	-5.780929	0.933608	0.800361
H	-7.198158	-1.061914	0.263524
H	-6.202315	-3.130823	-0.642979
H	1.857770	-4.386657	1.125197
H	5.312491	-1.335022	-0.926215
H	5.842523	-3.721839	-0.385307
H	4.148362	-5.209764	0.620670
H	3.494471	2.037539	-0.309555
H	-0.362267	5.228228	0.246946
H	1.993813	6.069750	0.023492
H	3.878405	4.494988	-0.246852
H	-3.756125	-3.304628	-1.050441
H	-1.226817	-1.647549	-0.841214
H	0.188434	-1.863131	0.964489

Linear benzo(b)thiophene trimer neutral solvated species: HF -2117.277793 a.u.

C	-0.134572	1.652795	1.646237
C	0.679846	1.968047	0.540960
C	0.922654	3.330912	0.249575
C	0.377408	4.364632	1.013045
C	-0.431100	4.027022	2.100413
C	-0.682648	2.677557	2.414149
C	1.355180	1.055456	-0.379931
C	2.089469	1.707461	-1.325890
S	2.016795	3.512193	-1.196202
C	3.813180	-0.787400	0.166344
C	2.488241	-1.229231	-0.027467
C	2.224920	-2.616103	0.052045
C	3.228713	-3.552757	0.305403
C	4.535031	-3.091690	0.482781
C	4.822217	-1.714939	0.415820
C	1.298188	-0.424645	-0.283399
C	0.144684	-1.161231	-0.396016
S	0.462460	-2.963513	-0.194957
C	-2.583550	-1.959188	1.069678
C	-2.433378	-1.120872	-0.054287
C	-3.596434	-0.539988	-0.614311
C	-4.872962	-0.781549	-0.105231
C	-4.996068	-1.625809	1.000268
C	-3.855105	-2.206547	1.584099
C	-1.206761	-0.716083	-0.744604
C	-1.443810	0.139516	-1.782656
S	-3.184988	0.541650	-2.020617
H	-0.332920	0.615324	1.890104
H	0.576818	5.402616	0.770430
H	-0.867341	4.813267	2.707789
H	-1.311843	2.433400	3.263633
H	2.677815	1.273147	-2.119951

H	4.037211	0.272558	0.124073
H	3.001148	-4.611532	0.362690
H	5.332201	-3.801711	0.677076
H	5.841039	-1.372327	0.564096
H	-1.712490	-2.409308	1.531302
H	-5.747361	-0.323557	-0.554328
H	-5.978760	-1.830423	1.412221
H	-3.965749	-2.854107	2.447669
H	-0.718101	0.575180	-2.450557

Linear benzo(b)thiophene trimer radical cation solvated species:
HF -2117.077019 a.u.

C	0.136579	1.784344	1.681003
C	0.975227	1.908502	0.555898
C	1.443788	3.196674	0.208649
C	1.087864	4.343030	0.917718
C	0.238016	4.195347	2.017910
C	-0.227541	2.923324	2.397764
C	1.521934	0.859040	-0.309246
C	2.399286	1.352030	-1.254161
S	2.581987	3.126177	-1.218845
C	3.682146	-1.338514	0.036699
C	2.283868	-1.557914	-0.045162
C	1.802142	-2.884083	0.091853
C	2.646879	-3.971340	0.266214
C	4.029695	-3.730213	0.304473
C	4.539532	-2.422454	0.195702
C	1.240221	-0.574588	-0.199127
C	-0.061628	-1.135920	-0.200882
S	-0.015673	-2.936326	0.043960
C	-3.026528	-1.871711	0.854814
C	-2.641631	-0.875084	-0.066401
C	-3.660664	-0.068004	-0.625869
C	-5.007792	-0.227281	-0.325801
C	-5.363242	-1.238970	0.577481
C	-4.377441	-2.046544	1.164218
C	-1.302875	-0.484961	-0.518657
C	-1.342966	0.594859	-1.400904
S	-2.963341	1.197340	-1.751007
H	-0.219187	0.809144	1.993848
H	1.465769	5.318625	0.634918
H	-0.053183	5.069658	2.588955
H	-0.872518	2.826921	3.263880
H	2.918890	0.792042	-2.017382
H	4.075437	-0.330070	-0.007313
H	2.258909	-4.977189	0.374731
H	4.709875	-4.564010	0.437630
H	5.609206	-2.258720	0.253117

H	-2.287296	-2.498894	1.336534
H	-5.763357	0.410552	-0.769309
H	-6.407308	-1.389474	0.827064
H	-4.665473	-2.816683	1.870432
H	-0.506534	1.035606	-1.917940

Linear benzo(b)selenophene trimer neutral solvated species:
HF -8120.296971 a.u.

C	-0.345746	-1.253785	1.981009
C	-1.137644	-1.567926	0.859164
C	-1.631149	-2.887859	0.724902
C	-1.342461	-3.873413	1.668310
C	-0.551709	-3.544569	2.769848
C	-0.057100	-2.236427	2.924147
C	-1.541903	-0.664101	-0.215350
C	-2.331359	-1.236071	-1.166858
SE	-2.699444	-3.087752	-0.852658
C	-3.547919	1.610812	0.258714
C	-2.182771	1.812635	-0.030491
C	-1.689444	3.138249	-0.077940
C	-2.520955	4.234038	0.154651
C	-3.870435	4.014133	0.434449
C	-4.379794	2.703734	0.487516
C	-1.177497	0.777277	-0.252110
C	0.094342	1.233446	-0.478248
SE	0.179881	3.174590	-0.462328
C	2.625628	1.609701	1.240362
C	2.499444	0.674348	0.193471
C	3.579445	-0.196223	-0.080487
C	4.761417	-0.138480	0.657248
C	4.871692	0.794886	1.689630
C	3.803727	1.663183	1.980152
C	1.327216	0.466794	-0.659526
C	1.467422	-0.532077	-1.577292
SE	3.169223	-1.397743	-1.514980
H	0.039749	-0.247838	2.101207
H	-1.725254	-4.881857	1.553268
H	-0.317900	-4.301520	3.511405
H	0.556297	-1.991195	3.784862
H	-2.733432	-0.734220	-2.034312
H	-3.940760	0.601243	0.303260
H	-2.130755	5.245321	0.111800
H	-4.528195	4.857957	0.615613
H	-5.429482	2.543114	0.710776
H	1.803512	2.287741	1.434635
H	5.585619	-0.809489	0.440149
H	5.785319	0.848354	2.272636
H	3.896582	2.382061	2.787536

H	0.715590	-0.842702	-2.285631

Linear benzo(b)selenophene trimer radical cation solvated species:
HF -8120.101166 a.u.

C	0.612332	1.453208	2.334511
C	0.891381	1.859586	1.014899
C	0.650853	3.204063	0.649120
C	0.148945	4.133219	1.559005
C	-0.120695	3.712239	2.863376
C	0.111075	2.378583	3.247455
C	1.446238	1.049501	-0.064222
C	1.722445	1.725993	-1.223287
SE	1.119242	3.521411	-1.185009
C	4.020199	-0.613854	0.016557
C	2.714025	-1.162163	-0.055163
C	2.558816	-2.571517	-0.111122
C	3.656663	-3.418026	-0.101762
C	4.942710	-2.856821	-0.047574
C	5.121155	-1.461583	0.012469
C	1.490568	-0.419870	-0.045876
C	0.301147	-1.188405	-0.110734
SE	0.714197	-3.071541	-0.158260
C	-2.335860	-2.720395	0.774360
C	-2.252869	-1.479725	0.108866
C	-3.468278	-0.832617	-0.216046
C	-4.710121	-1.394030	0.047481
C	-4.765502	-2.643674	0.677362
C	-3.580890	-3.291085	1.049390
C	-1.048411	-0.708199	-0.247188
C	-1.348649	0.548877	-0.793242
SE	-3.168616	0.889090	-1.006684
H	0.799940	0.429568	2.640996
H	-0.023913	5.163897	1.270691
H	-0.505450	4.421606	3.587481
H	-0.096987	2.070237	4.265920
H	2.133627	1.298044	-2.125822
H	4.148591	0.460460	0.081388
H	3.538423	-4.494541	-0.139280
H	5.808489	-3.509693	-0.042977
H	6.122248	-1.050118	0.064711
H	-1.444379	-3.230199	1.113202
H	-5.625415	-0.876687	-0.216140
H	-5.725673	-3.098457	0.891989
H	-3.624804	-4.242865	1.566103
H	-0.652324	1.314285	-1.091665

1,4,5,8,9,12-Hexamethyltriphenylene neutral solvated species:
HF -929.241923 a.u.

C	-1.274545	0.725972	-0.128548
C	-0.065105	1.439430	0.147295
C	1.166808	0.636310	0.327807
C	-1.274364	-0.726260	0.128571
C	-0.064759	-1.439420	-0.147306
C	1.166960	-0.636007	-0.327808
C	-2.376071	1.380051	-0.718215
C	-2.331929	2.768665	-0.842873
C	-1.190366	3.475716	-0.517451
C	-0.019566	2.838185	-0.096731
C	2.369984	1.073607	0.922135
C	3.564723	0.479656	0.502612
C	3.564843	-0.478809	-0.502564
C	2.370248	-1.073041	-0.922102
C	-2.375721	-1.380619	0.718244
C	-2.331237	-2.769226	0.842869
C	-1.189511	-3.475996	0.517402
C	-0.018876	-2.838169	0.096672
C	-3.550465	-0.670530	1.357873
C	1.226376	-3.698673	0.099542
C	-3.550648	0.669660	-1.357813
C	1.225471	3.698998	-0.099684
C	2.400646	-2.034593	-2.090251
C	2.400141	2.035113	2.090328
H	-3.181195	3.290461	-1.272931
H	-1.164401	4.546874	-0.689369
H	4.502763	0.813544	0.935095
H	4.502970	-0.812494	-0.935018
H	-3.180370	-3.291240	1.272929
H	-1.163285	-4.547153	0.689285
H	-4.477678	-0.814493	0.796073
H	-3.383121	0.399838	1.465277
H	-3.715419	-1.085278	2.356194
H	1.092740	-4.521288	0.804786
H	2.110794	-3.137830	0.402636
H	1.437248	-4.144104	-0.875874
H	-3.715721	1.084351	-2.356138
H	-4.477889	0.813402	-0.796001
H	-3.383042	-0.400668	-1.465202
H	2.110017	3.138365	-0.402790
H	1.436270	4.144524	0.875704
H	1.091601	4.521548	-0.804958
H	1.409880	-2.412421	-2.338777
H	3.069162	-2.883691	-1.926065
H	2.771554	-1.497669	-2.969612
H	2.771158	1.498234	2.969671
H	1.409284	2.412700	2.338857
H	3.068464	2.884374	1.926194

1,4,5,8,9,12-Hexamethyltriphenylene cation solvated species:
HF -929.038131 a.u.

C	1.271750	-0.722633	-0.149191
C	0.058504	-1.440756	0.132477
C	-1.140971	-0.647575	0.334527
C	1.271259	0.723491	0.149163
C	0.057531	1.440801	-0.132514
C	-1.141413	0.646821	-0.334542
C	2.354730	-1.370259	-0.751789
C	2.292066	-2.773034	-0.891163
C	1.162753	-3.487924	-0.553282
C	-0.000865	-2.854754	-0.102789
C	-2.346076	-1.056874	0.975949
C	-3.517691	-0.467630	0.531971
C	-3.518025	0.465317	-0.531860
C	-2.346823	1.055315	-0.975914
C	2.353794	1.371836	0.751788
C	2.290190	2.774567	0.891171
C	1.160405	3.488704	0.553265
C	-0.002781	2.854761	0.102748
C	3.547428	0.682132	1.362865
C	-1.241460	3.711645	0.049115
C	3.547924	-0.679767	-1.362834
C	-1.238968	-3.712468	-0.049162
C	-2.368885	1.990630	-2.162103
C	-2.367461	-1.992267	2.162089
H	3.141285	-3.292753	-1.322142
H	1.140941	-4.558038	-0.723414
H	-4.464120	-0.766553	0.970096
H	-4.464674	0.763612	-0.969942
H	3.139049	3.294850	1.322177
H	1.137876	4.558802	0.723404
H	4.459572	0.857532	0.785355
H	3.407993	-0.392245	1.465233
H	3.723085	1.095881	2.359474
H	-1.135081	4.542997	0.746957
H	-2.145941	3.165336	0.313481
H	-1.391546	4.146521	-0.942642
H	3.723896	-1.093417	-2.359429
H	4.460165	-0.854549	-0.785285
H	3.407775	0.394515	-1.465226
H	-2.143821	-3.166761	-0.313500
H	-1.388745	-4.147470	0.942587
H	-1.132040	-4.543732	-0.747025
H	-1.381604	2.382138	-2.400755
H	-3.059068	2.825429	-2.027171
H	-2.710284	1.426009	-3.035220

H	-2.709204	-1.427925	3.035251
H	-1.379904	-2.383126	2.400674
H	-3.057086	-2.827523	2.027140

Pyrrolo[3,2,1-jk]carbazole neutral solvated species: HF -593.804964 a.u.

C	2.223913	2.020373	0.000235
C	0.890898	2.375090	-0.000147
C	2.307694	0.564967	0.000378
C	0.980578	0.167240	0.000150
N	0.113449	1.211413	-0.000170
C	2.684951	-1.822892	-0.000177
C	1.304669	-2.136465	-0.000228
C	0.386759	-1.082232	0.000080
C	3.207712	-0.516692	0.000246
C	-2.207797	-1.547120	0.000147
C	-3.456085	-0.921764	0.000344
C	-3.560982	0.472155	0.000179
C	-1.052684	-0.770029	-0.000436
C	-1.185457	0.661730	-0.000503
C	-2.424105	1.284142	-0.000160
H	3.041106	2.725574	0.000341
H	0.444487	3.356366	-0.000535
H	3.388045	-2.648561	-0.000357
H	0.996723	-3.175692	-0.000478
H	4.282392	-0.373985	0.000378
H	-2.138514	-2.629103	0.000243
H	-4.541145	0.934900	0.000421
H	-2.510925	2.364176	-0.000197
H	-4.356690	-1.524590	0.000724

Pyrrolo[3,2,1-jk]carbazole cation solvated species: HF -593.592152 a.u.

C	2.186825	2.024803	0.000402
C	0.803748	2.367643	-0.000220
C	2.300675	0.587579	0.000345
C	0.986116	0.163546	-0.000394
N	0.080497	1.223928	-0.000651
C	2.731858	-1.786562	0.000402
C	1.363389	-2.120060	-0.000482
C	0.415310	-1.073400	-0.000541
C	3.234579	-0.468837	0.001042
C	-2.171963	-1.572723	-0.000101
C	-3.440205	-0.953184	0.000860
C	-3.576173	0.434616	0.001013
C	-1.042465	-0.781346	-0.001220
C	-1.204446	0.647468	-0.001166
C	-2.451398	1.263036	-0.000043
H	2.982820	2.755762	0.000667
H	0.356868	3.349645	-0.000446

H	3.447309	-2.599800	0.000552
H	1.071270	-3.162843	-0.001038
H	4.303795	-0.298428	0.001713
H	-2.096679	-2.653236	-0.000006
H	-4.563678	0.878054	0.001926
H	-2.552148	2.341465	0.000135
H	-4.328148	-1.573590	0.001667

Pyrrolo[3,2,1-jk]carbazole dimer neutral solvated species: HF

C	0.730254	-0.074246	-0.000236
C	1.535471	-1.153619	-0.350965
C	1.623276	1.030513	0.381199
C	2.892670	0.495785	0.221981
N	2.876964	-0.794139	-0.205647
C	2.887127	2.968167	1.102984
C	4.143473	2.341904	0.906366
C	4.157152	1.021021	0.441531
C	1.639891	2.355654	0.861881
C	6.436558	-0.259005	0.078659
C	6.980061	-1.487037	-0.314260
C	6.153035	-2.553373	-0.693537
C	5.050614	-0.097911	0.091042
C	4.221879	-1.207865	-0.303691
C	4.758654	-2.428599	-0.693529
C	-0.730211	-0.074330	-0.000087
C	-1.535363	-1.154091	0.349644
C	-1.623282	1.030264	-0.381852
C	-2.892646	0.495446	-0.222697
N	-2.876886	-0.794567	0.204676
C	-2.887254	2.968162	-1.102741
C	-4.143568	2.341950	-0.905819
C	-4.157168	1.020900	-0.441463
C	-1.639963	2.355506	-0.862250
C	-6.436562	-0.258833	-0.077710
C	-6.980068	-1.486822	0.315329
C	-6.153026	-2.553291	0.694195
C	-5.050601	-0.097919	-0.090584
C	-4.221822	-1.208013	0.303680
C	-4.758623	-2.428723	0.693582
H	1.242300	-2.133563	-0.709658
H	2.885163	3.992759	1.471525
H	5.056516	2.893338	1.124304
H	0.728102	2.914012	1.059562
H	7.088374	0.562641	0.372034
H	6.599538	-3.499313	-0.995183
H	4.119162	-3.258410	-0.988394
H	8.060779	-1.615924	-0.325312
H	-1.242082	-2.134242	0.707683

H	-2.885352	3.992951	-1.470736
H	-5.056660	2.893587	-1.123041
H	-0.728229	2.914133	-1.059766
H	-7.088365	0.562928	-0.370805
H	-6.599531	-3.499209	0.995907
H	-4.119201	-3.258738	0.987995
H	-8.060797	-1.615579	0.326773

Pyrrolo[3,2,1-jk]carbazole dimer cation solvated species: HF

C	0.707932	0.065109	0.007971
C	1.495052	-1.125689	-0.146801
C	1.655962	1.182415	0.167799
C	2.889236	0.568849	0.080099
N	2.804814	-0.795640	-0.109715
C	3.028022	3.139543	0.546254
C	4.244388	2.425672	0.428925
C	4.177810	1.047332	0.189297
C	1.746894	2.564372	0.433320
C	6.385930	-0.385206	0.021624
C	6.861702	-1.691166	-0.159009
C	5.983960	-2.768822	-0.333303
C	5.012250	-0.162913	0.025931
C	4.135112	-1.283919	-0.155065
C	4.596950	-2.579795	-0.333658
C	-0.707923	0.065042	-0.007906
C	-1.495017	-1.125869	0.146515
C	-1.655937	1.182331	-0.167947
C	-2.889200	0.568722	-0.080458
N	-2.804806	-0.795801	0.109216
C	-3.027941	3.139541	-0.546167
C	-4.244308	2.425680	-0.428804
C	-4.177760	1.047302	-0.189368
C	-1.746825	2.564332	-0.433360
C	-6.385937	-0.385054	-0.021235
C	-6.861786	-1.690969	0.159502
C	-5.984100	-2.768711	0.333539
C	-5.012238	-0.162897	-0.025872
C	-4.135137	-1.283974	0.154932
C	-4.597070	-2.579821	0.333554
H	1.154891	-2.145367	-0.302734
H	3.084824	4.207881	0.746986
H	5.190075	2.953343	0.538180
H	0.876878	3.195611	0.577294
H	7.081565	0.441317	0.156560
H	6.382572	-3.771972	-0.471393
H	3.911969	-3.414795	-0.469361
H	7.935295	-1.870496	-0.163517
H	-1.154889	-2.145588	0.302235

H	-3.084735	4.207915	-0.746707
H	-5.189987	2.953410	-0.537827
H	-0.876789	3.195582	-0.577175
H	-7.081516	0.441551	-0.155976
H	-6.382776	-3.771824	0.471713
H	-3.912171	-3.414908	0.469075
H	-7.935395	-1.870196	0.164282

2,5-dibenzoselenophene neutral solvated species: HF -3018.639618 a.u.

C	0.711345	1.676616	0.538449
C	1.317943	0.505508	0.166773
SE	-0.000003	-0.788877	-0.264939
C	-1.317939	0.505487	0.166814
C	-0.711356	1.676554	0.538631
C	-3.660270	1.237255	-0.260346
C	-2.752204	0.216379	0.072627
C	-3.263429	-1.069585	0.314574
C	-5.025618	0.982457	-0.332121
C	-5.517936	-0.299487	-0.088428
C	-4.628755	-1.324237	0.231394
C	3.660321	1.237320	-0.260012
C	5.025664	0.982498	-0.331814
C	5.517942	-0.299514	-0.088435
C	2.752203	0.216393	0.072636
C	3.263392	-1.069659	0.314254
C	4.628712	-1.324329	0.231069
H	1.284823	2.539859	0.855196
H	-1.284839	2.539770	0.855447
H	-3.287156	2.229766	-0.484121
H	-2.586670	-1.870325	0.592057
H	-5.706655	1.784998	-0.592994
H	-6.581748	-0.497825	-0.150525
H	-4.999426	-2.324444	0.426040
H	3.287262	2.229909	-0.483536
H	5.706728	1.785102	-0.592421
H	6.581747	-0.497882	-0.150554
H	2.586608	-1.870462	0.591492
H	4.999346	-2.324597	0.425469

2,5-dibenzoselenophene cation solvated species: HF -3018.440571 a.u.

C	0.690597	1.776564	0.016300
C	1.315498	0.512197	0.005267
SE	0.000000	-0.853647	-0.007725
C	-1.315498	0.512197	0.005264
C	-0.690596	1.776564	0.016300
C	-3.669230	1.291089	-0.007761
C	-2.722363	0.232384	0.002537
C	-3.210037	-1.099384	0.009671

C	-5.025987	1.023361	-0.010875
C	-5.482016	-0.298903	-0.003385
C	-4.567027	-1.358652	0.006932
C	3.669229	1.291089	-0.007757
C	5.025987	1.023361	-0.010873
C	5.482016	-0.298903	-0.003386
C	2.722363	0.232384	0.002540
C	3.210037	-1.099385	0.009668
C	4.567027	-1.358652	0.006928
H	1.258442	2.696861	0.026940
H	-1.258442	2.696861	0.026941
H	-3.337376	2.320648	-0.015235
H	-2.516709	-1.932965	0.019307
H	-5.735854	1.841280	-0.019455
H	-6.545984	-0.503973	-0.005560
H	-4.921928	-2.381787	0.013218
H	3.337376	2.320648	-0.015229
H	5.735854	1.841280	-0.019451
H	6.545984	-0.503973	-0.005563
H	2.516709	-1.932965	0.019301
H	4.921928	-2.381787	0.013210

2,5-dibenzo-3,4-selenophene neutral solvated species: HF -3050.720237 a.u.

N	0.675765	1.575520	0.000282
C	1.253994	0.410606	0.000121
SE	0.000002	-1.029229	-0.000101
C	-1.253996	0.410606	0.000093
N	-0.675769	1.575518	0.000277
C	-3.537710	1.374569	0.000363
C	-2.711539	0.237559	0.000023
C	-3.307633	-1.031018	-0.000364
C	-4.919902	1.236742	0.000309
C	-5.504050	-0.030920	-0.000094
C	-4.692631	-1.163852	-0.000430
C	3.537708	1.374569	-0.000571
C	4.919899	1.236743	-0.000642
C	5.504049	-0.030918	-0.000084
C	2.711538	0.237558	0.000060
C	3.307633	-1.031018	0.000637
C	4.692632	-1.163850	0.000556
H	-3.076688	2.353655	0.000667
H	-2.690436	-1.922939	-0.000616
H	-5.545472	2.122202	0.000585
H	-6.583142	-0.134240	-0.000134
H	-5.136874	-2.152538	-0.000748
H	3.076684	2.353653	-0.001013
H	5.545469	2.122202	-0.001137
H	6.583141	-0.134235	-0.000143

H	2.690436	-1.922939	0.001199
H	5.136876	-2.152536	0.001008

2,5-dibenzoselenophene neutral solvated species: HF -3050.494074 a.u.

N	-0.648262	1.547892	0.000077
C	-1.251189	0.341954	0.000019
SE	0.000000	-1.085398	-0.000062
C	1.251189	0.341955	0.000019
N	0.648262	1.547892	0.000076
C	3.466767	1.405450	0.000081
C	2.675212	0.221098	0.000017
C	3.320158	-1.042329	-0.000048
C	4.844767	1.314117	0.000078
C	5.464201	0.058641	0.000013
C	4.696786	-1.118558	-0.000049
C	-3.466767	1.405450	0.000120
C	-4.844767	1.314117	0.000123
C	-5.464201	0.058641	0.000009
C	-2.675212	0.221097	0.000006
C	-3.320158	-1.042329	-0.000114
C	-4.696786	-1.118558	-0.000112
H	2.969363	2.365789	0.000130
H	2.733912	-1.954292	-0.000096
H	5.446121	2.214737	0.000125
H	6.545935	-0.008607	0.000011
H	5.188409	-2.083347	-0.000099
H	-2.969363	2.365789	0.000206
H	-5.446121	2.214737	0.000216
H	-6.545935	-0.008606	0.000011
H	-2.733913	-1.954292	-0.000214
H	-5.188409	-2.083346	-0.000207

Chapter 5:

Indolo[3,2,1-jk]carbazole neutral solution species: HF -747.497336 a.u.

C	-3.547141	0.142635	0.000397
C	-2.160948	0.284062	-0.000335
C	-1.344168	-0.900184	-0.000567
C	-1.902132	-2.172332	-0.000254
C	-3.293818	-2.273791	0.000423
C	-4.106455	-1.134747	0.000749
C	-1.260652	1.444146	-0.000348
C	-0.000002	0.872806	-0.000670
N	0.000001	-0.492196	-0.000882
C	-0.000011	3.504343	0.000316
C	1.246482	2.845206	0.000163
C	1.260646	1.444150	-0.000251
C	-1.246502	2.845200	-0.000019

C	3.547144	0.142646	0.000427
C	4.106464	-1.134732	0.000637
C	3.293829	-2.273779	0.000299
C	2.160950	0.284071	-0.000103
C	1.344171	-0.900183	-0.000443
C	1.902143	-2.172329	-0.000252
H	-4.185425	1.019103	0.000606
H	-1.281758	-3.059747	-0.000555
H	-3.751334	-3.256446	0.000713
H	-5.184200	-1.248085	0.001332
H	-0.000010	4.588589	0.000727
H	2.157851	3.431997	0.000565
H	-2.157878	3.431979	0.000220
H	4.185424	1.019117	0.000590
H	3.751348	-3.256434	0.000501
H	1.281783	-3.059753	-0.000604
H	5.184209	-1.248074	0.001066

Indolo[3,2,1-jk]carbazole cation solution species: HF -747.286709 a.u.

C	-3.532332	0.136085	0.000094
C	-2.161904	0.288390	-0.000047
C	-1.336860	-0.891022	-0.000104
C	-1.870751	-2.177647	-0.000039
C	-3.262441	-2.298222	0.000109
C	-4.076729	-1.166838	0.000175
C	-1.260831	1.464746	-0.000120
C	0.000000	0.900382	-0.000293
N	0.000000	-0.471920	-0.000264
C	0.000000	3.514807	0.000163
C	1.254557	2.859058	0.000096
C	1.260831	1.464746	-0.000127
C	-1.254557	2.859058	0.000102
C	3.532332	0.136085	0.000061
C	4.076729	-1.166838	0.000129
C	3.262441	-2.298223	0.000067
C	2.161904	0.288390	-0.000062
C	1.336860	-0.891022	-0.000111
C	1.870751	-2.177647	-0.000062
H	-4.189515	0.997154	0.000152
H	-1.239179	-3.056323	-0.000103
H	-3.711195	-3.283329	0.000168
H	-5.153302	-1.286870	0.000288
H	0.000000	4.598431	0.000326
H	2.162311	3.449009	0.000247
H	-2.162311	3.449010	0.000256
H	4.189515	0.997154	0.000115
H	3.711195	-3.283329	0.000113
H	1.239178	-3.056323	-0.000123

H	5.153302	-1.286870	0.000229

5-aminoindolo[3,2,1-jk]carbazole neutral solution species: HF -802.878013 a.u.

C	3.894564	-0.149015	0.003136
C	2.527781	0.122922	0.002285
C	1.601841	-0.979685	0.000865
C	2.038705	-2.299124	0.000353
C	3.414485	-2.530813	0.001249
C	4.331344	-1.473337	0.002650
C	1.739133	1.360852	0.001744
C	0.430341	0.907556	0.000352
N	0.304642	-0.449279	0.000071
C	0.674059	3.529325	0.000245
C	-0.628274	2.987967	-0.001671
C	-0.772566	1.594763	-0.001824
C	1.853979	2.757355	0.001938
C	-3.170815	0.527142	-0.005130
C	-3.872710	-0.685688	-0.004310
C	-3.160018	-1.898472	-0.005416
C	-1.778795	0.524349	-0.003800
C	-1.077714	-0.727667	-0.003032
C	-1.766958	-1.931078	-0.003711
N	-5.274909	-0.694797	-0.067180
H	4.612660	0.663462	0.003994
H	1.337376	-3.124264	-0.001126
H	3.777612	-3.552225	0.000626
H	5.393636	-1.687715	0.003142
H	0.774360	4.608962	0.000005
H	-1.481208	3.657080	-0.003891
H	2.815767	3.257379	0.002915
H	-3.714816	1.466176	-0.012060
H	-3.710204	-2.833581	-0.013682
H	-1.245756	-2.880292	-0.003026
H	-5.724124	0.138921	0.283359
H	-5.713715	-1.529478	0.293963

5-aminoindolo[3,2,1-jk]carbazole cation solution species: HF -802.696017 a.u.

C	-3.866855	-0.165550	0.000462
C	-2.508565	0.111601	-0.000033
C	-1.582181	-0.985476	-0.000312
C	-1.997655	-2.310867	-0.000150
C	-3.371453	-2.554589	0.000366
C	-4.289454	-1.501183	0.000664
C	-1.728129	1.366896	-0.000321
C	-0.421890	0.936702	-0.000851
N	-0.278662	-0.443718	-0.000831
C	-0.686574	3.544206	0.000341
C	0.621782	3.020007	0.000073

C	0.768563	1.627094	-0.000532
C	-1.859932	2.761096	0.000251
C	3.149977	0.549925	-0.000018
C	3.844077	-0.696238	0.000470
C	3.120671	-1.927661	-0.000030
C	1.779441	0.554871	-0.000372
C	1.062072	-0.716067	-0.000444
C	1.747549	-1.943637	-0.000406
N	5.192563	-0.712833	0.000599
H	-4.594667	0.636772	0.000689
H	-1.291651	-3.131314	-0.000385
H	-3.728755	-3.576777	0.000525
H	-5.349982	-1.721611	0.001042
H	-0.798817	4.621790	0.000765
H	1.467719	3.696072	0.000364
H	-2.825675	3.251142	0.000701
H	3.713029	1.476302	-0.000098
H	3.672410	-2.860244	-0.000191
H	1.211998	-2.883831	-0.000718
H	5.730245	0.140925	0.001969
H	5.708179	-1.580133	0.002009

5-bromoindolo[3,2,1-jk]carbazole neutral solution species: HF -3321.039440 a.u.

C	4.831867	-0.367290	-0.000172
C	3.486964	-0.002964	0.000036
C	2.489499	-1.038782	0.000124
C	2.832368	-2.384485	0.000142
C	4.189233	-2.710533	-0.000005
C	5.175875	-1.718586	-0.000167
C	2.787201	1.288279	-0.000142
C	1.450323	0.929848	-0.000135
N	1.228439	-0.417135	0.000142
C	1.877859	3.526604	0.000223
C	0.541267	3.080183	0.000004
C	0.300360	1.699566	-0.000224
C	3.000631	2.672521	0.000114
C	-2.165258	0.796642	-0.000175
C	-2.911268	-0.377897	-0.000112
C	-2.313931	-1.640486	0.000036
C	-0.775137	0.701002	-0.000016
C	-0.161901	-0.600124	0.000090
C	-0.924145	-1.760824	0.000164
BR	-4.828241	-0.260234	-0.000005
H	5.603976	0.393780	-0.000282
H	2.076408	-3.159643	0.000277
H	4.481213	-3.754345	-0.000001
H	6.220818	-2.005577	-0.000317
H	2.054768	4.596195	0.000471

H	-0.262616	3.807082	0.000077
H	3.995267	3.103142	0.000263
H	-2.655958	1.761326	-0.000317
H	-2.931289	-2.529104	0.000001
H	-0.464059	-2.740744	0.000298

5-bromoindolo[3,2,1-jk]carbazole cation solution species: HF -3320.827191 a.u.

C	-4.796780	-0.394538	0.000002
C	-3.469592	-0.015362	0.000038
C	-2.459058	-1.040767	0.000066
C	-2.771771	-2.398025	0.000063
C	-4.122615	-2.747855	0.000024
C	-5.115565	-1.767186	-0.000005
C	-2.781432	1.296476	0.000060
C	-1.447314	0.958440	0.000098
N	-1.209386	-0.404585	0.000097
C	-1.895423	3.536449	-0.000021
C	-0.549152	3.104352	0.000002
C	-0.306315	1.729119	0.000056
C	-3.014039	2.675383	0.000000
C	2.152712	0.814684	-0.000026
C	2.906762	-0.381513	-0.000036
C	2.301551	-1.649121	-0.000001
C	0.779893	0.723812	0.000021
C	0.162054	-0.585869	0.000059
C	0.919679	-1.761859	0.000049
BR	4.784872	-0.260296	-0.000094
H	-5.587772	0.345389	-0.000017
H	-2.003551	-3.160186	0.000085
H	-4.401206	-3.793976	0.000017
H	-6.156851	-2.065813	-0.000032
H	-2.080848	4.603923	-0.000069
H	0.246053	3.839106	-0.000041
H	-4.010877	3.097912	-0.000037
H	2.657079	1.772125	-0.000050
H	2.918492	-2.537603	-0.000013
H	0.453075	-2.738156	0.000074

Indolo[3,2,1-jk]carbazole-5-carboxylic acid neutral solution species: HF -936.147176 a.u.

C	-4.451389	-0.358749	0.000486
C	-3.105336	0.000955	-0.000091
C	-2.112519	-1.038285	-0.000423
C	-2.458861	-2.382651	-0.000197
C	-3.816839	-2.704538	0.000365
C	-4.799667	-1.709081	0.000703
C	-2.401610	1.290856	-0.000186
C	-1.066590	0.929918	-0.000629

N	-0.847755	-0.420572	-0.000859
C	-1.486140	3.525947	0.000476
C	-0.150557	3.075439	0.000136
C	0.085519	1.694220	-0.000317
C	-2.611604	2.675983	0.000272
C	2.542468	0.769896	-0.000019
C	3.303042	-0.407197	0.000077
C	2.674792	-1.665172	-0.000260
C	1.158102	0.690645	-0.000375
C	0.535689	-0.610344	-0.000617
C	1.288911	-1.779958	-0.000637
C	4.777841	-0.272722	0.000275
O	5.383683	0.775328	-0.000432
O	5.424562	-1.470075	0.001407
H	-5.221017	0.404754	0.000742
H	-1.705168	-3.159928	-0.000470
H	-4.112272	-3.747323	0.000556
H	-5.845609	-1.992435	0.001150
H	-1.659525	4.596116	0.000889
H	0.656164	3.798994	0.000397
H	-3.604969	3.109399	0.000618
H	3.054711	1.724208	0.000209
H	3.285354	-2.558054	-0.000337
H	0.817271	-2.754242	-0.000941
H	6.371876	-1.270475	0.001174

Indolo[3,2,1-jk]carbazole-5-carboxylic acid cation solution species:
HF -935.930277 a.u.

C	-4.437425	-0.375987	0.000134
C	-3.109522	-0.003238	0.000050
C	-2.104570	-1.032485	-0.000041
C	-2.422066	-2.387732	-0.000054
C	-3.776850	-2.733272	0.000037
C	-4.763676	-1.750408	0.000129
C	-2.411217	1.302550	0.000030
C	-1.072697	0.948957	-0.000103
N	-0.852230	-0.399851	-0.000137
C	-1.494679	3.528867	0.000228
C	-0.149838	3.086342	0.000138
C	0.081976	1.712209	-0.000028
C	-2.629241	2.677651	0.000197
C	2.535029	0.774545	-0.000024
C	3.291083	-0.422669	-0.000051
C	2.669279	-1.671664	-0.000108
C	1.161183	0.699198	-0.000050
C	0.539189	-0.597724	-0.000104
C	1.274179	-1.776677	-0.000140
C	4.782604	-0.278856	-0.000020

O	5.343495	0.787612	-0.000054
O	5.415162	-1.465477	-0.000088
H	-5.225660	0.367021	0.000205
H	-1.656653	-3.152718	-0.000129
H	-4.058379	-3.778554	0.000033
H	-5.806576	-2.043120	0.000196
H	-1.670755	4.598154	0.000355
H	0.650702	3.815093	0.000216
H	-3.619945	3.114185	0.000318
H	3.062992	1.720286	0.000017
H	3.275105	-2.567473	-0.000130
H	0.797937	-2.748303	-0.000190
H	6.371124	-1.300356	-0.000122

5-chloroindolo[3,2,1-jk]carbazole neutral solution species: HF -1207.119527 a.u.

C	-4.211247	-0.271797	-0.000354
C	-2.856005	0.052369	-0.000556
C	-1.890128	-1.012971	-0.000256
C	-2.272965	-2.347830	0.000157
C	-3.638928	-2.633263	0.000092
C	-4.595488	-1.612208	-0.000027
C	-2.117406	1.321923	-0.000060
C	-0.791913	0.922961	0.000425
N	-0.611130	-0.429874	0.000512
C	-1.140088	3.531483	-0.000040
C	0.182310	3.044530	0.000358
C	0.381128	1.657266	0.000265
C	-2.288415	2.712045	-0.000072
C	2.818010	0.679247	-0.000045
C	3.527439	-0.517356	-0.000010
C	2.891759	-1.760728	0.000094
C	1.425865	0.626610	0.000054
C	0.773339	-0.655116	0.000008
C	1.499473	-1.838675	0.000117
CL	5.289217	-0.464461	-0.000246
H	-4.960334	0.511969	-0.000566
H	-1.540337	-3.145127	0.000224
H	-3.961967	-3.667887	0.000294
H	-5.648559	-1.867761	0.000156
H	-1.284311	4.605977	-0.000219
H	1.007899	3.746703	0.000248
H	-3.269401	3.172952	-0.000571
H	3.342725	1.626121	-0.000250
H	3.485940	-2.665182	0.000306
H	1.009134	-2.803744	0.000091

5-chloroindolo[3,2,1-jk]carbazole cation solution species: HF -1206.907263 a.u.

C	4.182384	-0.297265	0.000228

C	2.844707	0.041709	0.000003
C	1.865587	-1.014159	-0.000179
C	2.219012	-2.361589	-0.000167
C	3.579768	-2.670596	0.000074
C	4.542415	-1.660265	0.000264
C	2.116221	1.332053	-0.000141
C	0.793170	0.952683	-0.000372
N	0.597844	-0.416868	-0.000368
C	1.160627	3.543015	0.000184
C	-0.171802	3.069121	0.000050
C	-0.371524	1.687267	-0.000212
C	2.305823	2.717421	0.000112
C	-2.800862	0.696186	0.000034
C	-3.516291	-0.523432	0.000082
C	-2.872543	-1.771144	-0.000018
C	-1.426280	0.648432	-0.000120
C	-0.768232	-0.641026	-0.000211
C	-1.488046	-1.840306	-0.000175
CL	-5.239545	-0.466964	0.000268
H	4.951010	0.465859	0.000352
H	1.474050	-3.146499	-0.000309
H	3.889887	-3.707786	0.000111
H	5.592317	-1.927065	0.000435
H	1.312530	4.615777	0.000396
H	-0.989422	3.778830	0.000215
H	3.288881	3.171052	0.000326
H	-3.340059	1.634683	0.000105
H	-3.465838	-2.675724	0.000025
H	-0.990804	-2.801297	-0.000259

5-cyanoindolo[3,2,1-jk]carbazole neutral solution species: HF -839.771363 a.u.

C	4.086755	-0.243163	-0.001159
C	2.728346	0.066985	-0.001911
C	1.774833	-1.008119	-0.001041
C	2.169693	-2.338746	0.000805
C	3.538531	-2.610572	0.001421
C	4.484059	-1.579727	0.000497
C	1.977531	1.330205	-0.001647
C	0.656310	0.920191	-0.000674
N	0.487325	-0.436929	0.000469
C	0.979802	3.530510	0.001525
C	-0.337644	3.032157	0.001568
C	-0.522531	1.642576	-0.000678
C	2.135771	2.721567	0.000028
C	-2.943948	0.633567	-0.000443
C	-3.659591	-0.573886	-0.000227
C	-2.986113	-1.810990	0.000202
C	-1.556541	0.601359	0.000090
C	-0.888232	-0.676297	-0.000032

C	-1.598141	-1.872552	0.000292
C	-5.089008	-0.550022	-0.000060
N	-6.245168	-0.530651	-0.000186
H	4.827804	0.548041	-0.002045
H	1.445401	-3.143556	0.001108
H	3.872051	-3.641739	0.002751
H	5.539620	-1.824627	0.001386
H	1.114425	4.606160	0.002934
H	-1.169975	3.726088	0.002412
H	3.112435	3.191323	-0.000497
H	-3.478375	1.575633	-0.001795
H	-3.565878	-2.725405	0.000549
H	-1.091896	-2.829112	-0.000121

5-cyanoindolo[3,2,1-jk]carbazole cation solution species: HF -839.551823 a.u.

C	-4.068859	-0.264510	-0.000723
C	-2.729312	0.061534	-0.000626
C	-1.760905	-1.003677	-0.000283
C	-2.126758	-2.348217	0.000413
C	-3.491692	-2.645639	0.000277
C	-4.443125	-1.627304	-0.000308
C	-1.985872	1.343076	-0.000544
C	-0.663509	0.944869	-0.000164
N	-0.488487	-0.417735	0.000255
C	-0.997355	3.538190	0.000566
C	0.331282	3.048002	0.000543
C	0.513733	1.666016	-0.000125
C	-2.157109	2.727578	0.000017
C	2.931612	0.644120	-0.000088
C	3.643704	-0.584403	-0.000026
C	2.973220	-1.818360	0.000257
C	1.556474	0.614098	0.000201
C	0.887403	-0.662894	0.000133
C	1.582556	-1.869810	0.000388
C	5.069000	-0.556545	-0.000256
N	6.224553	-0.527525	-0.000318
H	-4.830875	0.505323	-0.001062
H	-1.389144	-3.140077	0.000885
H	-3.810605	-3.680077	0.000679
H	-5.495805	-1.882791	-0.000407
H	-1.135369	4.612931	0.001069
H	1.156721	3.748509	0.000834
H	-3.133024	3.196237	-0.000142
H	3.478493	1.578512	-0.000307
H	3.548397	-2.734908	0.000388
H	1.071830	-2.823579	0.000597

5-hydroxyindolo[3,2,1-jk]carbazole neutral solution species:

HF -822.751474 a.u.

C	-3.885842	-0.137543	0.000004
C	-2.518195	0.129748	0.000087
C	-1.596483	-0.975547	0.000051
C	-2.036658	-2.293365	0.000049
C	-3.413288	-2.520801	0.000024
C	-4.326565	-1.460514	-0.000022
C	-1.725907	1.365802	-0.000060
C	-0.418490	0.908947	-0.000105
N	-0.296253	-0.448190	-0.000083
C	-0.654371	3.531189	0.000042
C	0.646021	2.986902	-0.000005
C	0.786145	1.592684	-0.000028
C	-1.836771	2.762151	0.000016
C	3.181909	0.513603	-0.000012
C	3.857174	-0.706480	0.000027
C	3.157000	-1.919333	0.000016
C	1.786923	0.519364	-0.000013
C	1.083393	-0.730941	-0.000006
C	1.764811	-1.941076	-0.000047
O	5.228065	-0.787723	-0.000010
H	-4.601324	0.677166	-0.000014
H	-1.338122	-3.120812	0.000084
H	-3.779497	-3.541041	0.000022
H	-5.389489	-1.671553	-0.000099
H	-0.751980	4.611013	0.000110
H	1.500573	3.653912	0.000046
H	-2.797023	3.265002	0.000094
H	3.735565	1.447767	-0.000075
H	3.723075	-2.842442	0.000035
H	1.235773	-2.885722	-0.000066
H	5.606844	0.097081	0.000415

5-hydroxyindolo[3,2,1-jk]carbazole cation solution species:
HF -822.552578 a.u.

C	-3.856546	-0.158960	0.000016
C	-2.502061	0.118631	-0.000022
C	-1.572990	-0.979922	-0.000048
C	-1.988086	-2.308144	-0.000043
C	-3.361078	-2.553323	-0.000003
C	-4.278096	-1.499599	0.000026
C	-1.718794	1.375191	-0.000050
C	-0.415188	0.942057	-0.000088
N	-0.275613	-0.440778	-0.000081
C	-0.672927	3.547730	0.000026
C	0.636169	3.018440	0.000015
C	0.777625	1.627036	-0.000042
C	-1.848716	2.770000	0.000000

C	3.160028	0.536811	0.000038
C	3.830081	-0.712138	0.000065
C	3.120561	-1.939037	0.000042
C	1.785857	0.547813	-0.000009
C	1.068276	-0.718758	-0.000030
C	1.745008	-1.950711	-0.000007
O	5.161045	-0.807822	0.000106
H	-4.587451	0.640413	0.000033
H	-1.280750	-3.127296	-0.000066
H	-3.718481	-3.575301	0.000005
H	-5.338802	-1.719389	0.000053
H	-0.780458	4.625773	0.000070
H	1.483508	3.692592	0.000057
H	-2.812851	3.262847	0.000035
H	3.730742	1.459235	0.000053
H	3.692096	-2.858021	0.000064
H	1.205265	-2.888422	-0.000022
H	5.593390	0.056888	0.000134

5-methoxyindolo[3,2,1-jk]carbazole neutral solution species:
HF -862.052520 a.u.

C	4.203569	-0.482513	0.000105
C	2.872401	-0.070411	-0.000111
C	1.837071	-1.070510	-0.000165
C	2.134366	-2.428219	0.000039
C	3.478628	-2.801482	0.000252
C	4.500323	-1.844942	0.000275
C	2.218061	1.243123	-0.000171
C	0.869131	0.930441	-0.000330
N	0.601856	-0.406945	-0.000362
C	1.388108	3.512051	0.000150
C	0.035934	3.111123	0.000125
C	-0.253496	1.740904	-0.000128
C	2.479629	2.619859	0.000043
C	-2.747346	0.929575	0.000057
C	-3.561583	-0.209203	0.000043
C	-2.997225	-1.491662	-0.000120
C	-1.367339	0.782498	-0.000046
C	-0.800539	-0.540503	-0.000158
C	-1.608338	-1.663533	-0.000244
O	-4.908998	0.035726	0.000201
C	-5.802410	-1.067320	0.000198
H	5.002060	0.251029	0.000153
H	1.351336	-3.176161	0.000044
H	3.733745	-3.855061	0.000409
H	5.534530	-2.168694	0.000432
H	1.601778	4.575023	0.000314
H	-0.742473	3.865423	0.000317

H	3.488951	3.015183	0.000165
H	-3.215254	1.906561	0.000123
H	-3.627099	-2.370349	-0.000162
H	-1.188818	-2.661693	-0.000412
H	-5.674727	-1.687691	0.894462
H	-5.675149	-1.687354	-0.894347
H	-6.803558	-0.639071	0.000540

5-methoxyindolo[3,2,1-jk]carbazole cation solution species:
HF -861.853078 a.u.

C	4.173343	-0.511570	0.000080
C	2.856215	-0.087800	0.000006
C	1.813461	-1.077455	-0.000047
C	2.081290	-2.442109	-0.000037
C	3.419753	-2.835579	0.000040
C	4.446608	-1.888707	0.000097
C	2.216316	1.246030	-0.000030
C	0.871049	0.958947	-0.000119
N	0.580958	-0.397391	-0.000125
C	1.415529	3.520412	0.000093
C	0.056760	3.140128	0.000042
C	-0.238595	1.772739	-0.000063
C	2.499203	2.616300	0.000074
C	-2.722744	0.951212	-0.000012
C	-3.540227	-0.216962	0.000000
C	-2.969330	-1.513276	-0.000031
C	-1.361259	0.812741	-0.000049
C	-0.787311	-0.524955	-0.000074
C	-1.596345	-1.670208	-0.000070
O	-4.845173	0.025955	0.000037
C	-5.804626	-1.050451	0.000068
H	4.986104	0.204480	0.000122
H	1.289082	-3.179539	-0.000086
H	3.663116	-3.890603	0.000053
H	5.476836	-2.223387	0.000154
H	1.642594	4.579800	0.000173
H	-0.711653	3.902955	0.000096
H	3.511870	2.999800	0.000152
H	-3.211290	1.917512	0.000010
H	-3.602780	-2.388601	-0.000028
H	-1.163696	-2.662130	-0.000098
H	-5.692101	-1.659558	0.899120
H	-5.692201	-1.659518	-0.899025
H	-6.775742	-0.563747	0.000133

5-methylindolo[3,2,1-jk]carbazole neutral solution species: HF -786.823424 a.u.

C	3.901635	-0.161364	0.002426
C	2.535811	0.115391	0.001531

C	1.606994	-0.983616	0.000729
C	2.037872	-2.304322	0.000903
C	3.412940	-2.541496	0.001812
C	4.333237	-1.487379	0.002558
C	1.752274	1.357329	0.000933
C	0.442031	0.910607	-0.000260
N	0.309903	-0.447326	-0.000248
C	0.696622	3.529806	-0.000426
C	-0.607965	2.994267	-0.001659
C	-0.758056	1.601307	-0.001691
C	1.873586	2.753314	0.000833
C	-3.160443	0.529032	-0.006285
C	-3.866272	-0.677497	-0.007662
C	-3.149966	-1.886105	-0.009562
C	-1.766451	0.533327	-0.001845
C	-1.069136	-0.721188	-0.000841
C	-1.756482	-1.927436	-0.005707
C	-5.377210	-0.689653	0.016308
H	4.622716	0.648385	0.003003
H	1.333317	-3.126627	0.000360
H	3.772187	-3.564213	0.001905
H	5.394744	-1.705598	0.003231
H	0.801370	4.609014	-0.000465
H	-1.458143	3.666737	-0.002533
H	2.837418	3.249258	0.001665
H	-3.702499	1.469184	-0.010230
H	-3.698950	-2.822158	-0.015899
H	-1.233082	-2.875470	-0.009990
H	-5.781551	-1.443546	-0.664567
H	-5.786869	0.279722	-0.275520
H	-5.756108	-0.919361	1.018205

5-methylindolo[3,2,1-jk]carbazole cation solution species: HF -786.616461 a.u.

C	-3.877599	-0.180649	0.000037
C	-2.527718	0.108540	0.000010
C	-1.588892	-0.983183	-0.000006
C	-1.992533	-2.316309	-0.000004
C	-3.363625	-2.574196	0.000020
C	-4.288132	-1.528221	0.000040
C	-1.751273	1.370343	0.000004
C	-0.443124	0.941691	-0.000005
N	-0.299694	-0.434568	-0.000016
C	-0.712506	3.542854	-0.000011
C	0.600745	3.018776	-0.000017
C	0.749587	1.630281	-0.000013
C	-1.888664	2.761644	-0.000003
C	3.139444	0.538498	-0.000034
C	3.842530	-0.698282	-0.000045

C	3.122178	-1.906747	-0.000082
C	1.765473	0.551603	-0.000001
C	1.057713	-0.710224	-0.000017
C	1.733815	-1.933803	-0.000072
C	5.341324	-0.694322	0.000121
H	-4.616422	0.611430	0.000052
H	-1.276856	-3.128100	-0.000016
H	-3.712411	-3.599043	0.000023
H	-5.347162	-1.756130	0.000058
H	-0.823763	4.620653	-0.000009
H	1.444621	3.697129	-0.000011
H	-2.853916	3.252061	0.000004
H	3.699706	1.466824	-0.000047
H	3.667414	-2.842590	-0.000123
H	1.200522	-2.875571	-0.000097
H	5.751484	-1.703654	-0.001179
H	5.725933	-0.166652	0.879456
H	5.726258	-0.164146	-0.877530

5-nitroindolo[3,2,1-jk]carbazole neutral solution species: HF -952.069185 a.u.

C	-4.430312	-0.327765	0.000786
C	-3.081065	0.019166	0.000030
C	-2.098944	-1.029097	-0.000601
C	-2.456293	-2.370003	-0.000478
C	-3.817270	-2.679460	0.000358
C	-4.790520	-1.674981	0.000962
C	-2.365692	1.303336	-0.000279
C	-1.033927	0.931054	-0.001248
N	-0.826774	-0.421955	-0.001548
C	-1.429877	3.530515	0.001013
C	-0.098943	3.069458	0.000455
C	0.124102	1.685460	-0.000671
C	-2.563023	2.689642	0.000851
C	2.571520	0.743844	-0.000325
C	3.292032	-0.449565	-0.000161
C	2.678721	-1.706389	-0.000361
C	1.186070	0.672700	-0.000643
C	0.551191	-0.624371	-0.000982
C	1.292988	-1.803039	-0.000915
N	4.762126	-0.383091	0.000648
O	5.285356	0.726748	-0.002135
O	5.383963	-1.440586	0.003915
H	-5.192940	0.442588	0.001249
H	-1.710171	-3.154511	-0.001002
H	-4.122223	-3.719385	0.000513
H	-5.838941	-1.948734	0.001573
H	-1.594521	4.601936	0.001855
H	0.713994	3.785864	0.000991

H	-3.552364	3.131965	0.001700
H	3.099504	1.687510	-0.000191
H	3.298693	-2.591703	-0.000138
H	0.812404	-2.772527	-0.001251

5-nitroindolo[3,2,1-jk]carbazole cation solution species: HF -951.846420 a.u.

C	4.420969	-0.346649	-0.000423
C	3.090262	0.015251	-0.000188
C	2.094337	-1.021624	0.000111
C	2.422415	-2.374009	0.000193
C	3.781475	-2.709666	-0.000060
C	4.759360	-1.720333	-0.000361
C	2.381309	1.314402	-0.000176
C	1.043184	0.947570	0.000211
N	0.836599	-0.397800	0.000360
C	1.443010	3.531274	-0.000722
C	0.099677	3.077105	-0.000446
C	-0.119712	1.702965	0.000025
C	2.586253	2.690453	-0.000647
C	-2.566822	0.752769	0.000147
C	-3.281382	-0.456358	0.000247
C	-2.677320	-1.704005	0.000399
C	-1.189623	0.681837	0.000155
C	-0.559324	-0.609312	0.000324
C	-1.280273	-1.794069	0.000477
N	-4.770931	-0.387347	0.000250
O	-5.269477	0.726921	0.001387
O	-5.376129	-1.444992	-0.001079
H	5.203583	0.402345	-0.000653
H	1.663760	-3.145759	0.000438
H	4.070210	-3.752960	-0.000016
H	5.804789	-2.003659	-0.000548
H	1.609212	4.602168	-0.001082
H	-0.706027	3.800141	-0.000646
H	3.572444	3.137028	-0.000995
H	-3.107339	1.689950	0.000098
H	-3.294538	-2.592015	0.000430
H	-0.797694	-2.762260	0.000643

Chapter 6:

5-azaindolo[3,2,1-jk]carbazole neutral solution species: HF -763.541126 a.u.

C	3.540641	0.174656	0.000290
C	2.151512	0.296641	-0.000190
C	1.350824	-0.896992	-0.000370
C	1.919292	-2.163804	-0.000034
C	3.313965	-2.247932	0.000412
C	4.113709	-1.098210	0.000568

C	1.238348	1.449377	-0.000344
C	-0.016787	0.867322	-0.000681
N	-0.002961	-0.501672	-0.000781
C	-0.041720	3.499655	0.000233
C	-1.283762	2.831117	0.000099
C	-1.281493	1.428182	-0.000407
C	1.212932	2.850809	0.000046
C	-3.542102	0.067868	0.000392
N	-4.107611	-1.148047	0.000926
C	-3.303116	-2.227021	0.000179
C	-2.163677	0.254286	-0.000040
C	-1.332414	-0.919086	-0.000355
C	-1.909891	-2.182680	-0.000561
H	4.169997	1.061291	0.000499
H	1.310503	-3.062791	-0.000116
H	3.783607	-3.228104	0.000674
H	5.195698	-1.199301	0.000944
H	-2.203900	3.409501	0.000549
H	2.122081	3.446629	0.000387
H	-4.218807	0.921641	0.000812
H	-3.804165	-3.193502	0.000260
H	-1.328440	-3.099117	-0.001115
H	-0.050115	4.586645	0.000671

5-azaindolo[3,2,1-jk]carbazole cation solution species: HF -763.320753 a.u.

C	-3.541109	0.174729	0.000293
C	-2.164132	0.303473	0.000130
C	-1.359028	-0.882220	-0.000099
C	-1.903475	-2.155083	-0.000423
C	-3.306850	-2.255317	-0.000253
C	-4.106573	-1.120179	0.000148
C	-1.252936	1.461531	0.000047
C	0.014795	0.871466	-0.000098
N	-0.006305	-0.470942	-0.000104
C	0.047112	3.487153	0.000023
C	1.302440	2.819613	-0.000173
C	1.295278	1.431866	-0.000162
C	-1.225394	2.847751	0.000180
C	3.545209	0.063293	-0.000065
N	4.098799	-1.168769	0.000056
C	3.298120	-2.232339	0.000245
C	2.174831	0.252526	-0.000193
C	1.345158	-0.911488	-0.000122
C	1.887949	-2.174865	0.000425
H	-4.184262	1.051748	0.000520
H	-1.287437	-3.049637	-0.000681
H	-3.763632	-3.241169	-0.000415
H	-5.188485	-1.223626	0.000311

H	2.217998	3.405012	-0.000246
H	-2.126117	3.455932	0.000344
H	4.232466	0.907821	-0.000126
H	3.784282	-3.206601	0.000189
H	1.300682	-3.088162	0.000964
H	0.058684	4.575200	0.000056

7-azaindolo[3,2,1-jk]carbazole neutral solution species: HF -763.545174 a.u.

C	-3.527098	0.160002	0.000417
C	-2.139923	0.296804	-0.000396
C	-1.332299	-0.890735	-0.000662
C	-1.885547	-2.163207	-0.000294
C	-3.277479	-2.259216	0.000442
C	-4.087060	-1.117061	0.000800
C	-1.232164	1.453623	-0.000227
C	0.026574	0.876783	-0.000496
N	0.015579	-0.488494	-0.000903
C	0.039354	3.508782	0.000135
C	1.282736	2.846186	0.000155
C	1.290395	1.444255	-0.000033
C	-1.210451	2.853853	-0.000025
C	3.551581	0.069195	0.000622
C	4.016120	-1.249134	0.000704
C	3.105954	-2.307216	0.000198
C	2.179283	0.278831	-0.000169
C	1.350617	-0.903686	-0.000517
N	1.771713	-2.153314	-0.000408
H	-4.164351	1.037168	0.000663
H	-1.253077	-3.041604	-0.000575
H	-3.739074	-3.239971	0.000790
H	-5.165137	-1.228099	0.001457
H	0.042904	4.592953	0.000300
H	2.196505	3.429032	0.000435
H	-2.118944	3.445056	0.000055
H	4.246111	0.901890	0.000921
H	3.461955	-3.332588	0.000044
H	5.078504	-1.459532	0.001171

7-azaindolo[3,2,1-jk]carbazole cation solution species: HF -763.326483 a.u.

C	-3.512112	0.150408	0.000069
C	-2.144974	0.308844	0.000009
C	-1.321234	-0.873560	-0.000022
C	-1.845060	-2.166852	0.000004
C	-3.238448	-2.291227	0.000068
C	-4.052830	-1.162619	0.000098
C	-1.236519	1.482183	-0.000056
C	0.022428	0.908152	-0.000107
N	0.004622	-0.458372	-0.000081

C	0.040185	3.521044	0.000000
C	1.294400	2.854180	-0.000018
C	1.291710	1.462949	-0.000074
C	-1.218648	2.877795	-0.000008
C	3.546277	0.050408	0.000035
C	3.983135	-1.283766	0.000062
C	3.059976	-2.335429	0.000014
C	2.181021	0.275839	-0.000021
C	1.350323	-0.891320	-0.000041
N	1.731281	-2.148585	-0.000023
H	-4.177274	1.005472	0.000088
H	-1.191641	-3.030090	-0.000015
H	-3.684893	-3.277336	0.000094
H	-5.129476	-1.282587	0.000142
H	0.050644	4.604635	0.000045
H	2.205102	3.439607	0.000025
H	-2.121248	3.475553	0.000043
H	4.259430	0.865812	0.000060
H	3.398115	-3.365096	0.000071
H	5.042142	-1.509448	0.000117

7,9-diazaindolo[3,2,1-jk]carbazole neutral solution species: HF -779.591139 a.u.

C	3.536414	0.104334	0.000390
C	2.159177	0.285864	0.000023
C	1.348059	-0.905567	-0.000212
N	1.794036	-2.147179	-0.000287
C	3.134526	-2.279383	-0.000012
C	4.025113	-1.205331	0.000374
C	1.258554	1.441788	-0.000127
C	-0.000009	0.864414	-0.000481
N	-0.000079	-0.505461	-0.000615
C	0.000336	3.503355	0.000258
C	-1.246876	2.843863	-0.000135
C	-1.258459	1.441884	-0.000320
C	1.247362	2.843626	0.000300
C	-3.536571	0.104539	0.000189
C	-4.025144	-1.205117	0.000487
C	-3.134696	-2.279256	0.000470
C	-2.159246	0.286086	-0.000427
C	-1.348241	-0.905407	-0.000568
N	-1.794188	-2.147069	0.000130
H	4.216435	0.953237	0.000603
H	3.510616	-3.300573	-0.000100
H	5.094058	-1.397507	0.000608
H	-2.162526	3.429523	-0.000035
H	2.163178	3.428990	0.000657
H	-4.216607	0.953395	0.000728
H	-3.510906	-3.300376	0.000877

H	-0.000263	4.590345	0.000552
H	-5.094158	-1.397207	0.000255

7,9-diazaindolo[3,2,1-jk]carbazole cation solution species: HF -779.363624 a.u.

C	3.555196	0.099993	0.000220
C	2.182262	0.286974	0.000060
C	1.373555	-0.890332	-0.000071
N	1.784541	-2.129069	-0.000163
C	3.130439	-2.283739	-0.000058
C	4.027689	-1.221688	0.000187
C	1.284554	1.446961	-0.000041
C	0.000009	0.860386	-0.000340
N	0.000004	-0.466326	-0.000345
C	0.000080	3.480973	0.000122
C	-1.271458	2.826731	-0.000058
C	-1.284544	1.447051	-0.000259
C	1.271579	2.826587	0.000194
C	-3.555161	0.100034	0.000088
C	-4.027751	-1.221628	0.000264
C	-3.130544	-2.283685	0.000327
C	-2.182273	0.287063	-0.000168
C	-1.373615	-0.890291	-0.000248
N	-1.784619	-2.129007	0.000006
H	4.244757	0.941420	0.000353
H	3.488448	-3.310731	-0.000059
H	5.095269	-1.422856	0.000331
H	-2.176616	3.428753	0.000029
H	2.176964	3.428194	0.000450
H	-4.244765	0.941452	0.000100
H	-3.488530	-3.310685	0.000361
H	0.000235	4.569613	0.000276
H	-5.095342	-1.422672	0.000375

Cyanoacetic acid aqueous species: HF -321.442722 a.u.

C	-0.864131	0.147351	0.000057
O	-0.783926	1.342087	0.000081
O	-2.030358	-0.536833	-0.000166
C	0.297074	-0.840826	0.000143
C	1.607246	-0.204837	0.000015
N	2.660821	0.259576	-0.000161
H	0.199457	-1.490217	-0.875234
H	0.199712	-1.489781	0.875884
H	-2.751788	0.110804	-0.000128

Cyanoacetic acid deprotonated aqueous species: HF -320.986816 a.u.

C	-1.035138	0.136451	-0.001449
O	-0.813261	1.354019	0.045170
O	-2.092608	-0.518410	-0.083046

C	0.249609	-0.839765	0.082246
C	1.562949	-0.225572	-0.002441
N	2.609375	0.263751	-0.069790
H	0.147987	-1.583617	-0.711962
H	0.168816	-1.374194	1.033365

Chloroacetic acid aqueous species: HF -688.795738 a.u.

C	-0.948880	0.131141	0.000033
O	-0.945859	1.328309	0.000135
O	-2.077477	-0.621454	-0.000288
C	0.251709	-0.798935	0.000332
CL	1.810757	0.072707	-0.000144
H	-2.832873	-0.014140	-0.000003
H	0.209833	-1.435558	-0.882898
H	0.209884	-1.434401	0.884390

Chloroacetic acid deprotonated aqueous species: HF -688.338255 a.u.

C	-1.126144	0.112332	0.000000
O	-1.026394	1.346231	0.000031
O	-2.133541	-0.638180	-0.000061
C	0.158334	-0.782556	0.000078
CL	1.809039	0.069369	-0.000031
H	0.166318	-1.411264	-0.887780
H	0.166352	-1.411067	0.888074

Formic acid aqueous species: HF -189.844397 a.u.

C	-0.136550	0.398849	-0.000030
O	-1.135210	-0.264719	0.000008
O	1.117998	-0.089141	0.000003
H	-0.104656	1.496017	0.000076
H	1.061650	-1.058234	0.000021

Formic acid deprotonated aqueous species: HF -189.383009 a.u.

C	-0.000110	0.315231	-0.000089
O	-1.137251	-0.209119	0.000023
O	1.137380	-0.209012	0.000023
H	-0.000374	1.453662	0.000169

Acetic acid aqueous species: HF -229.179660 a.u.

C	1.393584	-0.124944	-0.000326
C	-0.089078	0.128004	-0.000712
O	-0.626802	1.206386	0.000097
O	-0.793073	-1.034416	-0.000142
H	1.925245	0.823363	-0.026323
H	1.667759	-0.734147	-0.864460
H	1.671890	-0.684854	0.895615
H	-1.732930	-0.798484	0.001758

Acetic acid deprotonated aqueous species: HF -228.712172 a.u.

C	-1.352226	-0.050109	-0.000123
C	0.211200	0.001242	-0.000211
O	0.803803	-1.105795	0.000038
O	0.701512	1.157975	0.000037
H	-1.724892	-1.078218	-0.007809
H	-1.736498	0.484289	-0.876688
H	-1.734976	0.469695	0.885901

Pivalic acid aqueous species: HF -347.150520 a.u.

C	0.943697	0.193060	-0.000176
O	1.518828	1.253175	-0.000169
O	1.623875	-0.984901	-0.000111
C	-0.571464	-0.012358	-0.000042
C	-1.262655	1.358707	-0.001667
C	-0.966287	-0.810110	-1.262985
C	-0.966062	-0.806940	1.265021
H	2.567098	-0.763821	-0.000003
H	-0.988418	1.941147	-0.883476
H	-0.988116	1.943386	0.878554
H	-2.347492	1.221957	-0.001324
H	-2.050857	-0.943189	1.284765
H	-0.678486	-0.271747	2.174364
H	-0.494260	-1.790628	1.280994
H	-0.678594	-0.277390	-2.173746
H	-2.051122	-0.946097	-1.282356
H	-0.494752	-1.793958	-1.276439

Pivalic acid deprotonated aqueous species: HF -346.679935 a.u.

C	-1.070189	0.030772	-0.000098
O	-1.617487	1.157954	0.000041
O	-1.607209	-1.103791	-0.000121
C	0.523744	0.009150	-0.000140
C	1.111329	1.426709	-0.000698
C	0.997388	-0.747427	1.254111
C	0.997565	-0.748626	-1.253185
H	0.776922	1.986238	0.876401
H	0.777294	1.985420	-0.878472
H	2.211356	1.393931	-0.000485
H	2.093387	-0.844703	-1.270991
H	0.691176	-0.223190	-2.164836
H	0.552340	-1.745657	-1.275522
H	0.690489	-0.221101	2.165062
H	2.093217	-0.843181	1.272334
H	0.552371	-1.744530	1.277210

2-bromoindolo[3,2,1-jk]carbazole neutral solution species: HF -3321.038922 a.u.

C	1.005692	3.550727	0.000069

C	0.872051	2.162678	-0.000185
C	2.057455	1.346885	-0.000350
C	3.329496	1.906476	-0.000389
C	3.425215	3.299985	-0.000152
C	2.283376	4.111888	0.000071
C	-0.285909	1.259133	-0.000170
C	0.288104	-0.000045	-0.000676
N	1.650298	0.000052	-0.000732
C	-2.325934	-0.000147	0.000210
C	-1.687280	-1.255595	-0.000256
C	-0.285765	-1.259285	-0.000550
C	-1.687359	1.255351	0.000390
C	1.006292	-3.550697	-0.000266
C	2.284088	-4.111609	0.000011
C	3.425788	-3.299548	0.000111
C	0.872332	-2.162680	-0.000415
C	2.057635	-1.346707	-0.000413
C	3.329779	-1.906047	-0.000108
BR	-4.259922	-0.000175	0.000657
H	0.124570	4.187856	0.000289
H	4.223548	1.290828	-0.000616
H	4.409764	3.760539	-0.000163
H	2.395053	5.192727	0.000289
H	-2.276740	-2.167393	-0.000178
H	-2.276636	2.167240	0.000829
H	0.125334	-4.188058	-0.000338
H	4.410404	-3.759946	0.000348
H	4.223676	-1.290177	-0.000070
H	2.395878	-5.192437	0.000140

2-bromoindolo[3,2,1-jk]carbazole cation solution species: HF -3320.826463 a.u.

C	-1.008259	3.537497	-0.000472
C	-0.864557	2.164970	-0.000077
C	-2.042555	1.341824	0.000390
C	-3.324913	1.875515	0.000716
C	-3.439598	3.271842	0.000418
C	-2.309285	4.085392	-0.000303
C	0.306832	1.262240	0.000168
C	-0.262548	-0.000041	0.000392
N	-1.621552	0.000098	0.000389
C	2.340834	-0.000176	-0.000042
C	1.696807	-1.264952	0.000035
C	0.306621	-1.262419	0.000289
C	1.696954	1.264645	-0.000072
C	-1.009007	-3.537383	0.000237
C	-2.310099	-4.085073	0.000064
C	-3.440273	-3.271344	-0.000162
C	-0.865023	-2.164909	0.000250

C	-2.042890	-1.341549	0.000134
C	-3.325392	-1.875016	-0.000131
BR	4.244794	-0.000237	-0.000382
H	-0.139612	4.191688	-0.000835
H	-4.211662	1.248755	0.001094
H	-4.428908	3.720959	0.000571
H	-2.426651	5.166067	-0.000569
H	2.288958	-2.175552	-0.000037
H	2.288832	2.175384	-0.000334
H	-0.140475	-4.191754	0.000327
H	-4.429642	-3.720326	-0.000334
H	-4.212108	-1.248250	-0.000287
H	-2.427587	-5.165729	0.000059

2,5-dibromoindolo[3,2,1-jk]carbazole neutral solution species:
HF -5894.580629 a.u.

C	3.582800	2.951712	0.000071
C	2.482243	2.095391	0.000285
C	1.159318	2.659837	0.000395
C	0.949148	4.032886	0.000174
C	2.074552	4.860417	-0.000034
C	3.371572	4.331097	-0.000064
C	2.339765	0.633210	0.000301
C	0.968966	0.442874	0.000641
N	0.239133	1.593343	0.000723
C	2.369142	-1.765315	-0.000203
C	0.967918	-1.898938	-0.000111
C	0.214768	-0.716688	0.000318
C	3.086213	-0.551757	-0.000092
C	-2.405746	-0.860542	0.000283
C	-3.549277	-0.068241	0.000140
C	-3.499381	1.328163	0.000205
C	-1.166711	-0.221337	0.000404
C	-1.112512	1.216496	0.000367
C	-2.268614	1.986668	0.000365
BR	-5.273080	-0.930168	-0.000250
BR	3.406781	-3.396376	-0.000485
H	4.592932	2.549388	-0.000020
H	-0.049957	4.457633	0.000174
H	1.936185	5.938520	-0.000191
H	4.224219	5.004627	-0.000237
H	0.513221	-2.884806	-0.000324
H	4.171999	-0.560744	-0.000294
H	-2.473776	-1.944636	0.000179
H	-4.416972	1.908285	0.000147
H	-2.236339	3.071763	0.000568

2,5-dibromoindolo[3,2,1-jk]carbazole cation solution species:

HF -5894.366491 a.u.

C	3.502523	3.003046	-0.000141
C	2.437470	2.125949	-0.000860
C	1.099910	2.656206	-0.000993
C	0.838165	4.022417	-0.000430
C	1.938062	4.886104	0.000209
C	3.241263	4.389805	0.000374
C	2.331677	0.649672	-0.001185
C	0.970656	0.426962	-0.001649
N	0.213127	1.569473	-0.001348
C	2.408541	-1.743604	-0.000582
C	1.000649	-1.903956	-0.000801
C	0.236227	-0.740158	-0.001151
C	3.103659	-0.510992	-0.000538
C	-2.380460	-0.901340	0.000125
C	-3.546430	-0.106370	0.000469
C	-3.508700	1.290340	0.000115
C	-1.162995	-0.258259	-0.000661
C	-1.124485	1.183352	-0.000871
C	-2.284752	1.955009	-0.000530
BR	-5.230358	-0.982374	0.001473
BR	3.461369	-3.336211	0.000345
H	4.527510	2.640000	-0.000004
H	-0.174024	4.416075	-0.000539
H	1.769251	5.959392	0.000536
H	4.077815	5.084037	0.000860
H	0.565823	-2.899243	-0.000160
H	4.189770	-0.498115	0.000042
H	-2.449431	-1.986132	0.000342
H	-4.431635	1.862409	0.000228
H	-2.258253	3.040645	-0.000881

5,10-dibromoindolo[3,2,1-jk]carbazole neutral solution species:
HF -5894.581365 a.u.

C	-3.547470	0.620193	0.000050
C	-2.158892	0.747318	0.000113
C	-1.343742	-0.438005	0.000187
C	-1.904856	-1.708410	-0.000024
C	-3.296894	-1.814324	-0.000112
C	-4.087319	-0.662398	-0.000040
C	-1.259905	1.908219	0.000113
C	-0.000001	1.334556	0.000287
N	0.000002	-0.030627	0.000414
C	-0.000004	3.969230	-0.000363
C	1.248252	3.310208	-0.000307
C	1.259904	1.908220	0.000048
C	-1.248256	3.310208	-0.000199
C	3.547473	0.620196	-0.000033

C	4.087318	-0.662397	0.000110
C	3.296893	-1.814322	0.000460
C	2.158895	0.747321	0.000101
C	1.343747	-0.437999	0.000369
C	1.904853	-1.708407	0.000634
BR	6.004673	-0.860053	-0.000217
BR	-6.004672	-0.860052	-0.000091
H	-4.187326	1.497934	0.000051
H	-1.294944	-2.606462	-0.000032
H	-3.759678	-2.796221	-0.000228
H	2.162983	3.897444	-0.000540
H	-2.162990	3.897440	-0.000338
H	4.187331	1.497936	-0.000273
H	3.759678	-2.796218	0.000591
H	1.294941	-2.606458	0.000895
H	-0.000004	5.056233	-0.000603

5,10-dibromoindolo[3,2,1-jk]carbazole cation solution species:
HF -5894.367818 a.u.

C	-3.523416	0.625853	-0.000229
C	-2.152663	0.763022	-0.000138
C	-1.326065	-0.421493	-0.000039
C	-1.869996	-1.706710	-0.000343
C	-3.254961	-1.826896	-0.000399
C	-4.056709	-0.679286	-0.000238
C	-1.254651	1.938675	0.000013
C	0.000011	1.375673	0.000135
N	-0.000006	-0.009813	0.000217
C	-0.000028	3.993498	-0.000276
C	1.251354	3.336845	-0.000340
C	1.254679	1.938661	-0.000069
C	-1.251374	3.336804	-0.000177
C	3.523380	0.625740	-0.000546
C	4.056704	-0.679354	-0.000143
C	3.254981	-1.826986	0.000590
C	2.152643	0.762926	-0.000193
C	1.326047	-0.421606	0.000317
C	1.869991	-1.706897	0.000799
BR	5.943380	-0.879863	-0.000170
BR	-5.943366	-0.879926	0.000364
H	-4.179637	1.492168	-0.000021
H	-1.248734	-2.597590	-0.000417
H	-3.710939	-2.812249	-0.000452
H	2.166511	3.922924	-0.000556
H	-2.166672	3.922601	-0.000263
H	4.179599	1.492070	-0.000850
H	3.711042	-2.812299	0.000993
H	1.248877	-2.597846	0.001318

H	-0.000056	5.080695	-0.000405

6-azapyrrolo[3,2,1-jk]carbazole neutral solution species: HF -609.852612 a.u.

C	-2.171617	2.038584	0.000159
C	-0.835592	2.375065	0.000050
C	-2.278678	0.582986	0.000020
C	-0.958203	0.163964	-0.000172
N	-0.077076	1.198011	-0.000184
C	-2.695990	-1.798929	0.000148
C	-1.322735	-2.136423	0.000042
C	-0.386929	-1.096967	-0.000117
C	-3.195869	-0.482867	0.000169
C	2.223434	-1.549698	0.000025
C	3.442008	-0.862119	0.000051
C	3.453321	0.532080	-0.000011
C	1.053192	-0.804914	-0.000069
C	1.208843	0.629953	-0.000155
N	2.344677	1.292965	-0.000120
H	-2.979261	2.754713	0.000294
H	-0.365002	3.344347	0.000093
H	-3.413608	-2.611864	0.000271
H	-1.032208	-3.180528	0.000110
H	-4.267963	-0.322125	0.000324
H	2.198163	-2.633630	0.000069
H	4.395320	1.071057	0.000009
H	4.380238	-1.403087	0.000116

6-azapyrrolo[3,2,1-jk]carbazole cation solution species: HF -609.632635 a.u.

C	-2.161272	2.024199	0.000079
C	-0.753949	2.357945	0.000088
C	-2.281940	0.602881	0.000004
C	-0.964638	0.164210	-0.000124
N	-0.053231	1.217032	-0.000109
C	-2.743485	-1.764993	0.000142
C	-1.372499	-2.112226	0.000065
C	-0.408202	-1.080337	-0.000070
C	-3.231597	-0.449685	0.000136
C	2.207355	-1.570950	0.000023
C	3.434169	-0.892495	0.000009
C	3.472311	0.505729	-0.000059
C	1.052544	-0.805755	-0.000035
C	1.239078	0.612493	-0.000134
N	2.369274	1.271706	-0.000140
H	-2.948198	2.765172	0.000190
H	-0.291690	3.334132	0.000175
H	-3.463926	-2.573693	0.000239
H	-1.093562	-3.158847	0.000127
H	-4.298396	-0.265435	0.000224

H	2.173527	-2.653661	0.000071
H	4.419101	1.032952	-0.000073
H	4.363601	-1.447867	0.000047

8-azapyrrolo[3,2,1-jk]carbazole neutral solution species: HF -609.848420 a.u.

C	-2.209043	2.025139	0.000024
C	-0.878468	2.381107	0.000000
C	-2.295206	0.568552	-0.000106
C	-0.970205	0.168146	-0.000230
N	-0.100125	1.214580	-0.000163
C	-2.677523	-1.817884	0.000107
C	-1.298685	-2.135018	0.000047
C	-0.378913	-1.082022	-0.000128
C	-3.197648	-0.510491	0.000048
C	2.232485	-1.511172	0.000009
N	3.449041	-0.953620	0.000091
C	3.535912	0.382703	0.000113
C	1.059061	-0.764408	-0.000018
C	1.189717	0.665265	-0.000013
C	2.444135	1.253782	0.000060
H	-3.026073	2.730593	0.000106
H	-0.431396	3.361896	0.000097
H	-3.382388	-2.641841	0.000239
H	-0.992619	-3.174453	0.000155
H	-4.271836	-0.365200	0.000152
H	2.200051	-2.597205	0.000018
H	2.585344	2.327347	0.000073
H	4.542800	0.789944	0.000169

8-azapyrrolo[3,2,1-jk]carbazole cation solution species: HF -609.626277 a.u.

C	-2.212936	2.011282	0.000265
C	-0.830472	2.371882	-0.000326
C	-2.296154	0.581636	-0.000020
C	-0.973057	0.174006	-0.000113
N	-0.093606	1.236171	-0.000172
C	-2.698009	-1.811833	0.000018
C	-1.330875	-2.125249	0.000040
C	-0.387317	-1.058049	-0.000048
C	-3.216929	-0.494854	-0.000030
C	2.213444	-1.525173	-0.000109
N	3.442050	-0.970781	0.000146
C	3.554450	0.348748	0.000222
C	1.059870	-0.759309	-0.000073
C	1.215153	0.662603	0.000027
C	2.458582	1.246523	0.000095
H	-3.019625	2.729914	0.000491
H	-0.395265	3.359572	-0.000455
H	-3.405127	-2.632143	0.000091

H	-1.021401	-3.163018	0.000068
H	-4.288864	-0.339542	0.000087
H	2.176154	-2.609728	0.000010
H	2.616228	2.317518	0.000047
H	4.564294	0.746424	0.000157

1-azacycl[2,3,2]azine neutral solution species: HF -456.170755 a.u.

N	1.758020	-1.264263	-0.000315
N	-0.170998	0.013296	0.001137
C	0.430559	-1.216812	0.000273
C	2.394019	-0.064985	-0.000222
C	1.789550	1.206202	0.000020
C	0.393532	1.263069	0.000217
C	-0.665850	-2.143507	-0.000344
C	-1.852337	-1.404951	-0.000155
C	-1.524958	-0.010391	0.000377
C	-1.896841	1.365413	-0.000215
C	-0.729947	2.146270	-0.000275
H	3.480376	-0.120285	-0.000302
H	2.405676	2.099662	-0.000398
H	-0.576178	-3.222022	-0.000402
H	-2.852715	-1.821050	-0.000740
H	-2.909477	1.751169	-0.000909
H	-0.683202	3.227439	-0.001066

1-azacycl[2,3,2]azine cation solution species: HF -455.958580 a.u.

N	1.754864	-1.276732	-0.000079
N	-0.140749	0.014279	0.000855
C	0.437530	-1.196791	0.000284
C	2.404133	-0.084097	-0.000184
C	1.808362	1.198567	-0.000219
C	0.421408	1.237418	0.000284
C	-0.708411	-2.128147	-0.000177
C	-1.878108	-1.385499	-0.000309
C	-1.530060	0.000411	0.000274
C	-1.901087	1.370891	-0.000129
C	-0.738763	2.138846	-0.000174
H	3.490932	-0.150233	-0.000381
H	2.423684	2.093126	-0.000667
H	-0.621866	-3.209549	-0.000507
H	-2.886233	-1.783677	-0.000747
H	-2.914583	1.755620	-0.000531
H	-0.680756	3.222293	-0.000498

1-azacycl[2,3,2]azine dimer neutral solution species: HF -911.140365 a.u.

N	4.575203	1.337740	0.508201
N	2.908444	-0.166172	-0.060630
C	4.238432	0.115535	0.125321

C	3.549866	2.200451	0.688932
C	2.179099	1.930064	0.504210
C	1.818802	0.647723	0.088696
C	4.899950	-1.121897	-0.174185
C	3.925497	-2.061282	-0.513123
C	2.638001	-1.438031	-0.435515
C	1.223699	-1.471993	-0.554802
C	0.699851	-0.198346	-0.237231
N	-4.575204	-1.337710	0.508252
N	-2.908457	0.166125	-0.060817
C	-4.238432	-0.115528	0.125303
C	-3.549874	-2.200436	0.688952
C	-2.179110	-1.930070	0.504180
C	-1.818811	-0.647750	0.088601
C	-4.899935	1.121941	-0.174089
C	-3.925480	2.061306	-0.513077
C	-2.638001	1.438001	-0.435637
C	-1.223694	1.471975	-0.554850
C	-0.699851	0.198330	-0.237260
H	3.841261	3.194741	1.010647
H	1.447003	2.703697	0.690583
H	5.965484	-1.280776	-0.135130
H	4.113636	-3.088793	-0.785629
H	0.634056	-2.320802	-0.866474
H	-3.841269	-3.194708	1.010717
H	-1.447012	-2.703689	0.690605
H	-5.965460	1.280854	-0.134932
H	-4.113608	3.088838	-0.785515
H	-0.634042	2.320796	-0.866475

1-azacycl[2,3,2]azine dimer cation solution species: HF -910.951365 a.u.

N	4.628307	1.339722	0.107254
N	2.893158	-0.174897	-0.013670
C	4.225884	0.085075	0.019952
C	3.645859	2.262638	0.161061
C	2.255676	2.011525	0.128938
C	1.846959	0.683987	0.027146
C	4.846476	-1.228114	-0.056829
C	3.850280	-2.180203	-0.128958
C	2.572527	-1.511263	-0.099488
C	1.184412	-1.545793	-0.116411
C	0.677409	-0.200746	-0.041389
N	-4.628302	-1.339722	0.107307
N	-2.893161	0.174884	-0.013881
C	-4.225884	-0.085080	0.019907
C	-3.645851	-2.262636	0.161103
C	-2.255670	-2.011521	0.128931
C	-1.846959	-0.683990	0.027038

C	-4.846478	1.228115	-0.056751
C	-3.850286	2.180205	-0.128903
C	-2.572533	1.511258	-0.099593
C	-1.184417	1.545799	-0.116407
C	-0.677410	0.200752	-0.041414
H	3.984356	3.290165	0.236254
H	1.568216	2.841778	0.187863
H	5.911127	-1.401247	-0.055131
H	3.998122	-3.247030	-0.193839
H	0.580568	-2.434507	-0.193790
H	-3.984344	-3.290159	0.236366
H	-1.568204	-2.841765	0.187935
H	-5.911129	1.401251	-0.054951
H	-3.998129	3.247037	-0.193700
H	-0.580573	2.434523	-0.193672

Chapter 7:

"trans"-2,3'-diindole neutral solution species: HF -726.658008 a.u.

C	4.064053	0.955762	0.636619
C	2.722899	0.676465	0.326227
C	2.409723	-0.558280	-0.304363
C	3.389215	-1.494946	-0.638197
C	4.707790	-1.185412	-0.327328
C	5.040741	0.026949	0.306775
C	1.485282	1.377426	0.505660
C	0.478252	0.589448	-0.005106
N	1.039866	-0.593596	-0.474249
C	-2.101759	-1.481888	0.378115
C	-2.033867	-0.115598	0.055787
C	-3.245811	0.598667	-0.137623
C	-4.498074	-0.012530	-0.045875
C	-4.530900	-1.367174	0.253724
C	-3.343786	-2.093042	0.469501
C	-0.952378	0.833734	-0.106751
C	-1.539386	2.046874	-0.383001
N	-2.910755	1.912880	-0.393448
H	4.332201	1.886820	1.124194
H	3.134124	-2.431884	-1.121586
H	5.492958	-1.890596	-0.575050
H	6.079209	0.234582	0.539061
H	1.344284	2.330534	0.991395
H	0.540286	-1.273113	-1.024026
H	-1.198994	-2.049621	0.572752
H	-5.413020	0.549475	-0.198143
H	-5.486444	-1.872819	0.331549
H	-3.405241	-3.145966	0.719538
H	-1.073464	2.996700	-0.592203

H	-3.561655	2.652162	-0.598590

"trans"-2,3'-diindole cation solution species: HF -726.477222 a.u.

C	4.110260	1.108526	0.088052
C	2.747422	0.719356	0.047700
C	2.416724	-0.669217	-0.039656
C	3.385196	-1.657401	-0.092847
C	4.717346	-1.239086	-0.054199
C	5.074979	0.125258	0.035850
C	1.541152	1.429433	0.071891
C	0.472876	0.484635	0.002860
N	1.032228	-0.764380	-0.055471
C	-2.225680	-1.548645	0.075500
C	-2.057281	-0.157935	0.011900
C	-3.215427	0.652473	-0.031289
C	-4.506454	0.143020	-0.027445
C	-4.639727	-1.242177	0.024770
C	-3.513340	-2.074332	0.078473
C	-0.917225	0.745510	-0.002294
C	-1.453317	2.049424	-0.046491
N	-2.791970	1.984830	-0.066077
H	4.379884	2.155397	0.157165
H	3.133470	-2.708752	-0.160241
H	5.501592	-1.985700	-0.093202
H	6.123641	0.393026	0.063787
H	1.422324	2.499322	0.142183
H	0.518876	-1.623126	-0.167731
H	-1.387521	-2.231570	0.136797
H	-5.374927	0.789889	-0.061042
H	-5.629340	-1.681871	0.028631
H	-3.648917	-3.147649	0.126905
H	-0.940486	2.997736	-0.075453
H	-3.405432	2.787096	-0.103617

"trans"-2,3'-di-5-methoxyindole neutral solution species: HF -955.766925 a.u.

C	3.901851	-0.805461	-0.606981
C	2.541883	-0.734219	-0.281885
C	2.063470	0.378589	0.462866
C	2.913599	1.391965	0.889229
C	4.266569	1.300064	0.566576
C	4.753667	0.208449	-0.180106
C	1.409505	-1.573246	-0.545076
C	0.304960	-0.981360	0.028564
N	0.696984	0.214367	0.616545
C	-2.524832	0.748389	-0.117045
C	-2.279928	-0.622404	0.032888
C	-3.380679	-1.515144	0.124782
C	-4.695524	-1.062677	0.092988

C	-4.920733	0.304541	-0.035895
C	-3.839826	1.203099	-0.145540
C	-1.077664	-1.428398	0.087004
C	-1.492277	-2.736001	0.205810
N	-2.866519	-2.796943	0.218233
O	6.074662	0.062451	-0.535547
C	7.002193	1.056039	-0.135556
O	-3.993467	2.559487	-0.288999
C	-5.304067	3.093367	-0.387138
H	4.309898	-1.630388	-1.178780
H	2.546275	2.239351	1.457781
H	4.935489	2.082646	0.896428
H	1.397307	-2.481759	-1.126861
H	0.114064	0.751852	1.236634
H	-1.722685	1.466100	-0.235740
H	-5.532686	-1.748377	0.162946
H	-5.939477	0.665751	-0.058036
H	-0.896783	-3.630290	0.300412
H	-3.406483	-3.637296	0.335938
H	7.061104	1.139587	0.956073
H	6.754881	2.036289	-0.559831
H	7.968930	0.734281	-0.521295
H	-5.885314	2.909236	0.523743
H	-5.841814	2.684844	-1.250285
H	-5.178535	4.167143	-0.519127

“trans”-2,3’-di-5-methoxyindole cation solution species: HF -955.586776 a.u.

C	3.992841	0.936680	0.159739
C	2.598415	0.747163	0.075387
C	2.065714	-0.566614	-0.112469
C	2.888878	-1.670608	-0.227282
C	4.268284	-1.461779	-0.148045
C	4.823116	-0.169408	0.046218
C	1.505938	1.624885	0.136674
C	0.313125	0.854861	-0.006656
N	0.678718	-0.458627	-0.137479
C	-2.627871	-0.765091	0.051453
C	-2.280868	0.582710	-0.011459
C	-3.312289	1.550070	-0.058903
C	-4.655885	1.210622	-0.064279
C	-4.989183	-0.140763	-0.019329
C	-3.985363	-1.124797	0.042419
C	-1.022118	1.318322	-0.007472
C	-1.369974	2.684695	-0.040694
N	-2.704413	2.807598	-0.074906
O	6.151993	0.069892	0.132013
C	7.079066	-1.012945	0.026113
O	-4.222839	-2.452415	0.101677

C	-5.572715	-2.929109	0.121603
H	4.426674	1.917430	0.307511
H	2.497474	-2.670333	-0.371007
H	4.922342	-2.318386	-0.235749
H	1.541531	2.692062	0.289961
H	0.051319	-1.209098	-0.376004
H	-1.908276	-1.568815	0.132797
H	-5.433852	1.964017	-0.099129
H	-6.032410	-0.422565	-0.025055
H	-0.728769	3.551519	-0.060182
H	-3.196999	3.688970	-0.115279
H	7.005045	-1.504087	-0.948797
H	6.930514	-1.741970	0.828409
H	8.063298	-0.561879	0.127760
H	-6.100533	-2.650091	-0.794642
H	-6.108456	-2.550716	0.996630
H	-5.496943	-4.012045	0.181836

“trans”-2,3’-di-5-methylindole neutral solution species: HF -805.309497 a.u.

C	3.960782	-0.738015	-0.599418
C	2.598975	-0.615167	-0.272436
C	2.171552	0.517687	0.466403
C	3.066324	1.502145	0.887751
C	4.404462	1.342937	0.555098
C	4.866810	0.232980	-0.189793
C	1.432937	-1.409109	-0.527121
C	0.355325	-0.769554	0.045718
N	0.803488	0.410814	0.627978
C	-2.393799	1.085834	-0.206043
C	-2.209121	-0.292374	0.005742
C	-3.350299	-1.124431	0.118727
C	-4.647350	-0.611372	0.051758
C	-4.790744	0.754029	-0.138819
C	-3.676765	1.615210	-0.276208
C	-1.047606	-1.150798	0.106890
C	-1.524535	-2.431558	0.271400
N	-2.902044	-2.421914	0.270730
C	6.335120	0.122832	-0.532331
C	-3.898443	3.092302	-0.506707
H	4.306196	-1.594218	-1.170474
H	2.733714	2.364622	1.455549
H	5.119217	2.094952	0.873848
H	1.380938	-2.320627	-1.102276
H	0.242879	0.983918	1.236827
H	-1.536085	1.737201	-0.336283
H	-5.515739	-1.255149	0.140520
H	-5.789230	1.175652	-0.193471
H	-0.976087	-3.350074	0.407695

H	-3.485463	-3.230809	0.402572
H	6.958672	0.145392	0.367307
H	-4.473974	3.271035	-1.420676
H	6.549303	-0.807843	-1.062279
H	-2.950194	3.625303	-0.602066
H	6.659134	0.951165	-1.171209
H	-4.455131	3.545721	0.319788

“trans”-2,3’-di-5-methylindole cation solution species: HF -805.129828 a.u.

C	4.044803	-0.872224	0.131852
C	2.648803	-0.630306	0.061667
C	2.172804	0.707568	-0.095529
C	3.040801	1.783008	-0.192748
C	4.404083	1.502634	-0.123865
C	4.925036	0.187502	0.039123
C	1.524521	-1.461938	0.112633
C	0.362949	-0.641688	-0.007391
N	0.786695	0.658257	-0.119443
C	-2.529696	1.100862	0.062928
C	-2.220596	-0.266022	0.001541
C	-3.284517	-1.192221	-0.043739
C	-4.618171	-0.808501	-0.050023
C	-4.886186	0.554997	-0.003384
C	-3.861438	1.519653	0.060132
C	-0.991599	-1.045827	-0.007541
C	-1.388464	-2.399959	-0.046127
N	-2.726188	-2.474198	-0.073393
C	6.418225	-0.013059	0.103165
C	-4.212095	2.984378	0.150558
H	4.411221	-1.884814	0.255675
H	2.688781	2.800222	-0.314433
H	5.104695	2.327648	-0.196030
H	1.517234	-2.533249	0.239834
H	0.186964	1.445606	-0.304484
H	-1.756312	1.856380	0.133923
H	-5.422067	-1.533950	-0.088771
H	-5.918330	0.886338	-0.010316
H	-0.778427	-3.288982	-0.072338
H	-3.253460	-3.335563	-0.106393
H	6.858621	0.575350	0.912664
H	-5.008363	3.243792	-0.550317
H	6.671783	-1.060141	0.271425
H	-3.351274	3.618452	-0.067084
H	6.896446	0.304682	-0.827866
H	-4.566645	3.236677	1.154853

“trans”-2,3’-diindole-5-carboxylic acid neutral solution species: HF -1103.960201 a.u.

C	3.815660	-0.714452	-0.454422
C	2.447244	-0.711821	-0.171947
C	1.892850	0.391549	0.535620
C	2.671747	1.469534	0.965440
C	4.026041	1.440465	0.678515
C	4.600004	0.357357	-0.028815
C	1.368671	-1.616624	-0.444228
C	0.223389	-1.072794	0.088727
N	0.545892	0.153520	0.667990
C	-2.702738	0.502179	-0.105856
C	-2.379091	-0.849174	0.042653
C	-3.434656	-1.800098	0.110625
C	-4.781228	-1.428537	0.060070
C	-5.074252	-0.082148	-0.066398
C	-4.043313	0.882220	-0.151827
C	-1.135319	-1.589502	0.120360
C	-1.482881	-2.914541	0.229559
N	-2.857277	-3.043083	0.214026
C	6.046259	0.316123	-0.342256
O	6.611758	-0.574336	-0.937964
O	6.726227	1.405921	0.111204
C	-4.338595	2.327456	-0.296464
O	-3.509433	3.208601	-0.342254
O	-5.669213	2.596727	-0.373690
H	4.283463	-1.529775	-0.992678
H	2.235220	2.303764	1.502832
H	4.661144	2.256494	0.995040
H	1.423143	-2.538605	-1.001459
H	-0.091196	0.710491	1.213944
H	-1.943646	1.268170	-0.203929
H	-5.572884	-2.167082	0.114792
H	-6.104362	0.244601	-0.106065
H	-0.848072	-3.779666	0.335920
H	-3.355779	-3.913061	0.303403
H	7.650108	1.275816	-0.146750
H	-5.750919	3.557341	-0.463679

“trans”-2,3’-diindole-5-carboxylic acid cation solution species:
HF -1103.768310 a.u.

C	-3.915065	0.788969	-0.000235
C	-2.506366	0.687765	-0.000121
C	-1.893171	-0.604496	0.000248
C	-2.635724	-1.773443	0.000530
C	-4.024857	-1.643020	0.000398
C	-4.660914	-0.376706	0.000013
C	-1.474617	1.635292	-0.000297
C	-0.233550	0.929631	0.000041
N	-0.521657	-0.410135	0.000338

C	2.807386	-0.509410	-0.000105
C	2.371598	0.816087	0.000032
C	3.346451	1.842431	0.000138
C	4.712764	1.595778	0.000192
C	5.119297	0.265107	0.000094
C	4.176225	-0.777125	-0.000062
C	1.073202	1.471611	0.000003
C	1.338486	2.855127	0.000054
N	2.665422	3.060898	0.000175
C	-6.151251	-0.243541	-0.000166
O	-6.730306	0.812844	-0.000484
O	-6.773601	-1.439583	0.000085
C	4.578744	-2.217400	-0.000191
O	3.790123	-3.131658	-0.000291
O	5.913625	-2.383039	-0.000252
H	-4.418805	1.747936	-0.000551
H	-2.171418	-2.751909	0.000833
H	-4.641607	-2.532181	0.000600
H	-1.583400	2.708540	-0.000560
H	0.160142	-1.151901	0.000376
H	2.144035	-1.364498	-0.000288
H	5.438237	2.400184	0.000301
H	6.173562	0.023471	0.000127
H	0.647799	3.683677	0.000089
H	3.104726	3.971377	0.000026
H	-7.730154	-1.279656	-0.000042
H	6.099995	-3.334840	-0.000342

“cis”-2,3’-diindole neutral solution species: HF -726.658875 a.u.

C	3.608256	1.532659	-0.510319
C	2.489113	0.709188	-0.306054
C	2.685740	-0.591288	0.231138
C	3.948342	-1.070522	0.581991
C	5.035352	-0.228551	0.378204
C	4.866469	1.058607	-0.166417
C	1.079762	0.862024	-0.522259
C	0.464582	-0.306502	-0.131382
N	1.444699	-1.194175	0.304904
C	-2.263379	1.526264	0.285986
C	-2.090373	0.159343	0.016042
C	-3.239864	-0.664165	-0.100844
C	-4.537219	-0.160940	0.021439
C	-4.676160	1.196637	0.272323
C	-3.549570	2.030698	0.408374
C	-0.935190	-0.695349	-0.157470
C	-1.422692	-1.967703	-0.363255
N	-2.800782	-1.953668	-0.324698
H	3.489509	2.526825	-0.927406

H	4.081420	-2.064454	0.995588
H	6.030135	-0.570184	0.640552
H	5.736573	1.687634	-0.316985
H	0.583955	1.712023	-0.963292
H	1.245276	-2.038813	0.815143
H	-1.404565	2.175081	0.406437
H	-5.404464	-0.805213	-0.072952
H	-5.668620	1.621233	0.371057
H	-3.693820	3.084627	0.616647
H	-0.890635	-2.882911	-0.571553
H	-3.391198	-2.753348	-0.479676

“cis”-2,3’-diindole cation solution species: HF -726.476359 a.u.

C	3.550536	1.640824	-0.294354
C	2.454241	0.751441	-0.151057
C	2.701349	-0.629925	0.131958
C	3.983743	-1.131890	0.291687
C	5.036876	-0.227724	0.153017
C	4.823807	1.141066	-0.138879
C	1.066223	0.915067	-0.228495
C	0.460071	-0.352599	-0.005252
N	1.473695	-1.266375	0.193945
C	-2.283403	1.548072	0.214151
C	-2.081003	0.175050	0.027116
C	-3.213822	-0.660558	-0.090498
C	-4.519336	-0.187961	-0.060102
C	-4.689408	1.184884	0.101039
C	-3.586005	2.037495	0.241044
C	-0.912831	-0.693907	-0.029682
C	-1.411821	-2.006307	-0.168978
N	-2.752614	-1.975150	-0.208838
H	3.381251	2.687446	-0.516265
H	4.171195	-2.176638	0.507417
H	6.052846	-0.586358	0.268330
H	5.679984	1.795977	-0.239374
H	0.533636	1.819958	-0.470249
H	1.344201	-2.216227	0.504714
H	-1.454875	2.228917	0.355320
H	-5.369768	-0.852954	-0.151107
H	-5.690434	1.596990	0.128905
H	-3.751133	3.098610	0.381100
H	-0.877692	-2.936741	-0.286131
H	-3.342076	-2.786474	-0.334689

“cis”-2,3’-di-5-methoxyindole neutral solution species: HF -955.768809 a.u.

C	3.215091	0.987479	-0.568134
C	2.123239	0.147921	-0.319579
C	2.336058	-1.092059	0.341440

C	3.598927	-1.484651	0.766973
C	4.674535	-0.631172	0.523503
C	4.481019	0.594545	-0.143843
C	0.718151	0.234631	-0.595181
C	0.122867	-0.913306	-0.118507
N	1.108066	-1.730348	0.425622
C	-2.642146	0.878985	0.069412
C	-2.444984	-0.507635	-0.079047
C	-3.564607	-1.367543	-0.152167
C	-4.873610	-0.879369	-0.100295
C	-5.050559	0.484894	0.031403
C	-3.943384	1.359915	0.122113
C	-1.265450	-1.340435	-0.149599
C	-1.714122	-2.641832	-0.257400
N	-3.089182	-2.662692	-0.253619
O	5.499084	1.477012	-0.420016
C	6.817902	1.142701	-0.023979
O	-4.274491	2.681953	0.266049
C	-3.224344	3.630380	0.374367
H	3.101621	1.936449	-1.078513
H	3.759449	-2.429906	1.273935
H	5.660514	-0.927864	0.853153
H	0.215259	1.020389	-1.135844
H	0.907855	-2.509806	1.030439
H	-1.789890	1.537774	0.152551
H	-5.729294	-1.542886	-0.158616
H	-6.043189	0.915630	0.074718
H	-1.150823	-3.554557	-0.373836
H	-3.655249	-3.487070	-0.361558
H	7.166449	0.224394	-0.511037
H	6.897955	1.027520	1.063345
H	7.444779	1.975063	-0.341647
H	-2.596543	3.434788	1.250946
H	-3.707494	4.599945	0.485617
H	-2.597831	3.639005	-0.524810

“cis”-2,3’-di-methoxyindole cation solution species: HF -955.585038 a.u.

C	3.167973	1.119786	-0.311827
C	2.103966	0.211637	-0.149005
C	2.374254	-1.153885	0.205731
C	3.669799	-1.604620	0.422222
C	4.702169	-0.687535	0.268242
C	4.459781	0.672154	-0.101109
C	0.710736	0.331236	-0.265552
C	0.134762	-0.932775	0.000604
N	1.167751	-1.822772	0.258150
C	-2.660274	0.882530	0.075208
C	-2.424827	-0.493664	-0.037241

C	-3.519978	-1.374259	-0.132170
C	-4.842082	-0.933670	-0.148470
C	-5.062150	0.428235	-0.061197
C	-3.986396	1.335797	0.055541
C	-1.223610	-1.323256	-0.030163
C	-1.673485	-2.659785	-0.108938
N	-3.013691	-2.672492	-0.174991
O	5.447084	1.579374	-0.262243
C	6.813855	1.203724	-0.066666
O	-4.346916	2.631964	0.149774
C	-3.343702	3.640355	0.279528
H	2.998490	2.152075	-0.589587
H	3.884700	-2.630900	0.693566
H	5.717537	-1.022919	0.429515
H	0.164802	1.208264	-0.570538
H	1.047875	-2.742385	0.651918
H	-1.845666	1.579592	0.197188
H	-5.673486	-1.624583	-0.221503
H	-6.066569	0.831496	-0.069371
H	-1.107185	-3.575707	-0.171798
H	-3.574237	-3.508522	-0.267533
H	7.114997	0.423893	-0.772030
H	6.990902	0.874808	0.961385
H	7.390186	2.105267	-0.259888
H	-2.760656	3.499473	1.194705
H	-3.883133	4.582723	0.336078
H	-2.683055	3.651539	-0.592895

“cis”-2,3’-di-5-methylindole neutral solution species: HF -805.310348 a.u.

C	-3.462629	1.209263	-0.498385
C	-2.347492	0.380539	-0.285180
C	-2.541047	-0.886712	0.320272
C	-3.802135	-1.322662	0.727357
C	-4.879201	-0.473615	0.511331
C	-4.727941	0.791176	-0.102890
C	-0.943892	0.505360	-0.549794
C	-0.329229	-0.650512	-0.119208
N	-1.305256	-1.503241	0.388069
C	2.426809	1.167311	0.147567
C	2.234189	-0.209659	-0.055959
C	3.368174	-1.050996	-0.160581
C	4.669535	-0.549120	-0.086594
C	4.821692	0.815594	0.100204
C	3.713329	1.686317	0.224450
C	1.065453	-1.056236	-0.163619
C	1.533106	-2.343757	-0.322015
N	2.911218	-2.345349	-0.315217
C	-5.941015	1.666975	-0.318826

C	3.945092	3.163832	0.441980
H	-3.334972	2.179141	-0.968997
H	-3.943899	-2.291458	1.194554
H	-5.869866	-0.791314	0.820690
H	-0.451697	1.325844	-1.047249
H	-1.099350	-2.321161	0.937647
H	1.571054	1.823803	0.255073
H	5.533155	-1.200103	-0.168911
H	5.823063	1.229928	0.159245
H	0.984945	-3.260241	-0.475915
H	3.488885	-3.157873	-0.449324
H	-6.439203	1.900087	0.627906
H	4.526882	3.346697	1.351128
H	-5.667472	2.612638	-0.791794
H	3.000270	3.702557	0.537441
H	-6.679752	1.175634	-0.960576
H	4.499434	3.607358	-0.391550

"cis"-2,3'-di-5methylindole cation solution species: HF -805.129698 a.u.

C	3.406362	1.326382	-0.260773
C	2.316599	0.427466	-0.123860
C	2.569124	-0.948271	0.178267
C	3.858271	-1.428056	0.362444
C	4.896479	-0.512104	0.228684
C	4.693635	0.865723	-0.084457
C	0.929166	0.577317	-0.224744
C	0.329792	-0.691238	0.003031
N	1.349432	-1.596831	0.226582
C	-2.440031	1.180595	0.126550
C	-2.219029	-0.195118	-0.016401
C	-3.335840	-1.048677	-0.125650
C	-4.644523	-0.582420	-0.124139
C	-4.827068	0.789986	-0.003978
C	-3.743695	1.682108	0.126052
C	-1.037727	-1.049486	-0.034651
C	-1.517435	-2.372889	-0.145050
N	-2.857875	-2.359444	-0.203410
C	5.889162	1.774355	-0.211558
C	-4.003868	3.160947	0.267642
H	3.219433	2.367400	-0.497914
H	4.060064	-2.467029	0.593221
H	5.914251	-0.862240	0.364390
H	0.393214	1.475156	-0.484219
H	1.222789	-2.542083	0.551684
H	-1.614432	1.868115	0.256791
H	-5.490915	-1.253890	-0.206824
H	-5.836397	1.185753	0.000055
H	-0.970454	-3.299196	-0.230115

H	-3.435639	-3.181371	-0.313153
H	6.570088	1.419990	-0.990856
H	-4.501127	3.557059	-0.622557
H	5.590430	2.792682	-0.462676
H	-3.078009	3.719684	0.411235
H	6.456086	1.809443	0.723375
H	-4.656525	3.364736	1.120913

"cis"-2,3'-diindole-5-carboxylic acid neutral solution species:
HF -1103.952910 a.u.

C	3.234304	0.832456	-0.432638
C	2.150447	-0.027047	-0.235741
C	2.379027	-1.298316	0.359379
C	3.648031	-1.710889	0.773497
C	4.705037	-0.838178	0.575460
C	4.505630	0.425812	-0.027947
C	0.744464	0.060366	-0.508686
C	0.165497	-1.116074	-0.095335
N	1.166278	-1.945168	0.414471
C	-2.651823	0.602508	0.105828
C	-2.411867	-0.760602	-0.085842
C	-3.518788	-1.642742	-0.212024
C	-4.839480	-1.191180	-0.170055
C	-5.046795	0.168763	-0.008846
C	-3.964514	1.070056	0.126318
C	-1.212941	-1.569343	-0.161163
C	-1.636616	-2.869507	-0.320009
N	-3.016295	-2.915736	-0.345645
C	5.630533	1.362924	-0.251469
O	5.543971	2.453278	-0.770604
O	6.825958	0.882373	0.191514
C	-4.163364	2.540139	0.327275
O	-3.338172	3.266123	0.814612
O	-5.357735	3.059373	-0.078456
H	3.110767	1.807725	-0.887368
H	3.807031	-2.680654	1.231584
H	5.702503	-1.121829	0.882190
H	0.234694	0.876693	-0.994390
H	0.986846	-2.787795	0.935825
H	-1.843414	1.307861	0.247084
H	-5.675890	-1.876269	-0.246187
H	-6.069512	0.523800	0.061589
H	-1.058935	-3.770881	-0.452900
H	-3.563310	-3.750334	-0.477294
H	7.482006	1.567348	-0.002107
H	-5.855537	2.406613	-0.584360

"cis"-2,3'-diindole-5-carboxylic acid cation solution species:
HF -1103.759828 a.u.

C	3.171220	0.905524	-0.217623
C	2.112705	-0.024573	-0.098900
C	2.404923	-1.394907	0.194348
C	3.701029	-1.846078	0.383630
C	4.723800	-0.904895	0.267307
C	4.465761	0.457326	-0.032978
C	0.722184	0.089675	-0.209773
C	0.158302	-1.200781	0.005472
N	1.200426	-2.073903	0.233867
C	-2.636984	0.611487	0.084544
C	-2.397166	-0.755364	-0.041055
C	-3.504107	-1.629200	-0.142831
C	-4.820518	-1.188549	-0.146251
C	-5.029102	0.184404	-0.052619
C	-3.952297	1.081464	0.056729
C	-1.201612	-1.590720	-0.042672
C	-1.661095	-2.918201	-0.139703
N	-3.003985	-2.929716	-0.202632
C	5.571376	1.458267	-0.161197
O	5.395810	2.620905	-0.420096
O	6.785652	0.909441	0.045630
C	-4.122176	2.573597	0.208477
O	-3.248722	3.265339	0.655939
O	-5.297782	3.114719	-0.173910
H	2.989469	1.949501	-0.442805
H	3.925776	-2.881628	0.607431
H	5.750612	-1.217295	0.405830
H	0.166415	0.979007	-0.457260
H	1.100998	-3.032957	0.527995
H	-1.849299	1.337708	0.227922
H	-5.654905	-1.876678	-0.204678
H	-6.052125	0.542137	-0.024234
H	-1.101339	-3.838688	-0.206460
H	-3.566060	-3.764360	-0.300738
H	7.450952	1.608524	-0.051248
H	-5.852695	2.485963	-0.650338

Appendix 2: Reprints of Published Papers.